TRANSACTIONS
OF THE ASME
Series C

Journal of HEAT TRANSFER

May 1960

RADIATION • CONDUCTION • CONVECTION • COMPLEX SYSTEMS • PHASE CHANGES AND MIXTURES • TRANSIENT PHENOMENA • THERMOPHYSICAL PROPERTIES • EXPERIMENTAL TECHNIQUES • THERMOMETRY • ANALOG METHODS • ANALYTICAL AND NUMERICAL METHODS • APPLICATIONS • DESIGN TECHNIQUES • HEAT EXCHANGERS • INSULATION • ECONOMIC FACTORS BIOTECHNOLOGY • ASTRONAUTICS

Published Quarterly by
THE AMERICAN SOCIETY OF MECHANICAL ENGINEERS

TRANSACTIONS
OF THE ASME
Series C

EDITORIAL DEPARTMENT

Editor, J. J. JAKLITSCH, JR.
Consulting Editor, LEO BLODGETT
Production, JEAN NORTH
Art Editor, HENRY BALFOUR

HEAT TRANSFER DIVISION

Chairman, H. A. JOHNSON
Secretary, S. OSTRACH
Papers Review, J. P. HARTNETT
Consulting Editor, S. P. KEZIOS

OFFICERS OF THE ASME

President, W. L. CISLER
Secretary, O. B. SCHIER, II
Treasurer, E. J. KATES
Assistant Treasurer, H. J. BAUER

PUBLICATIONS COMMITTEE

Chairman, B. G. A. SKROTZKI
HENDLEY N. BLACKMON
R. D. MINDLIN
MARTIN GOLAND
VITO L. SALERNO

Junior Representatives
A. S. GOLDSTEIN
J. W. FOLLANSBEE

REGIONAL ADVISORY BOARD

Region I, H. M. ROGERS, JR.
Region II, GLENN R. FRYLING
Region III, F. J. HEINZE
Region IV, FRANCIS C. SMITH
Region V, H. M. CATHER
Region VI, C. R. EARLE
Region VII, M. S. UMBENHAUER
Region VIII, CARL J. ECKHARDT

Published quarterly by The American Society of Mechanical Engineers. Publication office at 20th and Northampton Streets, Easton, Pa. The editorial department is located at the headquarters of the Society, 29 West Thirty-Ninth Street, New York 18, N. Y. Cable address, "Mechaneer," New York. Price $3.00 a copy, $10.00 annually; to members, $1.50 a copy, $5.00 annually. Add 50 cents for postage to all countries outside the United States and Canada. Changes of address must be received at Society headquarters seven weeks before they are to be effective on the mailing list. Please send old as well as new address. . . . By-Law: The Society shall not be responsible for statements or opinions advanced in papers or . . . printed in its publications (B13, Par. 4). . . . Second-class mail privileges authorized at Easton, Penna. . . . This publication is authorized to be mailed at the special rates of postage prescribed by Section 132.122 . . . © Copyrighted, 1960, by The American Society of Mechanical Engineers. Reprints from this publication may be made on condition that full credit be given the Transactions of the ASME, Series C—Journal of Heat Transfer, and the author, and that date of publication be stated.

TRANSACTIONS OF THE ASME
is indexed by the Engineering Index, Inc.

Journal of HEAT TRANSFER

VOL. 82 • SERIES C • NO. 2

May 1960

CONTENTS

77 **Heat Transfer From Transverse and Yawed Cylinders in Continuum, Slip, and Free Molecule Air Flows**
L. V. Baldwin, V. A. Sandborn, and J. C. Laurence

87 **Magnetohydrodynamic Effects Upon Heat Transfer for Laminar Flow Across a Flat Plate**
R. D. Cess

94 **Conical Turbulent Boundary Layer Experiments and a Correlation With Flat Plate Data**
W. S. Bradfield

101 **The Influence of Free Stream Turbulence on the Local Heat Transfer From Cylinders**
R. A. Seban

108 **Heat Transfer to Fully Developed Laminar Flow in a Circular Tube With Arbitrary Circumferential Heat Flux**
W. C. Reynolds

113 **Steam Slip—Theoretical Prediction From Momentum Model**
S. Levy

125 **Pressure Drop and Heat Transfer in a Duct With Triangular Cross Section**
E. R. G. Eckert and T. F. Irvine, Jr.

139 **Heat Transfer in Flow Through Rotating Ducts**
C. Y. Kuo, H. T. Iida, J. H. Taylor, and F. Kreith

TECHNICAL BRIEF

152 **Comparison of Turbulent Heat-Transfer Results for Uniform Wall Heat Flux and Uniform Wall Temperature**
R. Siegel and E. M. Sparrow

TRANSACTIONS OF THE ASME Series B

Journal of
ENGINEERING FOR INDUSTRY
Volume 82 • Series B • Number 2

CONTENTS FOR MAY, 1960

87 Simplified Approach to Understanding the Suction Problems for Reciprocating Mud Pumps, by W. E. Liljestrand. (59—Pet-23)
93 Prevention of Sulfide-Stress Cracking in Sour-Condensate Well Equipment, by W. J. McGuire and L. W. Vollmer. (59—Pet-36)
103 Overstrain Tests on Thick-Walled Cylinders, by S. M. Jorgensen. (59—Pet-1)
122 An Analytical Study of Drill-String Vibration, by J. J. Bailey and I. Finnie. (59—Pet-15)
129 An Experimental Study of Drill-String Vibration, by I. Finnie and J. J. Bailey. (59—Pet-16)
136 The Theory of the Ideal Design of a Compound Vessel, by S. J. Becker and L. Mollick. (59—A-125)
143 The Strength of Thick Cylinders Subjected to Repeated Internal Pressure, by J. L. M. Morrison, B. Crossland, and J. S. C. Parry. (59—A-167)
154 The Interaction of Textile Structures and High-Speed Textile Processes, by H. M. Morgan. (59—A-115)
159 Effect of Transient Loads on the Refrigerated-Space Temperature of a Cooling Complex, by C. F. Kayan. (59—A-181)
167 Uniform Two-Way Orientation of Plastic Films, by M. O. Longstreth and Turner Alfrey, Jr. (59—A-113)

TRANSACTIONS OF THE ASME Series A

Journal of
ENGINEERING FOR POWER
Volume 82 • Series A • Number 2

CONTENTS FOR APRIL, 1960

83 Critical Flow Velocities for Collapse of Reactor Parallel-Plate Fuel Assemblies, by D. R. Miller.
96 The Propeller Turbines of the St. Lawrence Power Project, by G. G. Fintak. (59—Hyd-11)
103 Influence of Trailing-Edge Geometry on Hydraulic-Turbine-Blade Vibration Resulting From Vortex Excitation, by Gunnar Heskestad and D. R. Olberts. (59—Hyd-7)
111 Water-Hammer Damage to Oigawa Power Station, by C. C. Bonin. (59—Hyd-8)
120 An Experimental Investigation of Radial Thrust in Centrifugal Pumps, by A. Agostinelli, D. Nobles, and C. R. Mockridge. (59—Hyd-2)
127 Design and Test of Mixed-Flow and Centrifugal Impellers, by J. J. Kramer, W. M. Osborn, and J. T. Hamrick. (59—Hyd-20)
136 Volute Pressure Distribution, Radial Force on the Impeller, and Volute Mixing Losses of a Radial Flow Centrifugal Pump, by H. W. Iversen, R. E. Rolling, and J. J. Carlson. (59—Hyd-10)
145 Relationship of Coal-Ash Viscosity to Chemical Composition, by W. L. Sage and J. B. McIlroy. (59—Fu-4)
156 Pressurization of Granular Solid Fuels, by M. N. Aref. (59—A-150)

TRANSACTIONS OF THE ASME Series D

Journal of
BASIC ENGINEERING
Vol. 82 • Series D • No. 1

CONTENTS FOR MARCH, 1960

1 Cavitation Effect on the Discharge Coefficient of the Sharp-Edged Orifice Plate, by F. Numachi, M. Yamabe, and R. Ōba. (58—A-93)
12 Measurement of Oil-Film Thickness Between Disks by Electrical Conductivity, by S. I. El-Sisi and G. S. A. Shawki. (58—A-253)
19 Performance Characteristics of Lubricating Oil Film Between Rotating Disks, by S. I. El-Sisi and G. S. A. Shawki. (58—A-254)
29 The Measurement of Oil-Film Thickness in Gear Teeth, by I. O. MacConochie and A. Cameron. (58—A-142)
35 A New Approach to Linear Filtering and Prediction Problems, by R. E. Kalman. (59—IRD-11)
46 Shannon's Theory and Feedback Systems, by S. S. L. Chang. (59—IRD-12)
51 Dynamic Response and Control of Multipass Heat Exchangers, by M. Masubuchi. (59—IRD-6)
66 Bang-Bang Versus Linear Control of a Second-Order Rate-Type Servomotor, by P. F. Meyfarth. (59—IRD-13)
73 The Design and Analysis of a Servovalve With Flow Feedback, by E. Bahniuk and S.-Y. Lee. (59—IRD-3)
81 A Thermocouple System for Measuring Turbine-Inlet Temperatures, by M. E. Ihnat and W. C. Hagel. (59—IRD-1)
87 Estimating the Roots of the Characteristic Determinant for Multicoupled Systems, by S. Lees, H. D. Felsenthal, and E. M. Goldberg. (59—IRD-2)
96 Human Body as an Inconstant Heat Source and Its Relation to Determination of Clothes Insulation, Part I, by A. S. Iberall. (59—IRD-7)
103 Human Body as an Inconstant Heat Source and Its Relation to Clothes Insulation, Part 2, by A. S. Iberall. (59—IRD-8)
113 Some General Considerations in Process Optimization, by G. E. P. Box.
120 Ejector-Nozzle Flow and Thrust, by H. E. Weber. (59—Hyd-5)
131 Pressure Losses in Smooth Pipe Bends, by H. Itō. (59—Hyd-4)
144 Discharge Coefficients and Steady-State Flow Forces for Hydraulic Poppet Valves, by J. A. Stone. (59—Hyd-18)
169 The Inception of Cavitation on Isolated Surface Irregularities, by H. W. Holl. (59—Hyd-12)
184 Indentation of Metals by Cavitation, by W. H. Wheeler. (59—Hyd-15)
195 A Shock-Tube Technique to Determine Steady-Flow Losses of Orifices and Other Duct Elements, by G. Rudinger. (59—Hyd-13)
201 Separation Prediction for Conical Diffusers, by J. M. Robertson and H. R. Fraser. (59—Hyd-14)

Journal of
BASIC ENGINEERING
Vol. 82 • Series D • No. 1

CONTENTS FOR MARCH, 1960
(continued)

210 Unsteady Transfer of Momentum and Heat Between Concentric Cylinders, by C.-S. Yih. (59—Hyd-17)
217 Chamber Dimension Effects on Induced Flow and Frictional Resistance of Enclosed Rotating Disks, by J. W. Daily and R. E. Nece. (59—Hyd-9)
233 On the Three-Dimensional Turbulent Boundary Layer Generated by Secondary Flow, by J. P. Johnston. (59—Hyd-6)
249 Addendum to a previously published paper by B. Sternlicht.

TRANSACTIONS OF THE ASME Series E

Journal of
APPLIED MECHANICS
Volume 82 • Series E • No. 1

CONTENTS FOR MARCH, 1960

TECHNICAL PAPERS

1 A Theory of Lubrication With Turbulent Flow and Its Application to Slider Bearings, L. N. Tao. (59—A-26)
5 Effect of the Wall on Two-Phase Turbulent Motion, S. L. Soo and C. L. Tien. (59—APMW-18)
16 The Melting of Finite Slabs, T. R. Goodman and J. J. Shea. (59—APMW-11)
25 Heat-Exchanger Tube-Sheet Design—3. U-Tube and Bayonet-Tube Sheets, K. A. Gardner. (59—A-81)
34 Mechanics of the Sheet-Bending Process, B. W. Shaffer and E. E. Ungar. (59—A-35)
41 Relaxation of a Cylinder on a Rigid Shaft, E. A. Davis. (59—A-31)
45 Strain-Hardening Solutions to Axisymmetric Disks and Tubes, Nicholas Perrone. (59—A-29)
54 Effect of Shear Deformations on the Bending of Rectangular Plates, V. L. Salerno and M. A. Goldberg. (59—A-66)
59 Plastic Stress Concentration at a Circular Hole in an Infinite Sheet Subjected to Equal Biaxial Tension, Bernard Budiansky and O. L. Mangasarian. (59—APMW-16)
65 Stresses in the Plastic Range Around a Normally Loaded Circular Hole in an Infinite Sheet, O. L. Mangasarian. (59—A-130)
74 On a Dynamical Saint Venant Principle, B. A. Boley. (59—A-61)
79 Correlation of Theoretical and Photothermoelastic Results on Thermal Stresses in Idealized Wing Structures, Herbert Tramposch and George Gerard. (59—A-36)
87 Stresses in a Circular Cylinder Having an Infinite Row of Spherical Cavities Under Tension, Akira Atsumi. (59—APMW-9)
93 Transient Thermal Stresses in a Semi-Infinite Slab, W. Jaunzemis and E. Sternberg. (59—A-63)
104 On Stress-Strain Relations and Strain-Energy Expressions in the Theory of Thin Elastic Shells, J. K. Knowles and Eric Reissner. (59—APMW-13)
107 On the Effect of Shear on Plastic Deformation of Beams Under Transverse Impact Loading, B. Karunes and E. T. Onat. (59—APMW-7)
111 The Half-Space Under Pressure Distributed Over an Elliptical Portion of Its Plane Boundary, H. Deresiewicz. (59—A-17)
120 Earth Motion Beneath a Prescribed Boundary Displacement, R. C. Geldmacher, J. W. Dunkin, and R. L. Anderson. (59—A-3)
125 On the Elastic Bending of Columns Due to Dynamic Axial Forces Including Effects of Axial Inertia, Eugene Sevin. (59—A-25)
132 Dominance of Shear Stresses in Early Stages of Impulsive Motion of Beams, H. H. Bleich and R. Shaw. (59—A-60)
139 The Elastic-Plastic Response of Thin Spherical Shells to Internal Blast Loading, W. E. Baker. (59—A-95)
145 Axially Symmetric Waves in Elastic Rods, R. D. Mindlin and H. D. McNiven. (59—APMW-2)
152 Vibrations and Waves in Elastic Bars of Rectangular Cross Section, R. D. Mindlin and E. A Fox. (59—APMW-23)
159 Subharmonic Oscillations of a Pendulum, Richard Skalak and M. I. Yarymovych. (59—A-94)
165 Plane-Stress Unloading Waves Emanating From a Suddenly Punched Hole in a Stretched Elastic Plate, Julius Miklowitz. (59—A-46)
172 Plastic-Wave Propagation Effects in Transverse Impact of Membranes, B. Karunes and E. T. Onat. (59—A-128)
177 The Motion and Loading of a Hinged Ramp Which Supports a Sliding Mass, B. Saelman. (59—A-85)
182 An Analytical Method for Locating the Burmester Points for Five Infinitesimally Separated Positions of the Coupler Plane of a Four-Bar Mechanism, J. C. Wolford. (59—A-11)
187 Steady-State Undamped Vibrations of a Class of Nonlinear Discrete Systems, P. R. Sethna. (59—A-67)
196 A Unified Criterion for the Degree of Constraint of Plane Kinematic Chains, B. Paul. (59—A-34)
201 Approximate Synthesis of Spatial Linkages, J. Denavit and R. S. Hartenberg. (59—A-24)

BRIEF NOTES

207 Buckling and Deflection of Isosceles-Triangular Plates, L. S. Han. 208 The Creep Deflection of a Rivet in Double Shear, L. N. Tao. 209 Torsion of Prismatical Rods With Isosceles-Triangle Cross Sections, H. D. Conway. 210 Buckling of a Beam on a Number of Elastic Restraints, J. P. Ellington. 211 The Second Approximation for Buckling Loads, M. M. Abbassi.

DISCUSSION

213 Discussion of previously published papers by S. J. Kline and P. W. Runstadler; J. H. Baltrukonis; J. Modrey; A. Dornig; E. W. Gaylord; B. Paul; W. F. Stokey and C. F. Zorowski; R. M. Rosenberg and C. P. Atkinson.

221 BOOK REVIEWS

Heat Transfer From Transverse and Yawed Cylinders in Continuum, Slip, and Free Molecule Air Flows[1]

LIONEL V. BALDWIN
VIRGIL A. SANDBORN
JAMES C. LAURENCE

Aeronautical Research Scientists, Lewis Research Center, National Aeronautics and Space Administration, Cleveland, Ohio

A general Nusselt number correlation is presented for transverse cylinders in subsonic and supersonic air flows where dissociation is negligible. New and existing data in the following experimental range have been correlated: Mach $M = 0.001$ *to 6.0, Reynolds* $N_{Re} = 0.02$ *to 300,000, Knudsen* $N_{Kn} = 4 \times 10^{-6}$ *to 37.*

In subsonic flow, heat transfer from a cylinder yawed at an angle to the air velocity is predicted by the transverse cylinder Nusselt number correlation when the normal velocity component is used as the characteristic velocity. Finally, recovery temperature data from cylinders are divided into three regimes by a Knudsen number criterion.

Introduction

FOR MANY YEARS PAPERS reporting experimental data of heat transfer from cylinders have appeared in the literature. This can probably be attributed not only to the relative ease with which electrically heated wires lend themselves to such an experiment, but also to the practical importance of cylinders as sensitive elements for instruments. For example, thermocouple response characteristics are important for many control applications. Similarly, hot-wire anemometers are valuable tools for studying both the mean and turbulent properties of air flows in aerodynamic research; and at very low density, hot wires find application as pressure gages of the Pirani-type. Despite these familiar applications, engineers do not generally realize that the accumulated data on heat transfer from cylinders are the most complete information available today for the prediction of heat transfer in rarefied air. The utility of individual contributions is greatly enhanced when these are viewed as part of a summary. But unfortunately, there has been little effort to correlate recent experimental data over a wide range of flow conditions. This paper presents the results of such an attempt with special emphasis on a general correlation of heat-transfer data from transverse and yawed cylinders in rarefied air flows. The discussion of this Nusselt number correlation stresses the primary dependence of the data on the flow characteristics, which vary from free molecule flow to continuum, and from speeds near those of natural convection to supersonic. Secondary effects, such as the dependence of the heat-transfer coefficient on cylinder and air temperature, are reviewed only briefly. Since data on the recovery temperature of cylinders give an insight to the boundary criterion for free molecule flow, these results are also presented herein.

[1] This paper has been written as a compilation of two papers, "Heat Transfer From Cylinders in Subsonic Slip Flow," presented at the 1958 Annual Meeting (Paper No. 58—A-202), and "Heat Transfer From Yawed Cylinders in Rarefied Air Flows," presented at the Heat Transfer Conference, 1959 (Paper No. 59—HT-5). Both papers were contributed by the Heat Transfer Division of THE AMERICAN SOCIETY OF MECHANICAL ENGINEERS.

NOTE: Statements and opinions advanced in papers are to be understood as individual expressions of their authors and not those of the Society. Manuscript received at ASME Headquarters, April 28, 1959.

Dimensionless Groups of Correlation

A significant portion of the experimental results which are to be presented were obtained in the last two years at the Lewis Research Center. The data from these experiments are correlated by dimensionless groups such as Nusselt, Reynolds, Mach, or Knudsen number. Like previous investigators, we were confronted with the problem of evaluating the air density, viscosity, and thermal conductivity for these dimensionless groups. The temperature at which to evaluate these air properties is the one that gives the "best correlation." Certainly the forms that were chosen in the past could be justified, but we hope that the success of the proposed Nusselt-number Reynolds-number correlation presents a good case for the method used in this paper.

The convective heat-loss rate defines the heat-transfer coefficient h:

$$q_c = h\pi Dl(T_w - T_e) \tag{1}$$

The heat-transfer coefficient is defined in terms of the recovery temperature T_e. The heat-transfer data are presented in terms

Nomenclature

a_s = $49.02\sqrt{T}$, speed of sound, ft/sec

exp = exponential, e^x, dimensionless

D = cylinder diameter, ft

$f(s)$ = dimensionless function of s; $f(s) = \pi\left[\exp\left(-\frac{s^2}{2}\right)\right] \times \left\{(s^2+3)I_0\left(\frac{s^2}{2}\right) + \left(s^2+\frac{7}{2}\right)s^2\left[I_0\left(\frac{s^2}{2}\right) + I_1\left(\frac{s^2}{2}\right)\right]\right\}$

$g(s)$ = dimensionless function of s; $g(s) = 3\pi\left[\exp\left(-\frac{s^2}{2}\right)\right] \times \left\{(1+s^2)I_0\left(\frac{s^2}{2}\right) + s^2 I_1\left(\frac{s^2}{2}\right)\right\}$

(Continued on next page)

of a Nusselt number based on air thermal conductivity (Hilsenrath [1][2]) at total air temperature

$$N_{Nu} = \frac{hD}{k_t} \tag{2}$$

The Reynolds number for the cylinder is defined by the free-stream density and velocity, but with air viscosity at total air temperature:

$$N_{Re} = \frac{\rho U_\infty D}{\mu_t} \tag{3}$$

The Knudsen number is based on the mean free path at free-stream conditions and cylinder diameter:

$$N_{Kn} = \frac{\lambda}{D} \tag{4}$$

Kennard, 1938 [2], Equation (126b), gives the mean free path in terms of the viscosity of a rarefied gas composed of hard elastic spheres having a Maxwellian velocity distribution; $\mu = 0.499\bar{v}\rho\lambda$. As is usually done, this relation together with experimental viscosity is taken as the definition of the mean free path. The Knudsen number is therefore related to the ratio of the Mach number to Reynolds number, since there is a simple relation between the acoustic speed and the mean molecular speed $\bar{v}$ (e.g., Stalder, Goodwin, and Creager [3]).

$$N_{Kn} = \sqrt{\frac{\pi\gamma}{2}}\,\frac{M}{N_{Re}}\,\frac{\mu_s}{\mu_t} \tag{5}$$

The ratio of viscosity at static temperature to that at total temperature is required by the definition of the Reynolds number which is used herein. All viscosities have been taken from Hilsenrath [1].

The Mach number is based on free-stream velocity and the acoustic velocity at static air temperature:

$$M = \frac{U_\infty}{a_s} \tag{6}$$

All the data presented have been converted to this basis. Where there has been a choice of measurements of different wire temperatures, the data nearest $(T_w - T_s) = 500$ F were used for reasons which will be given later.

[2] Numbers in brackets designate References at end of paper.

Nusselt-Number Correlation for Transverse Cylinders

The results of individual investigators are grouped according to experimental range for ease in the graphical presentation of results. In this presentation we are primarily concerned with demonstrating the variation of heat-transfer characteristics over a very wide range of flows.

A summary of some subsonic continuum data is given in Fig. 1. Hilpert's data [4] are the backbone of current engineering correlations (McAdams [5]). The results of Schmidt and Wenner [6] for large cylinders confirm the results of Hilpert at the high Reynolds numbers. The data of Collis and Williams [7] and Cole and Roshko [8] extend the familiar correlation for continuum flow by two decades to $N_{Re} = 0.01$. These data were obtained with small diameter wires having length to diameter ratios greater than 2000. In Fig. 1, the results of Cole and Roshko fall slightly below the Collis and Williams data. A possible explanation is that Cole and Roshko reported Nusselt numbers which were extrapolated to $\Delta T = 0$. The Collis and Williams data which are used here were obtained at $\Delta T \approx 420$ F. In this experimental range, the heat-transfer coefficient increases slightly as cylinder temperature is increased.

The effects of natural convection were observed by Collis and Williams as the Reynolds number decreases (e.g., in Fig. 1, 0.00021-in. cylinder $N_{Re} < 0.2$ or the 0.0000354-in. cylinder $N_{Re} < 0.03$). Cole and Roshko report that decreasing the aspect ratio of the cylinder increases the Nusselt number (after allowance for conduction losses at the ends). This observation is limited to very low N_{Re} results at nearly zero Mach number because no effect of aspect ratio is discernible in the rarefied flow results to be presented in the following discussion.

As the air velocity increases, the Mach number can be expected to be a flow parameter along with N_{Re}. Scadron and Warshawsky [9] varied cylinder diameter and air density for subsonic Mach numbers from 0.10 to 0.90. Their experimental procedure differed from that used by most of the investigators mentioned here in that they measured transient thermal response rather than steady-state he atloss. Therefore the Nusselt numbers that they calculate from the time-constant of step-current response are for very low cylinder temperatures. In terms of our equation (3), their results were correlated within 7.4 per cent average deviation of a single observation by:

$$N_{Nu} = 0.431\sqrt{N_{Re}}\,(1 + 0.20\,M^2)^{-1/2} \tag{7}$$

Nomenclature

$g(s \sin \Phi)$ = dimensionless function of $s \sin \Phi$; substitute $s \sin \Phi$ for s in $g(s)$ formula
g_c = unit conversion factor, $lb_M ft/lb_F sec^2$
h = average convective heat-transfer coefficient for whole cylinder, Btu/(sec)(sq ft)(deg R)
$I_0(x), I_1(x)$ = modified Bessel function of first kind; (0) zero and (1) first order, respectively, dimensionless
J = conversion factor, ft-lb_F/Btu
k_t = air thermal conductivity at total air temperature, Btu/(sec)(ft)(deg R)
l = cylinder length, ft
$\mathfrak{L}$ = turbulent integral scale, ft
M = free-stream Mach number, dimensionless
N_{Kn} = free-stream Knudsen number, dimensionless
N_{Nu} = Nusselt number, dimensionless
N_{Re} = Reynolds number, dimensionless
p = static pressure, lb_F/sq ft
q_c = over-all convective heat-transfer rate, Btu/sec
R = gas constant for air, ft-lb_F/lb_M-deg R
$s = \sqrt{\frac{\gamma}{2}}\,M$, molecular speed ratio, dimensionless
T = static or free-stream air temperature, deg R
T_s = recovery or equilibrium cylinder temperature, deg R
$T_{s,\infty}$ = theoretical recovery temperature of an infinitely long cylinder in a free-molecule flow of air, deg R
T_t = total air temperature, deg R
T_w = cylinder temperature, deg R
$\Delta T = T_w - T_s$, temperature difference, deg R
U_∞ = free-stream air speed, ft/sec
$\bar{v} = \sqrt{\frac{8g_cRT}{\pi}}$, mean molecular speed, ft/sec
$v_m = \sqrt{2g_cRT}$, most probable molecular speed, ft/sec
α = accommodation coefficient, dimensionless
γ = ratio of specific heats, 1.40 for air, dimensionless
$\eta = T_s/T_t$, recovery temperature ratio, deg R
λ = mean free path of air at free-stream conditions, ft
μ_t = air viscosity at total air temperature, lb_M/ft-sec
π = 3.14159
Φ = angle the free-stream velocity vector subtends with the cylinder axis, radians
ρ = air density at free-stream conditions, lb_M/cu ft

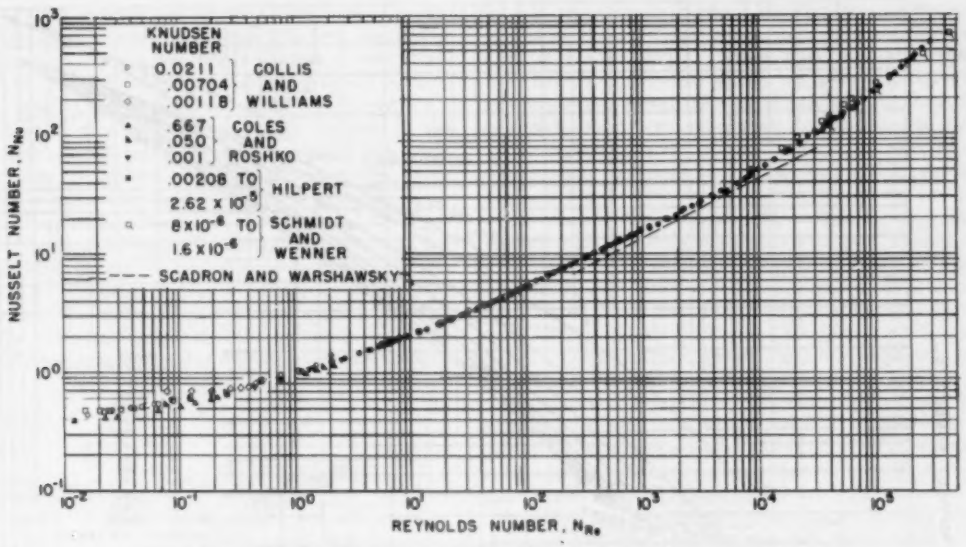

Fig. 1 Summary of subsonic continuum heat transfer from transverse cylinders

The 0.05 Mach line calculated from equation (7) is shown dashed in Fig. 1 in the range of their work $250 < N_{Re} < 30{,}000$. At least some of the difference in the dashed line and the summary curve is traceable to the secondary effect of cylinder temperature on the heat-transfer coefficient. The important point of the data of Scadron and Warshawsky is the relatively small effect of Mach number on heat transfer at constant Reynolds number that was observed [equation (7)] as $\mathbf{M}$ increased to 0.90. This Mach number effect is practically nil below $\mathbf{M} = 0.30$ and it decreases the Nusselt number by about 15 per cent at $\mathbf{M} = 0.90$. Naturally, more data are required before firm conclusions can be drawn, but until more data become available, an allowance of the order of $\sqrt{1 + 0.20\,M^2}$ might be used to account for the effect of compressibility in subsonic continuum flows.

The remainder of this section is devoted to heat-transfer data from cylinders in rarefied air flows. The data shown in Fig. 2 extend from the slip region to free molecule flow and are subsonic throughout. The Mach number is a parameter shown by solid line curves. The early results of Laurence and Landes [10], seemed anomalous when the Mach number was shown to be a parameter in the range of $0.10 \leq \mathbf{M} \leq 0.30$ at N_{Re} approaching 100. Subsequent experiments showed that this "Mach-number effect" was real and the anomalous features faded when it was noted that an equally effective correlating parameter would be the Knudsen number. Curves of constant Knudsen number are shown in Fig. 2 as dashed lines. The heat-loss characteristics shown in this figure differ markedly from the familiar N_{Re} correlation of continuum flow. The significant features of Fig. 2 are discussed as part of the summary correlation at the end of this section. For the moment, recall that the three flow parameters (N_{Re}, $\mathbf{M}$, N_{Kn}) are related by equation (5); so only two moduli can be regarded as independent. Therefore either $N_{Nu} = f(N_{Re}, \mathbf{M})$ or $N_{Nu} = f(N_{Re}, N_{Kn})$ completely specifies the correlation. Where it is convenient, both of these correlation forms are given for ready reference (as in Fig. 2).

The data of Baldwin [11, 12] and Cybulski and Baldwin [13] were obtained with tungsten wires about 0.00020 in. in diameter. The aspect ratio was about 350 in the earlier work and $l/D = 2500$ for the more recent measurements. The good agreement at $N_{Kn} < 0.01$ in Fig. 2 is evidence that the aspect ratio phenomenon discussed by Cole and Roshko, does not extend into the rarefied flow region. Although the data of Laurence and Landes and Baldwin are not in good agreement, both sets of data exhibit the same trends as the flow parameters are varied.

In Fig. 2, the data of Cybulski and Baldwin at $N_{Kn} = 4.70$ borders on the free molecule region, which will shortly be shown to exist for $N_{Kn} > 5.0$ from recovery temperature data. The following equation gives the heat-transfer coefficient h of a transverse cylinder of infinite length in a rarefied, diatomic gas flow (Stalder, Goodwin, and Creager [3])

$$h = \frac{p v_\infty \alpha g(s)}{2J\pi^{3/2}T} \tag{8}$$

Re-expressing equation (8) in terms of the Nusselt and Knudsen numbers:

$$N_{Nu} = \left(\frac{R\mu_t}{2J\pi k_t}\right) \alpha \frac{g(s)}{N_{Kn}} \frac{\mu_s}{\mu_t} \quad (\text{all } \mathbf{M}) \tag{9}$$

At a total air temperature of 85 F, the dimensionless constant in parentheses is 0.0322. $g(s)$ is a function of the Mach number (or molecular speed ratio); which is defined in the Nomenclature. At Mach numbers greater than about 2.4,

$$g(s) = 6\sqrt{\frac{\pi\gamma}{2}}\,\mathbf{M} \qquad (\mathbf{M} > 2.4) \tag{10}$$

Combining equations (10) and (5) with equation (9) and evaluating the gas properties for air streams at a total temperature of 85 F, we get

$$N_{Nu} = 0.193\,\alpha N_{Re} \qquad (\mathbf{M} > 2.4) \tag{11}$$

If the accommodation coefficient α of the metal-air system is known, equations (9) and (11) predict the heat transfer.

The data of Cybulski and Baldwin were found to be in best agreement with equation (9) when $\alpha = 0.57$. This agreement is shown in Fig. 2 for $N_{Kn} > 5.0$. The theory correctly predicts both the first power dependence at constant $\mathbf{M}$ and also the large separation of the constant $\mathbf{M}$ parametric curves.

The data of Spangenberg [14] are shown in Fig. 3. Spangenberg varied cylinder diameter from 0.00005 to 0.00152 in. and worked with three wire materials: tungsten, platinum, and a platinum 10 per cent rhodium alloy. He reported more data than have been plotted here, but the portion that is not shown confirmed

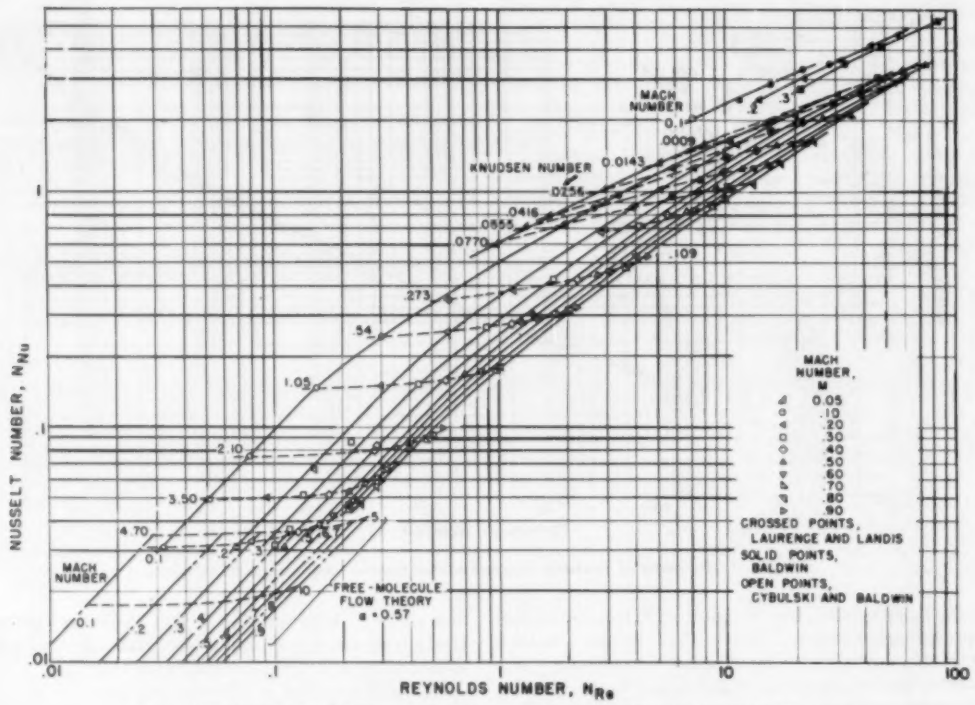

Fig. 2 Heat transfer from transverse cylinders in slip and transition to free-molecular flow

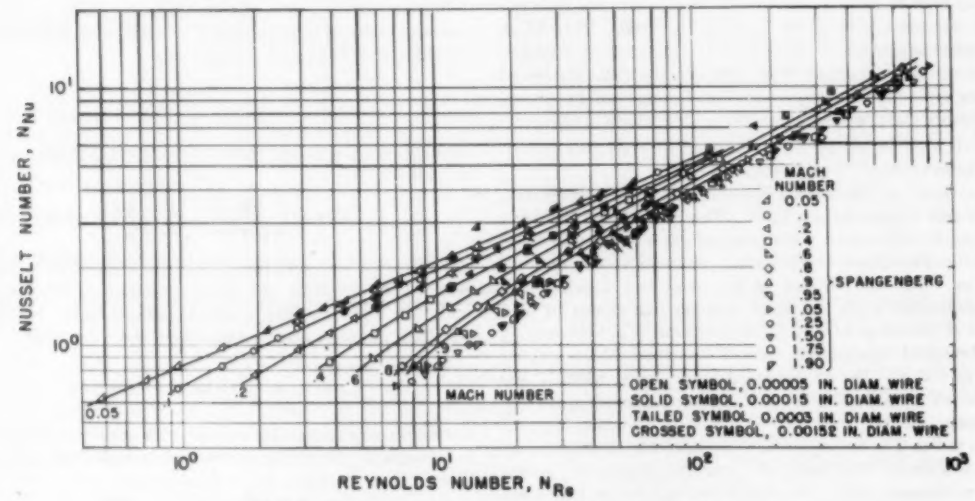

Fig. 3 Heat transfer from transverse cylinders in slip flow

and overlapped the data in Fig. 3. The subsonic data in Fig. 3 confirm all the trends noted in Fig. 2. The agreement between Figs. 2 and 3 is good for $M > 0.60$, but the low M results of Spangenberg are somewhat higher in N_{Nu} than the Baldwin data. Nevertheless, the similarity between Figs. 2 and 3 is considered a positive result, although the discrepancies at $M < 0.6$ are larger than would be expected for these experiments. The supersonic data of Fig. 3 group in a narrow band, so for $1.05 \leq M \leq 1.90$, the Nusselt number is adequately given by specifying the Reynolds number alone.

Some additional experimental data are given in Fig. 4. The results of Lowell [15] and Winovich and Stine [16] agree well in the transonic range. The supersonic data of Winovich and Stine groups in a single N_{Re} band as did that of Spangenberg in Fig. 3. However, Lowell reports that the supersonic N_{Nu} data have a systematic variation with Mach numbers greater than 1.0. Note that the supersonic N_{Nu} data of Lowell fall over the transonic results. However, the trend is relatively small and if it truly exists, there is no evidence of it in the data of either Spangenberg or Winovich and Stine.

A summary plot of all available supersonic data, including some not previously published, is given in Fig. 5. The data group in

a narrow band with a scatter of the order of ±15 per cent. The very low Reynolds number data of Stalder, Goodwin, and Creager [3], Wong [17], and Weltmann and Kuhns [18] were obtained in nitrogen rather than air, however, this is thought to have no effect on the heat transfer. While free-molecular theory predicts that the data should be represented by a single curve for $M > 2.4$ [see equation (11)], it was not foreseen that the data in the transition to free molecule and slip regions should also be a single curve. The data are limited to $N_{Re} < 1000$, however, there is no reason to suspect that the correlation will differ greatly at higher N_{Re} as long as dissociation does not occur.

The two curves given as Figs. 1 and 5 are the boundaries of the convective heat-transfer correlation for transverse cylinders which is given as Fig. 6. The continuum curve at very low Mach number (Fig. 1) is well established over a large range of Reynolds numbers. The mid-range between the incompressible, continuum flow data and the supersonic band of data is covered by the subsonic rarefied flows such as shown in Figs. 2 and 3. The data of Baldwin and Cybulski were chosen in preparing the suggested correlation curves of Fig. 6, because they cover the entire subsonic range of rarefied flows. Future work may alter these subsonic curves in the rarefied regime, but there is no doubt that the present curves correctly predict the trends and are sufficiently accurate for most engineering work. As discussed in the section on "Secondary Effects," future fundamental data on the accommodation coefficient should also help clarify the subsonic portion of Fig. 6.

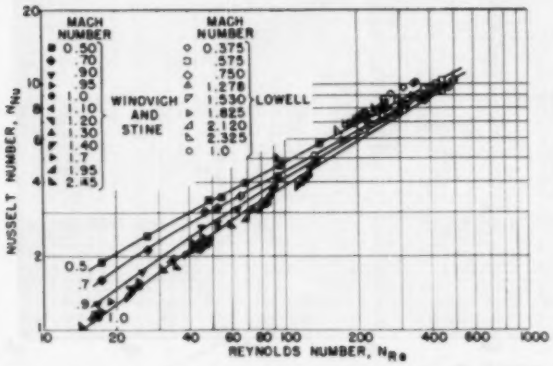

Fig. 4 Heat transfer from transverse cylinders in transonic slip flow

The subsonic flow data in the transition region from slip to free-molecular flow show the gradual change in slope of the constant Mach number curves necessary to approach the first power Reynolds-Nusselt number relation required for free-molecular flow. As the Reynolds number decreases, the heat transfer depends less on the air velocity (as compared to the continuum curve), and instead the Knudsen number becomes the governing parameter in subsonic flows.

The supersonic curve appears to fair in very closely with the subsonic continuum data at high Reynolds numbers. In the absence of supersonic data at Reynolds numbers greater than 10^3 it would appear necessary to assume that the subsonic curve is adequate to predict heat transfer in supersonic flows.

Recently, heat-transfer measurements for spheres have been correlated by Schaaf and Chambri [22], in the same manner as used for Fig. 6. The results for spheres are quite similar to Fig. 6, although the data for spheres are quite meager by comparison.

Secondary Effects on the Nusselt Number Correlation

This brief review will not adequately describe all the observed effects, because in some cases the basic parameters have not been isolated. However, the state of the art is better today than even a few years ago, and future research should clarify some of the phenomena which occur.

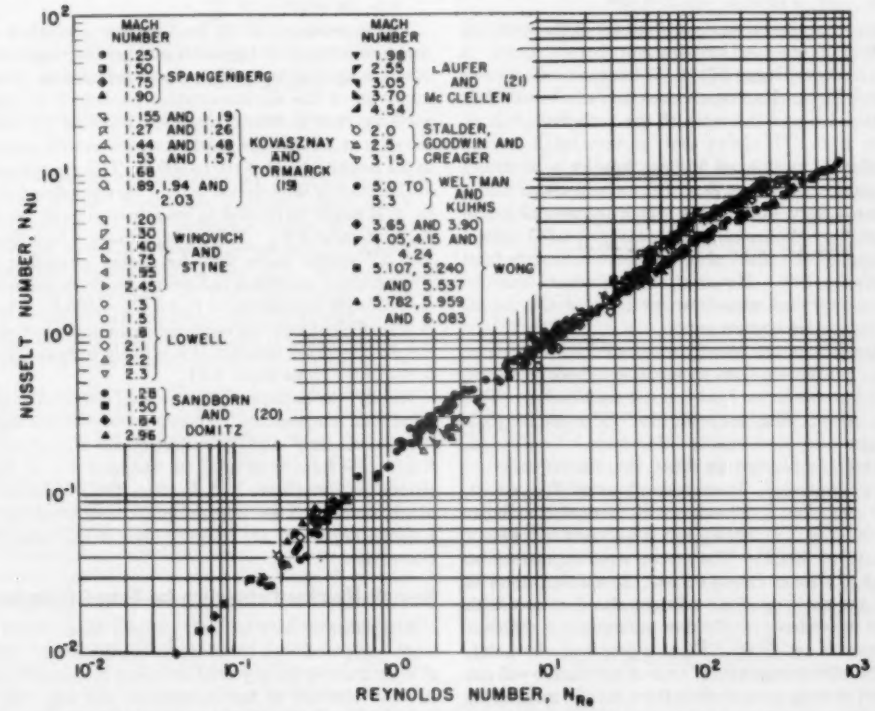

Fig. 5 Summary of supersonic heat transfer from transverse cylinders in rarefied air flow

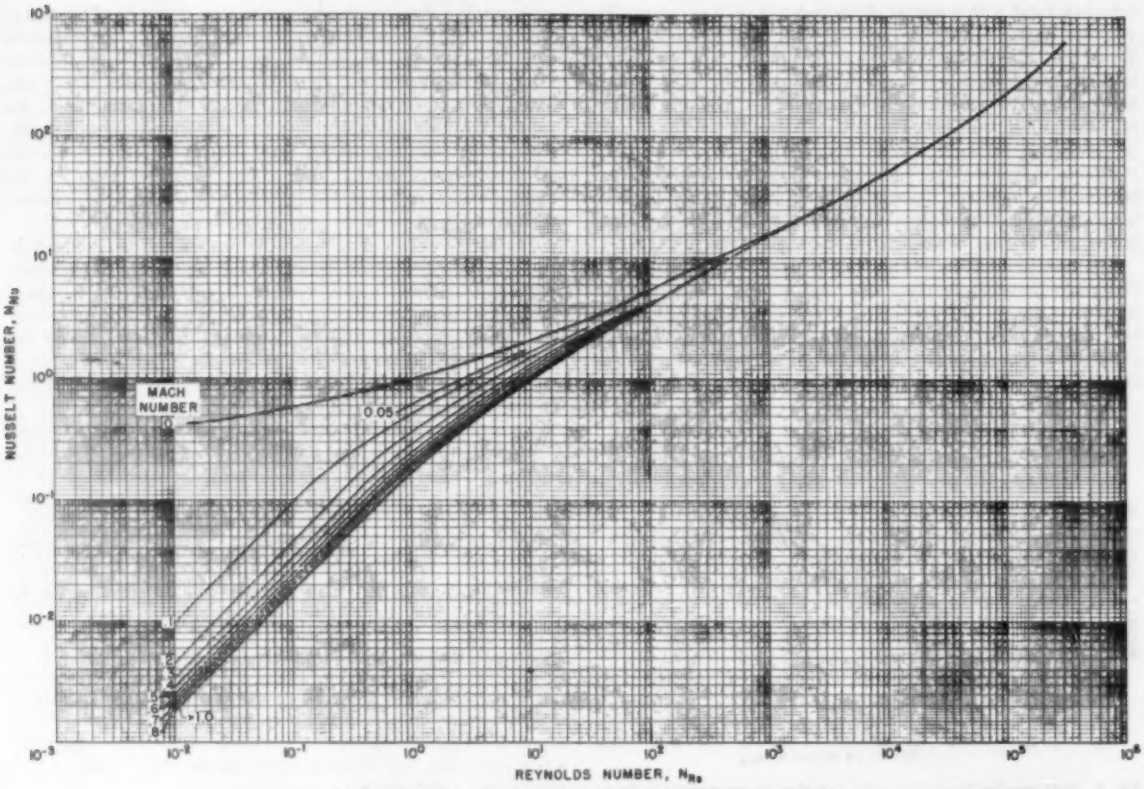

Fig. 6 Correlation of convective heat transfer from transverse cylinders

It has long been recognized that the turbulence of the approach air stream can affect the observed heat-transfer characteristics. A recent review by Van der Hegge Zijnen [23] seems to clarify this problem in subsonic flows. He characterizes the turbulent field by the turbulent intensity and the ratio of the turbulent scale to cylinder diameter $\mathcal{L}/D$. He shows that, at very small or very large $\mathcal{L}/D$, the effect of turbulence on heat transfer is relatively small for all intensities, but for $\mathcal{L}/D \approx 1.5$, an increase in turbulent intensity has a very large effect which is especially pronounced at large N_{Re}. Concerning the data presented herein, it seems safe to neglect the effect of turbulence on the data from fine wires (say $N_{Re} < 100$). However, the turbulence must be regarded as an uncontrolled parameter for most of the results referred to here in the continuum region.

Other secondary effects are usually associated with the wire temperature. For continuum flow, an increase in body temperature T_w causes an increase in the heat-transfer coefficient h. This effect led to the use of "film temperatures" for evaluating air properties in engineering correlations (McAdams, also Douglas and Churchill [24]). In rarefied air flows, the observations are more complex (e.g., Baldwin). In subsonic flows at $N_{Kn} > 0.02$, the heat-transfer coefficient h decreases with increasing cylinder temperature for $33 < \Delta T < 200$ F, but h assumed a constant value for $200 < \Delta T < 500$ F. The results were dependent on N_{Kn} (or N_{Re}) and to a lesser extent on M. In rarefied flows at supersonic speed, the heat-transfer coefficient also decreases with rising T_w, but this dependence on the flow parameters is different as shown by Winovich and Stine. From a practical viewpoint, this means that the "film temperature" type of correlation will not minimize the effect of body temperature from data in rarefied air flow, but rather will accentuate the systematic spread.

The dependence of the heat-transfer coefficient on body temperature reverses as Reynolds numbers corresponding to rarefied flow are approached. Very few fundamental data exist on the variation of the accommodation coefficient α with metal temperature, but a recent summary reported by Estermann [25] shows that α exhibits a marked variation with metal temperature in the neighborhood of 100 to 600 F. This variation is one possible explanation of the reversal noted. As more data become available on α, it might be fruitful to reanalyze some of the data from fine wires at various T_w. It is an experimental fact that data at very low ΔT scatter more than for higher operating temperatures. Furthermore, according to Estermann, there is less likelihood that α is strongly dependent on T_w for $T_w \approx 500$ F. The accommodation coefficient must be regarded as an uncontrolled parameter in the data reported herein and it is likely to have increasing importance as N_{Kn} rises above 0.01.

Finally, the data presented were all obtained at essentially ambient total temperature. There is some evidence that air temperature has a nearly negligible effect on the Nusselt-number correlation in the form used here for temperatures as high as 3000 F (Baldwin, also Glawe and Johnson [26]). However, very high Mach number (high temperature) flows where air dissociation becomes important are obviously out of the range of the data in this review.

Nusselt-Number Correlation for Yawed Cylinders

Experimental data for heat transfer from yawed cylinders are scant compared with the transverse orientation. This discussion of heat transfer from yawed cylinders is limited to subsonic free-stream velocities in the continuum and slip flow regimes. A theoretical solution for the heat transfer from a yawed cylinder

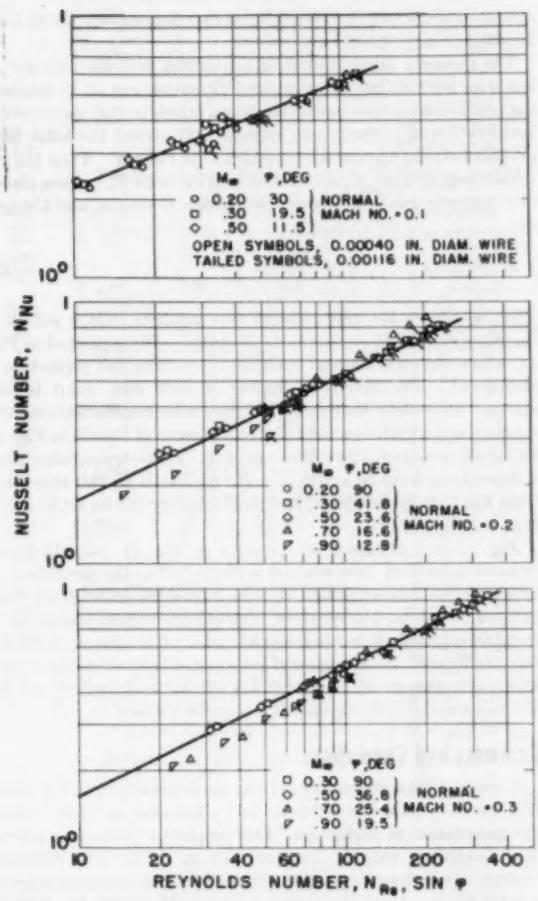

Fig. 7 Normal Mach number correlation of heat loss from yawed cylinders

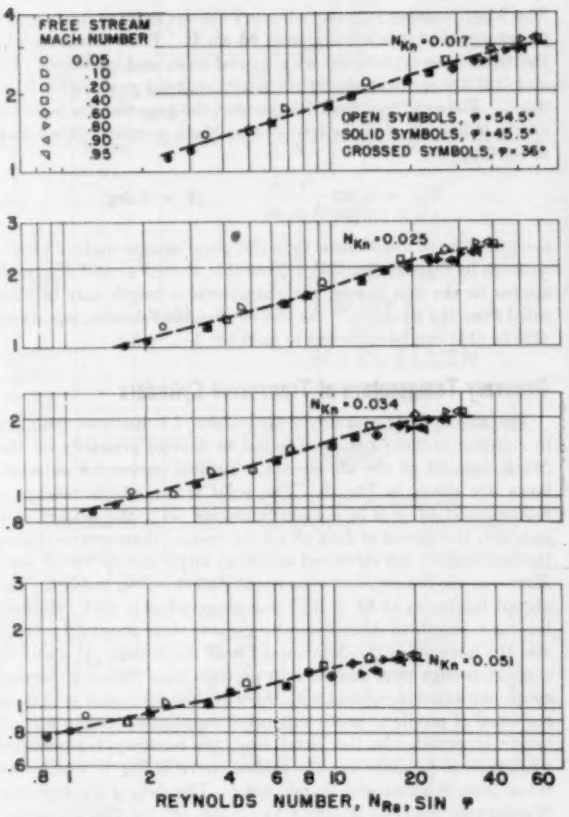

Fig. 8 Knudsen number correlation of heat loss from yawed cylinders

in a free molecule flow is now available for all Mach numbers.

For a transverse cylinder in subsonic continuum flow, N_{Nu} was found to be a function of N_{Re} with perhaps a 15 per cent variation at constant N_{Re} due to a Mach number effect at $0.5 < M < 1.0$ (Fig. 1 and also Scadron and Warshawsky [9]). Reshotko and Beckwith [27] give a solution of the compressible laminar boundary layer equations at the stagnation-line of yawed cylinders. For Mach numbers from zero to about 0.5, they found that the effect of yaw can almost be eliminated by giving N_{Nu} as a function of $\sqrt{N_{Re}} \sin \Phi$, where Φ is the angle the free-stream velocity vector subtends with the cylinder axis ($\Phi = 90$ deg for transverse case). Thus for angles from 90 to about 20 deg, use of the summary correlation (Fig. 6) with $N_{Re} \sin \Phi$ should give a good engineering estimate for $N_{Re} \sin \Phi > 400$ in subsonic flows.

The anemometer data of Schubauer and Klebanoff [28] are sometimes cited as experimental evidence for the validity of $N_{Re} \sin \Phi$ as the correlating parameter for yawed cylinders. Actually, these authors' contribution was to show that $U \sin \Phi$ correlated heat loss data obtained at various velocities and angles. That is, for their application, they did not need to vary D or ρ systematically. Data were subsequently obtained with fine wires at various N_{Re} by Spangenberg and by Sandborn and Laurence [29] but, as could be expected from the transverse cylinder discussion, an additional flow parameter is required along with $N_{Re} \sin \Phi$ due to slip effects. The importance of N_{Kn} for transverse orientation in slip flow suggests that the heat-transfer results for yawed cylinders should correlate using N_{Kn} and $N_{Re} \sin \Phi$ as parameters. By equation (5) it can be seen that $M \sin \Phi$ is the related modulus.

The data of Sandborn and Laurence have been reanalyzed by Baldwin, Sandborn, and Laurence [30] to test the use of $N_{Re} \sin \Phi$ and N_{Kn} (or $M \sin \Phi$) for correlation. The results are shown in Fig. 7. The points are keyed to values of the free stream Mach number and the angle of yaw. Some of the data at $M = 0.70$ and 0.90 fail to align with the transverse cylinder data ($\Phi = 90$ deg). However, the general agreement of the majority of the yawed results with $\Phi = 90$ deg and the grouping of the yawed wire data for $M \sin \Phi = 0.10$, shows that this form of correlation is an adequate assumption for most engineering purposes in the subsonic slip flow regime.

Fig. 8 shows the subsonic data of Spangenberg. The data of Figs. 7 and 8 show that either $M \sin \Phi$ or N_{Kn} is adequate to correlate the data for angles between 90 and 20 degrees.

Although there appear to be no experimental data for yawed cylinders in very rarefied flow, the change in orientation only slightly modifies the free molecule flow analysis. The transverse cylinder problem is detailed by Stalder, Goodwin, and Creager [31]; and Talbot [32] outlined the yawed cylinder solution. The similarity is clear when the result is written as:

$$N_{Nu} = 0.0322\, \alpha \frac{g(s \sin \Phi)}{N_{Kn}} \frac{\mu_s}{\mu_1} \qquad \text{(all } M\text{)} \qquad (12)$$

or for $M > 2.4$,

$$N_{Nu} = 0.193\, \alpha N_{Re} \sin \Phi \qquad (M > 2.4) \qquad (13)$$

The Mach number function $g(s \sin \Phi)$ is the same as in equation (9) except that it is a function of $\mathbf{M} \sin \Phi$. These forms include the transverse orientation as a special case, and equations (12) and (13) are applicable over the entire range of yaw angles, 90 to 0 deg. For axial flow past the cylinder, the heat transfer becomes nearly independent of the free-stream Mach number. A solution of the form,

$$N_{Nu} = 0.303 \frac{\alpha}{N_{Kn}} \frac{\mu_s}{\mu_t} \qquad (\Phi = 0 \text{ deg}) \qquad (14)$$

is equivalent to the solution for a flat plate at zero angle of attack as given by Oppenheim [33]. Note that since N_{Nu} and N_{Kn} each appear to the first power, the characteristic length may be canceled from the equation. As will be discussed shortly, equations (12) to (14) can be expected to hold for $N_{Kn} > 5.0$.

Recovery Temperature of Transverse Cylinders

The adiabatic or recovery temperature of transverse cylinders in continuum flows has been found to depend primarily on the Mach number of the air stream. Typical curves for subsonic flows are given in Fig. 9. The solid curve which reaches a minimum at $\mathbf{M} \approx 0.75$ is from Simmons [34]; the shaded area indicates the spread of data about the mean. Simmons used long thermocouple wires stretched across an airjet and he varied wire diameter, air density, and velocity at $20{,}000 > N_{Re} > 1000$. The abrupt minimum at $\mathbf{M} \approx 0.75$ was observed only with cylinders having a length to diameter ratio greater than about 50. Note also the increase in the data spread near this hump. If a pair of support prongs were moved into position near the long thermocouple wire (not in contact with the wire, but in front of it to form the usual H profile of probe supported couples) the hump was no longer observed. In the latter case, the recovery temperature was found to be more like the dashed curve of Fig. 9, which was taken from Scadron and Warshawsky. The data of Scadron and Warshawsky are from $30{,}000 > N_{Re} > 250$, but the thermocouples were probe supported. It seems probable that the disappearance of the distinct minimum at $\mathbf{M} \approx 0.75$ is associated with an interference of the wire supports with the flow over the cylinder at aspect ratios less than 50.

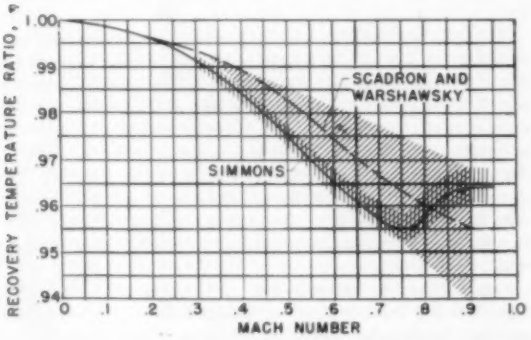

Fig. 9 Recovery temperature in continuum flow

The preceding discussion is intended to show that, although the recovery temperature data are correlated by Mach number alone, there may be applications where the cylinder aspect ratio is a significant factor. However, the data given in Fig. 10 were all obtained with fine wires having length to diameter ratios greater than 100, and these curves have no sharp minimums. In Fig. 10, the Reynolds number range is lower and extends well into the slip regime ($1000 > N_{Re} > 0.10$). From the general agreement between the data of Figs. 9 and 10, we conclude that within experimental scatter the recovery temperature data are almost entirely free of Reynolds number dependence for at least $30{,}000 > N_{Re} > 0.10$.

The recovery temperatures of continuum and slip flow are all less than the total air temperature. However, one of the interesting predictions of free-molecular-flow analysis is that the recovery temperature of a transverse cylinder will exceed the total temperature of the gas stream in which it is located. Thus the recovery temperature of an infinitely long cylinder $T_{s,\infty}$ when placed in a diatomic gas flow is given by Stalder, Goodwin, and Creager as:

$$\eta = \frac{T_{s,\infty}}{T_t} = \frac{T}{T_t} \frac{f(s)}{g(s)} \qquad (15)$$

That is, theory for very rarefied flow predicts that η will be a function only of Mach number. Equation (16) is plotted in Fig. 11, where the experimental evidence supporting this prediction is also given. The Knudsen number of each data point is also shown. It is clear that there is a transition region between the continuum and slip flow behavior of the curve of Lowell in Fig. 11 and the free molecule flow limiting curve. In this transition region, η depends on both $\mathbf{M}$ and N_{Kn}. Rough limits on this transition from slip to fully developed free molecule flow can be set at $5.0 > N_{Kn} > 0.2$.

Fig. 12 is a crossplot of the data of Fig. 11 (on which the measured recovery temperature is compared to the prediction of free-molecule-flow analysis). Unlike inferences drawn from Nusselt number data, the recovery temperature results enable us to test free-molecule-flow analysis independent of the accommodation coefficient. So, the general grouping of both the subsonic and supersonic data at $N_{Kn} > 5.0$ in Fig. 12 is excellent evidence for the existence of fully developed free-molecule flow.

Summary and Conclusions

A general Nusselt-number correlation is presented as Fig. 6 for transverse cylinders in subsonic and supersonic air flows where air dissociation is negligible. This empirical correlation covers flow conditions varying from continuum to the free molecule regime. It is based on data obtained in the following experimental range: Mach $\mathbf{M} = 0.001$ to 6.0, Reynolds N_{Re} 0.02 to 300,000, Knudsen N_{Kn} 4×10^{-4} to 37. The familiar Nusselt-number correlation in subsonic continuum flow is a function only of Reynolds number. This curve has been extended by two decades at low Reynolds numbers to $N_{Re} = 0.01$. The first deviation from the continuum correlation occurs at about $N_{Re} = 400$, and for $N_{Re} < 400$, an additional flow parameter along with N_{Re} is required to specify the Nusselt number. This additional parameter may be taken to be either the Knudsen number or the Mach number, because there is a relation between the three groups (N_{Re}, N_{Kn}, $\mathbf{M}$). As a reminder of the physical significance of the additional parameter, it is preferable to use the Knudsen

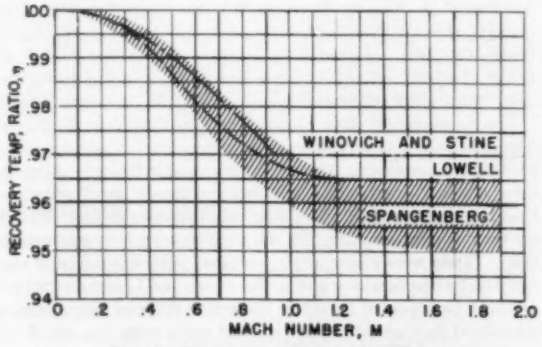

Fig. 10 Recovery temperature in slip flow

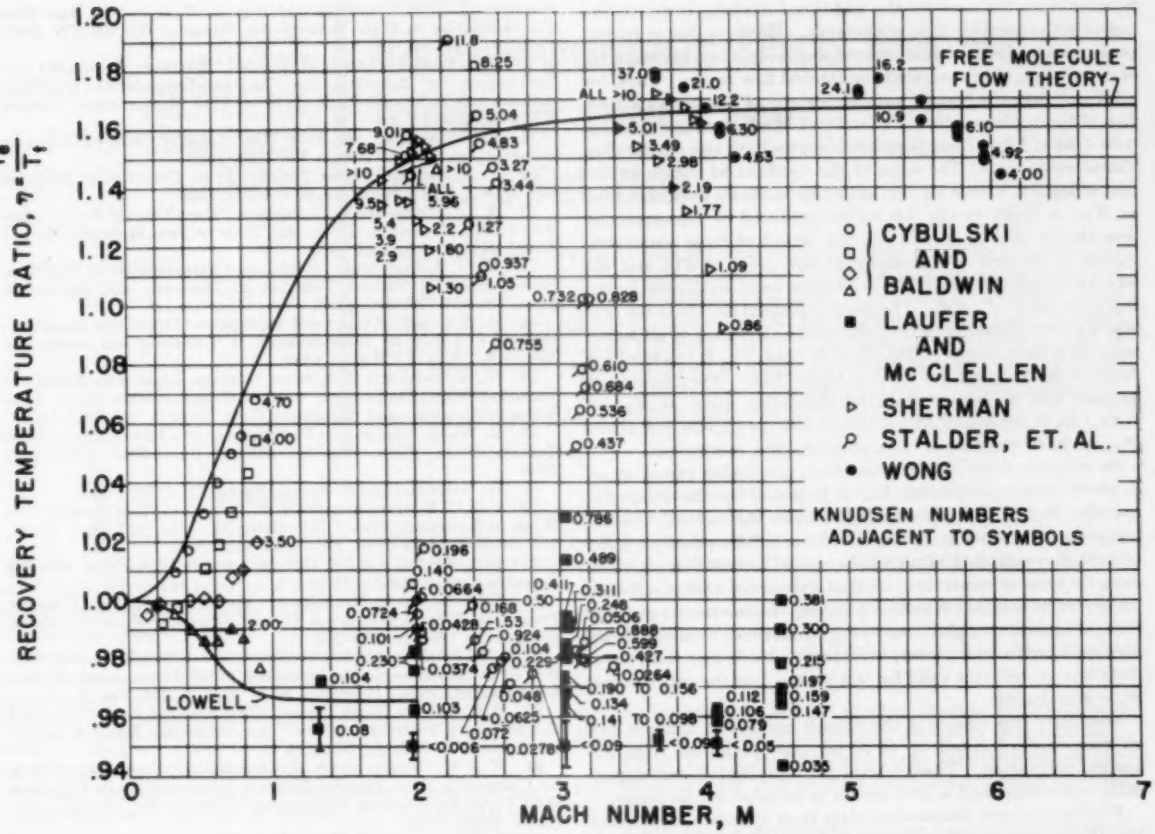

Fig. 11 Recovery temperature over a wide range of Knudsen numbers

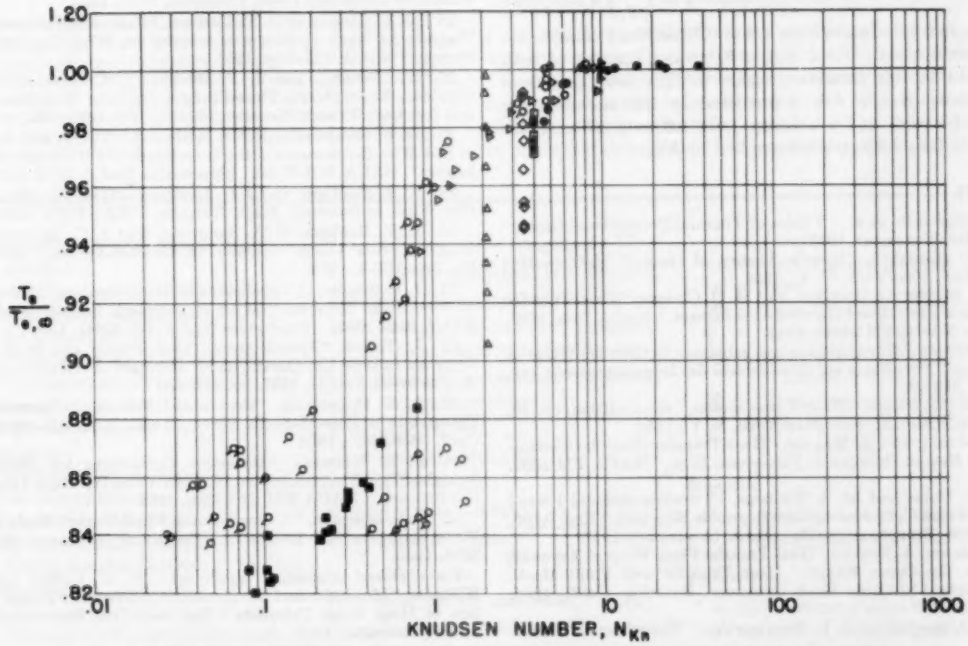

Fig. 12 Comparison of measured recovery temperature with predictions of free-molecular-flow theory

number since the need for the additional modulus is due to the beginning of rarefied flow phenomena. However, for graphical presentation it is more convenient to specify the correlation by $N_{Nu} = f(N_{Re}, M)$ throughout the rarefied flow region. Thus, for all $N_{Re} < 400$, the Nusselt number is given as a continuous function of Reynolds number by a family of Mach number curves for $0.05 < M < 1.0$. These parametric curves have two outstanding characteristics: (*a*) The slope of the constant M curves on the plot of log N_{Nu} versus log N_{Re} gradually increases from about 0.5 at $N_{Kn} = 0.001$ to the 1.0 values predicted by free-molecule-flow theory at $N_{Kn} = 5.0$; (*b*) the spread of these parametric curves is greatest in free-molecule flow ($N_{Kn} > 5.0$) and the M curves gradually converge to a common point on the continuum N_{Re} curve at $N_{Re} > 400$. The other important feature of the general N_{Nu} correlation in rarefied flows is the grouping of all supersonic-flow data into a single band, so that N_{Nu} is essentially a function of N_{Re} only for all N_{Re} below 1000. Furthermore, it appears safe to assume that the correlation given as $N_{Nu} = f(N_{Re})$ for all supersonic M will persist into continuum flow above $N_{Re} = 1000$, but lack of data prohibits firm conclusions.

In subsonic flow, heat transfer from a cylinder yawed at an angle Φ to the air velocity U_∞ is predicted by the transverse cylinder Nusselt number correlation when the normal velocity component $U_\infty \sin \Phi$ is used as the characteristic velocity. That is, both Reynolds and Mach numbers must be based on $U_\infty \sin \Phi$ even for slow subsonic flow, so that the yawed wire results are compared at constant Knudsen number. In continuum and slip flows, N_{Nu} data at angles from 90 deg (transverse) to about 20 deg are correlated in this manner, while free-molecule-flow theory predicts this procedure is valid for this regime over the entire range, 90 to zero degrees.

Secondary dependence of the Nusselt number on cylinder and air temperatures causes up to 20 per cent deviations from the general correlation. These effects are complicated, but apparently systematic, and a brief review is included in this paper.

Finally, recovery temperature data from cylinders are divided into three parts by a Knudsen number criterion: $N_{Kn} < 0.2$, the ratio of recovery to total air temperature $\eta \equiv \left(\frac{T_r}{T_t}\right)$ is independent of N_{Kn} and η decreases from 1.0 to 0.95 as Mach number increases from 0 to 4.0; $0.2 < N_{Kn} < 5.0$, η is a function of both N_{Kn} and M in this transition region to fully developed free-molecule flow; $N_{Kn} > 5.0$, η predicted by free-molecule-flow theory is observed, and η increases from 1.0 to 1.167 as M increases from 0 to 7.0 again independent of N_{Kn}.

References

1 J. Hilsenrath, et al., "Tables of Thermal Properties of Gases," cir. 564, NBS, November, 1955.

2 E. H. Kennard, "Kinetic Theory of Gases," McGraw-Hill Book Co., Inc., New York, N. Y., 1938.

3 J. R. Stalder, G. Goodwin, and M. O. Creager, "Heat Transfer to Bodies in a High-Speed Rarefied-Gas Stream," NACA Rep. 1093. (Supersedes NACA TN 2438), 1952.

4 R. Hilpert, "Wärmeabgabe von geheizten Drahten und Rohren im Luftstrom," Forschung auf dem Gebiete des Ingenieurwesens, vol. 4, 1933, pp. 215–222.

5 W. H. McAdams, "Heat Transmission," third edition, ch. 10, McGraw-Hill Book Co., Inc., New York, N. Y., 1954.

6 E. Schmidt and K. Wenner, "Heat Transfer Over the Circumference of a Heated Cylinder in Transverse Flow," NACA TM 1050, 1943.

7 D. C. Collis and M. J. Williams, "Two-Dimensional Forced Convection From Cylinders at Low Reynolds Numbers," Rep. A105, Res. and Dev. Branch, Aero. Res. Labs. (Australia), 1957.

8 J. Cole and A. Roshko, "Heat Transfer From Wires at Reynolds Numbers in the Oseen Range," Heat Transfer and Fluid Mech. Inst. Preprints, California Book Company, Berkeley, Calif., 1954, pp. 13–23.

9 M. D. Scadron and I. Warshawsky, "Experimental Determination of Time Constants and Nusselt Numbers for Bare-Wire Thermocouples in High Velocity Air Streams," NACA TN 2599, 1952.

10 J. C. Laurence and L. G. Landes, "Auxiliary Equipment and Techniques for Adapting the Constant-Temperature Hot-Wire Anemometer to Specific Problems in Air-Flow Measurement," NACA TN 2843, 1952.

11 L. V. Baldwin, "Slip-Flow Heat Transfer From Cylinders in Subsonic Airstreams," NACA TN 4369, 1958.

12 L. V. Baldwin, "Heat Transfer From Cylinders in Subsonic Slip Flow," ASME Paper No. 58—A-202, 1958.

13 R. J. Cybulski and L. V. Baldwin, "Heat Transfer From Cylinders in the Transition From Slip Flow to Free-Molecular Flow," NASA MEMO 4-27-59E, 1959.

14 W. G. Spangenberg, "Heat-Loss Characteristics of Hot-Wire Anemometers at Various Densities in Transonic and Supersonic Flow," NACA TN 3381, 1955.

15 H. H. Lowell, "Design and Application of Hot-Wire Anemometers for Steady-State Measurements at Transonic and Supersonic Airspeeds," NACA TN 2117, 1950.

16 W. Winovich and H. A. Stine, "Measurements of the Nonlinear Variation With Temperature of Heat-Transfer Rate From Hot-Wires in Transonic and Supersonic Flow," NACA TN 3965, 1957.

17 H. Wong, "Design and Development of a Free-Molecule Heat Transfer Probe," Proj. Rep. HE-100-143, Univ. Calif. (Berkeley), 1956.

18 R. Weltmann and P. Kuhns, NASA TN-D267 (1960).

19 L. S. G. Kovasznay and S. I. A. Tormarck, "Heat Loss of Hot-Wires in Supersonic Flow," Bumblebee Rep. No. 127, Dept. Aero., The Johns Hopkins Univ., Baltimore, Md., 1950.

20 V. A. Sandborn and S. Domitz, unpublished research at Lewis Research Center, NASA, 1956.

21 J. Laufer and R. McClelland, "Measurement of Heat Transfer From Fine Wires in Supersonic Flows," *Journal of Fluid Mechanics*, vol. 1, pt. 3, 1956, pp. 276–289.

22 S. A. Schaaf and P. L. Chambri, "Flow of Rarefied Gases," Sec. H of "Fundamentals of Gas Dynamics," H. W. Emmons, ed., Princeton University Press, Princeton, N. J., 1958, p. 726 (Fig. H, 17(c)).

23 B. G. Van der Hegge Zijnen, "Heat Transfer From Horizontal Cylinders to a Turbulent Airflow," *Applied Science Research*, sec. A, vol. 7, No. 2–3, 1958, pp. 205–223.

24 W. J. M. Douglas and S. W. Churchill, "Recorrelation of Data for Convective Heat Transfer Between Gases and Single Cylinders With Large Temperature Differences," Preprint No. 16, Am. Inst. Chem. Engr., 1955.

25 I. Estermann, "Gases at Low Densities," sec. I, ch. 4 of "Thermodynamics and Physics of Matter," F. D. Rossini, ed., Princeton University Press, Princeton, N. J., 1955.

26 G. E. Glawe and R. C. Johnson, "Experimental Study of Heat Transfer to Small Cylinders in a Subsonic, High-Temperature Gas Stream," NACA TN 3934, 1957.

27 E. Reshotko and I. E. Beckwith, "Compressible Laminar Boundary Layer Over a Yawed Infinite Cylinder With Heat Transfer and Arbitrary Prandtl Number," NACA TN 3986, 1957.

28 G. B. Schubauer and P. S. Klebanoff, "Theory and Application of Hot-Wire Instruments in the Investigation of Turbulent Boundary Layers," NACA WR W-86. (Supersedes NACA ACR 5K27), 1946.

29 V. A. Sandborn and J. C. Laurence, "Heat Loss From Yawed Hot Wires at Subsonic Mach Numbers," NACA TN 3563, 1955.

30 L. V. Baldwin, V. A. Sandborn, and J. C. Laurence, "Heat Transfer From Yawed Cylinders in Rarefied-Airflow," ASME paper No. 59—HT-5, 1959.

31 J. R. Stalder, G. Goodwin, and M. O. Creager, "A Comparison of Theory and Experimental for High-Speed, Free-Molecule Flow," NACA Rep. 1032. (Supersedes NACA TN 2244), 1951.

32 L. Talbot, "Free-Molecule Flow Forces and Heat Transfer From an Infinite Circular Cylinder at Angle of Attack," *Journal of Aero Sciences*, vol. 24, 1957, pp. 458–459.

33 A. K. Oppenheim, "Generalized Theory of Convective Heat Transfer in a Free-Molecule Flow," Tech. Rep. HE-150-93, Univ. Calif. (Berkeley), 1952.

34 F. S. Simmons, "Recovery Corrections for Butt-Welded, Straight-Wire Thermocouples in High-Velocity, High-Temperature Gas Streams," NACA RM E54G22a, 1954.

35 F. S. Sherman, "A Low Density Wind-Tunnel Study of Shock-Wave Structure and Relaxation Phenomena in Gases," NACA TN 3298, 1955.

For a recent interesting report see: D. C. Collins and M. J. Williams, "Molecular and Compressibility Effects on Forced Convection of Heat From Cylinders," Res. and Dev. Branch, Aero Res. Labs. (Australia), 1958.

R. D. CESS
Heat Transfer Section,
Mechanics Department,
Westinghouse Electric Corporation
Research Laboratories,
Pittsburgh, Pa.
Assoc. Mem. ASME

Magnetohydrodynamic Effects Upon Heat Transfer for Laminar Flow Across a Flat Plate

Forced-convection heat transfer for laminar flow of electrically conducting fluids across a flat plate is considered for a magnetic field of constant inductance acting normal to the free stream velocity and fixed relative to the plate. The boundary condition on the surface of the plate is taken to be either a constant temperature or constant heat flux, and solutions are presented for the following cases: (a) Fluids having a Prandtl number of unity for which both Joule heating and frictional heating are accounted for; (b) fluids having moderate and large Prandtl numbers for negligible Joule and frictional heating; and (c) fluids having low Prandtl numbers for negligible frictional heating.

Introduction

CONSIDERABLE INTEREST has recently developed in regard to forced-convection heat transfer involving electrically conducting fluids in the presence of magnetic fields. The primary motivation of this interest has been the prospect of reducing aerodynamic heat transfer [1, 2, 3, 4, 5].[1] Rossow [1] has considered a fluid with a Prandtl number of unity flowing across a flat plate for which a magnetic field of constant inductance acts normal to the free stream velocity. The magnetic field was considered fixed relative to the plate or relative to the fluid, and solutions were obtained for the plate temperature equal to the free stream temperature and for an adiabatic plate.

Although the fluids of most common concern have been conducting gases, it is not hard to envision practical heat-transfer problems involving other types of electrically conducting fluids, such as salt water or liquid metals.

The purpose of the present investigation is to extend certain of Rossow's results for laminar flow across a flat plate to include more general boundary conditions on the plate surface as well as more general types of fluids. The magnetic field is considered to be fixed relative to the plate and to act normal to the free stream velocity with constant magnetic inductance. It is further considered that the plate surface has either a constant temperature or constant heat flux, and solutions are presented for the following cases:

1 Fluids having a Prandtl number of unity for which both Joule heating and frictional heating are taken into account.

2 Fluids having moderate and large Prandtl numbers (approximately greater than one) for negligible Joule and frictional heating.

3 Fluids having low Prandtl numbers for negligible frictional heating.

The first case would be approximately representative of many gases, and is essentially the same problem considered by Rossow with the exception that the boundary conditions are more general. The second case would correspond to ordinary types of conducting liquids, such as salt water, for which both Joule heating and frictional heating are generally negligible. The third case applies to liquid metals such that frictional heating is negligible whereas

[1] Numbers in brackets designate References at end of paper.

Contributed by the Heat Transfer Division of THE AMERICAN SOCIETY OF MECHANICAL ENGINEERS and presented at the ASME-AIChE Heat Transfer Conference, Storrs, Conn., August 9–12, 1959.
NOTE: Statements and opinions advanced in papers are to be understood as individual expressions of their authors and not those of the Society. Manuscript received at ASME Headquarters, May 4, 1959. Paper No. 59—HT-14.

Nomenclature

$\vec{B}_0$ = magnetic induction vector (magnitude B_0)
c_p = specific heat at constant pressure
f_0, f_1 = dimensionless stream functions
h_s = total enthalpy, $c_p t + u^2/2$
H = dimensionless enthalpy function, see Equations (14) and (25)
k = thermal conductivity
m = magnetic parameter, $\sigma B_0^2/\rho u_\infty$
P = pressure
Pe = Peclet number, $u_\infty x/\alpha$
Pr = Prandtl number, ν/α
q = local surface heat flux
Re = Reynolds number, $u_\infty x/\nu$
s = Laplace transform variable
t = temperature
T = dimensionless temperature difference, see Equations (33) and (42)
$\vec{U}$ = velocity vector (magnitude U)
u = velocity component in x-direction
v = velocity component in y-direction
x = distance co-ordinate measured along plate from leading edge
y = distance co-ordinate measured normal to plate
z = $(\beta_0 \mathrm{Pr}/12)\eta^3$
α = thermal diffusivity
β_0 = $f_0''(0) = 0.332$
β_1 = $f_1''(0) = -0.894$
Γ = gamma function
η = $y\sqrt{u_\infty/\nu x}$
Θ = temperature difference, $t - t_\infty$
$\overline{\Theta}$ = Laplace transform of Θ
ν = kinematic viscosity
ρ = density
σ = electrical conductivity
τ = time
Φ = hydrodynamic potential function
Φ_d = dissipation function
ϕ = unit hydrodynamic potential function, Φ/u_∞
Ψ = hydrodynamic stream function
ψ = unit hydrodynamic stream function, Ψ/u_∞

Subscripts

w = conditions at the plate surface
∞ = free stream conditions

Superscripts

$'$ = differentiation with respect to η
$*$ = conditions for no magnetic field present

Joule heating may be significant. For cases 1 and 2 only first-order heat-transfer results will be considered.

Basic Equations

The present analysis is based upon the following assumptions:

1 The flow is incompressible, steady, and two-dimensional.

2 The properties of the fluid, including electrical conductivity, are constant.

3 Both the induced magnetic field and the charge density are negligible.

In accord with these assumptions the equations expressing the conservation of mass, momentum, and energy for laminar flow may be written, respectively, as [1]

$$\text{div } \vec{U} = 0 \tag{1}$$

$$\frac{D\vec{U}}{D\tau} = \nu\nabla^2\vec{U} - \frac{1}{\rho}\,\text{grad } P + \frac{\sigma}{\rho}(\vec{U} \times B_0) \times B_0 \tag{2}$$

$$\frac{Dt}{D\tau} = \alpha\nabla^2 t + \frac{1}{\rho c_p}\frac{DP}{D\tau} + \frac{\nu}{c_p}\Phi_d + \frac{\sigma}{\rho c_p}(\vec{U} \times B_0)^2 \tag{3}$$

where Φ_d is the dissipation function [6]. The last terms on the right side of Equations (2) and (3) represent, respectively, the induced magnetic force and Joule heat generation within the fluid due to the resulting electric current.

From Rossow [1] the boundary layer form of Equation (2) for flow across a flat plate becomes

$$u\frac{\partial u}{\partial x} + v\frac{\partial u}{\partial y} = \nu\frac{\partial^2 u}{\partial y^2} - \frac{\sigma B_0^2}{\rho}u \tag{4}$$

and from this equation Rossow has shown that the zero-order and first-order terms for the velocity components u and v are[2]

$$u = u_\infty[f_0' + mxf_1' + \ldots] \tag{5}$$

$$v = \frac{\eta}{2}\sqrt{\frac{u_\infty\nu}{x}}\,[f_0' + mxf_1' + \ldots] - \frac{1}{2}\sqrt{\frac{u_\infty\nu}{x}}\,[f_0 + 3mxf_1 + \ldots] \tag{6}$$

where the primes denote differentiation with respect to η. The function $f_0(\eta)$ is the dimensionless Blasius stream function [6], and $f_1(\eta)$ is given by

$$f_1''' + \frac{1}{2}f_0f_1'' - f_0'f_1' + \frac{3}{2}f_0''f_1 = f_0' \tag{7}$$

with the boundary conditions

$$f_1 = f_1' = 0;\ \eta = 0$$

$$f_1' = -1;\ \eta = \infty$$

Tabulated values of $f_1(\eta)$ and its first two derivatives are given in reference [1],[3] and the derivatives f_0' and f_1' are shown in Fig. 1.

It is of further interest to determine the velocity components for the potential flow occurring outside the region of viscous effects (momentum boundary layer). For this case Equation (4) becomes

$$\frac{\partial u}{\partial x} = -\frac{\sigma B_0^2}{\rho}$$

and

$$u = u_\infty - \frac{\sigma B_0^2}{\rho}x \tag{8}$$

[2] Rossow has also considered second-order terms.

[3] In reference [1] the first-order stream function is denoted by $f_2(\eta)$.

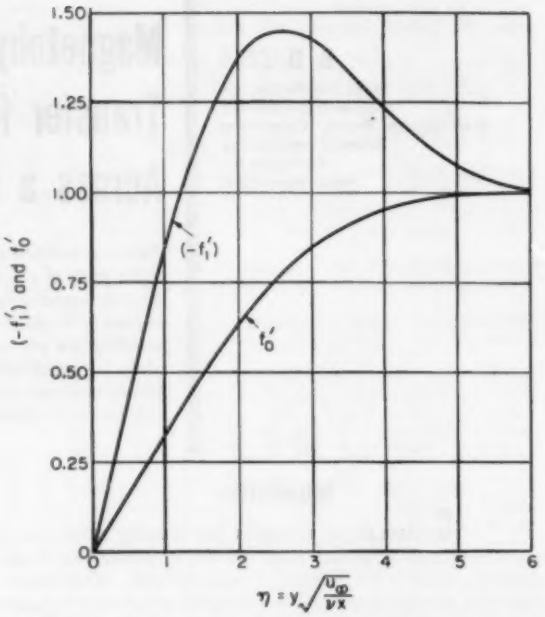

Fig. 1 Zero-order and first-order stream function derivatives from references [1] and [6]

Correspondingly, from continuity

$$\frac{\partial v}{\partial y} = -\frac{\partial u}{\partial x} = \frac{\sigma B_0^2}{\rho}$$

such that

$$v = \frac{\sigma B_0^2}{\rho}y \tag{9}$$

The stream and potential functions Ψ and Φ thus become

$$\Psi = \int_{0,0}^{x,y}(-vdx + udy) = u_\infty y - \frac{\sigma B_0^2}{\rho}xy$$

$$\Phi = \int_{0,0}^{x,y}(udx + vdy) = u_\infty x - \frac{\sigma B_0^2}{2\rho}(x^2 - y^2)$$

Further, defining unit stream and potential functions as $\psi = \Psi/u_\infty$ and $\phi = \Phi/u_\infty$, then

$$\psi = y - mxy \tag{10}$$

$$\phi = x - \frac{1}{2}m(x^2 - y^2) \tag{11}$$

These potential flow results will be employed when considering fluids with low Prandtl number.

Prandtl Number of Unity

Taking into account both Joule heating and frictional heating the boundary-layer form of Equation (3) reduces to

$$u\frac{\partial t}{\partial x} + v\frac{\partial t}{\partial y} = \alpha\frac{\partial^2 t}{\partial y^2} + \frac{\nu}{c_p}\left(\frac{\partial u}{\partial y}\right)^2 + \frac{\sigma B_0^2}{\rho c_p}u^2 \tag{12}$$

However, it is more convenient in this case to employ the total energy equation rather than Equation (12). Upon multiplying Equation (4) by u and adding the result to Equation (12), the total energy equation for $\text{Pr} = 1$ becomes [1]

$$u\frac{\partial h_s}{\partial x} + v\frac{\partial h_s}{\partial y} = \nu\frac{\partial^2 h_s}{\partial y^2} \tag{13}$$

where h_s is the total enthalpy given by

$$h_s = c_p t + u^2/2$$

Constant Surface Temperature. For the case of a constant surface temperature on the plate, a dimensionless enthalpy function will be defined as

$$H = \frac{h_s - h_{s\infty}}{h_{sw} - h_{s\infty}} = \frac{c_p\Theta + \frac{1}{2}(u^2 - u_\infty^2)}{c_p\Theta_w - \frac{1}{2}u_\infty^2} \tag{14}$$

and Equation (13) becomes

$$u\frac{\partial H}{\partial x} + v\frac{\partial H}{\partial y} = \nu\frac{\partial^2 H}{\partial y^2} \tag{15}$$

The zero-order and first-order terms of the enthalpy function may be expressed as

$$H = H_0(\eta) + mxH_1(\eta) + \ldots \tag{16}$$

Upon substituting Equations (5), (6), and (16) into Equation (15), and collecting like powers of mx, the equations for H_0 and H_1 become

$$H_0'' + \frac{1}{2}f_0 H_0' = 0 \tag{17}$$

$$H_1'' + \frac{1}{2}f_0 H_1' - f_0' H_1 = -\frac{3}{2}f_1 H_0' \tag{18}$$

with the boundary conditions

$$H_0 = 1, \quad H_1 = 0; \quad \eta = 0$$

$$H_0 = 0, \quad H_1 = 0; \quad \eta = \infty$$

The solution of Equation (17) has been shown by Pohlhausen [6] to be

$$H_0 = 1 - f_0' \tag{19}$$

and correspondingly Equation (18) becomes

$$H_1'' + \frac{1}{2}f_0 H_1' - f_0' H_1 = \frac{3}{2}f_1 f_0'' \tag{20}$$

If a transformation is considered of the form

$$H_1 = -g - 2f_0' f_1' \tag{21}$$

it may readily be shown that the function $g(\eta)$ is analogous to the temperature function considered by Rossow [1] for the case of equal plate and free stream temperatures, and it follows that $g'(0) = -0.352$.

From Equations (19) and (21)

$$H_0'(0) = -0.332$$

$$H_1'(0) = 0.352$$

such that

$$\left(\frac{\partial t}{\partial y}\right)_{y=0} = -\left(\Theta_w - \frac{u_\infty^2}{2c_p}\right)\sqrt{\frac{u_\infty}{\nu x}}\,[0.332 - 0.352(mx) + \ldots]$$

Further

$$q = -k\left(\frac{\partial t}{\partial y}\right)_{y=0}$$

and the expression for the heat flux from the surface of the plate becomes

$$q = 0.332k\left(\Theta_w - \frac{u_\infty^2}{2c_p}\right)\sqrt{\frac{u_\infty}{\nu x}}\,[1 - 1.06(mx) + \ldots] \tag{22}$$

This may be written in terms of a heat-flux ratio as

$$\frac{q}{q^*} = 1 - 1.06(mx) + \ldots \tag{23}$$

where q^* is the heat flux with no magnetic field present given by

$$q^* = 0.332\left(\frac{k}{x}\right)\left(\Theta_w - \frac{u_\infty^2}{2c_p}\right)(\mathrm{Re})^{1/2} \tag{24}$$

which is the well-known result obtained by Pohlhausen [6].

One may note that the ratio q/q^* is independent of the temperature difference Θ_w, and thus Rossow's results for $\Theta_w = 0$ are identical with Equation (23). This invariance with Θ_w is not obtained for Prandtl numbers other than unity, except for cases in which Joule and frictional heating are negligible.

Constant Surface Flux. For the case of a constant surface heat flux the dimensionless enthalpy function will be defined as

$$H = \frac{(h_{s\infty} - h_s)}{c_p q/k}\sqrt{\frac{u_\infty}{\nu x}} \tag{25}$$

Again letting

$$H = H_0(\eta) + mxH_1(\eta) + \ldots$$

then from Equations (5), (6), and (13)

$$H_0'' + \frac{1}{2}f_0 H_0' - f_0' H_0 = 0 \tag{26}$$

$$H_1'' + \frac{1}{2}f_0 H_1' - \frac{3}{2}f_0' H_1 = \frac{1}{2}f_1' H_0 - \frac{3}{2}f_1 H_0' \tag{27}$$

with the boundary conditions

$$H_0' = 1, \quad H_1' = 0; \quad \eta = 0$$

$$H_0 = 0, \quad H_1 = 0; \quad \eta = \infty$$

Numerical solution of Equations (26) and (27) has been carried out on a Datatron computer, giving the results

$$H_0(0) = -2.18$$

$$H_1(0) = -1.59$$

Thus

$$H(\eta = 0) = -2.18 - 1.59(mx) + \ldots$$

such that the expression for the surface temperature difference becomes

$$\Theta_w = \frac{u_\infty^2}{2c_p} + 2.18\frac{q}{k}\sqrt{\frac{\nu x}{u_\infty}}\,[1 + 0.729(mx) + \ldots] \tag{28}$$

This may be written in terms of a temperature difference ratio as

$$\frac{\Theta_w - u_\infty^2/2c_p}{\Theta_w^* - u_\infty^2/2c_p} = 1 + 0.729(mx) + \ldots \tag{29}$$

where Θ_w^* is the surface temperature difference with no magnetic field present given by

$$\Theta_w^* - \frac{u_\infty^*}{2c_p} = 2.18\left(\frac{qx}{k}\right)(\mathrm{Re})^{-1/2} \tag{30}$$

It may be noted from Equation (28) that the adiabatic wall temperature is independent of the magnetic field, which is the same result found by Rossow [1].

Moderate and High Prandtl Numbers

Neglecting both Joule heating and frictional heating, the boundary layer form of Equation (3) becomes

$$u\frac{\partial t}{\partial x} + v\frac{\partial t}{\partial y} = \alpha\frac{\partial^2 t}{\partial y^2} \tag{31}$$

It will now be convenient to employ an approximation in regard to the velocity components given by Equations (5) and (6). For nonmagnetic flows ($mx = 0$) Fage and Falkner [7], as well as others, have considered the stream function derivative f_0' to be a linear function of η. This approximation is reasonable for fluids with large Prandtl numbers, since for a large Prandtl number the thickness of the thermal boundary layer is much less than that of the momentum boundary layer, and thermal gradients are consequently restricted to the region for which f_0' is approximately linear with η. For low Prandtl numbers this would not be the case. However, from the heat-transfer results of Fage and Falkner for nonmagnetic flow across an isothermal flat plate, it is found that for a Prandtl number as low as 0.77 the linear approximation is in error by only 2.3 per cent.

In the present analysis it will be assumed that both f_0' and f_1' are linear functions of η, such that

$$f_0 = \frac{1}{2}\beta_0\eta^2$$
$$f_1 = \frac{1}{2}\beta_1\eta^2 \tag{32}$$

where $\beta_0 = f_0''(0) = 0.332$ and $\beta_1 = f_1''(0) = -0.894$ from references [6] and [1], respectively. As may be seen from Fig. 1 the linear approximation is more restrictive in regard to f_1' than f_0'. However, it will be shown later that first-order heat-transfer results obtained by this means are approximately valid for Prandtl numbers as low as one.[4]

Constant Surface Temperature. For a constant temperature on the surface of the plate, a dimensionless temperature difference will be defined as

$$T = \frac{t - t_\infty}{t_w - t_\infty} = \frac{\Theta}{\Theta_w} \tag{33}$$

and Equation (31) becomes

$$u\frac{\partial T}{\partial x} + v\frac{\partial T}{\partial y} = \alpha\frac{\partial^2 T}{\partial y^2} \tag{34}$$

Upon letting

$$T = T_0(\eta) + mxT_1(\eta) + \dots$$

the equations for the zero-order and first-order temperature functions, T_0 and T_1, are found from Equations (5), (6), and (34) to be

$$T_0'' + \frac{1}{2}\mathrm{Pr}f_0T_0' = 0 \tag{35}$$

$$T_1'' + \frac{1}{2}\mathrm{Pr}f_0T_1' - \mathrm{Pr}f_0'T_1 = -\frac{3}{2}\mathrm{Pr}f_1T_0' \tag{36}$$

with the boundary conditions

$$T_0 = 1, \quad T_1 = 0; \quad \eta = 0$$
$$T_0 = 0, \quad T_1 = 0; \quad \eta = \infty$$

From Equations (32), Equation (35) may be rewritten as

$$T_0'' + \frac{1}{4}\beta_0\mathrm{Pr}\eta^2T_0' = 0$$

for which the solution is

$$T_0 = 1 - \gamma_1\left(\frac{\beta_0\mathrm{Pr}}{2}\right)^{1/3}\int_0^\eta \exp\left(-\frac{\beta_0\mathrm{Pr}}{12}\xi^3\right)d\xi \tag{37}$$

where

$$\gamma_1 = \frac{1}{6^{1/3}\Gamma(4/3)}$$

Correspondingly, Equation (36) becomes

$$T_1'' + \frac{1}{4}\beta_0\mathrm{Pr}\eta^2T_1' - \beta_0\mathrm{Pr}\eta T_1 = \frac{3}{4}\gamma_1\beta_1\mathrm{Pr}\left(\frac{\beta_0\mathrm{Pr}}{2}\right)^{1/3}\eta^2\exp\left(-\frac{\beta_0\mathrm{Pr}}{2}\eta^3\right)$$

and it may readily be verified that the solution of this equation is

$$T_1 = -\frac{3}{7}\gamma_1\left(\frac{\beta_1}{\beta_0}\right)\left(\frac{\beta_0\mathrm{Pr}}{2}\right)^{1/3}\eta\exp\left(-\frac{\beta_0\mathrm{Pr}}{2}\eta^3\right) \tag{38}$$

From Equations (37) and (38)

$$T_0'(0) = -\gamma_1\left(\frac{\beta_0\mathrm{Pr}}{2}\right)^{1/3}$$
$$T_1'(0) = -\frac{3}{7}\gamma_1\left(\frac{\beta_1}{\beta_0}\right)\left(\frac{\beta_0\mathrm{Pr}}{2}\right)^{1/3}$$

such that

$$\left(\frac{\partial T}{\partial y}\right)_{y=0} = -\gamma_1\Theta_w\left(\frac{\beta_0\mathrm{Pr}}{2}\right)^{1/3}\sqrt{\frac{u_\infty}{\nu x}}\left[1 + \frac{3}{7}\left(\frac{\beta_1}{\beta_0}\right)(mx) + \dots\right]$$

and the heat flux from the surface of the plate is given by

$$q = \gamma_1 k\Theta_w\left(\frac{\beta_0\mathrm{Pr}}{2}\right)^{1/3}\sqrt{\frac{u_\infty}{\nu x}}\left[1 + \frac{3}{7}\left(\frac{\beta_1}{\beta_0}\right)(mx) + \dots\right] \tag{39}$$

This may be written in terms of a heat-flux ratio as

$$\frac{q}{q^*} = 1 - 1.15(mx) + \dots \tag{40}$$

where

$$q^* = 0.338\left(\frac{\Theta_w k}{x}\right)(\mathrm{Pr})^{1/3}(\mathrm{Re})^{1/2} \tag{41}$$

One may note that the ratio q/q^* is independent of Prandtl number for the present case of moderate and large Prandtl numbers.

Constant Surface Flux. For the case of a constant surface heat flux the dimensionless temperature difference will be defined as

$$T = \frac{(t_\infty - t)}{q/k}\sqrt{\frac{u_\infty}{\nu x}} \tag{42}$$

Again letting

[4] From reference [1] the linear approximation would not appear applicable to terms higher than the first-order.

$$T = T_0(\eta) + mxT_1(\eta) + \dots$$

then from Equations (5), (6), and (31)

$$T_0'' + \frac{1}{2}\,\mathrm{Pr} f_0 T_0' - \frac{1}{2}\,\mathrm{Pr} f_0' T_0 = 0 \tag{43}$$

$$T_1'' + \frac{1}{2}\,\mathrm{Pr} f_0 T_1' - \frac{3}{2}\,\mathrm{Pr} f_0' T_1 = \frac{1}{2}\,\mathrm{Pr} f_1' T_0 - \frac{3}{2}\,\mathrm{Pr} f_1 T_0' \tag{44}$$

with the boundary conditions

$$T_0' = 1, \quad T_1' = 0; \quad \eta = 0$$

$$T_0 = 0, \quad T_1 = 0; \quad \eta = \infty$$

From Equations (32), Equation (43) becomes

$$T_0'' + \frac{1}{4}\,\beta_0 \mathrm{Pr}\eta^3 T_0' - \frac{1}{2}\,\beta_0 \mathrm{Pr}\eta T_0 = 0$$

Letting $z = (\beta_0 \mathrm{Pr}/12)\eta^3$, this equation reduces to Kummer's differential equation [8, 9], such that the solution may be written in terms of the Kummer function $F(a, c, z)$ as

$$T_0 = -\gamma_2 \left(\frac{2}{\beta_0 \mathrm{Pr}}\right)^{1/3} \left[F\left(\frac{4}{3}, \frac{2}{3}, z\right) - \frac{1}{\gamma_2}\,(6z)^{1/3} F\left(\frac{5}{3}, \frac{4}{3}, z\right)\right] e^{-z} \tag{45}$$

where $$\gamma_2 = \frac{2}{3}\left[\frac{\Gamma(4/3)}{\Gamma(5/3)}\right]^3 6^{1/3}$$

Correspondingly, Equation (44) becomes

$$T_1'' + \frac{1}{4}\,\beta_0 \mathrm{Pr}\eta^3 T_1' - \frac{3}{2}\,\beta_0 \mathrm{Pr}\eta T_1 = \frac{1}{2}\,\beta_1 \mathrm{Pr}\eta T_0 - \frac{3}{4}\,\beta_1 \mathrm{Pr}\eta^3 T_0'$$

and the solution of this equation may also be written in terms of Kummer functions as

$$T_1 = \frac{4}{7}\,\gamma_3 \left(\frac{\beta_1}{\beta_0}\right)\left(\frac{2}{\beta_0 \mathrm{Pr}}\right)^{1/3} \left[F\left(\frac{8}{3}, \frac{2}{3}, z\right) - \frac{1}{\gamma_3}\,(6z)^{1/3} F\left(3, \frac{4}{3}, z\right)\right] e^{-z} + \frac{1}{7}\left(\frac{\beta_1}{\beta_0}\right)\left[T_0 + 3\eta \frac{dT_0}{d\eta}\right] \tag{46}$$

where $$\gamma_3 = \frac{5}{9}\,6^{1/3}\Gamma(4/3)$$

From Equations (45) and (46)

$$T_0(0) = -\gamma_2 \left(\frac{2}{\beta_0 \mathrm{Pr}}\right)^{1/3}$$

$$T_1(0) = \frac{\gamma_2}{7}\left(\frac{\beta_1}{\beta_0}\right)\left(\frac{2}{\beta_0 \mathrm{Pr}}\right)^{1/3}\left(4\,\frac{\gamma_3}{\gamma_2} - 1\right)$$

and it follows that the surface temperature difference is given by

$$\Theta_w = \gamma_2 \left(\frac{2}{\beta_0 \mathrm{Pr}}\right)^{1/3} \frac{q}{k}\sqrt{\frac{u_\infty}{\nu x}} \left[1 - \frac{1}{7}\left(\frac{\beta_1}{\beta_0}\right)\left(4\,\frac{\gamma_3}{\gamma_2} - 1\right)(mx) + \dots\right] \tag{47}$$

or

$$\frac{\Theta_w}{\Theta_w^*} = 1 + 0.789(mx) + \dots \tag{48}$$

where

$$\Theta_w^* = 2.16\left(\frac{qx}{k}\right)(\mathrm{Pr})^{-1/3}(\mathrm{Re})^{-1/3} \tag{49}$$

Again it may be noted that for the present case magnetic effects are independent of Prandtl number.

Low Prandtl Numbers

For negligible frictional heating Equation (3) may be written approximately as

$$u\,\frac{\partial t}{\partial x} + v\,\frac{\partial t}{\partial y} = \alpha\left(\frac{\partial^2 t}{\partial x^2} + \frac{\partial^2 t}{\partial y^2}\right) + \frac{\sigma B_0^2}{\rho c_p} U^2 \tag{50}$$

The method that will be employed to solve this equation is similar to that presented by Grosh and Cess [10] for nonmagnetic flows. For fluids with very low Prandtl numbers the thickness of the thermal boundary layer is much greater than that of the momentum boundary layer. This in turn indicates that viscous effects are limited to a small portion of the thermal boundary layer, and to a first approximation inviscid potential flow may be assumed such that the velocity components u and v occurring in Equation (50) are given by Equations (8) and (9). A discussion of the applicability of this assumption for nonmagnetic flow across an isothermal flat plate is given in reference [10], for which good agreement was found to exist between inviscid flow and viscous flow solutions within the Prandtl number range of typical liquid metals.

Following reference [10], Boussinesq's transformation [11] will be employed. Thus Equation (50) may be written in terms of the independent variable ϕ and ψ as

$$u_\infty \frac{\partial \Theta}{\partial \phi} = \alpha\left(\frac{\partial^2 \Theta}{\partial \phi^2} + \frac{\partial^2 \Theta}{\partial \psi^2}\right) + \frac{m u_\infty^2}{c_p}$$

where ϕ and ψ are given by Equations (10) and (11). From the usual boundary layer assumptions this equation reduces to

$$u_\infty \frac{\partial \Theta}{\partial \phi} = \alpha \frac{\partial^2 \Theta}{\partial \psi^2} + \frac{m u_\infty^2}{c_p} \tag{51}$$

for which the boundary condition with respect to ϕ may be taken as $\Theta = 0$ for $\phi = 0$. Applying a Laplace transform with respect to ϕ, then

$$\overline{\Theta}(s, \psi) = \int_0^\infty \Theta(\phi, \psi) e^{-s\phi} d\phi$$

and Equation (51) transforms to

$$\frac{d^2\overline{\Theta}}{d\psi^2} - \left(\frac{u_\infty^2}{\alpha}\right)\overline{\Theta} = -\left(\frac{m u_\infty^2}{\alpha c_p^2}\right) \tag{52}$$

such that the solution may be carried out for specified boundary conditions with respect to ψ.

Constant Surface Temperature. For a constant temperature on the surface of the plate, the boundary conditions with respect to ψ become

$$\Theta = \Theta_w; \quad \psi = 0$$

$$\frac{\partial \Theta}{\partial \psi} = 0; \quad \psi = \infty$$

and it follows that the transformed boundary conditions are

$$\bar{\Theta} = \frac{\Theta_w}{s}; \quad \psi = 0$$

$$\frac{d\bar{\Theta}}{d\psi} = 0; \quad \psi = \infty$$

The solution of Equation (52) satisfying these conditions is

$$\bar{\Theta} = \left(\frac{\Theta_w}{s} - \frac{mu_\infty{}^2}{c_p s^2}\right) \exp\left(-\psi \sqrt{\frac{u_\infty s}{\alpha}}\right) + \frac{mu_\infty{}^2}{c_p s^2}$$

Correspondingly

$$\left(\frac{d\bar{\Theta}}{d\psi}\right)_{\psi=0} = -\sqrt{\frac{u_\infty}{\alpha}} \left[\frac{\Theta_w}{s^{1/2}} - \frac{mu_\infty{}^2}{c_p s^{3/2}}\right]$$

and taking the inverse it follows that

$$\left(\frac{\partial\Theta}{\partial\psi}\right)_{\psi=0} = -\sqrt{\frac{u_\infty}{\pi\alpha x}} \left(\frac{\Theta_w}{\sqrt{1 - \frac{1}{2}mx}}\right) \left[1 - 2\left(\frac{u_\infty{}^2}{\Theta_w c_p}\right)(mx)\left(1 - \frac{1}{2}mx\right)\right]$$

To obtain an expression for the heat flux from the surface of the plate

$$q = -k\left(\frac{\partial\Theta}{\partial\psi}\frac{\partial\psi}{\partial y}\right)_{y=0} = -k(1 - mx)\left(\frac{\partial\Theta}{\partial\psi}\right)_{\psi=0}$$

and

$$q = \Theta_w \sqrt{\frac{k\rho c_p u_\infty}{\pi x}} \left(\frac{1 - mx}{\sqrt{1 - \frac{1}{2}mx}}\right) \left[1 - 2\left(\frac{u_\infty{}^2}{\Theta_w c_p}\right)(mx)\left(1 - \frac{1}{2}mx\right)\right] \quad (53)$$

Again expressing the results in terms of a heat-flux ratio

$$\frac{q}{q^*} = \left(\frac{1 - mx}{\sqrt{1 - \frac{1}{2}mx}}\right) \left[1 - 2\left(\frac{u_\infty{}^2}{\Theta_w c_p}\right)(mx)\left(1 - \frac{1}{2}mx\right)\right] \quad (54)$$

where

$$q^* = 0.564\left(\frac{\Theta_w k}{x}\right)(\mathrm{Pe})^{1/2} \quad (55)$$

The ratio q/q^* is shown in Fig. 2. For most cases of practical interest the effect of Joule heating, as represented by the parameter $(u_\infty{}^2/\Theta_w c_p)$, will be negligible.

Constant Surface Flux. For the case of a constant surface heat flux

$$\left(\frac{\partial\Theta}{\partial y}\right)_{y=0} = -\frac{q}{k}$$

and since

$$\left(\frac{\partial\Theta}{\partial y}\right)_{y=0} = (1 - mx)\left(\frac{\partial\Theta}{\partial\psi}\right)_{\psi=0} = \sqrt{1 - 2m\phi}\left(\frac{\partial\Theta}{\partial\psi}\right)_{\psi=0}$$

then in terms of ϕ and ψ the temperature gradient at the surface becomes

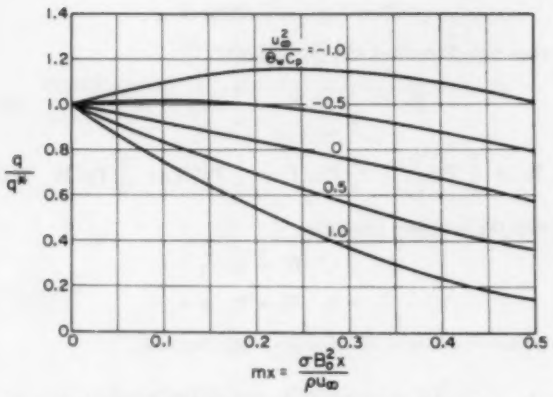

Fig. 2 Variation of the heat-flux ratio for fluids with low Prandtl numbers

$$\left(\frac{\partial\Theta}{\partial\psi}\right)_{\psi=0} = -\frac{q}{k}\frac{1}{\sqrt{1 - 2m\phi}}$$

Letting $Q(s)$ represent the Laplace transform of this quantity, the boundary conditions for Equation (52) become

$$\frac{d\bar{\Theta}}{d\psi} = Q(s); \quad \psi = 0$$

$$\frac{d\bar{\Theta}}{d\psi} = 0; \quad \psi = \infty$$

The solution of Equation (52) satisfying these conditions is

$$\bar{\Theta} = -\sqrt{\frac{\alpha}{u_\infty s}}\, Q(s) \exp\left(-\psi\sqrt{\frac{u_\infty s}{\alpha}}\right) + \frac{mu_\infty{}^2}{c_p s^2}$$

from which it follows

$$\bar{\Theta}(s, 0) = -\sqrt{\frac{\alpha}{u_\infty}}\left(\frac{1}{s^{1/2}}\right) Q(s) + \frac{mu_\infty{}^2}{c_p s^2} \quad (56)$$

Recalling that

$$\mathfrak{L}^{-1}[Q(s)] = -\frac{q}{k}\frac{1}{\sqrt{1 - 2m\phi}}$$

then with the aid of the convolution integral the inverse of Equation (56) becomes

$$\Theta(\phi, 0) = \frac{q}{k}\sqrt{\frac{\alpha}{\pi u_\infty}} \int_0^\phi \frac{1}{\sqrt{1 - 2m\phi + 2m\xi}} \frac{d\xi}{\xi^{1/2}} + \frac{mu_\infty{}^2}{c_p}\phi$$

Evaluating the integral in this equation, the surface temperature difference is given by

$$\Theta_w = q\sqrt{\frac{1}{\pi\rho c_p k u_\infty}}\sqrt{\frac{2}{m}} \ln\left[\frac{1 + \sqrt{mx(2 - mx)}}{1 - mx}\right] + \frac{u_\infty{}^2}{c_p}(mx)\left(1 - \frac{1}{2}mx\right) \quad (57)$$

or

$$\frac{\Theta_w}{\Theta_w{}^*} = \left(\frac{1}{2\pi x}\right)^{1/2} \ln\left[\frac{1 + \sqrt{mx(2 - mx)}}{1 - mx}\right] + \left(\frac{u_\infty{}^2}{\Theta_w{}^* c_p}\right)(mx)\left(1 - \frac{1}{2}mx\right) \quad (58)$$

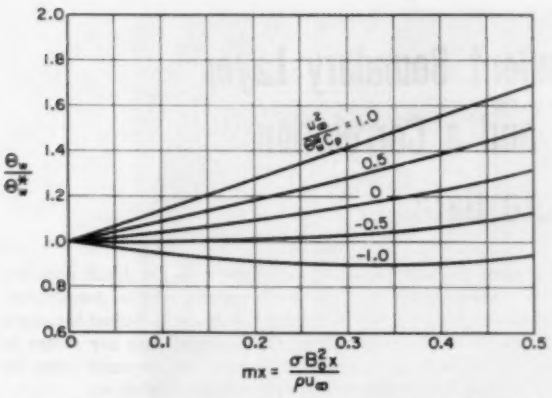

Fig. 3 Variation of the temperature difference ratio for fluids with low Prandtl numbers

where

$$\theta_w^* = 1.128 \left(\frac{qx}{k}\right) (\mathrm{Pe})^{-1/3} \tag{59}$$

The temperature difference ratio θ_w/θ_w^* is shown in Fig. 3. In most cases the effect of Joule heating will again be negligible.

Discussion of Results

Mathematically, the solutions for moderate and large Prandtl numbers represent asymptotic solutions for $\mathrm{Pr} \to \infty$, whereas the low Prandtl number results correspond to $\mathrm{Pr} \to 0$. It is of interest to compare these solutions as well as those for a Prandtl number of unity to determine the effect of Prandtl number upon convective heat transfer in a magnetic field. In order to put the results for all three cases on a comparable basis, both Joule and frictional heating will be neglected; i.e., the parameters $(u^2_\infty/\theta_w c_p)$ and $(u_\infty{}^2/\theta_w{}^* c_p)$ will be set equal to zero. Further, Equations (54) and (58) will be expanded in series form and only the first two terms retained. For a constant surface temperature this gives

$$\mathrm{Pr} \to \infty: \quad \frac{q}{q^*} = 1 - 1.15(mx) + \ldots$$

$$\mathrm{Pr} = 1: \quad \frac{q}{q^*} = 1 - 1.06(mx) + \ldots$$

$$\mathrm{Pr} \to 0: \quad \frac{q}{q^*} = 1 - 0.75(mx) + \ldots$$

whereas for a constant surface heat flux

$$\mathrm{Pr} \to \infty: \quad \frac{\theta_w}{\theta_w^*} = 1 + 0.789(mx) + \ldots$$

$$\mathrm{Pr} = 1: \quad \frac{\theta_w}{\theta_w^*} = 1 + 0.729(mx) + \ldots$$

$$\mathrm{Pr} \to 0: \quad \frac{\theta_w}{\theta_w^*} = 1 + 0.417(mx) + \ldots$$

It may be noted that magnetic effects increase with increasing Prandtl number. However, this variation is not great, and for all practical purposes the first-order terms may be considered independent of Prandtl number for Prandtl numbers greater than approximately one. It should be mentioned, however, that this would probably not be the case for higher-order terms.

In addition to altering the momentum and thermal transfer processes, the application of a magnetic field may also alter the flow regime. For example, separation can occur as a result of the retarding magnetic force, and from reference [1] a second-order approximation for the laminar separation point is found to be $mx \simeq 0.5$. A second effect upon the flow regime concerns transition from laminar to turbulent flow, and from the stability analysis presented by Rossow [12] it is found that the transition Reynolds number is reduced through application of a transverse magnetic field fixed relative to the plate.

In the present analysis it has been assumed that the induced magnetic field is negligible. In most applications this is a plausible assumption providing the electrical conductivity of the fluid under consideration is not large. However, for fluids with high electrical conductivities, such as liquid metals, the induced magnetic field may in some instances be appreciable. This effect is discussed by Cowling [13].

References

1 V. J. Rossow, "On Flow of Electrically Conducting Fluids Over a Flat Plate in the Presence of a Transverse Magnetic Field," NACA Report 1358, 1958.

2 J. L. Neuringer and W. McIlroy, "Hydromagnetic Effects on Stagnation-Point Heat Transfer," *Journal of the Aeronautical Sciences*, vol. 25, 1958, p. 332.

3 V. J. Rossow, "Magnetohydrodynamic Analysis of Heat Transfer Near a Stagnation Point," *Journal of the Aeronautical Sciences*, vol. 25, 1958, p. 334.

4 P. S. Lykoudis, "On a Class of Magnetic Laminar Boundary Layers," Heat Transfer and Fluid Mechanics Institute, Preprints of Papers, Stanford University Press, Stanford, California, 1958, p. 176.

5 R. C. Meyer, "On Reducing Aerodynamic Heat-Transfer Rates by Magnetohydrodynamic Techniques," *Journal of Aero/Space Sciences*, vol. 25, 1958, p. 561.

6 H. Schlichting, "Boundary Layer Theory," McGraw-Hill Book Company, Inc., New York, N. Y., 1955.

7 "Modern Developments in Fluid Dynamics," edited by S. Goldstein, vol. II, Oxford Universty Press, London, England, 1938, pp. 633–636.

8 E. Jahnke and F. Emde, "Tables of Functions," Dover Publications, New York, N. Y., 1945, p. 275.

9 W. Magnus and F. Oberhettinger, "Special Functions of Mathematical Physics," Chelsea Publishing Company, New York, N. Y., 1949, pp. 86–88.

10 R. J. Grosh and R. D. Cess, "Heat Transfer to Fluids With Low Prandtl Numbers for Flow Across Plates and Cylinders of Various Cross Section," TRANS. ASME, vol. 80, 1958, p. 667.

11 M. J. Boussinesq, "Calcul du Pouvoir Refroidissant des Courants Fluids," *Journal de Mathematique*, vol. 1, 1905, p. 285.

12 V. J. Rossow, "Boundary-Layer Stability Diagrams for Electrically Conducting Fluids in the Presence of a Magnetic Field," NACA TN 4282, 1958.

13 T. G. Cowling, "Magnetohydrodynamics," Interscience Publishers, Inc., New York, N. Y., 1957, pp. 4–17.

Conical Turbulent Boundary Layer Experiments and a Correlation With Flat Plate Data

W. S. BRADFIELD
Senior Staff Scientist, Convair, Scientific Research Laboratory, San Diego, Calif.

Measurements in the turbulent boundary layer of unyawed cones for Mach numbers from 1 to 6 are presented. Specifically, the first measurements of total temperature profiles, directly determined skin friction, and local heat flux in the turbulent boundary layer of cone models are given. In addition, these experimental data are shown to justify the calculation of turbulent friction and heat transfer on unyawed cones by means of an incompressible plate friction law and simple auxiliary relations.

Experimental Methods

THE EXPERIMENTAL INVESTIGATION was performed in the wind tunnel facilities of the University of Minnesota Rosemount Aeronautical Laboratory. In Fig. 1 is shown a photograph of the 15-deg cone model with boundary layer probes installed in the $M_\infty = 3$, 6 × 9-in. test section. An impact temperature probe [1][1] was mounted on the upper surface of the cone and an impact pressure probe on the lower surface at the meridional plane. The probes were adjustable from outside the tunnel during operation by means of push rods projecting through the model skin as shown. The probe tips were approximately 5 inches downstream from the tip of the model.

The impact pressure probe was made of $^1/_{32}$-in. OD stainless steel tubing. The tip opening was 1.5 mils[2] high and 17 mils wide with outside dimensions of 3.2 × 20 mils. The probe was designed for fast response [2], the response time being about 15 seconds.

The locations of the probes relative to the surface of the model were measured with a 20-power stereoscopic microscope.

The surface of the model was instrumented with static pressure taps and thermocouples [3]. Static pressure orifices were 14 mils

[1] Numbers in brackets designate References at end of paper.

Contributed by the Heat Transfer Division of THE AMERICAN SOCIETY OF MECHANICAL ENGINEERS, and presented at the ASME-AIChE Heat Transfer Conference, Storrs, Conn., August 9–12, 1959.

NOTE: Statements and opinions advanced in papers are to be understood as individual expressions of their authors and not those of the Society. Manuscript received at ASME Headquarters, April 28, 1959. Paper No. 59—HT-6.

[2] 1 mil = 0.001 in.

Nomenclature

A = area of surface
C_f = local skin friction coefficient, τ/q_1
C_F = average or total skin friction coefficient $= \frac{1}{A}\int_A C_f(A')dA'$
c_p = specific heat at constant pressure
h = heat-transfer coefficient (quantity of heat per unit time per unit area per temperature difference)
k = thermal conductivity
M = Mach number without subscript indicates local value of Mach number in undisturbed boundary layer
mil = one thousandth of an inch . . . roughly 1/40 of a millimeter
n = exponent in turbulent velocity profile
Pr = Prandtl number $= \frac{c_p\mu}{k}$ based on thermal equilibrium at the wetted surface
$q = \frac{\rho u^2}{2}$
St = Stanton number $= \frac{h}{\rho_1 c_p u_1}$ based on conditions just outside boundary layer
T = temperature
u = velocity in the x-direction
x = distance downstream from boundary layer origin on cone or plate
y = distance perpendicular to the wetted surface
δ = boundary layer thickness determined by taking $y = \delta$ when $u = 0.995u_1$
δ^* = boundary layer displacement thickness, $\int_0^\delta \left[1 - \frac{\rho u}{\rho_1 u_1}\right] dy$
γ = ratio of specific heats c_p/c_v
θ = boundary layer momentum defect thickness, $\int_0^\delta \frac{\rho u}{\rho_1 u_1}\left[1 - \frac{u}{u_1}\right] dy$
ν = kinematic viscosity μ/ρ
μ = viscosity
ρ = density
σ = boundary layer recovery factor $\frac{T_s - T_1}{T_0 - T_1}$

Subscripts

∞ = upstream conditions
1 = conditions locally at outer edge of boundary layer
0 = stagnation conditions
e = properties based on recovery temperature (surface temperature at condition of zero heat transfer)
i = incompressible
t = either "transition" or "thermal boundary layer" as appropriate
w = conditions on surface of model
x = as in R_x, characteristic length used in calculating R_l

Superscripts

* = indicates values corresponding to equation (9)

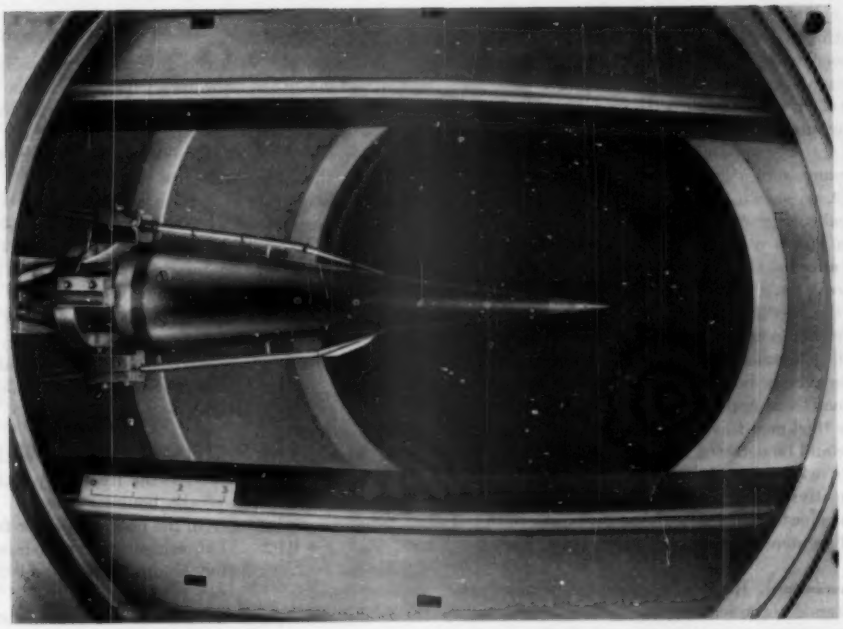

Fig. 1 Installation of impact pressure and impact temperature probes on 15-deg total angle cone

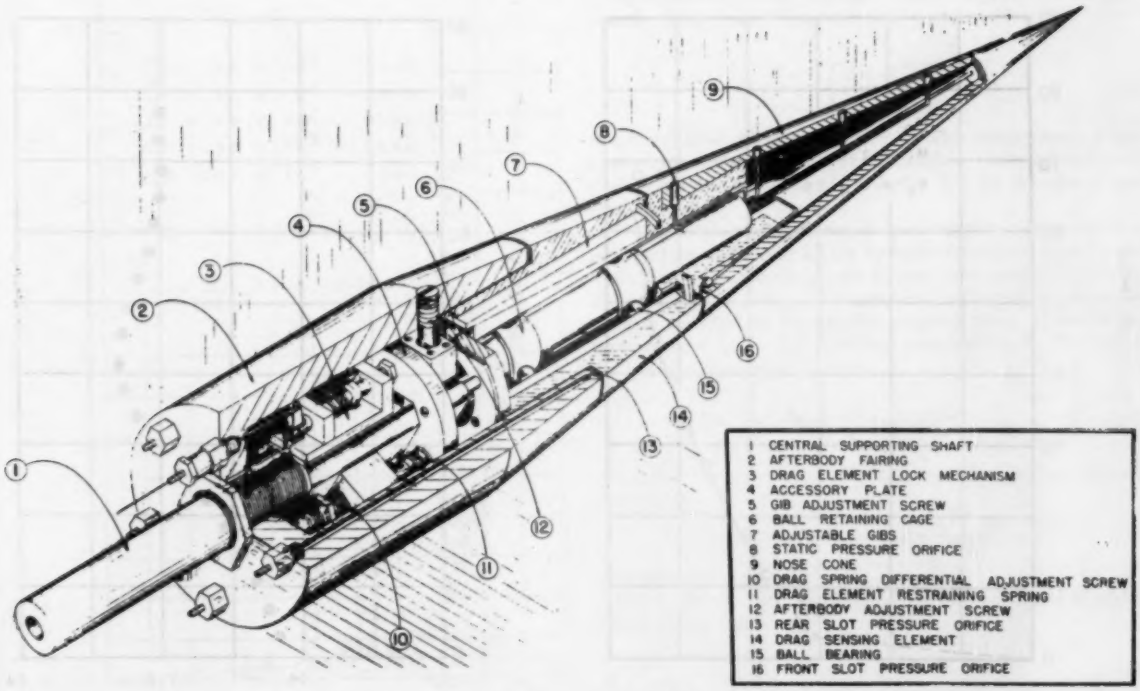
1 CENTRAL SUPPORTING SHAFT
2 AFTERBODY FAIRING
3 DRAG ELEMENT LOCK MECHANISM
4 ACCESSORY PLATE
5 GIB ADJUSTMENT SCREW
6 BALL RETAINING CAGE
7 ADJUSTABLE GIBS
8 STATIC PRESSURE ORIFICE
9 NOSE CONE
10 DRAG SPRING DIFFERENTIAL ADJUSTMENT SCREW
11 DRAG ELEMENT RESTRAINING SPRING
12 AFTERBODY ADJUSTMENT SCREW
13 REAR SLOT PRESSURE ORIFICE
14 DRAG SENSING ELEMENT
15 BALL BEARING
16 FRONT SLOT PRESSURE ORIFICE

Fig. 2 15-deg cone drag balance

in diameter and opened into 1/16-in. OD brass tubing pressure leads. Orifice fittings were soldered into the model skin. Iron-constantan thermocouples were installed by soft soldering in holes drilled through the 1/32-in-thick model skin.

A combination of an upstream directed air jet issuing from the cone tip and a roughness trip (shown in Fig. 1) was used to insure the existence of a turbulent boundary layer.

Direct measurements of skin friction were made using the balance system [4, 5] shown as Fig. 2. A segment (truncated cone) of the conical surface was supported from the central shaft on 6 steel balls in such a way that it was free to "float" with a clearance of 1 mil afforded at the leading edge and trailing edge of the floating surface. Lateral adjustment of the floating element was achieved by the selective adjustment of an internal parallel inclined wedge system. A conservative estimate of the maximum floating element misalignment with the conical surface was 3/10 mil. However, the average boundary layer thickness for the skin friction measurements was approximately 120 mils giving a ratio of boundary layer thickness to surface step of 400. During the testing no waves could be detected as originating from either the front or rear crack when observed with a double pass schlieren system at high sensitivity.

Determinations of local values of heat flux were made both from electrically heated segmented models [6] and from a "heat sink" cone [7].

Accuracy of Measurements. Random errors in temperature ratio, or in flow parameters determined by probing due to uncertainty in pressure and temperature measurement are:[3] $T_s/T_0 = \pm 1$ per cent; momentum thickness ± 5 per cent to ± 7 per cent; displacement thickness ± 3 per cent to ± 5 per cent.

For measurements on the model with the balance system, the experimental uncertainties are as follows: Reynolds number ± 3 per cent; friction coefficient ± 3.4 per cent; Mach number ± 1.5 per cent.

In connection with the direct determinations of skin friction (carried out in the blowdown wind tunnel), the pressure force on the floating element was determined by measurements of pressure on both the exterior and interior surfaces of the floating element. The pressure force was always less than 20 per cent of the friction drag for these measurements.

The accuracy of heat-transfer measurements was determined from the uncertainties in the terms in the heat-balance equation. They are: $(T_w - T_s) \pm 2$ deg F; slope $\pm 4\%$; $\Delta W/\Delta A \pm 1\%$. Thus the uncertainty in h was $\pm 5\%$. The corresponding uncertainty in Stanton number was $\pm 8\%$.

Mach Number and Total Temperature Profiles. The first measurement of a cone flow turbulent thermal boundary layer total temperature profile was accomplished for this investigation. Simultaneously, an impact pressure profile was obtained. The measurements were obtained at $M_1 = 2.8$ and $R_x = 4 \times 10^6$. The results are shown as Fig. 3.

As expected for a gas (Prandtl number less than unity), local total enthalpy values above the freestream value are observed near the outer edge of the boundary layer. The surface, in adiabatic equilibrium with the boundary layer flow, stabilized at $T_0/T_{01}]_{y=0} = 0.928$. This temperature ratio is one per cent lower than the recovery factor, according to the relation $\sigma = (\mathrm{Pr})^{1/3}$, would indicate.

Comparison [7] of the present data with existing two dimensional, nearly adiabatic data [8, 9], indicates that the cone boundary layer total temperature profile is similar to two-dimensional profiles in the y/δ_t versus $T_0(y)/T_{01}$ presentation. Further, indications are that similarity with respect to Reynolds number variations is also obtained over a moderate Reynolds number range at $M_1 = 3$.

[3] See reference [7] for details.

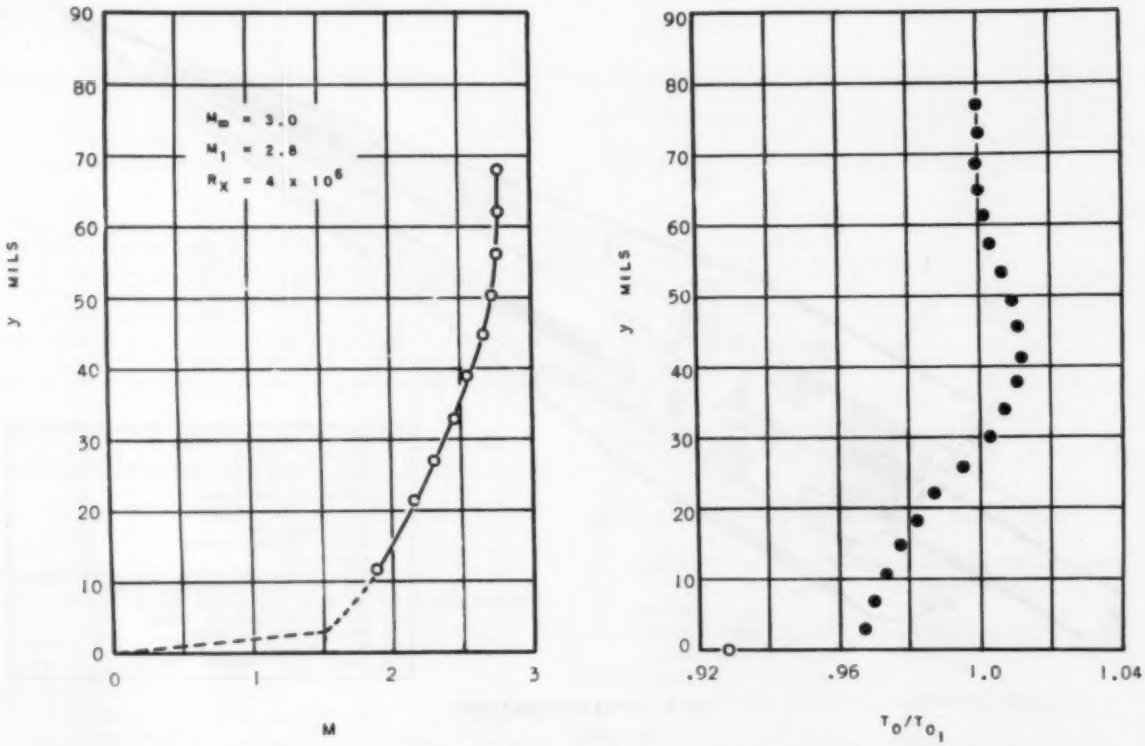

Fig. 3 Mach number and total temperature profiles in the turbulent boundary layer of 15-deg total angle cone

Turbulent Boundary Layer Velocity Profiles. Velocity profiles may be calculated from the Mach profile number and free stream total temperature. A set of turbulent velocity profiles from a cone at $M_1 = 3.7$ is presented as Fig. 4. The data were obtained from a fifteen-degree total angle cone at zero yaw and in thermal equilibrium with the flow. A combination roughness (sand) and air trip [4, 5] was used to produce fully turbulent boundary layer for three of the five sets of data. One set was obtained with sand trip only and one with air trip only.

Just as in the case of existing flat-plate data over a relatively wide range of Reynolds number and Mach number, the cone data are well represented by $^1/_7$-power profiles for the outer region in combination with linear profiles assumed for the laminar sublayer.

An Engineering Prediction of Turbulent Skin Friction and Heat Transfer on a Cone at Zero Yaw at Supersonic Speeds. It was indicated by the results of the present investigation [7] that velocity profiles from the turbulent boundary layer of both plate and cone at the same M_1 are congruent when presented as u/u_1 versus y/θ. In other words

$$\frac{u}{u_1} = a(y/\theta)^{1/n} \tag{1}$$

for both plate and cone where a has the same dependence on Mach number for both cases over the range of Mach number investigated. It was found that $n = 7$ for the moderate range of Reynolds numbers investigated.

If it is now assumed that a friction law of form $C_f = B(R_\delta)^k$ holds, this law together with equation (1) results in

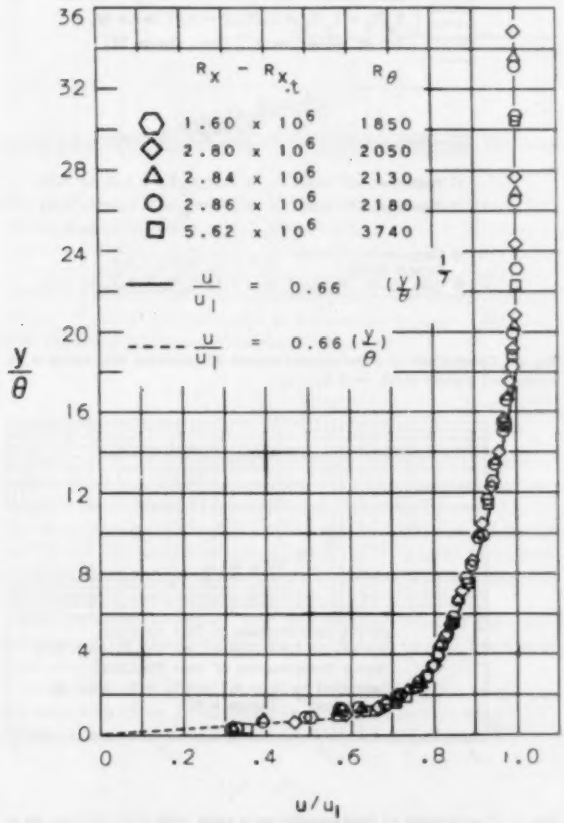

Fig. 4 Turbulent velocity profiles on a cone

$$C_f = \frac{B}{\left[\frac{u_1\delta}{\nu_1}\right]^{\frac{2}{n+1}}} \tag{2}$$

for both cases. It is further assumed that B, a parameter depending on Mach number, has the same dependence on Mach number for both cases. It follows that the friction coefficients will be related by

$$\frac{C_f}{\bar{C}_f} = \left[\frac{\bar{\delta}}{\delta}\right]^{\frac{2}{n+1}} \tag{3}$$

Here and in what follows, a bar over a quantity indicates a two-dimensional (plate or axial flow cylinder) boundary layer quantity.

For the plate,

$$\frac{\bar{C}_f}{2} = \frac{d\bar{\theta}}{dx} \tag{4}$$

while for the cone

$$\frac{C_f}{2} = \frac{d\theta}{dx} + \frac{\theta}{x} \tag{5}$$

Again, as a consequence of the congruence of velocity and temperature profiles for plate and cone, the momentum defect thickness for both cases has the same dependence on M_1. That is,

$$\frac{\theta}{\delta} = \frac{\bar{\theta}}{\bar{\delta}} = f(M_1, n) \tag{6}$$

Using equations (2) and (6), equations (4) and (5) can be integrated. These results together with equation (3) give

$$\frac{C_f}{\bar{C}_f} = \left[\frac{2(n+2)}{n+1}\right]^{\frac{2}{n+3}} \tag{7}$$

at a specified M_1, n, u_1/ν_1, and $x = \bar{x}$. This development, which explicitly considers variable Mach number, yields precisely the same result as that obtained by Gazley [10] for the case of constant properties.

It is general practice to obtain heat-transfer coefficients from skin friction coefficients for the turbulent boundary layer by use of the Reynolds analogy (see, for example, reference [11], p. 107). For compressible flow plate experiments, a form of the Reynolds analogy modified to account for property value variation has proved useful [12]. This relation, proposed by A. P. Colburn [18], for incompressible flow, is

$$\bar{St} = \frac{\bar{C}_f}{2}(Pr^*)^{-2/3} \tag{8}$$

where the Prandtl number (Pr^*) is evaluated at the reference temperature

$$T^* = T_1 + 0.5(T_w - T_1) + 0.22(T_r - T_1) \tag{9}$$

proposed by Eckert [12].

If it is assumed that equation (8) holds for cone flow as well as for plate flow, then

$$\frac{St}{\bar{St}} = \frac{C_f}{\bar{C}_f} \tag{10}$$

if $T^* = \bar{T}^*$.

For $n = 7$, equation (7) yields for local values of Stanton number and skin friction

$$\frac{\overline{St}}{St} = \frac{C_f}{\overline{C_f}} = 1.18 \tag{11}$$

for $T^* = \overline{T^*}$ and $R_x = \overline{R_x}$ independent of Reynolds number and Mach number over the range covered by the experimental data discussed here. Note that for $5 < n < 10$, equation (7) shows $1.23 < C_f/\overline{C_f} < 1.13$. Thus the effect of variations of n on the transformation relation is small in this range.

For obtaining the relation between mean skin friction and heat transfer on plates and cones, the relations

$$\overline{C_F} = \frac{1}{x}\int_0^x \overline{C_f}(x')dx' \quad \text{and} \quad C_F = \frac{2}{x^2}\int_0^x C_f(x')x'dx'$$

are employed. It follows from the above that for average friction and heat-transfer coefficients

$$\frac{C_F}{\overline{C_F}} = \frac{St_T}{\overline{St_T}} = 2\left[\frac{n+1}{2(n+2)}\right]^{\frac{n+1}{n+3}} = 1.05 \tag{12}$$

for $n = 7$. The effect of variations of n on the transformation relation equation (12) is negligible; for $5 < n < 10$, $1.065 < C_F/\overline{C_F} < 1.035$.

Correlations of Direct Measurements of Turbulent Skin Friction and Heat Transfer. The results of the measurements at $M_1 = 3.7$ are shown as Fig. 5 in comparison with the data of Coles [13] on a flat plate in the form C_f versus $(R_x - R_{x_t})$ where the dashed line and the line through the cone data are drawn parallel to the faired line representing Coles' data. R_{x_t} is the Reynolds number based on the distance between the measuring station and the beginning of transition as determined from schlieren observations. The dashed line is higher than the plate data by 18 per cent in accord with equation (11). The cone data are about 10 per cent higher than predicted by equation (11).

Fig. 6 is adapted from Fig. 2 of reference [14]. It shows the relation between the heat-transfer data (at constant surface temperature) from two cones and a secant ogive and from the flat plate data of Pappas [15]. The mean line of the cone flow data is higher than the corresponding mean line of the flat plate data and parallel to the flat plate data mean line. The lines were obtained by least squares procedure from the data points. As predicted by equation (11), the mean line of the cone data is about 18 per cent higher than the plate data mean line.

Fig. 7 shows a comparison between measured heat transfer and transformed skin friction measurements on cones at $M_1 = 3.7$. Stanton numbers are calculated from measured skin friction coefficients by the Colburn relation, equation (8), where the Prandtl number is evaluated at the reference temperature proposed by Eckert [12], equation (9). The agreement is satisfactory.

Fig. 8 shows a comparison between heat-transfer results and skin friction results for cones and plates over the present Mach number range. The data are evaluated at $R_x = \overline{R_x} = 3 \times 10^6$. In order to provide a comparison of results on a $T^* = \overline{T^*}$ basis, all Stanton number data were adjusted to $T_w = T_r$ using the theory of Van Driest [17] (the same procedure was used in comparing the data of Fig. 7). The maximum adjustment required amounted to 5 per cent of the measured value. The average adjustment required was 3 per cent of the measured values.

In nondimensionalizing the Stanton numbers and skin friction coefficients, incompressible flat plate theory was used in both cases. Values of Stanton number (incompressible) were calculated utilizing equations (8) and (9). The reference temperature value used to calculate St_i was calculated using the wind tunnel adiabatic wall temperature at each Mach number.

The vertical bars through many of the data points in Fig. 8 indicate the maximum scatter of the data at that Mach number. The symbol location in each case represents the mean value of the data. Where no vertical bar appears, the scatter of the data is represented by the symbol size.

The solid curve is the experimentally determined mean curve through the plate data points. Obviously, this relation should not be expected to hold for flow around cones at subsonic speeds or for cones with detached shocks.

The data correlations indicated by Figs. 5 through 8 are regarded as justification for the calculation of turbulent friction

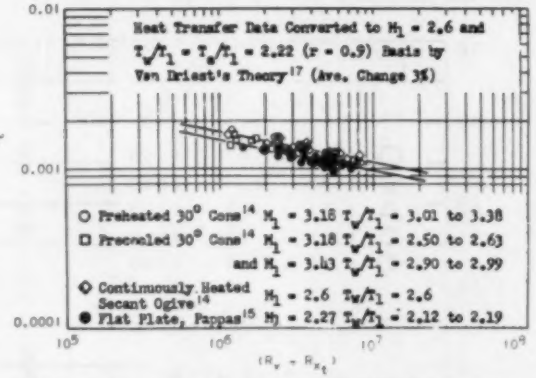
0.01
0.001
0.0001
St
Heat Transfer Data Converted to M1 = 2.6 and
Tw/T1 = Tr/T1 = 2.22 (r = 0.9) Basis by
Van Driest's Theory17 (Ave. Change 3%)
Preheated 30° Cone14 M1 = 3.18 Tw/T1 = 3.01 to 3.38
Precooled 30° Cone14 M1 = 3.18 Tw/T1 = 2.50 to 2.63
and M1 = 3.43 Tw/T1 = 2.90 to 2.99
Continuously Heated
Secant Ogive14 M1 = 2.6 Tw/T1 = 2.6
Flat Plate, Pappas15 M1 = 2.27 Tw/T1 = 2.12 to 2.19
10^5
10^6
10^7
10^8
(Rx - Rxt)

Fig. 6 Comparison of direct measurements of turbulent heat transfer on cones and a plate at $M_1 = 2.6$

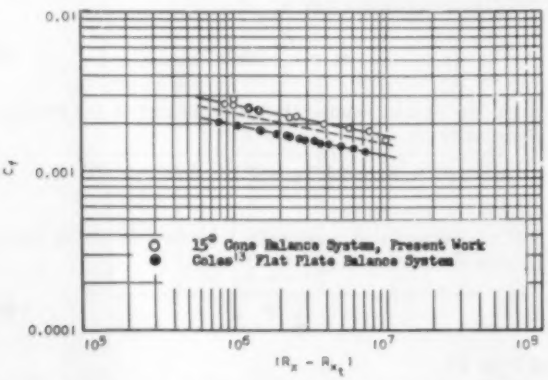

Fig. 5 Comparison of direct measurements of turbulent skin friction on a cone and a plate at $M_1 = 3.7$

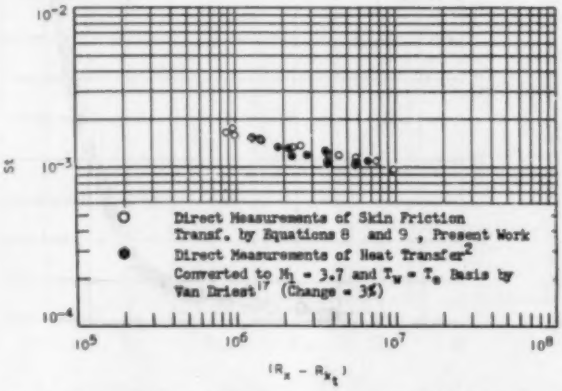

Fig. 7 Comparison of heat transfer on a cone with skin friction on a cone at $M_1 = 3.7$

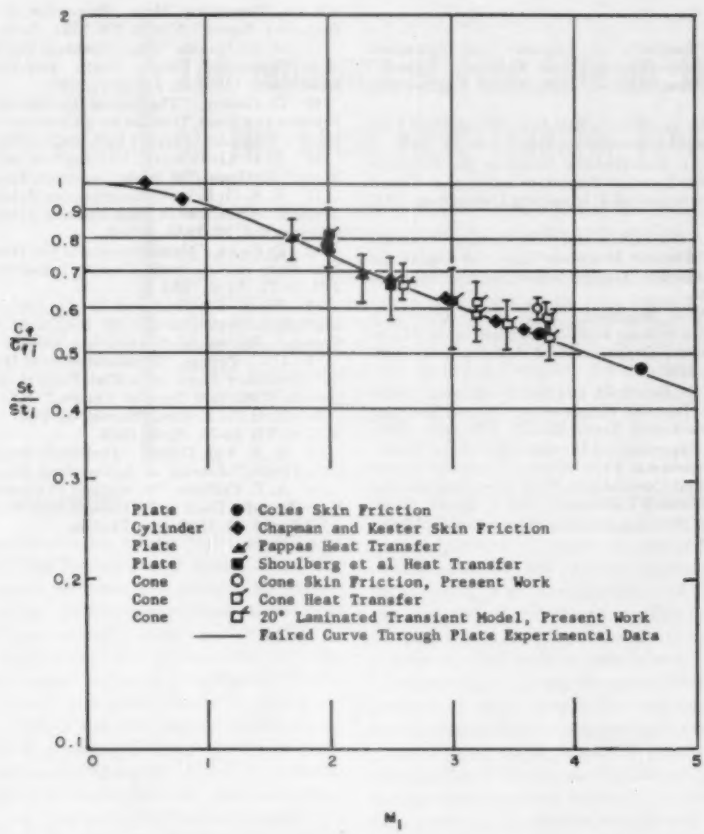

Fig. 8 A comparison between heat-transfer and skin-friction measurements on plates, axial flow cylinders, and cones

and heat transfer on unyawed cones at supersonic speeds by means of an incompressible plate friction law and the simple auxiliary relations given as equations (8), (9), (11), and (12).

As a summary of this procedure, suppose it is desired to calculate the local heat flux at the surface of a cone at Mach number M_i and R_x at the outside edge of the boundary layer. Starting with the Schultz-Grunow local skin friction law

$$\overline{C_{fi}} = \frac{0.370}{(\log_{10} \overline{R_x})^{2.584}} \tag{13}$$

where $\overline{R_x} = R_x$, the corresponding incompressible plate Stanton number $\overline{St_i}$ is calculated by equation (8). The compressible flow flat plate $\overline{St}$ is obtained by multiplying St_i by $\overline{St}/\overline{St_i}$ from Fig. 8. The cone Stanton number St is obtained by increasing $\overline{St}$ by 18 per cent in accordance with equation (11). The same procedure is followed for average values except the relation between cone and plate values is given by equation (12).

Summary and Conclusions. The first measurements of the total temperature distribution through a turbulent conical boundary layer are presented.

A comparison of directly measured local skin friction values on the cone with those on the plate at constant Mach number indicates that cone skin friction is higher but that it has the same dependence on Reynolds number as plate skin friction (Fig. 5). A comparison of local heat-transfer values on cone and plate similarly shows higher heat transfer on a cone at the same M_i and Reynolds number based on property values just outside the boundary layer (Fig. 6).

It is confirmed that the modified Reynolds analogy of Colburn, equation (5), together with the reference temperature of Eckert, equation (6), permits the calculation of cone heat-transfer values from known cone skin-friction values (Figs. 7 and 8).

Finally, an analysis is presented which predicts that skin-friction and heat-transfer values on unyawed cone in supersonic flow should be approximately a constant times the corresponding flat-plate values and this prediction is confirmed by experiment.

Acknowledgment

The present paper is excerpted from the doctoral dissertation of the author [7]. Prof. E. R. G. Eckert, Department of Mechanical Engineering, University of Minnesota, served as thesis adviser. The writer wishes to express his deep appreciation to Professor Eckert for the many constructive criticisms which brought the work into its final form. It is a pleasure to acknowledge that discussions with M. Sibulkin and R. D. Linnell of Convair Scientific Research Laboratory have contributed to the present paper.

References

1 W. S. Bradfield, "Research on Laminar and Turbulent Boundary Layers at Supersonic Speeds, Final Summary Report," University of Minnesota, Department of Aeronautical Engineering, RR 131, December, 1957.

2 W. S. Bradfield and G. E. Yale, "Small Pitot Tubes With Fast Response Time," *Journal of Aeronautical Sciences*, vol. 18, 1951.

3 D. G. DeCoursin, "An Experimental Study of the Effect of Small Angles of Attack on the Laminar Boundary Layer of a Cone," University of Minnesota, Aeronautical Engineering Department, RR 121, August, 1955.

4 W. S. Bradfield, D. G. DeCoursin, and C. B. Blumer, "Characteristics of Laminar and Turbulent Boundary Layer at Supersonic Velocity," University of Minnesota, Department of Aeronautical Engineering, RR 83, July, 1952.

5 C. B. Blumer and W. S. Bradfield, "Final Modification of a Conical Skin Friction Balance System and Measurements at $M_1 = 2.6$," University of Minnesota, Department of Aeronautical Engineering, RR 111, February, 1955.

6 D. G. DeCoursin, W. S. Bradfield, and J. J. Sheppard, "Aerodynamic Heating and Heat-Transfer Phenomena at Mach Numbers 2.7 Through 5.7," WADC Technical Report 53-379, February, 1954.

7 W. S. Bradfield, "An Experimental Investigation of the Turbulent Boundary Layer in Supersonic Flow Around Unyawed Cones With Small Heat Transfer and Correlations With Two-Dimensional Data," Convair Scientific Research Laboratory, RR 1, March, 1958.

8 G. J. Nothwang, "An Evaluation of Four Experimental Methods for Measuring Mean Properties of a Supersonic Turbulent Boundary Layer," NACA TN 3721, June, 1956.

9 H. M. Spivak, "Experiments in the Turbulent Boundary Layer of a Supersonic Flow," North American Aviation, Aerophysics Laboratory, CM-615, January, 1950.

10 C. Gazley, "Theoretical Evaluation of the Turbulent Skin Friction and Heat Transfer on a Cone in Supersonic Flight," General Electric Company, Report R49A0524, 1949.

11 E. R. G. Eckert, "Introduction to the Transfer of Heat and Mass," McGraw-Hill Book Company, Inc., New York, N. Y., 1950.

12 E. R. G. Eckert, "Engineering Relations for Friction and Heat Transfer to Surfaces in High Velocity Flow," *Journal of Aeronautical Sciences*, vol. 22, 1955, p. 585.

13 D. Coles, "Measurements in the Boundary Layer on a Smooth Flat Plate in Supersonic Flow," California Institute of Technology, JPL 20-71, June, 1953.

14 W. S. Bradfield and D. G. DeCoursin, "Measurements of Turbulent Heat Transfer on Bodies of Revolution at Supersonic Speeds," *Journal of Aeronautical Sciences*, vol. 23, 1956, p. 272.

15 C. C. Pappas, "Measurements of Heat Transfer in the Turbulent Boundary Layer on a Flat Plate in Supersonic Flow and Comparison With Skin Friction Results," NACA TN 3222, June, 1954.

16 E. R. G. Eckert, "Survey on Heat Transfer at High Speeds," WADC TR 54-70, April, 1954.

17 E. R. Van Driest, "Turbulent Boundary Layer in Compressible Fluids," *Journal of Aeronautical Sciences*, vol. 18, 1951.

18 A. P. Colburn, "A Method of Correlating Forced Convection Heat-Transfer Data and a Comparison With Fluid Friction," *Trans. AIChE*, vol. 29, 1933, pp. 174–210.

The Influence of Free Stream Turbulence on the Local Heat Transfer From Cylinders

R. A. SEBAN
Professor of Mechanical Engineering, University of California, Berkeley, Calif. Mem. ASME

Local heat-transfer coefficients and recovery factors are presented for three different cylinders in a two-dimensional subsonic air flow, with emphasis on the effect of screen-produced turbulence on these quantities. The increase in turbulent intensity so realized produced larger local heat-transfer coefficients, in a way dependent upon the location on the cylinders, through a direct increase in the heat transfer to the laminar boundary layer, through an earlier transition to turbulence, or through an alteration in the character of the separated flow. Alternatively, recovery factors were affected less, being invariant with respect to the turbulent intensity for attached boundary layer flow, but demonstrating large changes in those separated flow regions for which increased free stream turbulence produced substantial changes in the nature of the separated flow.

Introduction

It has been known for a long time that the heat transfer from a body to a fluid flowing over it is increased if the turbulence level of the stream increases, and recently the experimental results demonstrating the effect have been augmented, particularly for over-all heat transfer from circular cylinders placed transverse to an air stream. For systems like this, the gain in the over-all heat transfer is due to a number of effects, such as an increase in the rate of heat transfer to the laminar layer, an earlier transition to turbulent flow with its higher heat transfer, and movement of the separation point and alteration of the character of the flow in the separated region. Giedt [1][1] was the first to achieve a separation of these effects by measuring local heat-transfer coefficients on a circular cylinder placed normal to an air stream, and these results demonstrated in particular the increased rate of heat transfer to the laminar boundary layer on the front of the cylinder. Kestin [2] has recently presented additional results on the effect of screen-produced turbulence on the over-all heat transfer from circular cylinders in air stream, to show that slight increases in the turbulent intensity produce substantial increases in the heat transfer, with a slight continued augmentation as the turbulent intensity is increased further. Sato [3] has presented results for the over-all heat transfer from spheres, which apply to higher turbulence levels and indicate a more sustained increase as the turbulence level rises.

The purpose of this paper is the presentation of additional evidence on the effect of screen-produced turbulence on the local heat transfer from cylinders. These results are not in as homogeneous a form as might be expected, for they were obtained largely as an adjunct to other experimental programs, but they do have the co-ordinating element of all having been obtained in the same wind tunnel with similar screens. They are also so far unique in embracing air speeds of sufficient magnitude so that recovery factors could be determined. But these aspects imposed a disadvantage, not discovered in detail until near the end of the program, in that apparent low frequency oscillations in the wind tunnel rendered partly ambiguous the relative turbulence increase attained with the screens. While, therefore, no quantitative specification of the increase in the heat transfer relative to the turbulence level has been achieved, the results in one sense indicate that possibly none should be expected.

Apparatus and Procedure

The models for which results have been obtained were a 1:3 elliptical cylinder, with 6-in. major axis, a 1.25-in. diameter circular cylinder, and a 1.87-in. diameter circular cylinder fitted with a downstream splitter plate. All were made of bakelite, with Nichrome ribbons on their surfaces for heating by electric dissipation. The elliptic cylinder described previously [4] contained three longitudinal ribbons, 0.002 in. thick and 1 in. wide; the 1.87-in. circular cylinder was wound helically with such a ribbon, and the 1.25-in. cylinder was wound helically with a similar ribbon 0.001 in. thick and 0.50 in. wide. Thermocouples were located beneath the ribbons and pressure taps in small spaces between them, and on the circular cylinders all instrumentation was situated on one cylinder generator and local results were obtained by altering this location by rotation of the cylinder. All the models were mounted centrally in and spanned the 6-in. width of the 6 × 9-in. rectangular test section of the wind tunnel.

Data were obtained at air velocities from 150 to 350 ft/sec, with

[1] Numbers in brackets designate References at end of paper.

Contributed by the Heat Transfer Division of The American Society of Mechanical Engineers and presented at the ASME-AIChE Heat Transfer Conference, Storrs, Conn., August 9–12, 1959.

Note: Statements and opinions advanced in papers are to be understood as individual expressions of their authors and not those of the Society. Manuscript received at ASME Headquarters, April 30, 1959. Paper No. 59—HT-3.

Nomenclature

c_p = specific heat at constant pressure
C_p = pressure coefficient, defined as $\frac{p - p_\infty}{p_s - p_\infty}$
d = diameter of circular cylinder
D = major axis of elliptical cylinder
F = spectrum function
h = local heat-transfer coefficient
k = thermal conductivity
M = screen mesh
p = pressure
T = temperature
u = mean velocity, ft/sec, u_∞, free stream velocity
$\overline{u'^2}$ = mean square value of the longitudinal component of the turbulence
x = distance downstream
δ = screen wire diameter
ν = kinematic viscosity
θ = angular position from stagnation point
ω = frequency

stagnation temperatures near 90 deg F and atmospheric stagnation pressure, with heating sufficient to give temperature differences of from 15 to 20 deg F between ribbon surface and stagnation temperature. The results are presented conventionally as pressure coefficients or local free-stream velocity deduced from the surface pressure observations, and heat-transfer coefficients determined from the heat dissipation in the ribbons and the effective temperature difference. These were evaluated directly from the data without correction and the errors due to the omission of the effects of internal conduction and surface radiation are small. They vary with the model and the conditions of observation but as a categorical specification it can be stated that all recovery factors shown are accurate to 2 per cent and heat-transfer coefficients to 5 per cent.

The screens were hardware mesh having the dimensions given in Table 1, where M is the distance in inches between wire centers and δ the wire diameter.

Table 1

Mesh/in., nominal	M (in.)	δ (in.)	M/δ
2	1/2	0.108	4.63
3	11/32	0.062	5.37
4	1/4	0.050	5.00
8	1/8	0.028	4.47
16	1/16	0.013	4.82

These screens were mounted at the end of the nozzle contraction, which was the beginning of the test section, and the leading edges of the models were located at the following distances downstream of the screens: Elliptic cylinder, 9 in.; 1.25-in. cylinder, 8 3/8 in.; 1.87-in. cylinder, 8 in.

Turbulence determinations were made with a Flow Corporation HWB hot-wire system, using a 0.35-mil diameter wire. Total output was determined on a Ballantine Model 320 rms meter and a Hewlett-Packard Model 300A wave analyzer was used for spectral determinations.

Results With the Elliptic Cylinder

Fig. 1 shows the effect of turbulence produced by the insertion of the 2 and 4-mesh screens on the heat transfer from this model, with the magnitudes for clear tunnel operation being shown as the curve which correlated these results in the earlier report [4]. There is apparent from the figure a negligible effect on the free-stream velocity distribution and this is so because of the relatively small change in the character of the small separated region that existed at the end of this model.

Two effects appear in the results for the local heat-transfer coefficient. The value at the stagnation point is increased in the order of 30 per cent and an increase is maintained in diminishing magnitude with increasing distance from the stagnation point. Also, the increased turbulence promoted earlier transition to turbulent flow in the boundary layer, after which it can be seen from the figure that the heat-transfer coefficients are predicted satisfactorily by the Colburn equation, $hs/k = 0.027\ (us/\nu)^{0.8}$. In the case of the elliptic cylinder, it is this change in the point of transition that produces the major effect of the turbulence on the over-all heat transfer. With the turbulent separation, occurring farther downstream than the laminar separation evidenced with clear tunnel operation, the heat-transfer coefficients at the rear of the cylinder are reduced slightly.

Recovery factors are not shown in the figure; insertion of the screens gave values typical of turbulent flow after the indicated transition points, while in the upstream laminar region the magnitudes were unaffected by the insertion of the screens.

Other results of the same general nature, presented elsewhere [5] were obtained with the cylinder at ±6 deg angle of attack. These support the evidence as presented in Fig. 1.

Results With the 1.25-In. Circular Cylinder

The results for the circular cylinder are presented in terms of the pressure coefficient, recovery factor, and correlating group for the heat-transfer coefficient. Here the recovery factor differs, being referred to the upstream rather than to the local velocity. Fig. 2 shows the performance with a clear tunnel, and makes the comparison to values predicted by the method of Seban [6] in the laminar flow region. The correspondence between predicted and measured values is good. Beyond the separation point the rather uncorrelated behavior of the local heat-transfer coefficient is typical for this range of Reynolds numbers, and there the recovery factors decrease continually to a negative value at the rear stagnation point.

Only the 4-mesh screen was used with this cylinder, to give the results shown in Fig. 3 which reveal for this bluff body a more drastic alteration than with the elliptic cylinder of flow and heat-transfer characteristics. The drag is reduced due to an apparent delay in separation until 120 deg and the velocity distribution over the front of the cylinder is slightly altered. In the region of

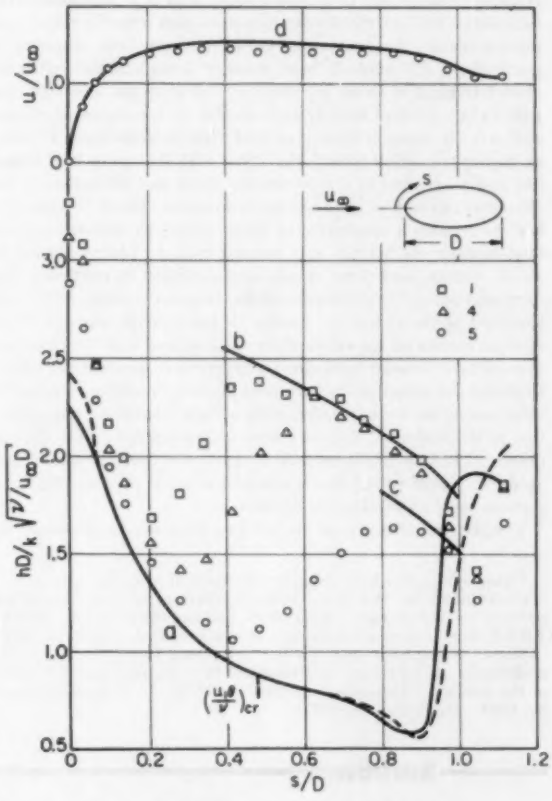

Fig. 1 Heat transfer on the elliptical cylinder

Curves *a*, *d*, Performance with clear tunnel. The dashed line near "a" applies for the higher Reynolds number.

b, *c*, Predictions for turbulent boundary layer flow for the high and low Reynolds numbers.

Run	Mesh	$u_\infty D/\nu$	u_∞, ft/sec
1	2	8.14 × 105	284
4	4	8.14	284
5	4	4.63	160

laminar flow there exists the increase in local heat-transfer coefficient similar to that found on the elliptic cylinder, now more extensive in effect. Remarkably, the recovery factor is unaltered, and is predicted as satisfactorily as before for the laminar flow region, and this laminar region appears to persist at least to 90 deg. There the heat-transfer coefficient rises, but to values less than would be predicted by the Colburn equation, while the recovery factor diminishes to values below any that would be associated with known boundary-layer effects. The behavior here is suggestive of a laminar separation near 90 deg, a transition to turbulent flow and a subsequent reattachment near 110 deg, with a new separation in the region of 120 to 130 deg. The final separated flow is so altered that the low recovery factors typical of the operation in the clear tunnel are no longer obtained.

Fig. 3 also contains curves which define the low speed result of Giedt [1] obtained with a larger cylinder in a different wind tunnel behind a rope net of the same relative geometry as the screen. Similarity is evident except for the difference in pressure coefficient behind the cylinder, an alteration due to wake blockage in the closed tunnel used with the $1^1/_4$-in. cylinder.

Results With the 1.87-In. Circular Cylinder

The 1.87-in. cylinder was examined with an extended range of screen sizes but, because of defects in the model, the results in their totality are somewhat less acceptable than those so far exhibited. This was caused by surface irregularities connected with the relatively larger helix angle of the wider ribbon winding on this cylinder, which irregularities, though being less than 0.001 in., were sufficient to disturb the flow near the separation line, particularly at high speeds. The use of a downstream splitter plate, 0.09 in. thick and extending downstream 12 in. from the rear stagnation point, ameliorated this difficulty in part, and the exigencies of the experimental program at that time dictated the use of this cylinder. The results are pertinent here in being typical at least in the region of laminar flow, to demonstrate further the effect of screen size. Further details on the operation of this cylinder in the clear tunnel are given in Reference [8].

Fig. 4 shows results for this cylinder with the clear tunnel and with the 4-mesh screen, at velocities from 190 to 380 ft/sec and irregularity is demonstrated directly by the pressure coefficient at an angle of 70 deg with clear tunnel operation. Here there is scatter in the results which are themselves averages of a spanwise variation of 10 per cent per inch in the velocity, a variation which was this serious only in this locality. Some of this variation is shown also in the heat-transfer correlation, which in the laminar flow region fails to resolve the performance at different speeds, an effect basically consequent on changes in the distribution of the local free-stream velocity. The two higher speed runs do, however, agree fairly with the prediction, made for the corresponding pressure coefficient. The recovery factors, shown here on a local basis, agree with the expected value of about 0.84. Because of the poor behavior in that region, separation is ill defined but apparently occurred at about 80 deg. Downstream of separation the heat-transfer coefficient varies considerably and the correla-

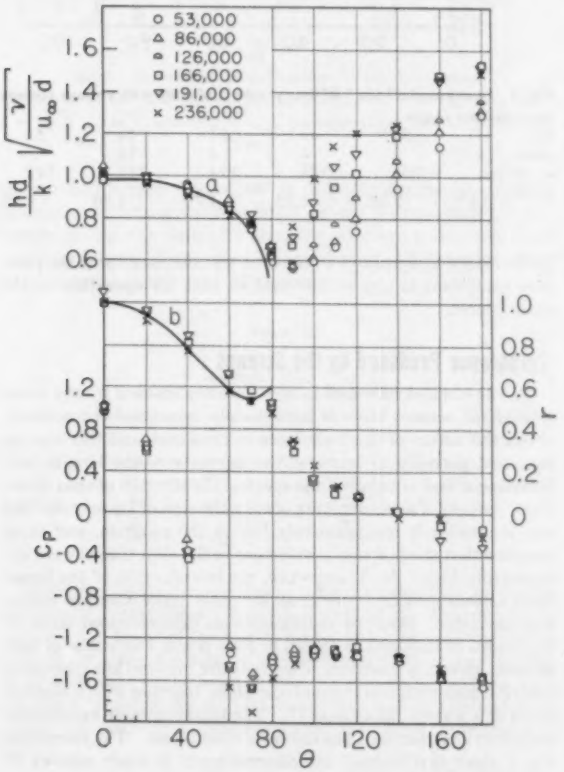

Fig. 2 Results for the 1.25-in. circular cylinder

Reynolds numbers, $u_\infty d/\nu$, are indicated in the figure. Here the recovery factor, r, is taken as $(T_s - T_1)/u_\infty^2/2c_p$.

Curves *a*, Predicted value for laminar boundary layer heat transfer.

b, Recovery factor predicted from a local value of 0.84.

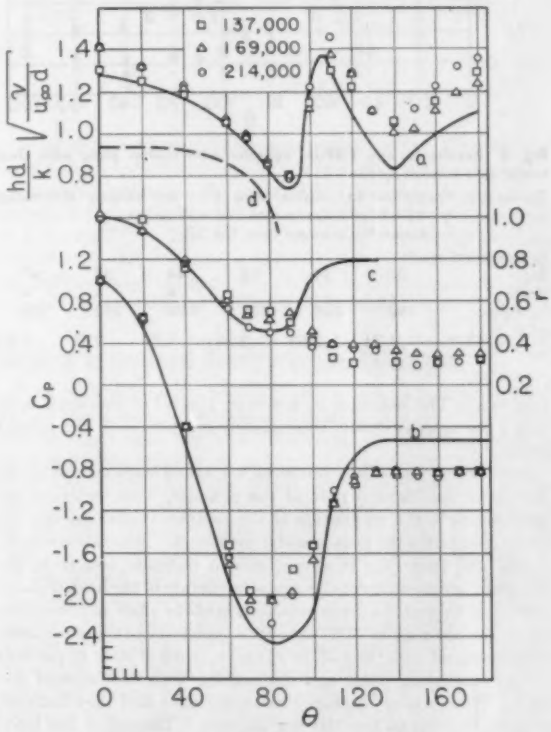

Fig. 3 Results for the 1.25-in. cylinder with 4-mesh screen

The representation is the same as that of Fig. 2.

Curves *a*, *b*, Heat-transfer and pressure coefficients from Giedt [1], for cylinder downstream of rope net at a Reynolds number of 170,000.

c, Predicted value of the recovery factor, from a local value of 0.84 for $\theta < 90$ deg and 0.89 for $\theta > 90$ deg.

d, Heat-transfer prediction.

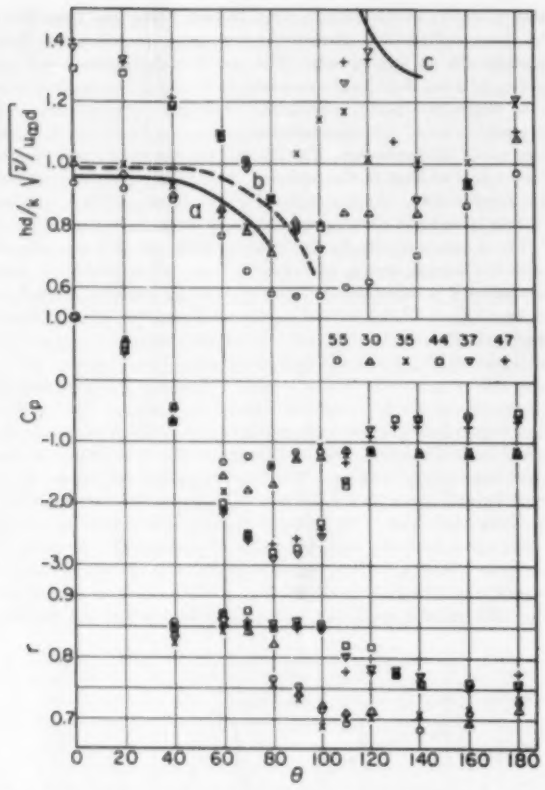

Fig. 4 Results for the 1.87-in. cylinder with splitter plate with clear tunnel and 4-mesh screen

Curves a, b, Predictions for laminar flow from the velocity distribution for 280 ft/sec, clear tunnel and with screen.
c, Prediction for turbulent flow, Run 37.

Experimental results						
Run	55	30	35	44	37	47
Mesh	...	...	...	4	4	4
u_∞ ft/sec	192	288	382	194	282	338
$\frac{u_\infty d}{\nu} \times 10^{-5}$	1.71	2.50	3.24	1.71	2.50	2.80

tion fails. The behavior is, however, typical of this system, in which the separated flow is ultimately reattached to the splitter plate.

Insertion of the screen produced a marked stabilization of the flow over the forward part of the cylinder, with resultant improvements in the correlation of the pressure coefficient and the group containing the heat-transfer coefficient. Separation was retarded and there was in consequence a sufficient change in the pressure coefficient to require a new prediction of the heat-transfer coefficient to enable a proper evaluation of the effect of turbulence in the laminar region. The increase is seen to be of the same order as experienced with the 1.25-in. cylinder, being of 30 to 40 per cent at the stagnation point and diminishing with downstream distance. The recovery factors remain the same and they indicate laminar flow up to the 100 deg position. Thereafter the heat-transfer coefficient increases and the recovery factor decreases in a way that suggests flow separation rather than the occurrence of any turbulent flow.

Fig. 5 shows additional results for the forward region of this cylinder, to illustrate primarily the effect of changing the screen size. There is little trend with screen size, except that the results for the 16-mesh screen are substantially closer to the clear tunnel

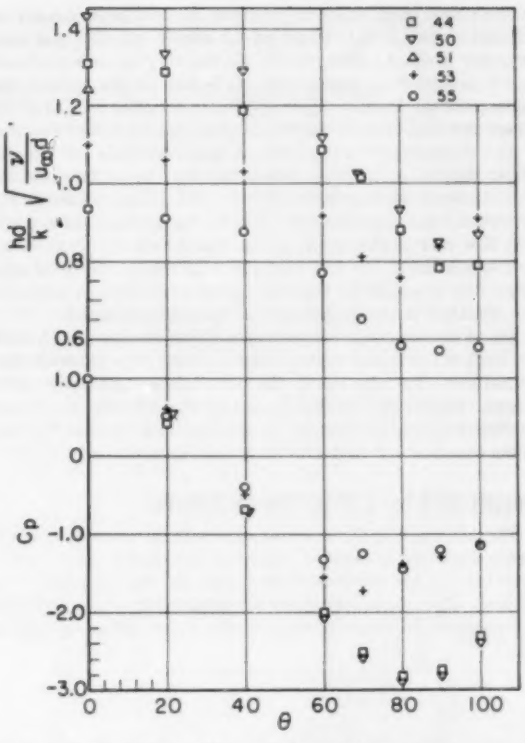

Fig. 5 Heat transfer from 1.87-in. cylinder and plate with various screens

Experimental results					
Run	50	44	51	53	55
Mesh	2	4	8	16	...
u_∞ ft/sec	260	194	194	195	192
$\frac{u_\infty d}{\nu} \times 10^{-5}$	2.25	1.70	1.70	1.70	1.70

performance with respect to the heat transfer, and for it the pressure coefficient is almost identical to that for operation in the clear tunnel.

Turbulence Produced by the Screens

To the obvious increases in heat transfer realized by the insertion of the screens there is immediately associated the question about the nature of the turbulence so produced, and this was determined partially in terms of the intensity of the longitudinal component and in terms of the spectral distribution of that quantity. Adequate measurements of even the first of these quantities was realized only comparatively late in the program, and these revealed that the turbulent intensities in the clear tunnel were unexpectedly high. In consequence, the introduction of the larger mesh screens provided very small increases in the observed turbulent intensity. Spectral determinations demonstrated some of the causes of this, and as shown in Figs. 6 and 7 in terms of normalized spectrum functions, they indicate unusual low frequency contributions with clear tunnel operation, together with a discrete input at a wave number near 17. The source of these exceptional turbulent contributions has not been established. The spectra in Fig. 7 show that at least the discrete input at wave number 17 was eliminated by the screens, though the low wave number energy in part remained.

The intensities presented in Table 2 are to be viewed in this regard, where as a specific example the introduction of the 4-mesh screen led to turbulent intensities of the same magnitude as given

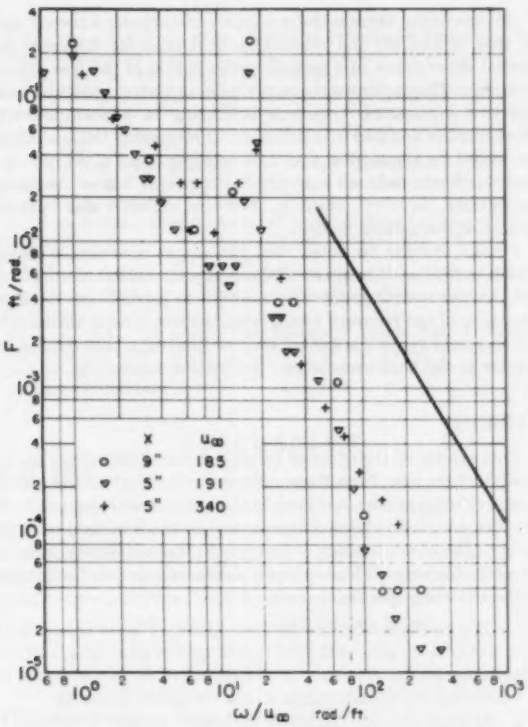

Fig. 6 Normalized power spectra for the clear tunnel

The line shown is a reference line having a slope of $-5/3$. The ordinate is $F = \overline{[u'^2]}_{u_\infty} / \overline{[u'^2]}$, where $\overline{[u'^2]}_{u_\infty}$ is the intensity per unit wave number.

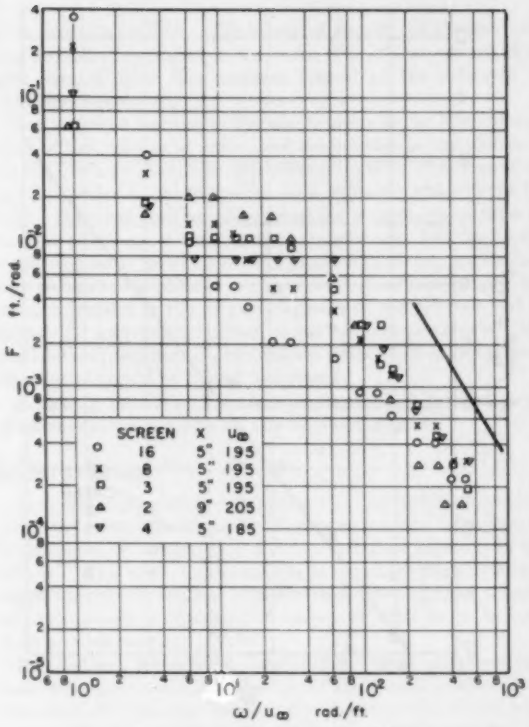

Fig. 7 Normalized power spectra for various screens

by the clear tunnel. As a contrast to emphasize the difference in intensities at higher wave numbers, Table 2 contains also a few values giving the intensity above an arbitrarily selected wave number of 40 and these show the substantial and expected effect of the screens in this spectral region.

Table 2

	Intensity $100\,\overline{u'^2}/u_\infty^2$			for $\frac{\omega}{u_\infty} > 40$	
Total Speed, ft/sec	150	250	340	190	340
Clear	1.5	1.0	0.90	0.10	0.07
4 mesh	1.6	1.1	1.0	0.94	
3	2.0	1.6	1.4	1.0	
2	3.3	2.6	1.0	1.0	

While the intensities existing in the clear tunnel are subject to no absolute comparison, those produced by the screens can be appraised in terms of the known results obtained at lower speeds behind rod grids of similar relative spacing. This is done in Fig. 8, to show that at the lower speeds the expected intensities were attained, while at the highest speeds the values attained were much too low. It is estimated that this latter difficulty was associated with possibly inadequate compensation, whereby the energy at the higher wave numbers was inadequately sampled.

Another appraisal of the screen data is possible through comparison of the scale with the mesh size, with the scale determined as $L = (\pi/2)F(0)$. Because of the low frequency energy that was still existent with the screens, the "zero" value is estimated from the flat portion of the spectra, with the results shown in Table 3. The values of scale are of the order of the mesh size.

Relation of the Heat Transfer to the Turbulence

It is evident from the results that the heat transfer is affected by the free stream turbulence in a number of ways. There is a definite effect upon the heat transfer to the laminar boundary layer, upon the point of transition and extent of the subsequent flow, possibly upon the point of separation and certainly upon the character of the separated flow and the region of the body adjacent hereto. The cumulative effect of each of these depends upon their relative importance on the particular body form considered, as can be assessed, for instance, by comparing the present results for the elliptical and circular cylinders. Of the individual effects the increase in the heat-transfer coefficient and invariability of the recovery factor of the laminar boundary-layer flow are phenomenologically the most definite in the present results and the relatively well-known behavior of the heat transfer in this region enables a more specific appraisal of the effect of increase in the turbulence level.

Table 3

Screen mesh	2	3	4	8	16	Clear
M inches	0.50	0.34	0.25	0.12	0.07	
F("0")ft/rad	0.017	0.10	0.008	0.005	0.002	> 0.20
L inches	0.32	0.20	0.15	0.10	0.04	> 3.8

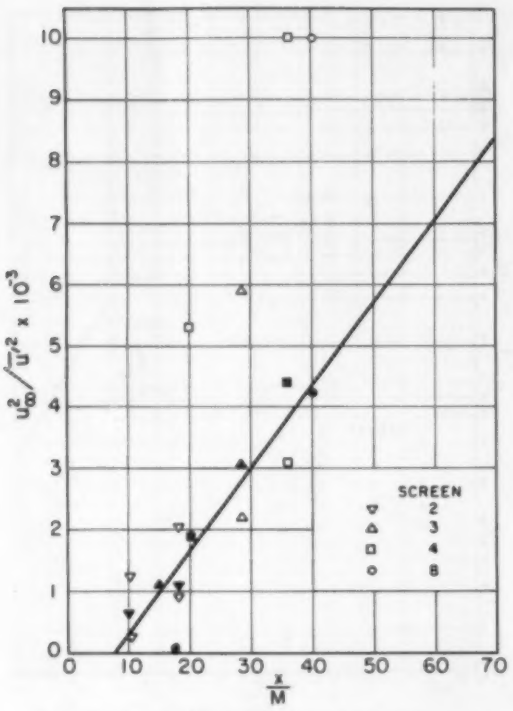

Fig. 8 Turbulence levels for various speeds and positions

The results are mostly for three speeds, of the magnitudes 145, 190, and 340 ft/sec. At any position the results for the intermediate speed are distinguished by solid points and the results for the higher and lower speed are open points, respectively, above and below the solid points. Here the distance x is the distance downstream of the screen position. The line is Batchelor's [7] specification for $M/\delta = 5.5$.

A uniform effect of the introduction of the screens was an increase in the heat transfer in the region of laminar flow. This was a maximum at the stagnation point and diminished with increasing distance downstream, to suggest a possible strong dependence upon pressure gradient. There is a variable sensitivity to turbulence level, with a slight increase over the clear tunnel value providing an increase of the order of 30 per cent in the coefficient at the stagnation point, with additional increases in turbulence providing only slight additional increases in the heat transfer. The failure to make this relation quantitative is an unfortunate aspect of the present result which is due, as already noted, to the abnormally high total intensity of clear tunnel operation. This appears to be due primarily to low frequency components which apparently exercised no influence on the laminar flow, so that inferentially some special spectral dependence is also anticipated for the ultimate rationalization of the increase in the heat-transfer coefficient which is realized by the insertion of the screens.

Finally, there arises the question of theoretical explanation of the increase, for which two general arguments might equally apply. It has been suggested that Görtler type instability might occur near the stagnation point where the onstream flow turns in a concave way to pass over the body surface. The wave length of such an instability would be of the order of 10 momentum thicknesses, which for the operating conditions embraced by these results would be from 0.04 to 0.10 in., at least of the order of what might be expected as a scale produced by the screens, though certainly not by the clear tunnel. In this sense such oscillations are a possibility.

Alternatively, there is the possibility of applying a theory such as that of Lin [8] and accounting in it both for temporal and spatial dependence of a periodic perturbation of the free stream velocity. This indicates that a periodic oscillation gives rise to an effective momentum transport increasing in importance with wave number and also with intensity. Presumably the heat transfer would be augmented also, but considerations along this line really indicate only an increased influence of higher frequency oscillations, an effect which is, of course, inferred also from the nature of the present results.

Finally, it must be noted that the as yet unavailable theory which would be descriptive of the presently exhibited effects on the laminar boundary layer would need to predict also the independence of the recovery factor from the free-stream turbulence, which would require a special kind of similarity between the increases in the heat-transfer and the friction coefficients.

Summary

This exhibit of the effect of screen-produced turbulence on the local heat transfer from three different cylindrical bodies reveals varied effects, due to alterations in the viscid flow which produced changes both in its local character and in the flow field over the body. The over-all effect of increase in the turbulence is an increase in the over-all heat-transfer coefficient, due to the totality of the following specific changes.

1 The coefficient for the laminar boundary layer is increased, with a maximum gain at the point of largest pressure gradient and a minimum at the smallest. The local recovery factor, however, is unaffected by the alteration of the turbulent intensity.

2 As expected, the transition Reynolds number is reduced to lower values, but the results for the elliptical cylinder indicate no effect of the turbulence on the heat transfer to the region of turbulent boundary layer flow.

3 The results from the circular cylinders reveal no effect on the separation point per se but the alteration of the wake flow is sufficient to alter substantially the position of separation by changes in the free-stream velocity distribution.

4 If the flow remains laminar at separation, as it apparently did on the 1.25-in. circular cylinder, then the increase in free stream intensity promotes earlier transition in the separated region, with probable reattachment before a final separation. This, of course, reduces the drag in the classic effect whereby bodies of this type have been used as turbulence indicators. The great attendant alteration of flow conditions in the rear of the cylinder alters completely the distribution of local heat-transfer and recovery factor in such a complicated way as to be discerned only by observation of the results as pictured here. Of the many effects a noteworthy one is the complete elimination at the rear of the cylinder of the low recovery factors that are characteristic of subcritical flow.

Acknowledgment

A major portion of this work was accomplished under the sponsorship of the United States Air Force, under AF 33(616)-348 and because of the duration of the effort there were many participants. Among them special mention is due to A. Levy, A. Emery, P. Gildea, and D. Doughty.

References

1 W. H. Giedt, "Effect of Turbulence Level of Incident Air Stream on Local Heat Transfer and Skin Friction on a Cylinder," *Journal of Aeronautical Sciences*, vol. 18, 1951, pp. 725–730, 766.

2 J. Kestin and P. Maeder, "Influence of Turbulence on Transfer of Heat From Cylinders," National Advisory Committee for Aeronautics, TN 4018, 1957.

3 K. Sato and B. H. Sage, "Thermal Transfer in Turbulent Gas Streams—Effect of Turbulence on Macroscopic Transport From Spheres," TRANS. ASME, vol. 80, 1958, p. 1380.

4 R. Drake, R. Seban, D. Doughty, and S. Levy, "Local Heat Transfer Coefficients on the Surface of an Elliptical Cylinder, Axis Ratio 1:3, in a High Speed Air Stream," TRANS. ASME, vol. 75, 1953, p. 1291.

5 R. Seban, "The Effect of Free Stream Turbulence on the Heat Transfer From Cylinders," Wright Air Development Command, USAF, TR-57-480, 1957.

6 R. A. Seban, "Heat Transfer to Laminar Boundary Layers With Variable Free-Stream Velocity," TRANS. ASME, vol. 79, 1957, p. 1545.

7 G. Batchelor and A. Townsend, "Decay of Isotropic Turbulence in the Initial Period," *Proceedings of the Royal Society*, series A, vol. 193, p. 539.

8 C. C. Lin, "Motion in the Boundary Layer With a Rapidly Oscillating External Flow," presented at the Ninth International Congress of Applied Mechanics, Brussels, 1956, General Electric Company GER-1355.

DISCUSSION

B. H. Sage[2]

This paper represents an additional contribution to the growing background of information concerning the influence of grid-induced turbulence upon the local thermal transfer from cylinders. Apparently an important difficulty in obtaining satisfactory agreement between different investigators is the lack of understanding of the details of the turbulent degradations taking place in the wake of a grid system. The author appears to recognize this, and the information portrayed in Fig. 8 illustrates some of the difficulties in relating turbulence level as measured with a hot wire anemometer to the geometry of the screen or grid for a range of flow conditions. The agreement with the work of Giedt [1] is as good as should be expected, and the scatter of the experimental points in the after portion of the cylinder is typical for such measurements.

The author is to be commended for his frankness in regard to the inadequacy of the data on the 1.87-in. cylinder. This laboratory also has found that small surface irregularities cause unusually large variations in the thermal transfer, particularly in the after part of a cylinder. The increased stability of the flow pattern around the cylinder in the wake of a grid as compared to open channel shear flow appears typical of the behavior of cylinders and spheres.

The indicated increase in thermal transfer in the forward segment of the cylinder as a result of the increase in turbulence in the wake of a grid is not greatly different in total effect from that found by other investigators for both cylinders and spheres [1, 2, 3]. However, this laboratory found a progressive increase in the rate of change of local thermal transfer with increase in the apparent level of turbulence. The markedly differing trends thus indicated as to the effect of apparent level of turbulence upon the thermal transfer in the forward segment of the cylinder and in spheres [3] may well be related to the microscopic aspects of the degradation phenomena in the wake of grids which at the present time do not appear to be well understood.

In closing, the author is to be complimented on bringing to an effective conclusion a difficult experimental program.

[2] Chemical Engineering Laboratory, California Institute of Technology, Pasadena, Calif.

Author's Closure

Professor Sage correctly indicates the question that remains about the relation between the increase in the local heat transfer in the region of laminar flow and the turbulent intensity of the stream. In his work, results have been obtained which indicate a simple functional relation between the increased heat transfer and the turbulent intensity. A survey of those given here reveals no such relation.

For example, if results at the stagnation point are chosen and these are represented as a function of the intensity, there is an indication of a trend of increasing heat-transfer coefficient with increased turbulence level. Considerable scatter exists and the question of a relation is confounded by the abnormally high turbulence level of the "clear" tunnel. Removal of this contradiction by using intensities over a wave number of 40, as indicated by the last columns in Table 2, does not minimize the scatter of those results representing increases of the order of 30 per cent in the heat-transfer coefficient. Hence, as indicated in the paper, the present results establish no functional relationship in this regard and additional experimental results are needed to clarify this aspect of the problem.

Heat Transfer to Fully Developed Laminar Flow in a Circular Tube With Arbitrary Circumferential Heat Flux

W. C. REYNOLDS
Assistant Professor,
Department of Mechanical Engineering,
Stanford, Calif. Assoc. Mem. ASME

A solution is presented for fully developed laminar heat transfer in a circular tube with arbitrary circumferential heat flux. Examples included indicate that the influence of circumferential heat-flux variation on wall temperatures can be quite significant and provide some insight into the nature of the effects. The analysis allows calculation of wall temperatures for any arbitrary peripheral heat-flux variation for fully developed laminar flow under the restriction of constant axial heat input.

Introduction

THE CIRCULAR TUBE has been the subject of a considerable amount of heat-transfer analysis and experimentation. The theories are now sufficiently advanced that it is possible to predict the heat-transfer performance in either laminar or turbulent flow, with arbitrary axial wall temperature [1, 2][1] or heat flux [3, 4]. The essential restrictions of these theories are: 1 That the velocity profile be fully established at the entrance of the tube; 2 that the fluid properties be constant; and 3 that the temperature field is radially symmetric, i.e., the heat flux and wall temperature do not vary around the circumference of the tube. For the special case of constant wall temperature, the effects of a developing velocity profile have been investigated [5, 6]. The effect of fluid property variation has also been studied [7]. The present paper treats fully established laminar flow in a circular tube with constant axial heat input but variable circumferential heat flux. Although restricted to a particularly simple case, the present analysis provides some general insight into the nature and magnitude of the effects of circumferential heat-flux variation.

The method of analysis is as follows: First, a solution is obtained for the case of a tube with constant heat flux over a portion of its circumference, insulated over the remainder; reduction of this solution to the limiting case of heating over a differential segment of circumference leads to a superposition kernel which in turn allows the arbitrary circumferential flux problem to be handled. Throughout, both the temperature and velocity profiles are assumed to be fully established, the heat flux is taken as constant in the axial direction, fluid properties are assumed constant, and viscous dissipation is neglected. An example illustrates how circumferential heat-flux variations might influence the wall temperatures in a nuclear reactor.

[1] Numbers in brackets designate References at end of paper.

Contributed by the Heat Transfer Division of THE AMERICAN SOCIETY OF MECHANICAL ENGINEERS and presented at the ASME-AIChE Heat Transfer Conference, Storrs, Conn., August 9–12, 1959.
NOTE: Statements and opinions advanced in papers are to be understood as individual expressions of their authors and not those of the Society. Manuscript received at ASME Headquarters, May 11, 1959. Paper No. 59—HT-13.

Analysis

Under the previously mentioned assumptions, application of an energy balance and suitable rate equations to a differential element of the fluid leads to the following governing differential equation for the fluid temperature [8]:

$$\frac{\partial^2 t}{\partial r^2} + \frac{1}{r}\frac{\partial t}{\partial r} + \frac{1}{r^2}\frac{\partial^2 t}{\partial \theta^2} = \frac{V}{\alpha}\frac{\partial t}{\partial x} \tag{1}$$

The velocity profile may be shown to be [8]

$$V = 2V_m(1 - r^{*2}) \tag{2}$$

If the temperature profile is fully established, then the rate of change of temperature with length must be the same at every point, and therefore

$$\frac{\partial t}{\partial x} = \frac{dt_m}{dx} = \text{const} \tag{3}$$

If the heat input is constant in the axial direction, then an energy balance dictates that, for the tube heated as shown by Fig. 1,

$$\pi r_0^2 \rho V_m c_p \frac{dt_m}{dx} = 2r_0\beta q'' \tag{4}$$

Again using the fact that the temperature profile is fully established, one can introduce the temperature difference as dependent variable,

$$\Delta t(r, \theta) = t(r, \theta, x) - t_m(x) \tag{5}$$

Nomenclature

A = flow area, ft²
c_p = specific heat at constant pressure, Btu/lb deg F
C_n = Fourier expansion coefficients
h = local convective heat-transfer coefficient, Btu/hr ft² deg F
k = thermal conductivity of fluid, Btu/hr ft deg F
Nu = Nusselt number, Nu = $2hr_0/k$
r = radius from tube axis, ft
r_0 = radius of tube, ft
r^* = r/r_0
t = temperature, deg F
t_m = mixed mean fluid temperature, deg F
t_w = local wall temperature, deg F
Δt = $t - t_m$, deg F
Δt_w = $t_w - t_m$, deg F
V = fluid velocity, ft/sec
V_m = mean fluid velocity, ft/sec
x = distance along tube, ft
α = thermal diffusivity of fluid, $2\alpha = k/\rho c_p$, ft²/hr
β = half angle of heated segment, radians
λ_n = eigenvalues
ρ = fluid density, lb/ft³
θ, ω = angle in polar co-ordinate system

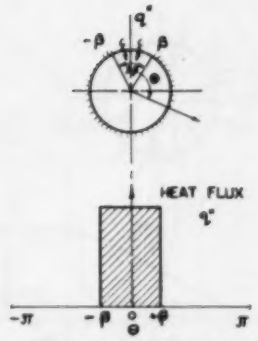

Fig. 1 Tube with heated segment centered at $\theta = 0$ deg

Equation (1) may now be written as follows:

$$\frac{\partial^2 \Delta t}{\partial r^{*2}} + \frac{1}{r^*}\frac{\partial \Delta t}{\partial r^*} + \frac{1}{r^{*2}}\frac{\partial^2 \Delta t}{\partial \theta^2} = a(1 - r^{*2}) \tag{6}$$

Here

$$a = 4\beta r_0 q''/\pi k \tag{7}$$

For the problem of Fig. 1, Equation (6) is to be solved subject to the boundary conditions

$$k\left(\frac{\partial t}{\partial r}\right)_{r=r_0} = q'' \qquad -\beta \le \theta \le +\beta \tag{8a}$$

$$k\left(\frac{\partial t}{\partial r}\right)_{r=r_0} = 0 \qquad \beta < \theta < 2\pi - \beta \tag{8b}$$

The analysis is simplified by the change of dependent variable,

$$\Delta t = F(r^*, \theta) + a\left(\frac{r^{*2}}{4} - \frac{r^{*4}}{16}\right) \tag{9}$$

Substituting (9) in (6) one sees that the variable F must satisfy Laplace's equation,

$$\frac{\partial^2 F}{\partial r^{*2}} + \frac{1}{r^*}\frac{\partial F}{\partial r^*} + \frac{1}{r^{*2}}\frac{\partial^2 F}{\partial \theta^2} = 0 \tag{10}$$

F must also satisfy the boundary conditions,

$$\left(\frac{\partial F}{\partial r^*}\right)_{r^*=1} = \frac{q''r_0}{k}\left(1 - \frac{\beta}{\pi}\right) \qquad -\beta \le \theta \le +\beta \tag{11a}$$

$$\left(\frac{\partial F}{\partial r^*}\right)_{r^*=1} = -(q''r_0/k)(\beta/\pi) \qquad \beta < \theta < 2\pi - \beta \tag{11b}$$

Equation (10) may be solved by separation of variables. Let $F(r^*, \theta) = R(r^*)\cdot T(\theta)$. Under this assumption, the functions R and T must satisfy the following equations:

$$R'' + (1/r^*)R' - \frac{1}{r^{*2}}\lambda^2 R = 0 \tag{12a}$$

$$T'' + \lambda^2 T = 0 \tag{12b}$$

Equations (12) have the solutions

$$R = A_1 r^{*\lambda} + A_2 r^{*-\lambda} \tag{13a}$$

$$T = B_1 \cos \lambda\theta + B_2 \sin \lambda\theta \tag{13b}$$

Because of symmetry,

$$\left(\frac{\partial \Delta t}{\partial \theta}\right)_{\theta=0} = 0 \tag{14a}$$

$$\left(\frac{\partial \Delta t}{\partial \theta}\right)_{\theta=\pi} = 0 \tag{14b}$$

These symmetry conditions lead to

$$B_2 = 0 \tag{15a}$$

$$\sin \lambda\pi = 0 \tag{15b}$$

Therefore the eigenvalues are simply integers,

$$\lambda = 0, 1, 2, \ldots n, \ldots \tag{16}$$

Moreover, since the temperature must be finite at the tube center,

$$A_2 = 0 \tag{17}$$

Equation (10) is linear, and therefore the linear combination of an infinite number of solutions may be taken in order to satisfy the boundary conditions (1). The solution for F then takes the form

$$F = C_0 + \sum_1^\infty C_n r^{*n} \cos n\theta \tag{18}$$

The boundary conditions are to be applied to the derivative and lead to the evaluation of the expansion coefficients C_n in the usual Fourier manner. One finds the following:

$$C_n = \left(\frac{2}{n^2\pi}\right)\left(\frac{q''r_0}{k}\right)\sin n\beta \qquad n = 1, 2, \ldots \tag{19}$$

The solution now takes the form

$$\Delta t = a\left(\frac{r^{*2}}{4} - \frac{r^{*4}}{16}\right) + C_0 + \sum_1^\infty \frac{2q''r_0}{n^2\pi k}\sin n\beta \cdot r^{*n} \cdot \cos n\theta \tag{20}$$

The single remaining unknown, C_0, must be such that the mixed mean temperature is

$$t_m = \frac{1}{AV_m}\int_A Vt\,dA \tag{21}$$

Equation (21) may be written as

$$\int_0^1 \int_0^{2\pi} (1 - r^{*2})r^* \Delta t\, d\theta\, dr^* = 0 \tag{22}$$

When (20) is used to evaluate the integral of (22), the cosine terms all drop out in the integration over θ. The remaining terms may be readily integrated, and one finds for C_0

$$C_0 = -14\beta/48\pi \tag{23}$$

The wall-temperature difference, $\Delta t_w(\theta) = \Delta t(r_0, \theta)$, may now be expressed as (for problem of Fig. 1)

$$\Delta t_w(\theta)/(q''2r_0/k) = \frac{11}{48}\frac{\beta}{\pi} + \sum_1^\infty \frac{1}{n^2\pi}\sin n\beta \cdot \cos n\theta \tag{24}$$

Note that this is simply the inverse of the local Nusselt number, and that for $\beta = \pi$, or constant circumferential heat flux, the Nusselt number has the familiar value of $48/11 = 4.364$. This completes the first part of the analysis.

We next consider the temperature distribution produced in a tube heated as shown by Fig. 2. The tube is insulated around its periphery, except for θ between ω and $\omega + \Delta\omega$, where the tube is heated with a constant flux $q''(\omega)$. The solution for this problem may be obtained by a simple shift of axes. We will denote the solution to this problem by

$$\delta\Delta t(r, \theta; \omega)$$

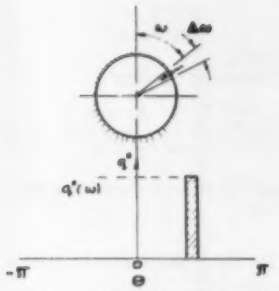

Fig. 2 Tube with heated segment at $\theta = \omega$

which denotes a small temperature difference induced by heating between ω and $\omega + \Delta\omega$ at a rate $q''(\omega)$. The wall temperature for this case is, from Equation (24),

$$\delta\Delta t_w(\theta;\ \omega) = \frac{q''(\omega)2r_0}{k}\left\{\frac{11}{48}\ \frac{\Delta\omega}{2\pi} + \sum_{n=1}^{\infty}\frac{1}{n^2\pi}\sin\left(\frac{n\Delta\omega}{2}\right)\cdot\cos n\left(\theta - \omega - \frac{\Delta\omega}{2}\right)\right\} \quad (25)$$

This solution can be used to obtain the solution for the temperature distribution in the tube heated at different rates over *several* segments of its circumference, as shown by Fig. 3.

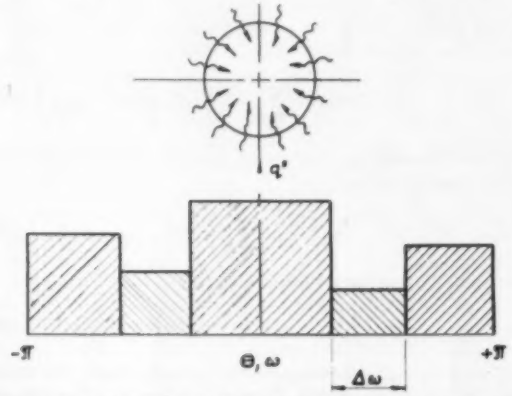

Fig. 3 Tube with different heat fluxes over different segments

Imagine that only the m^{th} segment was heated at $q''(\omega_m)$, and the remainder of the tube was insulated. The temperature distribution would be

$$\delta_m t(r,\ \theta,\ x;\ \omega_m)$$

Since the governing differential equation (1) is *linear* in temperature, the sum of M such solutions is also a solution, and hence

$$t(r,\ \theta,\ x) = \sum_{m=1}^{M}\delta_m t(r,\ \theta,\ x;\ \omega_m) \quad (26)$$

is *also* a solution of the differential equation. Moreover, such a solution satisfies the boundary conditions that

$$k\left(\frac{\partial t}{\partial r}\right)_{r=r_0} = q''(\theta) \quad (27)$$

where $q''(\theta)$ represents the heat flux at any point θ prescribed as shown in Fig. 3. Since (26) satisfies both the differential equation and the imposed boundary conditions, it must represent the solution to the problem of Fig. 3. The wall temperature is therefore given by

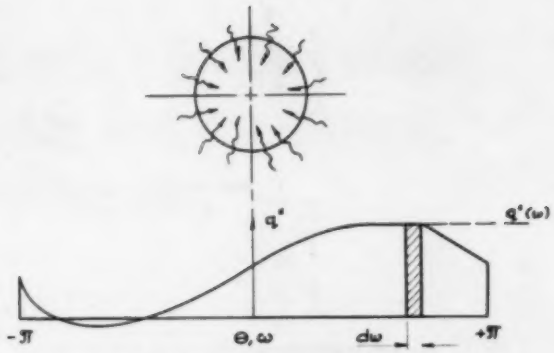

Fig. 4 Tube with arbitrary heat flux

$$\Delta t_w(\theta) = \sum_{m=1}^{M}\delta_m\Delta t_w(\theta;\ \omega_m) = \sum_{m=1}^{M}\left\{\frac{q''(\omega_m)2r_0}{k}\left[\frac{11}{48}\ \frac{\Delta\omega_m}{2\pi} + \sum_{n=1}^{\infty}\frac{1}{n^2\pi}\sin\left(\frac{n\Delta\omega_m}{2}\right)\cos n\left(\theta - \omega_m - \frac{\Delta\omega_m}{2}\right)\right]\right\} \quad (28)$$

The problem of completely arbitrary circumferential heat flux, shown in Fig. 4, can be solved simply by letting $\Delta\omega$ be infinitesimal, $d\omega$. The summation over the elemental segments $d\omega$ in Equation (28) is then replaced by an integral around the circumference and the solution reduces to

$$\Delta t_w(\theta) = \int_{\omega=0}^{2\pi}\frac{q''(\omega)2r_0}{k}\left[\frac{11}{48} + \sum_{n=1}^{\infty}\frac{\cos n(\theta - \omega)}{n}\right]\frac{d\omega}{2\pi} \quad (29)$$

The infinite series appearing in Equation (29) has the sum [9]

$$\sum_{1}^{\infty}\frac{\cos n(\theta - \omega)}{n} = -\ln\left\{2\sin\frac{\theta - \omega}{2}\right\} \quad (30)$$

We now denote an *integration kernel*, $g(\theta;\ \omega)$, by

$$g(\theta;\ \omega) = \frac{11}{48} + \sum_{n=1}^{\infty}\frac{\cos n(\theta - \omega)}{n} \quad (31a)$$

or alternatively, using (30)

$$g(\theta;\ \omega) = \frac{11}{48} - \ln\left\{2\sin\frac{\theta - \omega}{2}\right\} \quad (31b)$$

It then follows that the wall-temperature distribution is given by

$$\Delta t_w(\theta) = (2r_0/k)\int_0^{2\pi}q''(\omega)g(\theta;\ \omega)\frac{d\omega}{2\pi} \quad (32)$$

Equation (32) represents the general solution to the arbitrary circumferential flux problem. Knowing the heat-flux variation around the circumference, $q''(\theta)$, one need only perform the integration of (32) to evaluate the wall-temperature distribution. In some cases the series form of the integration kernel (31*a*) will be easier to use. The closed form expression of the kernel (31*b*) makes numerical integration extremely easy in problems where exact integration is not possible.

It should be noted that the kernel has a singularity at the point $\theta - \omega$. At this point the series of (31*a*) behaves like $1/n$, and therefore diverges. However, the integrated series behaves

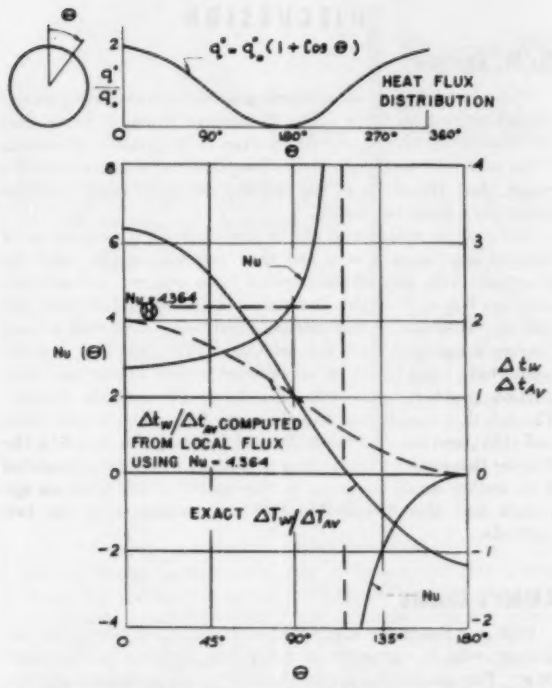

Fig. 5 Illustration of effect of circumferential heat-flux variation on fully established laminar heat transfer

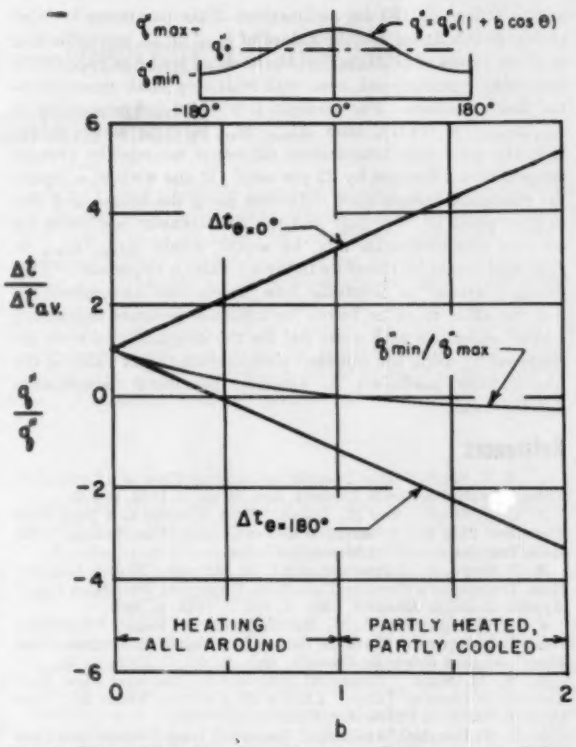

Fig. 6 Effect of heat-flux depression on wall-temperature variation

like $1/n^2$, which converges, and therefore the wall temperature, as expressed by (32), is finite. At all other points the convergence is absolute.

Examples

Constant Heat Flux. For the special case of constant heat flux, $q''(\theta) = q_0'' = \text{const}$, and the integration of (32) yields

$$\Delta t_w(\theta) = (2r_0 q_0''/k)(11/48) = \text{const} \tag{33}$$

The Nusselt number for constant heat flux is then equal to [7]

$$\text{Nu} = 48/11 = 4.364 \text{ (constant heat input)} \tag{34}$$

Cosine Circumferential Flux Distribution. Consider the heat-flux distribution shown at the top of Fig. 6,

$$q''(\theta) = q_0''(1 + b\cos\theta) \tag{35}$$

This might represent the sort of circumferential flux distribution found in a nuclear reactor. For this example the most convenient form of the integrating kernel is the series form (31*a*). From (32) the wall-temperature distribution is given by

$$\Delta t_w(\theta) = \int_0^{2\pi} q_0''(1 + b\cos\omega)(2r_0/k) \left[\frac{11}{48} + \sum_1^{\infty} \frac{\cos n(\theta - \omega)}{n}\right] \frac{d\omega}{2\pi} \tag{36}$$

Performing the indicated integrations one finds

$$\Delta t_w(\theta) = (q_0''2r_0/k)\left(\frac{11}{48} + b\frac{\cos\theta}{2}\right) \tag{37}$$

The local Nusselt number can be calculated from the local heat-flux and temperature difference,

$$\text{Nu}(\theta) = (1 + b\cos\theta)\Big/\left(\frac{11}{48} + b\frac{\cos\theta}{2}\right) \tag{38}$$

The results of this example for $b = 1$ are shown by Fig. 5. Note that the local Nusselt number varies substantially from the constant heat-input value previously determined as 4.364. This indicates a substantial variation of the heat-transfer coefficient around the tube periphery. The Nusselt number is *infinite* at the point where the wall temperature equals the mean fluid temperature, and is *negative* where the wall temperature is less than the mean temperature. The ratio of the local wall-temperature difference to the average temperature difference Δt_{avg} is shown in Fig. 5. Note that the local temperature difference is more than *three times* the average difference for $\theta = 0$! This indicates the profound influence of the circumferential heat-flux variation. It might be thought that the local heat flux, together with the heat-transfer coefficient from the constant heat-input solution, could be used to estimate the wall-temperature variation. But as the comparison of Fig. 5 shows, this is not very satisfactory because the flux variation markedly alters the heat-transfer coefficient.

Fig. 6 shows the extreme temperature differences which occur

at $\theta = 0$ deg and 180 deg as functions of the parameter b.—Also shown in this figure are the values of q_{min}''/q_{max}'' corresponding to given values of b. Note that the effect of heat-flux variation is surprisingly pronounced, even with relatively small circumferential flux variations. For example, if $b = 0.1$ (corresponding to $q_{min}''/q_{max}'' = 0.817$), then $\Delta t_{max}/\Delta t_{avg} = 1.22$, which means that the maximum temperature difference exceeds the average temperature difference by 22 per cent! If one were to compute the maximum temperature difference using the actual heat flux at that point ($\theta = 0$ deg) and the heat-transfer coefficient for *constant* circumferential flux, he would obtain $\Delta t_{max}/\Delta t_{avg} = 1.10$, and would be therefore in error by about 12 per cent. This example serves to illustrate how severe the circumferential flux variation must be before its influence becomes important, and provides one with some feel for the magnitude of error introduced by using the constant circumferential flux value of the heat-transfer coefficient to estimate peripheral temperature distributions.

References

1. S. N. Singh, "Heat Transfer by Laminar Flow in a Cylindrical Tube," *Applied Scientific Research*, sect. A, vol. 7, 1958, p. 325.
2. C. A. Sleicher and M. Tribus, "Heat Transfer in a Pipe With Turbulent Flow and Arbitrary Wall-Temperature Distribution," 1956 Heat Transfer and Fluid Mechanics Institute.
3. R. Siegel, E. M. Sparrow, and T. M. Hallman, "Steady Laminar Heat Transfer in a Circular Tube With Prescribed Wall Heat Flux," *Applied Scientific Research*, sect. A, vol. 7, 1958, p. 386.
4. E. M. Sparrow, T. M. Hallman, and R. Siegel, "Turbulent Heat Transfer in the Entrance Region of a Pipe With Uniform Heat Flux," *Applied Scientific Research*, sect. A, vol. 7, 1958, p. 37.
5. W. M. Kays, "Numerical Solutions for Laminar Flow Heat Transfer in Circular Tubes," TR-No. 20, Contract N6onr 251, Task Order 6, Stanford University, October 15, 1953.
6. R. G. Deissler, "Analysis of Turbulent Heat Transfer and Flow in the Entrance Region of Smooth Passages," NACA TN 3016, October, 1953.
7. W. M. Kays and A. L. London, "Compact Heat Exchangers," National Press, Palo Alto, California, 1955.
8. M. Jacob, "Heat Transfer," vol. 1, John Wiley & Sons, Inc., New York, N. Y., 1949, p. 451.
9. K. Knopp, "Theory and Application of Infinite Series," Blackie and Son, Ltd., London, England, 1928, p. 378.

DISCUSSION

E. M. Sparrow[2]

This paper provides an interesting addition to the heat-transfer literature on pipe flows. The illustrative example shows that circumferential heat-flux variations can be important. However, if the flow were turbulent rather than laminar as assumed in the paper, then the effects of the imposed circumferential variation would very likely be smaller.

The analysis was carried out by first finding the response to an isolated heating at $\theta = \omega$ and then generalizing this result by superposition to provide the response to an arbitrary circumferential heat flux $q''(\theta)$. This is certainly a correct and elegant procedure. However, if this discusser had been faced with solving Laplace's equation (10) for arbitrary $q''(\theta)$, his first impulse would have been to call on his experience with similar heat conduction problems and utilize Fourier series methods directly. The solution would have had the same form as equations (13*a*) and (13*b*), and the coefficients B_{1n} and B_{2n} would be found by the Fourier theorems by integrating $q''(\theta)$. It would be appreciated if the author would comment on the validity of this alternate approach and also discuss the relative advantages of the two methods.

Author's Closure

Professor Sparrow's suggestion is of particular interest to the author, who is currently studying this problem in turbulent flow. For this case it appears that the resulting eigenvalue problem is somewhat simpler to handle for a cosine flux distribution than for the pulse treated in the present paper. Both methods are of course identical in the end result. The difference is merely in the way the convolution notion is employed to reduce the superposition integral to the form of equations (31) and (32).

---

[2] NASA Lewis Research Center, Cleveland, Ohio. Assoc. Mem. ASME. Present address: Professor of Mechanical Engineering, University of Minnesota, Minneapolis, Minn.

Steam Slip—Theoretical Prediction From Momentum Model[1]

S. LEVY

Specialist, Heat Transfer and Fluid Flow, Engineering Development, Atomic Power Equipment Department, General Electric Company, San Jose, Calif. Assoc. Mem. ASME

Theoretical equations governing slip effects in forced circulation of boiling water are derived. The equations indicate that steam slip is dependent upon channel geometry, inlet water velocity, and rate of heat addition. A simplified momentum model is postulated which leads to equal friction and head losses of two phases. The model gives good agreement with available experimental results in horizontal and vertical test sections with and without heat addition at pressures from 12 to 2000 psia. Discussion of the model in terms of nonquasi steady-state unbalances of friction and head losses of the two phases explains experimental deviations from the predictions and the previously noted effects of water inlet velocity. It also gives trends for the effects of channel geometry and rate of heat addition. Application of the simplified model to calculating two-phase pressure drops is included.

Introduction

STEAM AND SATURATED WATER have different properties and cannot be expected to flow at the same velocity in forced circulation boiling systems. Unequal density and viscosity of the two phases usually force the steam to attain a relative velocity or "slip" with respect to the water. Knowledge of this slip velocity is of utmost importance because it determines the density, i.e., driving head, of natural circulation boilers and void distribution or neutron economy of boiling water reactors.

In recent years, considerable information has been accumulated about the density of two phase mixtures. Flinn and Lottes [1],[2] Cook [3], and Marchaterre [2] have measured the density of boiling water in a rectangular channel at pressures between 115 and 600 psia. Egen, Dingee, and Chastain [4] have investigated the same problem at 2000 psia. Additional data have been obtained by other investigators for steam-water mixtures in circular pipes. They include the work of Schwarz [5], Behringer [6], Dengler [7], Schurig [8], Smith and Hoe [9], Isbin, Sher, and Eddy [10], and Larson [11]. Similar information has also been compiled for air-water and air-oil mixtures by Petrick [12], Lockhart and Martinelli [13], Alves [14], Johnson and Abou-Sabe [15], Zmola and Bailey [16], Bergelin and Gazley [17], and Baker [18].

Most of the work to date has, however, been of an experimental nature. Correlation of data has always been empirical and even the widely used predictions of Martinelli and Nelson [19] were obtained by introducing an empirical pressure dependency in the relations proposed in reference [13]. It is proposed herein to theoretically analyze the problems of steam slip in forced circulation of boiling water. The basic equations will first be derived and the most important variables established. Next, a simplified momentum model will be postulated to obtain a theoretical prediction of steam slip and two-phase pressure drop.

Basic Equations

Derivation of Equations. In a boiling water system with heat addition in the direction of flow, each fluid phase satisfies a momentum equation of the Bernouilli type. The equations are derived in the Appendix for an element length dy in the flow direction. They are:

$$dP + \rho_L \frac{V_L dV_L}{g} = \left(\frac{dP}{dy}\right)_{LTP} dy - \rho_L (\sin\theta) dy \qquad (1)$$

$$dP + \frac{1}{gA_G} d(A_G \rho_G V_G^2) + \frac{V_L}{gA_G} d(A_L \rho_L V_L) = \left(\frac{dP}{dy}\right)_{GTP} dy - \rho_G (\sin\theta) dy \qquad (2)$$

Equations (1) and (2) assume that the static pressure drop for

[1] The author wishes to acknowledge the assistance of Dr. R. O. Niemi and E. E. Polomik. Critical discussions with them helped the author formulate changes in the basic equations.

[2] Numbers in brackets designate References at end of paper.

Contributed by the Heat Transfer Division of THE AMERICAN SOCIETY OF MECHANICAL ENGINEERS and presented at the ASME-AIChE Heat Transfer Conference, Storrs, Conn., August 9–12, 1959.

NOTE: Statements and opinions advanced in papers are to be understood as individual expressions of their authors and not those of the Society. Manuscript received at ASME Headquarters, May 4, 1959. Paper No. 59—HT-15.

Nomenclature

- A = cross-sectional area of flow, ft²
- C = heat generation per unit volume of coolant, Btu/hr ft³
- D = pipe diameter or equivalent hydraulic diameter, ft
- f = friction factor, nondimensional
- G = mass flow rate per unit area, lb/hr ft²
- g = gravitational constant, ft/hr²
- h_{fg} = heat of vaporization, Btu/lb
- K = nondimensional grouping
- P = pressure lb/ft²
- V = velocity, ft/hr
- W = mass flow rate, lb/hr
- x = steam quality, nondimensional
- y = distance measured in direction of flow, ft
- α = void content, nondimensional
- β = nondimensional pressure drop difference
- θ = angle of inclination of test section
- ρ = density, lb/ft³
- τ_w = shear stress at wall, lb/ft²
- ψ = frictional plus static pressure, lb/ft²

Subscripts

- e = exit end of heated section
- i = initial value corresponding to $x = 0$
- G = steam or gas
- GTP = steam in two-phase flow
- L = liquid or fluid
- LSP = water alone
- LTP = water in two-phase flow
- 0 = corresponding to 100 per cent water flow
- TP = two-phase mixture

the liquid and gas phase are equal and constant at every cross section and that the boiling system is inclined at an angle θ from the horizontal direction.

Multiplication of Equation (1) by A_L and Equation (2) by A_G and addition yields

$$dP + \frac{1}{gA}\, d[A_G\rho_G V_G^2 + A_L\rho_L V_L^2] = \left(\frac{dP}{dy}\right)_{TP} dy - \left(\rho_L \frac{A_L}{A} + \rho_G \frac{A_G}{A}\right) \sin\theta\, dy \quad (3)$$

The term $\left(\frac{dP}{dy}\right)_{TP}$ represents the two phase frictional drop and is equal to

$$\left(\frac{dP}{dy}\right)_{TP} = \frac{A_L}{A}\left(\frac{dP}{dy}\right)_{LTP} + \frac{A_G}{A}\left(\frac{dP}{dy}\right)_{GTP} \quad (4)$$

Equation (3) is the basic equation proposed by Martinelli and Nelson to calculate steam-water pressure drop. It states that the total pressure drop is made up of a momentum loss (represented by the second term on the left side of the equation) plus a frictional loss and a head loss (given by the last term on the right). Similarly, another important relation can be obtained from Equations (1) and (2) by subtracting one from the other.

$$\frac{1}{g}\{d[A_G\rho_G V_G^2 + A_L\rho_L V_L^2] - A\rho_L V_L dV_L\} = A_G\left[\left(\frac{dP}{dy}\right)_{GTP} - \left(\frac{dP}{dy}\right)_{LTP} + (\rho_L - \rho_G)\sin\theta\right]dy \quad (5)$$

The advantage of writing a momentum equation for each of the phases is now apparent. In addition to the accepted pressure drop relation of Equation (3), there results a second expression, Equation (5), which can be used to predict steam slip.

Equation (5) can be rewritten by substituting the following:

$$\rho_L A_L V_L = GA(1 - x) \quad (6)$$

$$\rho_G A_G V_G = GAx \quad (7)$$

$$\frac{A_G}{A} = \alpha \quad \text{and} \quad \frac{A_L}{A} = 1 - \alpha \quad (8)$$

Equation (5) becomes for ρ_L assumed constant

$$\frac{G^2}{g\rho_L}\, d\left[\frac{(1-x)^2}{(1-\alpha)} + \frac{x^2}{\alpha}\frac{\rho_L}{\rho_G} - \frac{1}{2}\frac{(1-x)^2}{(1-\alpha)^2}\right] = \alpha\left[\left(\frac{dP}{dy}\right)_{GTP} - \left(\frac{dP}{dy}\right)_{LTP} + (\rho_L - \rho_G)\sin\theta\right]dy \quad (9)$$

It is possible to relate the two variables y and x from a heat balance. Assuming thermal equilibrium at any cross section and a heat generation C per unit volume of coolant, one obtains

$$Cdy = Gh_{fg}dx \quad (10)$$

In order to make Equation (9) nondimensional let us introduce the liquid phase pressure drop for the initial flow of 100 per cent water or

$$\left(\frac{dP}{dy}\right)_o = -\frac{f_o G^2}{2gD\rho_L} \quad (11)$$

Equation (9) becomes

$$d\left[\frac{(1-x)^2}{(1-\alpha)} + \frac{x^2}{\alpha}\frac{\rho_L}{\rho_G} - \frac{1}{2}\frac{(1-x)^2}{(1-\alpha)^2}\right] = -\frac{\alpha G h_{fg} f_o}{2DC}\left\{\frac{\left(\frac{dP}{dy}\right)_{GTP} - \left(\frac{dP}{dy}\right)_{LTP} + (\rho_L - \rho_G)\sin\theta}{\left(\frac{dP}{dy}\right)_o}\right\}dx \quad (12)$$

Equation (12) in its most general form is the steam slip equation.

Discussion of the Equations. For a given heat generation, mass flow rate per unit area, system pressure, and hydraulic diameter, Equation (12) is a differential equation which relates α and x (i.e., defines steam slip with respect to water) if $(dP/dy)_{GTP}/(dP/dy)_o$ and $(dP/dy)_{LTP}/(dP/dy)_o$ could be expressed in terms of x and α and the system parameters G, D, C, and pressure. Even before considering such expressions, several important conclusions can be drawn about steam slip from Equation (12).

1 Steam slip depends not only upon pressure, but also upon the inlet velocity, hydraulic diameter, and distribution of heat production along the flow direction. The grouping $K = Gh_{fg}f_o/DC$ can be expected to control.

2 Steam slip will vary with flow pattern if the functions $(dP/dy)_{GTP}/(dP/dy)_o$ and $(dP/dy)_{LTP}/(dP/dy)_o$ vary with flow pattern.

3 The functions $(dP/dy)_{LTP}/(dP/dy)_o$ and $(dP/dy)_{GTP}/(dP/dy)_o$ have not been found susceptible to accurate correlation. Since these functions are expected to exhibit a scatter of 10 to 30 per cent steam slip may be expected to exhibit the same order of scatter.

A relation between α and x can be derived from Equation (11) by two means. First, one could utilize experimental measurements of $(dP/dy)_{LTP}/(dP/dy)_o$ and $(dP/dy)_{GTP}/(dP/dy)_o$. Second, a theoretical model could be postulated to define all these functions. The first method, a priori, appears to be the most accurate one. However, upon close examination of test results it is found that the important ratios $(dP/dy)_{LTP}/(dP/dy)_o$ and $(dP/dy)_{GTP}/(dP/dy)_o$ cannot be measured experimentally and the only recourse is to a theoretical model. Such a theoretical model, referred to as the "momentum exchange model" will be discussed next. It has the important advantage of being physically acceptable without requiring expressions for $(dP/dy)_{LTP}/(dP/dy)_o$ and $(dP/dy)_{GTP}/(dP/dy)_o$.

Momentum Exchange Model

Definition of Model. Equation (9) can be rewritten

$$\frac{G^2}{g\rho_L}\, d\left[\frac{(1-x)^2}{(1-\alpha)} + \frac{x^2}{\alpha}\frac{\rho_L}{\rho_G} - \frac{1}{2}\frac{(1-x)^2}{(1-\alpha)^2}\right] = \alpha\left[\left(\frac{d\psi}{dy}\right)_{GTP} - \left(\frac{d\psi}{dy}\right)_{LTP}\right]dy \quad (13)$$

where ψ is used to represent the combined frictional and head losses. For instance,

$$\left(\frac{d\psi}{dy}\right)_{GTP} = \left(\frac{dP}{dy}\right)_{GTP} - \rho_G \sin\theta$$

Let us first consider the simplified case of no heat addition and of no other source of variation of x, α, or ρ_L/ρ_G. Equation (13) reduces to

$$\left(\frac{d\psi}{dy}\right)_{GTP} = \left(\frac{d\psi}{dy}\right)_{LTP} \quad (14)$$

which states that the frictional and head loss of the liquid must equal the frictional and head loss of the gas. This postulate was the basis of the semiempirical relations proposed by Lockhart and Martinelli [13]. Consider next small localized disturbances

of x, α, or ρ_L/ρ_G. Following these local disturbances the system will once again satisfy Equation (14) even though x and α are now slightly modified. If the changes occur slowly enough, one can assume that Equation (14) is satisfied at all times. This constitutes the basis of the momentum exchange model. In other words, momentum is exchanged between water and steam every time x, α, or ρ_L/ρ_G vary and the exchange tends to maintain the equality of frictional and head losses of the two phases.

It is important to note that the model was tacitly utilized by Martinelli and Nelson when they extrapolated the unheated test data of reference [13] at atmospheric pressure to an evaporating system where x changes rapidly. The model also gives a possible explanation for the agreement of two-phase pressure drop data taken with and without heat addition in horizontal and inclined test sections.

Derivation of Equations. Mathematically speaking, the model corresponds to writing

$$\frac{d}{dx}\left[\frac{(1-x)^2}{(1-\alpha)} + \frac{x^2}{\alpha}\frac{\rho_L}{\rho_G} - \frac{1}{2}\frac{(1-x)^2}{(1-\alpha)^2}\right] = 0 \quad (15)$$

Note that if Equation (14) holds Equation (15) is valid whether the flow is horizontal or vertical.

Integration of Equation (15) with zero voids at zero quality gives

$$\frac{(1-x)^2}{(1-\alpha)} + \frac{x^2}{\alpha}\frac{\rho_L}{\rho_G} - \frac{1}{2}\frac{(1-x)^2}{(1-\alpha)^2} = 0 \quad (16)$$

Equation (16) can be rewritten to give

$$x = \frac{\alpha(1-2\alpha) + \alpha\sqrt{(1-2\alpha)^2 + \alpha\left[2\frac{\rho_L}{\rho_G}(1-\alpha)^2 + \alpha(1-2\alpha)\right]}}{2\frac{\rho_L}{\rho_G}(1-\alpha)^2 + \alpha(1-2\alpha)} \quad (17)$$

In the event that α is not equal to zero at $x = 0$ but equal to α_i (as often reported in test results), Equation (16) becomes

$$\frac{(1-x)^2}{(1-\alpha)} + \frac{x^2}{\alpha}\frac{\rho_L}{\rho_G} - \frac{1}{2}\frac{(1-x)^2}{(1-\alpha)^2} - \frac{1}{1-\alpha_i} + \frac{1}{2}\frac{1}{(1-\alpha_i)^2} = 0 \quad (18)$$

and it can be solved to yield a solution equivalent to Equation (17).

It is important to note that Equation (17) gives $\alpha = 1$ when $x = 1$ and reduces to the accepted relation $x = \alpha$ at the critical pressure where $\rho_L = \rho_G$. At low pressures where the quantity $(1 - x)$ may be set equal to one even at high void contents, Equation (17) reduces to

$$x^2 = 2\frac{\alpha^2}{(1-\alpha)^2}\frac{\rho_G}{\rho_L}\alpha \quad (19)$$

and the ratio of liquid to gas velocity is

$$\frac{V_G}{V_L} = \sqrt{\frac{\rho_L}{\rho_G}}\sqrt{2\alpha} \quad (20)$$

The slip ratio, according to the momentum model may, therefore, be expected at low pressures to vary with the square root of the ratio ρ_L/ρ_G, a dependence once proposed by Untermeyer [20]. On the other hand, the homogeneous model where V_L equals V_G would yield

$$x^2 = \left(\frac{\rho_G}{\rho_L}\right)^2 \frac{\alpha^2}{(1-\alpha)^2} \quad (21)$$

and the quality x would vary as ρ_G/ρ_L instead of $\sqrt{\rho_G/\rho_L}$ as obtained from Equation (19).

The slip ratio according to Equation (20) is not constant but increases with void content. This is in agreement with the prediction of Martinelli and Nelson. Machaterre's plot of this ratio at 115 psia along a heated channel verifies the predicted trend of Equation (20). The slip ratio starts below one, increases along the test section, and appears to reach a constant value. Over the exit half of the test section the per cent change in steam volume is small and this partly accounts for the approximate constancy of the slip ratio. Equation (20) suggests a further note of caution. Empirical correlations of slip ratios versus inlet velocity are best done when the void content or quality, at which those slip ratios are plotted, are held constant. The effect of quality has been recognized and noted by Petrick.

Comparison With Test Data. The validity of the model is best demonstrated by comparison with experimental data. The prediction and test results of Larson are shown in Fig. 1 for a horizontal pipe at 1000 psia without heat addition. The agreement is good in the region of high steam quality and void content where the experimental errors are small. The comparison with the Martinelli and Nelson prediction is also satisfactory, with the simplified model giving higher slip values particularly at low qualities. Similar comparisons with the data of Sher [10] and Schwarz [5] are given in Fig. 2 for unheated vertical and horizontal pipes at pressures of 14.7 and 1180 psia. The momentum model again yields lower than measured steam voids, the deviation ranging from about 20 to 30 per cent.

Figs. 3, 4, 5, and 6 show the predictions and test results at various pressures in a vertical system with heat addition. Fig. 3 deals with the data of Dengler and the agreement of theory and tests is good. Fig. 4 gives a check of the model at high pressure. The momentum model curve falls about 20 per cent below the results of Egen, Dingee, and Chastain[4].[3] Fig. 5 compares Marchaterre's measurements at 115 psia with the theoretical analysis. The predicted void volumes at 115 psia are about 25 to 40 per cent too low, but the deviation decreases for the higher pressure runs of Marchaterre. The most comprehensive check of the model is obtained from the data of Cook. Fig. 6 shows predictions and experimental measurements when the parameter $K = Gh_{fg}f_0/CD$ is below 15. The agreement is good. Here again, the momentum model falls below the experimental measurements and appears to be a lower limit for the test data.

This trend is understandable since the derivation assumed that Equation (15) is satisfied along the entire test section, while in reality departures may be expected when the steam quality varies. Unbalances of the steam and water pressure losses in Equation (15) account for the deviations as discussed in the next section.

Momentum Model for Nonquasi Steady-State Conditions

The preceding model assumed that the change in quality and fluid properties were slow enough for the water and steam pressure losses to remain equal. This is particularly true of horizontal and vertical flow in unheated channel with pressure drops small enough not to cause sizable changes in steam density or water flashing. (Note, however, a major difference between verti-

[3] Assuming α different from zero at zero quality does not lower the deviation at high qualities between tests and prediction. The test results confirm that the steam voids are not highly dependent upon the initial void value at zero quality.

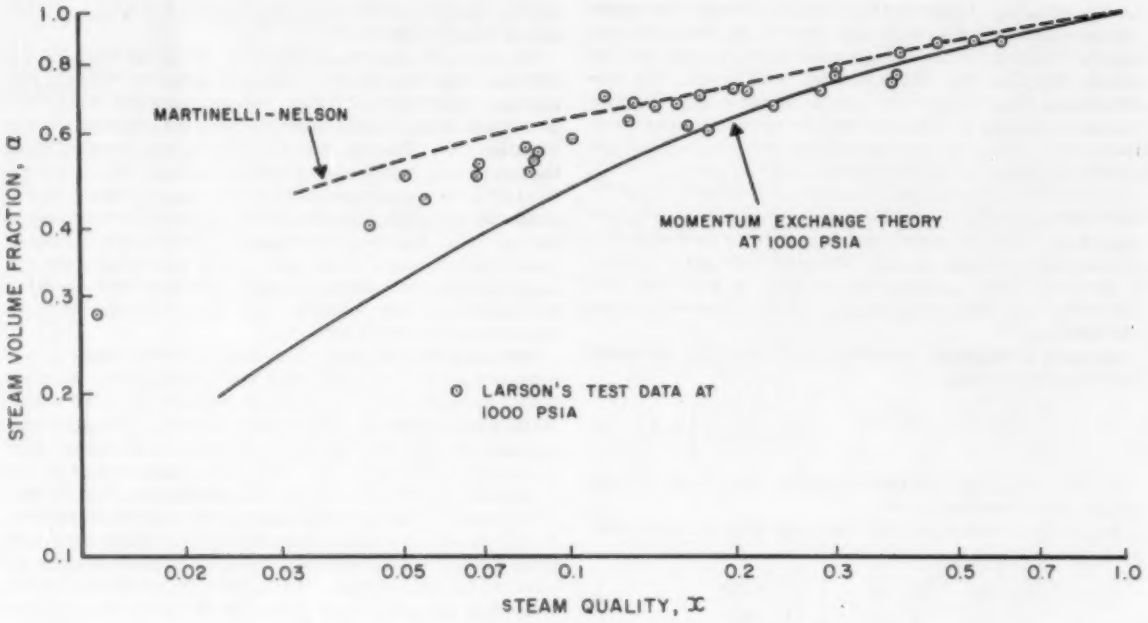

Fig. 1 Comparison of momentum exchange theory with Larson's data

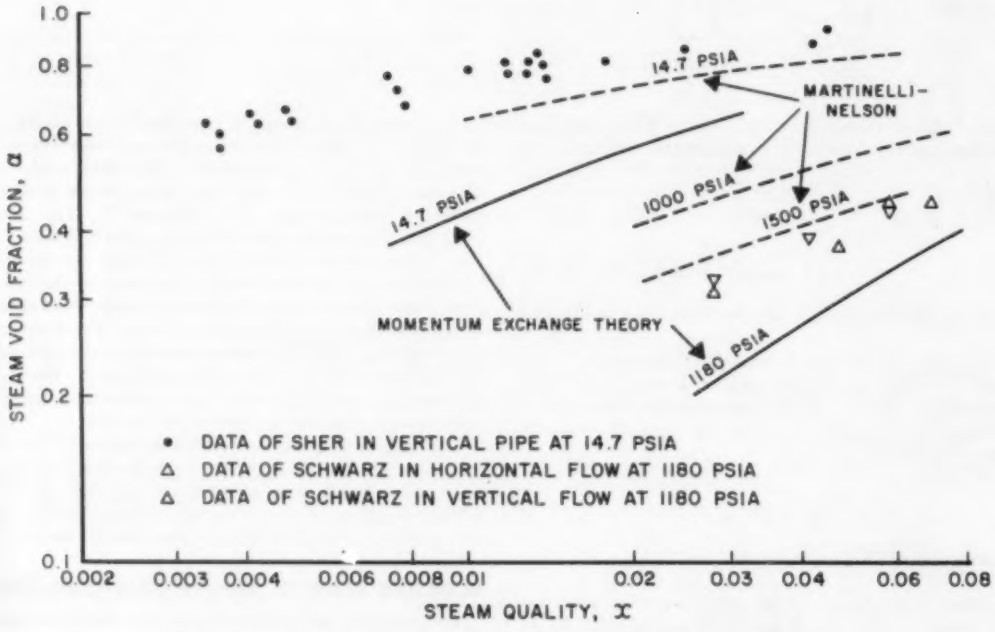

Fig. 2 Comparison of momentum exchange theory with data of Sher and Schwartz

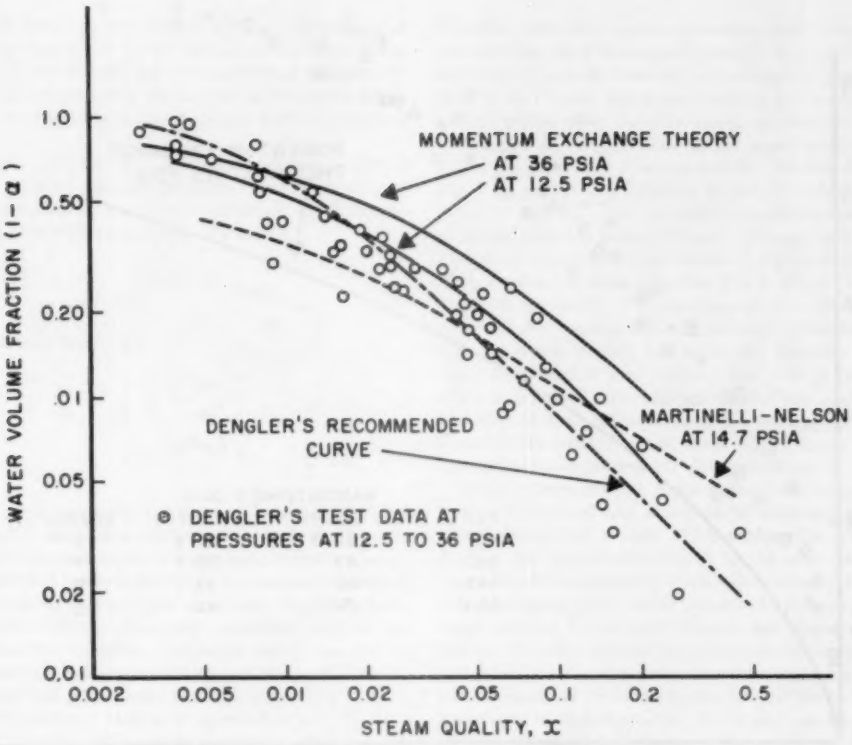

Fig. 3 Comparison of momentum exchange theory with Dengler's data

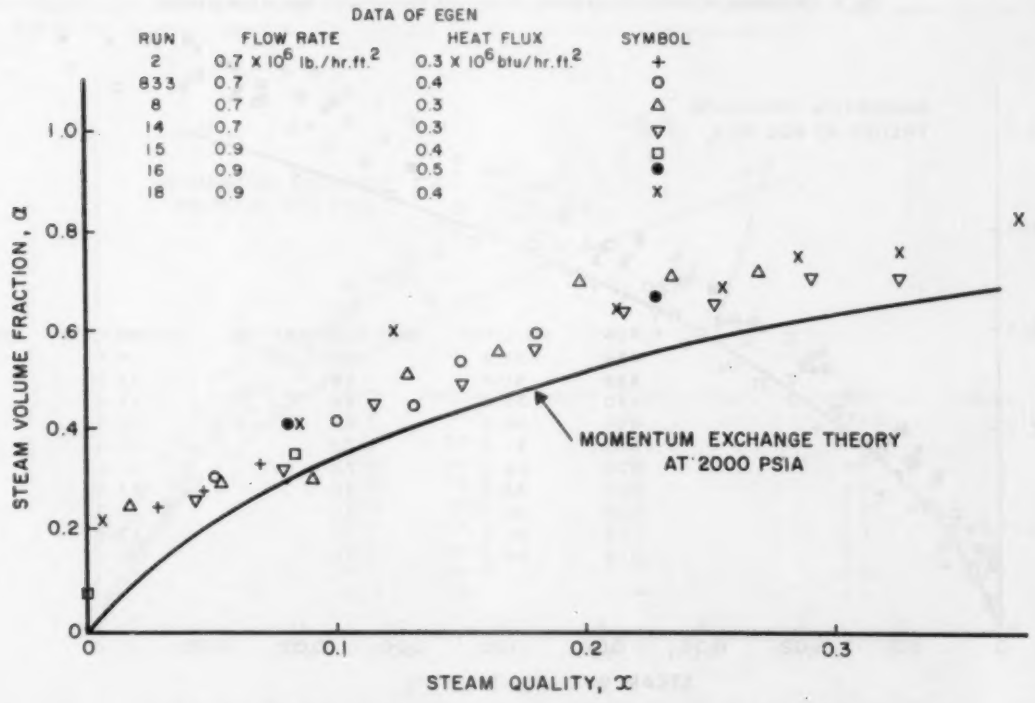

Fig. 4 Comparison of momentum exchange theory with data of Egen, Dingee, and Chastain

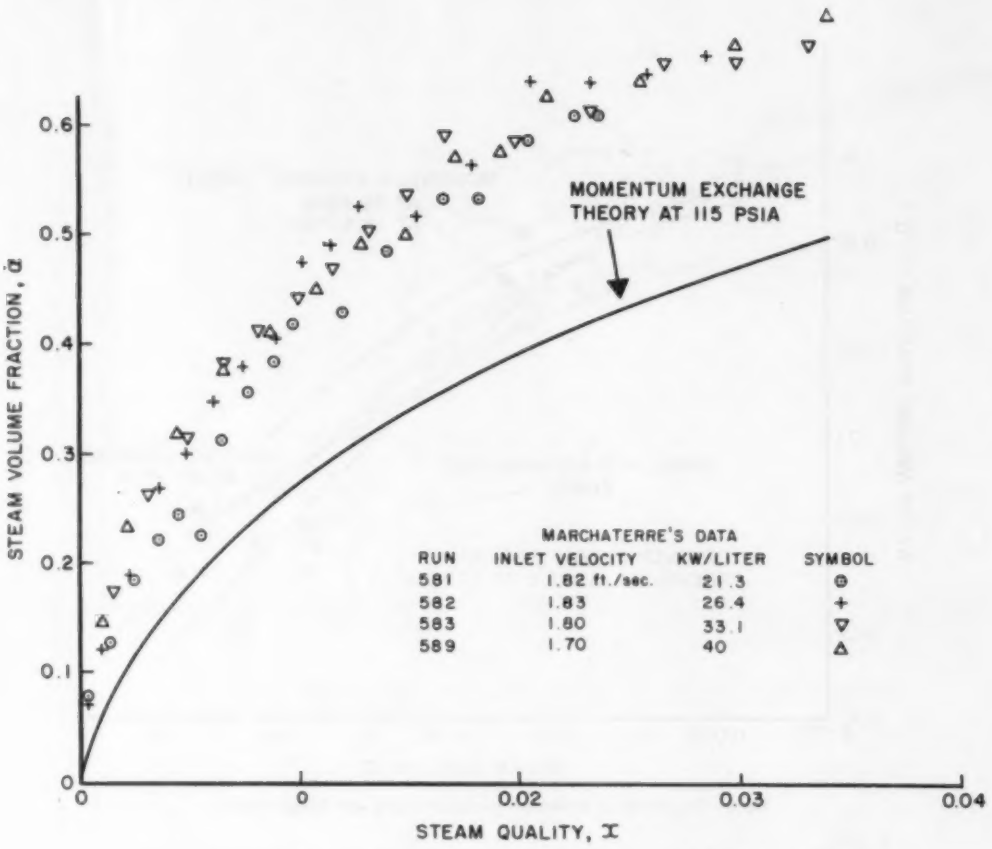

Fig. 5 Comparison of momentum exchange theory with Marchaterre's data at low pressure

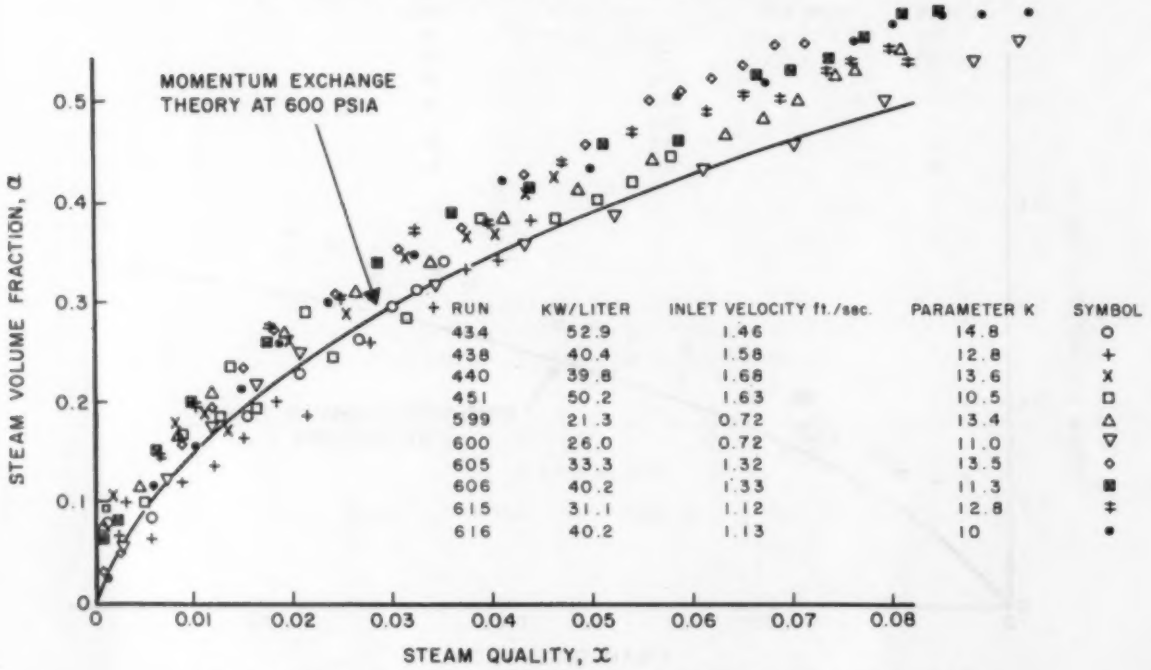

Fig. 6 Comparison of momentum exchange theory with Cook's data for parameter *K* below 15

cal and horizontal flow. In the vertical channel $(dP/dy)_{OTP}$ is much larger rather than equal to $(dP/dy)_{LTP}$ due to hydrostatic head differences. Even though the void content is the same in both systems at a given quality x, the flow pattern must be different to produce the higher gaseous frictional losses in vertical flow.)

In most practical cases the rate of change of steam quality is rapid enough to produce different pressure losses of steam and water. If the steam quality were continuously changed the unbalance could be preserved and during this period

$$\frac{(d\psi/dy)_{OTP} - (d\psi/dy)_{LTP}}{(dP/dy)_0} = \beta \tag{22}$$

Equation (12) can now be written

$$\frac{d}{dx}\left[\frac{(1-x)^2}{(1-\alpha)} + \frac{x^2}{\alpha}\frac{\rho_L}{\rho_G} - \frac{1}{2}\frac{(1-x)^2}{(1-\alpha)^2}\right] = -\frac{\alpha G h_{fg} f_0}{2DC}\beta = -\frac{\alpha}{2}K\beta \tag{23}$$

Equation (23) gives lower slip values than Equation (15) if β is positive and higher ones if β is negative. Nonquasi steady-state unbalances of the two-phase pressure losses may, therefore, be expected to give different void content than the momentum model. The role of the grouping K is now also apparent. Its effects upon slip cannot, however, be quantitatively described until an expression for β becomes available. Tentative trends can still be obtained by examining limiting conditions of the parameter K. First, consider the case where heat addition is small or $C \to 0$, i.e., $K \to \infty$. We assumed that as β approaches zero that the left-hand side of Equation (23) approaches zero. This was the single major assumption made in deriving the preceding momentum exchange model. Next consider the case of very high heat addition or $C \to \infty$, i.e., $K \to 0$. The term β approaches a constant corresponding to the pressure drop ratio of 100 per cent steam flow to 100 per cent water flow. The left-hand side of Equation (23) once again approaches zero. One can, therefore, presume that as K increases from zero to infinity the slip values will first agree with those of the momentum model, then deviate from it, and finally agree again with it at very high values of K.

Cook's data offer the only major opportunity of determining the role of K. Fig. 6 showed the experimental measurements where the parameter K was below 15. Similar plots are given in Fig. 7 for values of K between 15 and 20 and in Fig. 8 for K between 20 and 30. The increased departure from the momentum exchange model is noticeable as K is raised and in particular at the higher values of α as predicted by Equation (23). The role of K appears to have leveled off in Fig. 9 where Cook's data for K above 30 are shown. The decrease of slip with initial increase of K means that raising the inlet velocity decreased slip while increasing power density and hydraulic diameter would raise the slip. The trend of inlet velocity has already been noted at the Argonne National Laboratory but the effects of channel geometry and rate of heat addition have not been previously mentioned. Quantitative predictions of these effects must, however, await theoretical or experimental determinations of the function β.

While expressions for β are beyond the scope of this paper, further theoretical and experimental work suggests itself. Simplified theoretical models which neglect the frictional pressure drop of one phase with respect to the other could be utilized. These and other simplified models are presently being considered. A test program which would consist of applying heat to a steam-water mixture over a short distance and measuring voids before, during, and after heating would help to determine the function β and establish the proposed momentum exchange model. Cook's measurements of voids in the riser beyond the heated section were a first step in that direction. For those runs where the slip ratio appears stabilized an increase in slip was noted with the absence of heat production. This may be construed as a partial verification of the assumption that as $K \to \infty$ the momentum model is again satisfied. Unfortunately, the riser flow area was twice that of the heated section and the conclusion cannot be final due to the change in the parameter G.

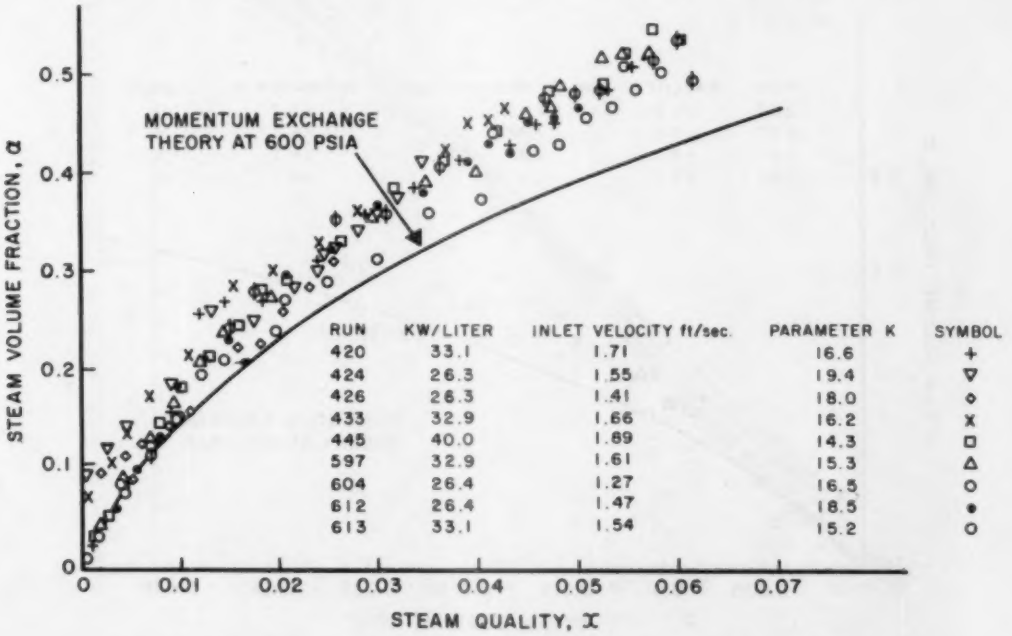

Fig. 7 Comparison of momentum exchange theory with Cook's data for parameter K between 15 and 20

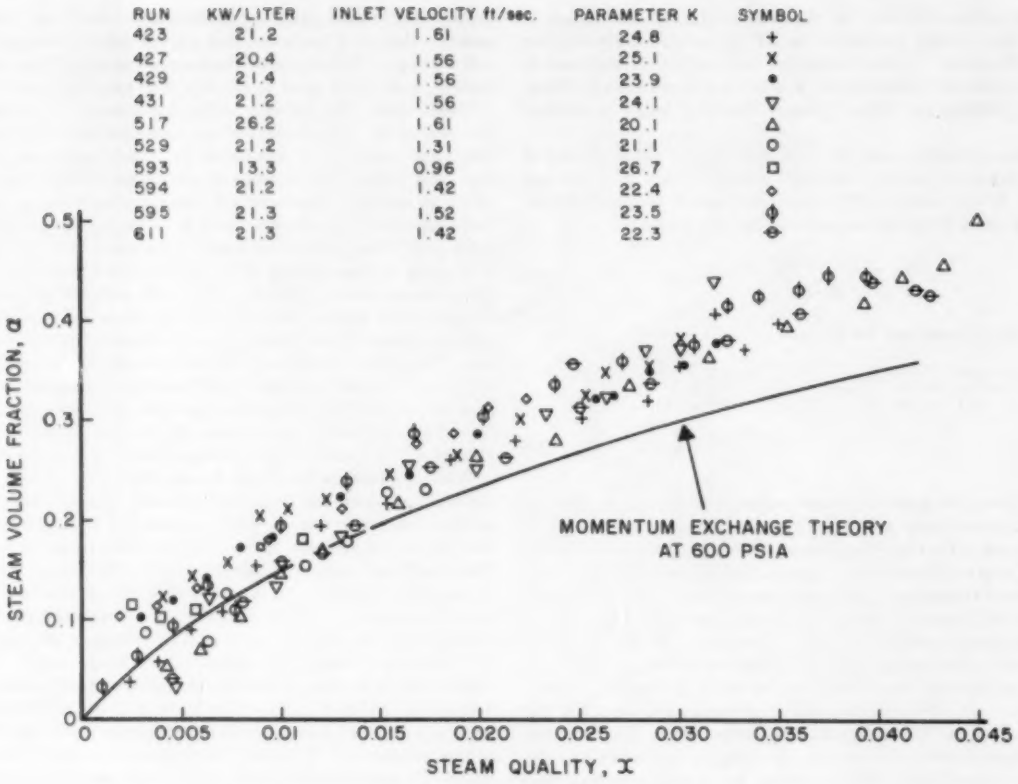

Fig. 8 Comparison of momentum exchange theory with Cook's data for parameter K between 20 and 30

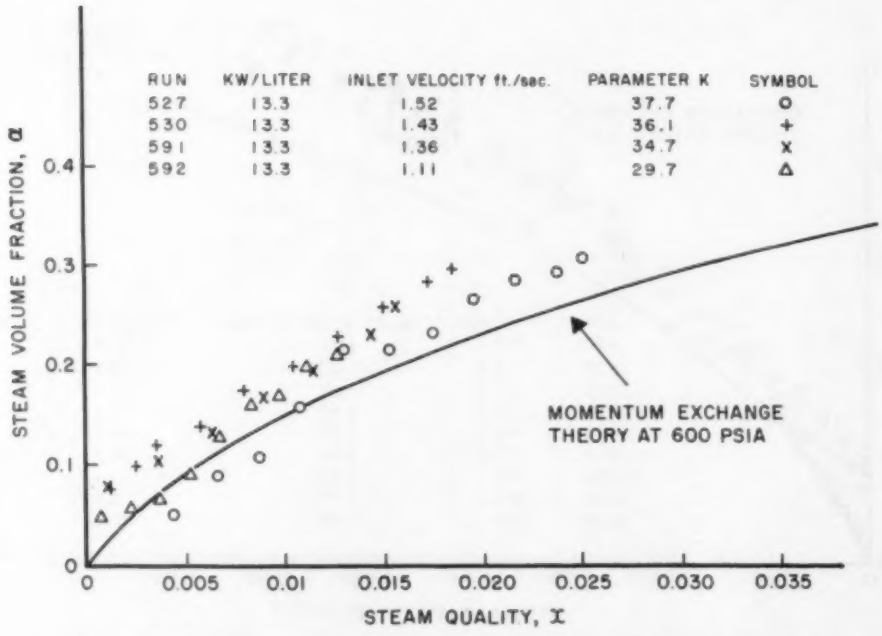
RUN KW/LITER INLET VELOCITY ft./sec. PARAMETER K SYMBOL
527 13.3 1.52 37.7 ○
530 13.3 1.43 36.1 +
591 13.3 1.36 34.7 X
592 13.3 1.11 29.7 △
STEAM VOLUME FRACTION, α
0 0.1 0.2 0.3 0.4
0 0.005 0.01 0.015 0.020 0.025 0.030 0.035
STEAM QUALITY, x
MOMENTUM EXCHANGE THEORY AT 600 PSIA

Fig. 9 Comparison of momentum exchange theory with Cook's data for parameter K above 35

Two-Phase Pressure Drop Prediction From the Momentum Model

Once the void content is specified in terms of the quality x, the acceleration and static losses in Equation (3) can be readily computed. The remaining term $(dP/dy)_{TP}$ can be obtained if the frictional losses are expressed in terms of the void content and other known system parameters. A simplified relation consists of writing[4]

$$\frac{(dP/dy)_{TP}}{(dP/dy)_{LSP}} = \frac{1}{(1-\alpha)^3} \tag{24}$$

where $(dP/dy)_{LSP}$ represents the pressure drop per unit length of the liquid phase if it were assumed to flow alone in the system.

$$\left(\frac{dP}{dy}\right)_{LSP} = \frac{f_{LSP}G^2(1-x)^2}{\rho_L D 2g} \tag{25}$$

[4] Equation (24) is an approximate relation because it does not account for the flow dependency reported in several two-phase investigations.

A relation similar to Equation (24) was previously derived for an annular pattern by Levy [21] and has been proposed by Flinn and Lottes. It can be derived if one assumes that most of the liquid phase is in contact with the channel walls. The two-phase frictional loss for equal shear forces at steam-water interface can be expressed as

$$\left(\frac{dP}{dy}\right)_{TP} = \frac{4\tau_w}{D} \tag{26}$$

where the shear stress at the wall τ_w is obtained from water flow conditions

$$\tau_w = \rho_L f_{LTP} \frac{V_L^2}{2g} \tag{27}$$

If one uses the average water flow velocity and assumes that the wetted perimeter is confined to water-channel interface, then

$$V_L = \frac{G(1-x)}{(1-\alpha)} \tag{28}$$

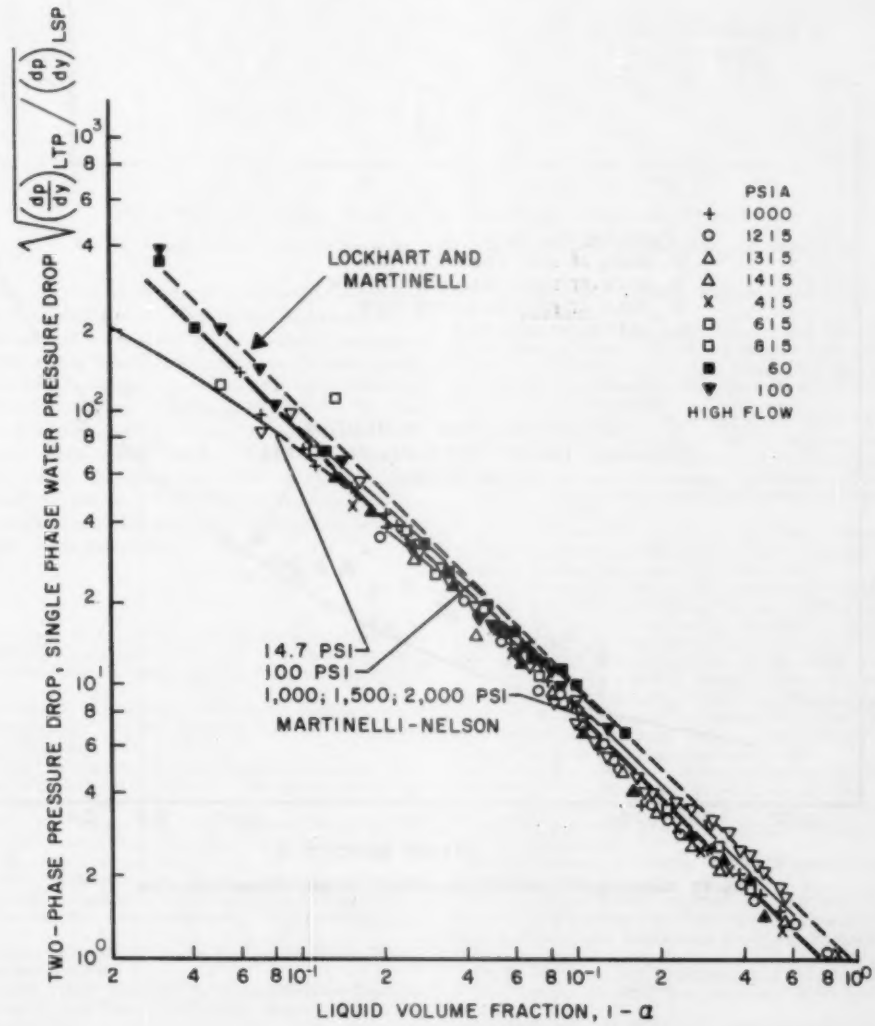

Fig. 10 Two-phase pressure drop data from Moen's thesis

$$D_{LTP} = (1 - \alpha)D \tag{29}$$

Since the friction factor f depends only upon Reynolds number

$$f_{LSP} = f_{LTP} \tag{30}$$

Substitution of Equations (27), (28), (29), and (30) into (26) gives the relation of Equation (24).

The validity of Equation (24) has been verified experimentally. A plot in reference [22] has been reproduced in Fig. 10. It is seen that the data of Martinelli and Lockhart and Martinelli and Nelson are in good agreement with it. Further, the data of Moen, Wickey, and Mosher at high flow rate give a further check of the model if the steam void contents are evaluated from the Martinelli and Nelson correlations.

The two-phase pressure gradient can be obtained by integrating Equation (24) from start of heating where $x = 0$ to end of the heated section where $x = x_e$ and

$$\left(\frac{\Delta P}{\Delta L}\right)_{TP} = \frac{C}{x_e}\int_0^{x_e} \frac{1}{C}\left(\frac{dP}{dy}\right)_{TP} dx \tag{31}$$

Equation (31) can be rewritten [19]

$$\frac{(\Delta P/\Delta L)_{TP}}{(dP/dy)_0} = \frac{C}{x_e}\int_0^{x_e} \frac{1}{C}(1 - x)^{1.75}\frac{1}{(1 - \alpha)^2} dx \tag{32}$$

and substitution of Equation (17) means that the ratio $(\Delta P/\Delta L)_{TP}/(dP/dy)_0$ is only a function of α and pressure, or again the mean void fraction $\bar{\alpha}$ obtained from

$$\bar{\alpha} = \frac{C}{x_e}\int_0^{x_e} \frac{\alpha}{C} dx \tag{33}$$

Equations (17) and (24) were used to predict two-phase pressure

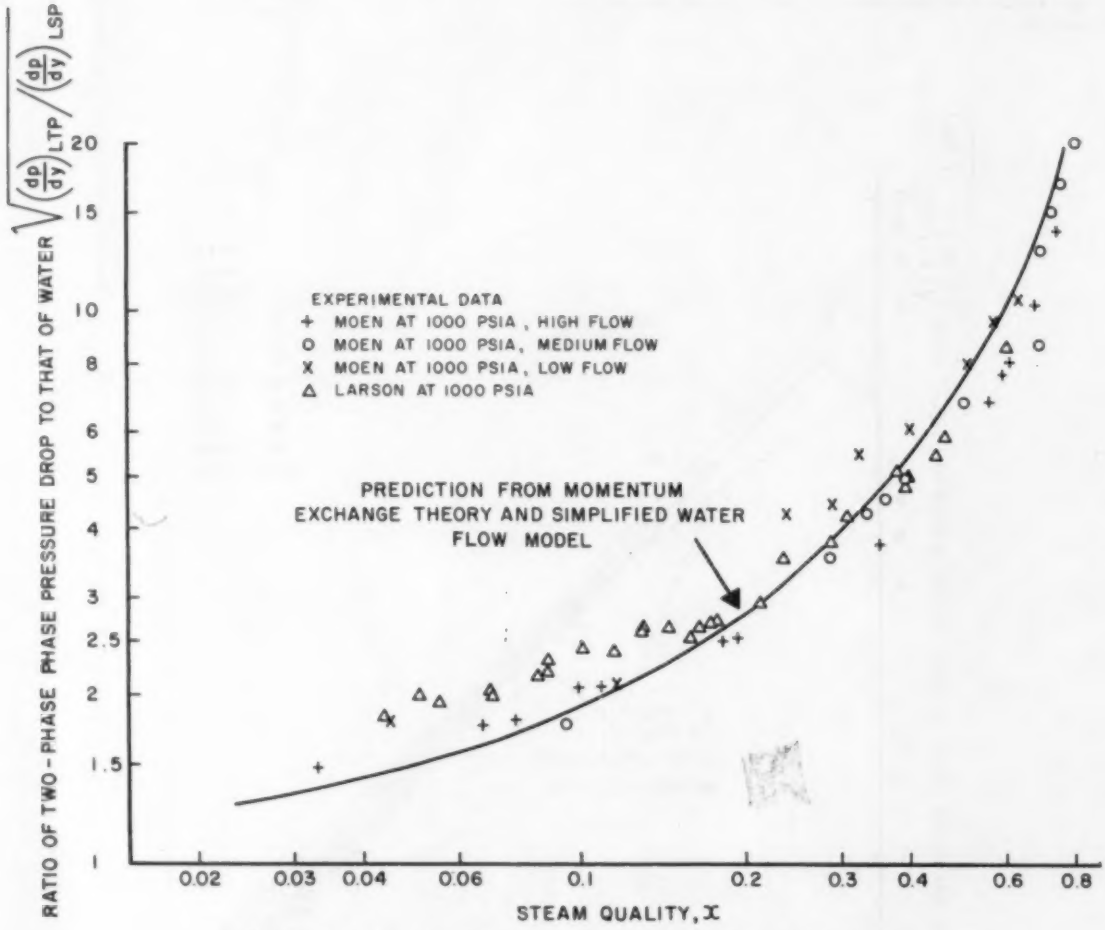

Fig. 11 Comparison of predicted pressure drop with data of Moen and Larson

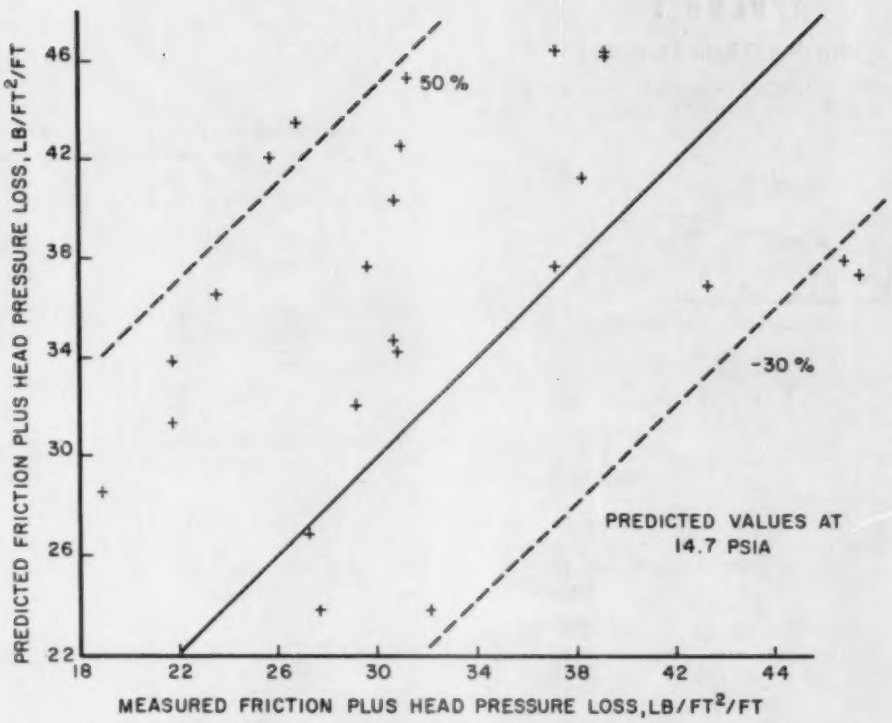

Fig. 12 Comparison of predicted two-phase pressure drop with data of Isbin, Sher, and Eddy

drop in two instances. Fig. 11 shows the two-phase pressure drop for the tests of Moen and Larson. Values for quality above 0.8 were purposely not plotted as these are more readily computed from 100 per cent steam flow. The comparison between theory and tests is satisfactory and the flow effects have been somewhat masked. A similar comparison is shown in Fig. 12 with the data of Sher and the prediction for frictional plus head losses fall 50 per cent above and 30 per cent below the experimental measurements. The deviations are partly due to the large void content measured by Sher and partly to scatter in the test results. The scatter in test results is probably caused by the effects of flow rate which were neglected in the analysis.

References

1 W. S. Flinn and P. A. Lottes, "Unrestricted and Restricted Natural Circulation Boiling Studies of 1/2 × 2 × 60 inch Channel," Argonne National Laboratory Memorandum to A. S. Jameson, February 2, 1956.

2 J. F. Marchaterre, "The Effect of Pressure on Boiling Density in Multiple Rectangular Channel," Argonne National Laboratory Report No. 5522, February, 1956.

3 W. H. Cook, "Boiling Density in Vertical Rectangular Multi-Channel Sections With Natural Circulation," Argonne National Laboratory Report No. 5621, November, 1956.

4 R. A. Egen, D. A. Dingee, and J. W. Chastain, "Vapor Formation and Behavior in Boiling Heat Transfer," Battelle Memorial Institute Report No. 1163, February, 1957.

5 K. Schwarz, "Untersuchungen Uber die Wichteverteilung, die Wasser und Dampfgeschwindigkeit soure den Reibungsdruckabfall in Lotrechen and Wasgerechten Kesselsteigrehren," VDI Forschungsheft 455, 1954.

6 P. Behringer, "Velocity of Steam Bubbles in Boiler Pipes," VDI Forschungsheft 365, 1934.

7 C. E. Dengler, "Heat Transfer and Pressure Drop for Evaporation of Water in a Vertical Tube," PhD thesis, Massachusetts Institute of Technology, 1952.

8 W. Schurig, "Water Circulation in Steam Boilers and the Motion of Liquid-Gas Mixtures in Tubes," VDI Forschungsheft 365, 1934.

9 G. R. Smith and Y. L. Hoe, "Water Velocities in the Two-Phase Flow of Steam and Water in 4.06 and 6.06 inch Diameter Horizontal Pipelines," C. E. 174, Report No. DL 118/6, Dominion Laboratory, Department of Scientific and Industrial Research of New Zealand, September, 1956.

10 H. S. Isbin, N. C. Sher, and K. C. Eddy, "Void Fractions in Two-Phase Steam Water Flow," *AIChE Journal*, March, 1957.

11 H. C. Larson, "Void Fractions of Two-Phase Steam-Water Mixture," MS thesis, University of Minnesota, 1957.

12 M. Petrick, "Two-Phase Air-Water Flow Phenomena," ANL-5787, March, 1958.

13 R. W. Lockhart and R. C. Martinelli, "Proposed Correlation of Data for Isothermal Two-Phase, Two-Component Flow in Pipes," *Chemical Engineering Progress*, vol. 45, 1944.

14 C. E. Alves, "Co-Current Liquid Gas Flow in a Pipe Line Contractor," *Chemical Engineering Progress*, vol. 50, 1954.

15 H. A. Johnson and A. H. Abou-Sabe, "Heat Transfer and Pressure Drop for Turbulent Flow of Air-Water Mixtures in a Horizontal Pipe," TRANS. ASME, vol. 74, 1952, p. 977.

16 P. C. Zmola and R. V. Bailey, "Power Removal From Boiling Nuclear Reactors," Report of Oak Ridge National Laboratory, 1955.

17 O. P. Bergelin and G. Gazley, Jr., "Co-Current Gas-Liquid Flow-I-Flow in Horizontal Tubes," Heat Transfer and Fluid Mechanics Institute, Berkeley, California, 1949.

18 C. Baker, "Design of Pipelines for the Simultaneous Flow of Oil and Gas," *The Oil and Gas Journal*, vol. 53, 1954.

19 R. C. Martinelli and D. B. Nelson, "Prediction of Pressure Drop During Forced-Circulation Boiling of Water," TRANS. ASME, vol. 70, 1948, p. 695.

20 S. Untermeyer, "Use of Boiling Water as a Reactor Coolant," ASME Paper No. 57—NESC-80, 1957.

21 S. Levy, "Theory of Pressure Drop and Heat Transfer for Annular Steady-State Two-Phase Two-Component Flow in Pipes," Second Midwestern Conference on Fluid Mechanics, Proceedings, 1952.

22 R. H. Moen, "An Investigation of the Steam-Water System at High Pressures and High Temperatures," PhD thesis, University of Minnesota, 1956.

23 H. S. Isbin, R. H. Moen, and D. R. Mosher, "Two-Phase Pressure Drop," AECU-2994, November, 1954.

APPENDIX

Derivation of Basic Equations

The net pressure forces are obtained by considering an elemental length of fluid stream tube. The net force is according to the sketch below

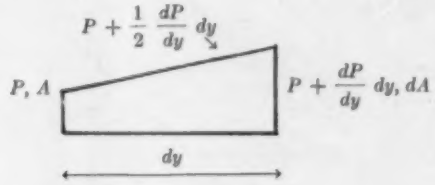

$$PA + \left(P + \frac{1}{2}\frac{dP}{dy}\,dy\right)dA - \left(P + \frac{dP}{dy}\,dy\right)(A + dA) = -A\frac{dP}{dy} \quad (34)$$

The momentum change for each fluid has been given in reference [23]. For the liquid phase flowing at a rate W_L lb/hr one has

$$\frac{1}{g}\left[(W_L + dW_L)(V_L + dV_L) - W_L V_L - V_L dW_L\right] = \frac{1}{g} W_L dV_L \quad (35)$$

Equation (35) assumes that dW_L lb/hr of fluid are converted to gas. The corresponding gaseous momentum change is

$$\frac{1}{g}\left[(W_G + dW_G)(V_G + dV_G) - W_G V_G + V_L dW_L\right] = \frac{1}{g}\left[d(W_G V_G) + V_L dW_L\right] \quad (36)$$

The gravity forces are computed as follows. For the liquid phase they are equal to

$$\rho_L\left(A + \frac{1}{2}\,dA\right)dy = \rho_L A\,dy \quad (37)$$

The frictional forces are expressed by means of expression (34) so that for the liquid phase they are

$$A\left(\frac{dP}{dy}\right)_{LTP} dy \quad (38)$$

Combination of Equations (34) to (38) yields Equations (1) and (2).

Pressure Drop and Heat Transfer in a Duct With Triangular Cross Section[1]

E. R. G. ECKERT

Professor of Mechanical Engineering, University of Minnesota, Minneapolis, Minn. Mem. ASME

T. F. IRVINE, JR.

Associate Professor of Mechanical Engineering, University of Minnesota, Minneapolis, Minn.

Friction factors have been measured for a duct whose cross section has the shape of an isosceles triangle with a side ratio 5 to 1 in the fully developed flow region for laminar, transitional, and turbulent conditions. In addition, local and average heat-transfer coefficients and the temperature field in the duct wall have been determined for the condition of constant heat generation per unit volume of the duct walls.

Friction factors in laminar flow agreed well with analytical predictions. In the turbulent flow range they were by 20 per cent lower than values calculated from relations for a round tube with the use of the "hydraulic diameter." Heat-transfer coefficients averaged over the circumference of the duct were only half as large as values calculated from round tube relations in the Reynolds number range from 4300 to 24,000. The measurements also revealed that thermal starting lengths were in excess of 100 diameters. In round tubes a length of 10 to 20 diameters has been found sufficient to develop the temperature field.

Introduction

Because of their wide technical applications, pressure drop and heat transfer in duct flow have been studied extensively in the past. The majority of these investigations have been concerned with ducts having a circular cross section.

In many present-day cooling problems, such as in nuclear reactors, in high performance heat exchangers, or in rocket power plants, design considerations dictate ducts with noncircular cross sections. Papers in the literature which investigated the pressure drop and heat transfer in ducts with noncircular cross sections (ref. [1])[2] indicate that turbulent pressure drop can be calculated with good accuracy from relations for circular ducts when the diameter in these relations is replaced by the "hydraulic diameter" of the particular cross section. This rule has also been used to calculate average heat-transfer coefficients in noncircular ducts. It has, however, not been verified as well by experiments.

Engineering applications which utilize cooling ducts at a high temperature level make it necessary to predict not only the average heat-transfer condition, but also the local temperature distributions in the duct walls. Theoretical studies [2–5] as well as experimental investigations [6 and 7] which have been made in this connection cast some doubt on the general applicability of the hydraulic diameter concept. The authors of this paper have, in addition, demonstrated [9] that for laminar flow, not only the local heat-transfer conditions, but also the average heat-transfer coefficients depend very strongly on the prescribed local temperature distribution of the duct wall in lengthwise and especially in peripheral direction. The analysis for a particular cross section demonstrated that the Nusselt number averaged over the periphery may differ by an order of magnitude depending on whether a constant wall temperature or a constant heat flux from the duct wall into the fluid is prescribed peripherally.

It appeared important to investigate whether the heat-transfer coefficient in noncircular ducts is as sensitive to the boundary conditions in turbulent flow. The present paper presents the results of an experimental study on the flow characteristics and heat transfer for a duct whose cross section has the shape of a narrow isosceles triangle with an apex angle of 11.46 degrees, correspond-

[1] Publication of the Heat Transfer Laboratory, University of Minnesota.

[2] Numbers in brackets designate References at end of paper.

Contributed by the Heat Transfer Division of The American Society of Mechanical Engineers and presented at the ASME-AIChE Heat Transfer Conference, Storrs, Conn., August 9–12, 1959.

Note: Statements and opinions advanced in papers are to be understood as individual expressions of their authors and not those of the Society. Manuscript received at ASME Headquarters, May 11, 1959. Paper No. 59—HT-10.

Nomenclature

C = perimeter of duct
A = cross-sectional area of duct
b = duct wall thickness
c_p = specific heat of air at constant pressure
D_h = hydraulic diameter
f = friction factor, see Equation (3)
h = convective heat-transfer coefficient
k = heat conductivity
k_w = heat conductivity of duct wall
L = distance between pressure taps
$\dot{m}$ = mass flow through duct
Nu = Nusselt number, see Equation (8)
p = static pressure
Pr = Prandtl number
q_w = local heat flow from inner duct wall surface to air stream
q_{el} = heat generated electrically per unit time and duct surface area minus heat loss to outside
Re = Reynolds number, see Equation (10)
T = air temperature
T_B = air bulk temperature
T_w = duct wall temperature
w = velocity in z-direction
x = co-ordinate along duct wall in circumferential direction
z = co-ordinate in direction of duct axis
α = thermal diffusivity
ϵ_m = turbulent diffusivity for momentum
ϵ_q = turbulent diffusivity for heat
η = Cartesian co-ordinate in plane of duct cross section
μ = dynamic viscosity
ν = kinematic viscosity
ρ = density of fluid
τ_w = wall shear stress
ξ = Cartesian co-ordinate in plane of duct cross section

Indexes

* = reference state
$\bar{}$ = average over circumference or cross section of duct
B = bulk value
w = duct wall

ing to a side ratio 5 to 1. This shape was chosen because it was expected that with such a strong asymmetry of the cross section and with the sharp corner, conditions would differ in a pronounced way from those in a circular tube. In addition, coolant passages with triangular cross sections are used in various of the applications that have been mentioned.

Experimental Apparatus

The experimental apparatus consisted of a duct with triangular cross section, partially wood and partially metal, with an over-all length of 209 hydraulic diameters. As illustrated in Fig. 1, under the influence of a downstream blower, air flows through an assembly (*a*) consisting of fine mesh screens to remove disturbances from the stream and enters the duct through a rounded entrance.

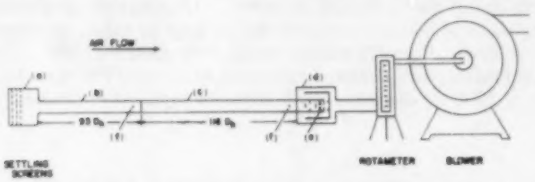

Fig. 1 Diagram of experimental flow circuit

Next, a wooden duct section (*b*) 93 hydraulic diameters in length, allows the flow to become fully developed hydrodynamically before entering the heated section. This wooden section was removed in some experiments. The heat-transfer section (*c*) which is made from a stainless-steel plate, 0.039 in. thick, is 116 hydraulic diameters long, has 119 thermocouples to measure the duct wall temperatures, and is surrounded by a wooden box filled with "Santocel A" insulation. (Thermal conductivity = 0.0142 Btu/hr ft F at a temperature of 150 F.) The box runs the whole length of the metal duct section with overlaps at both ends. The minimum thickness of the insulation was 5 in.

Downstream from the duct are a mixing chamber (*d*) for measuring the exit bulk temperature of the air with thermocouples (*e*), flow measuring instruments (either rotameters or orifices) and the blower which returns the heated air to the room. Located at the ends of the wooden and metal sections are pressure taps (*f*) to measure the static pressure level at those respective cross sections.

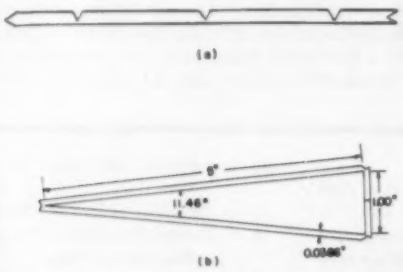

Fig. 2 Construction details (a) and final dimensions (b) of heat-transfer duct

The metal heat-transfer duct was formed from a single sheet of stainless steel 0.039 in. thick. The construction details and final dimensions of the metal duct are shown in Fig. 2. Grooves were milled along lines representing the corners which were then bent to the correct angle. The grooves served to simplify bending and eliminate excess corner material. The single seam, which occurs in the center of the triangle base, is a tongue and groove connection held together with glass fiber tape painted with "glyptol," and tested for leaks. The hydraulic diameter of the duct is 0.904 in. and the apex angle is 11.46 deg. The duct was arranged in such a way that the height of the triangular cross section and the axis were in a horizontal plane.

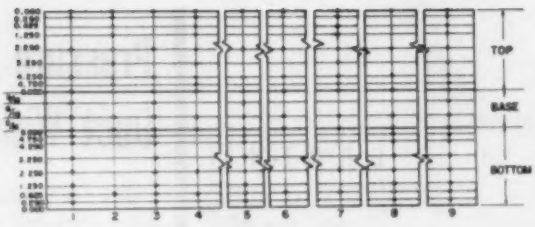

LOCATION OF MEASURING STATIONS

SECTION NO.	DISTANCE FROM START OF METAL DUCT	
	INCHES	HYDRAULIC DIAM
1	0.91	1
2	3.64	4
3	7.28	8
4	14.56	16
5	27.30	30
6	44.00	49
7	64.00	71
8	84.00	93
9	103.00	114

Fig. 3 Thermocouple locations in heat-transfer duct

As mentioned previously, 119 thermocouples were installed in the metal duct at locations shown in Fig. 3. For convenience in data representation, the locations of the measuring stations are given in the figure to the nearest hydraulic diameter. The thermocouple installation was performed by drilling a small hole slightly larger than the thermocouple junction part way through the duct wall, filling the hole with copper oxide cement, and then carefully holding the junction in place away from contact with the duct until the cement hardened. The junctions were thus not in electrical contact with the duct, avoiding spurious voltages, and were located approximately 0.010 in. from the inner duct wall.

The metal test section was heated under the condition of constant heat generation per unit wall volume by passing an alternating current through the stainless-steel wall. Power was supplied and controlled by means of a transformer and "Variac" combination with the current entering and leaving the duct through a large number of fine wires attached at either end around the periphery of the duct and passing the electric current in parallel. The purpose of these wires was to insure a constant electrical potential around the end cross sections and simultaneously to prevent or at least reduce conduction losses from the duct ends.

Accuracy of Measurements

The important measurements in these experiments included wall temperatures, entering and leaving air temperatures, air mass flows, static pressures, and heat-generation rates. In the following paragraphs the accuracy of these measurements is examined.

Thirty-gage iron-constantan thermocouples were used to make wall temperature measurements. The following calibration procedure was followed. In order to avoid the necessity of individually calibrating 119 thermocouples, special thermocouples of uniform length were made from each of five rolls of iron-constantan wires. These thermocouples were then calibrated against mercury-in-glass thermometers which had been certified by the National Bureau of Standards to be accurate to 0.05 F. The thermocouple emf's were read with a Brown self balancing potentiometer whose error is believed to be less than the equivalent of 0.1 F. When all calibrations were compared, it was found that the maximum difference between thermocouples was 0.3 F. This latter figure was then taken as the uncertainty in the temperature measurements.

The temperatures measured in the duct wall are not the inner surface values, because the thermocouple junctions were positioned within the stainless-steel duct wall. A calculation indicated that even under the most unfavorable conditions this difference between the measured and the surface temperature should be less than 0.3 F or the calibration uncertainty and thus no corrections were made for this effect. Every effort was made to minimize conduction errors by running the thermocouple wires along the outer surface of the duct in flow direction (where the temperature gradients are least) before taking them to the potentiometer. Under these conditions it is felt that 0.3 F is a reasonable uncertainty figure for measurement of the wall inner surface temperature.

The temperature of the air entering the heated section was measured by a thermocouple two inches upstream from the end of the wooden section. The thermocouple was shielded from any radiation coming from the metal section and since the air temperature measured in this way always agreed with the room temperature measured in the vicinity of the entrance with a mercury thermometer, it is felt that these data are reliable.

The temperature of the air leaving the heated section was measured by a seven-junction averaging thermocouple after the air had been thoroughly mixed by a series of baffles. Radiation and conduction errors in these measurements were shown by calculation to be negligible.

Mass flows of the air were measured by either an orifice, built to standard ASME specifications, or a rotameter depending upon the flow range. In the region of overlap between the two methods, the measurements agreed to within one per cent.

Static pressures were measured through wall pressure taps having a diameter of 0.020 in. with no inside ridges to disturb the flow. Pressure differences were determined using a micromanometer (Meriam Type A-750) which can be read within 0.002 in. of water. In the worst case, when laminar pressure drops were being measured, the accuracy was estimated to be within two per cent.

The heat-generation rate was determined by reading the total power dissipated in the duct. The current through the duct was measured by a calibrated laboratory ammeter (Westinghouse Type PY 5) and a current transformer. The meter accuracy was 0.25 per cent of full scale or 0.0125 ampere. The electric potential difference across the duct was measured by a Weston model 904 voltmeter with a guaranteed accuracy of $\frac{1}{2}$ per cent of full scale of 0.015 volts. In these experiments, the uncertainty in the power input varied between one and two per cent.

The amount of heat transferred to the air could be determined from the mass flow of the air and its entering and leaving temperature. The difference between the electric power input and the energy absorbed by the air was between 2 and 10 per cent. This difference is interpreted as external heat loss of the apparatus and is listed in Table 1. The losses determined in this way were later applied to the data as correction factors. Relaxation calculations of the heat loss through the insulation surrounding the duct had previously established the validity of the correction procedure.

An investigation was also made of the possibility of unequal rates of heat generation in various sections of the duct due to the change in duct temperature and to the temperature dependence of the electric resistance of stainless steel. A rather lengthy numerical calculation showed this effect to be negligible.

Dimensionless Parameters and Their Determination

The results of the present investigation are appropriately presented in the form of dimensionless parameters. The type and number of the parameters, which describe heat transfer under the conditions as outlined before, will be determined by a dimensional analysis.

The flow field for fully established turbulent flow is described by the following differential equation

$$\frac{\partial}{\partial \xi}\left[(\nu + \epsilon_m)\frac{\partial w}{\partial \xi}\right] + \frac{\partial}{\partial \eta}\left[(\nu + \epsilon_m)\frac{\partial w}{\partial \eta}\right] = \frac{1}{\rho}\frac{dp}{dz} \quad (1)$$

The symbols appearing in this and the following equations are contained in the Nomenclature. The fluid properties related to the present investigation will be assumed as constants. If Equation (1) is made dimensionless in the customary way (see for instance ref. [10]), then it can be anticipated that the solution to this equation must have the following form

$$\frac{w}{\bar{w}} = \phi\left(\mathrm{Re}, \frac{\epsilon_m}{\nu}, \frac{\xi}{D_h}, \frac{\eta}{D_h}\right) \quad (2)$$

In developed flow it can be assumed that the turbulence level is determined by the internal flow process and that it can not be influenced by changes in the inlet condition. As long as the duct walls are hydraulically smooth, the ratio ϵ_m/ν can therefore not be regarded as a free parameter. The solution of Equation (1) also leads to a relation between the pressure gradient and the mean velocity.

The pressure drop in the duct may be described by a friction factor defined by the following equation

$$f = \frac{2D_h}{L}\frac{\Delta p}{\rho \bar{w}^2} = \frac{2D_h}{L}\rho \Delta p \left(\frac{A}{\dot{m}}\right)^2 \quad (3)$$

The temperature field in the duct wall can be described by the following differential equation, assuming that temperature variations through the duct wall normal to its surface are negligibly small.

$$b\frac{\partial}{\partial x}\left(k_w \frac{\partial T_w}{\partial x}\right) = q_{s1} + k\left(\frac{\partial T}{\partial n}\right)_w \quad (4)$$

The left-hand term in Equation (4) describes the net heat flux into a volume element of the wall by heat conduction in the peripheral direction x. A corresponding term for the direction z of the duct axis was omitted because it was found to be small as compared with the contribution of conduction in x-direction.

The temperature field in the fluid flowing through the duct is described by the equation

$$\frac{\partial}{\partial \xi}\left[(\alpha + \epsilon_q)\frac{\partial T}{\partial \xi}\right] + \frac{\partial}{\partial \eta}\left[(\alpha + \epsilon_q)\frac{\partial T}{\partial \eta}\right] = w\frac{\partial T}{\partial z} \quad (5)$$

Heat transport by conduction and turbulent mixing is again neglected in z-direction. The form of the solution to the two equations (4) and (5), which describes the duct wall and the fluid temperatures can again be anticipated by making these equations dimensionless. This process indicates that a relation of the following form must exist for the wall temperature:

$$\frac{k\Delta T_w}{q_{s1} D_h} = \phi\left(\frac{k_w b}{k D_h}, \mathrm{Re}, \mathrm{Pr}, \frac{x}{D_h}, \frac{z}{D_h}\right) \quad (6)$$

The Reynolds number appears in this equation because the relation (2) for the flow velocity w has to be introduced into Equation (5). The wall temperature is indicated in this equation as a parameter ΔT_w because Equations (4) and (5) are obviously independent of temperature level as long as the properties are constant. The temperature can then be measured from any reference value and the fluid bulk temperature is used for this purpose in the following presentations.

A heat-transfer coefficient $\bar{h}$ averaged over the periphery of a particular cross section will be defined in the following way

$$q_{s1} = \bar{h}(\bar{T}_w - T_B) \quad (7)$$

The average Nusselt number, as a dimensionless expression for this heat-transfer coefficient, is then determined by an equation of the following form

$$\overline{\mathrm{Nu}} = \frac{\bar{h}D_h}{k} = \phi\left(\frac{k_w b}{kD_h}, \mathrm{Re}, \mathrm{Pr}, \frac{z}{D_h}\right) \tag{8}$$

The parameter on the left side of Equation (6) is therefore equal to $1/\overline{\mathrm{Nu}}$ when ΔT_w is interpreted as $\bar{T}_w - T_B$. The relation (8) is presented later on. In addition, the dimensionless parameter $(T_w - T_B)/(\bar{T}_w - T_B)$ as a representation of the local wall temperature will be shown as well as a local heat-transfer coefficient h which is defined by the equation

$$q_w = h(T_w - T_B) \tag{9}$$

The parameters appearing in these relations are obtained from the measured values in the following way. The Reynolds number is defined as

$$\mathrm{Re} = \frac{\rho \bar{v} D_h}{\mu} = \frac{\dot{m} D_h}{A\mu} \tag{10}$$

The properties are generally introduced into the dimensionless parameters at the local fluid bulk temperature. The average wall temperature is obtained by an integration of the measured wall temperatures around the periphery of the duct. The fluid bulk temperature rises linearly from the beginning to the end of the heated duct provided the heat addition to the fluid per unit length and the specific heat of the air is constant. The local bulk temperature was determined in this way from the measured entrance and exit temperatures of the heated section. The average Nusselt number then was obtained from Equations (7) and (8). The heat conductivity of the duct wall material was taken from the literature as 9.27 Btu/hr ft deg F. This value, the length dimensions of the duct, and the heat conductivity of the air determine the parameter $(k_w b)/(kD_h)$. It varied in the present experiments between 23.2 and 24.9. This variation is considered small and the value 24 has been assigned to the results presented later on in this paper. The Prandtl number of air varied in the experiments between 0.709 and 0.700.

The calculation of the local Nusselt number is somewhat more involved. A heat balance was made for this purpose on an element with 1 in. × 1 in. dimensions located in the wall as indicated in Fig. 4. The heat balance on the wall element can then be approximated by the following equation when the heat conduction in z-direction can be neglected.

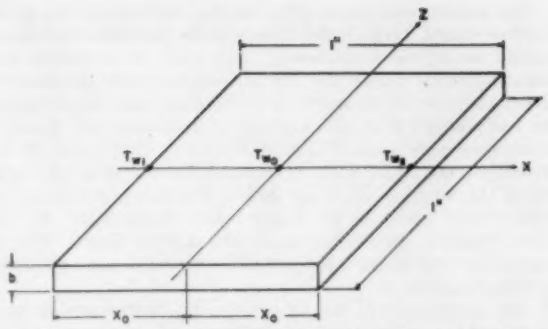

Fig. 4 Control volume for calculating local heat-transfer coefficients

$$h = \frac{q_{w1} + \dfrac{k_w b}{2x_0^2}(T_{w1} + T_{w2} - 2T_{w0})}{T_{w0} - T_B} \tag{11}$$

The temperatures T_{w0}, T_{w1}, and T_{w2} are obtained from the measured temperature profiles along the duct periphery; the measurement of the other quantities appearing in this equation has already been described.

Results of Pressure Drop Measurements

The first series of measurements are concerned with the static pressure drop for the fully developed isothermal flow through the metal heat-transfer duct. The purpose was to obtain a partial check on the duct dimensions, sealing integrity, and flow transition by comparison of the measurements with analytical laminar flow solutions and with previous measurements [7 and 8]. The pressure drop information which is conveniently presented as friction factor against Reynolds number with the hydraulic diameter taken as the characteristics length dimension is shown in Fig. 5.

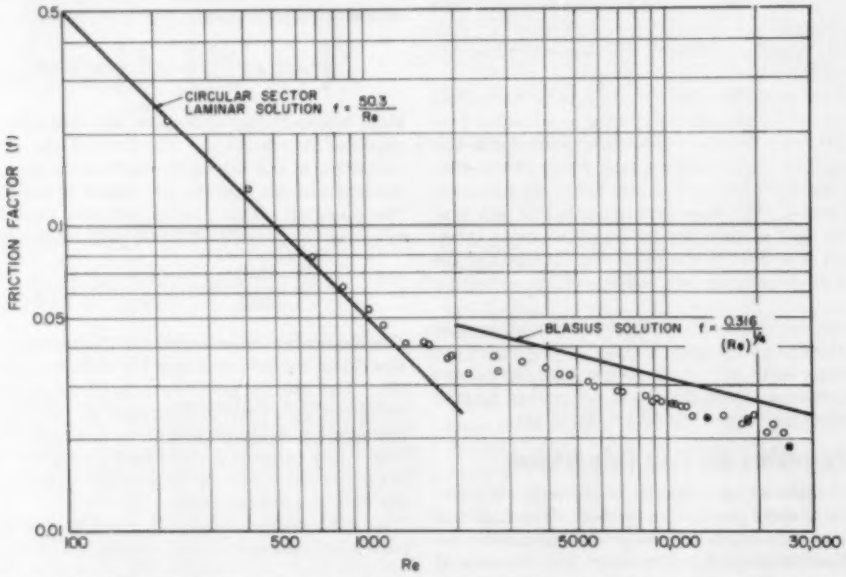

Fig. 5 Fully developed friction factors in 11.46 degree duct. Solid points calculated by method of ref. [5].

Table 1

Run no.	Mass flow rate, lbm/sec	Reynolds number Entrance	Reynolds number Exit	Total bulk temp rise, deg F	Total heating power input to duct, Btu/hr	Average losses, per cent
1	0.02097	7440	6840	62.5	1222	5.2
2	0.01326	4725	4340	65.8	795	5.3
3	0.03005	10580	9640	69.9	1817	2.0
4	0.04381	15620	14380	61.2	2472	6.5
5	0.04500	16000	14740	59.9	2463	5.5
6	0.0618	21750	20330	51.3	2940	7.0
7	0.0682	24100	22570	48.7	3070	6.7
8	0.0379	13420	12510	58.3	1990	4.2
9	0.01806	6400	5950	53.1	904	8.2
10	0.0143	4990	4615	59.0	810	9.9
11	0.0210	7360	6830	56.1	1093	6.5
12	0.02864	10160	9420	56.8	1054	6.6
13	0.0450	15850	14820	50.2	2107	7.3
14	0.0608	21660	20340	46.7	2650	7.3
15	0.0673	23800	22200	51.2	3210	7.3

In the laminar flow regime, the experimental friction factors are compared with the calculated friction factors for a circular sector duct with the same opening angle. Below a Reynolds number of 1000 the agreement appears to be satisfactory. It can be seen that at Reynolds numbers larger than 1000, the data gradually depart from the laminar solution. This is in agreement with previous measurements [7 and 8], in which it was found that the transition process in such a duct is a gradual one with the turbulent flow appearing first in the duct core near the triangle base and filling more and more of the duct as the Reynolds number increases.

When the flow becomes fully turbulent, it is seen that the experimental data fall approximately 20 per cent below the Blasius expression for a circular tube. This does not agree with either our previous experience on a triangular duct with 23-deg apex angle [8], or with the measurements of others on ducts with various cross sections [1] where it has been found that pressure drop can be represented by the circular duct relation if the hydraulic diameter is used to define the friction factor and Reynolds number. A search of the literature, however, failed to reveal any measurements on a triangular duct with such a small apex angle.

In an attempt to account for the departure of the experimental data from the circular tube solution, a calculation of the velocity field was made using the method of Deissler and Taylor [4 and 5]. They assume that on lines normal to the lines of constant velocity, the turbulent velocity distribution may be represented by the universal velocity profiles found to describe the flow in circular ducts. With this assumption, it is possible by an iterative procedure to calculate the velocity field and thus the friction factor in a duct such as the present one. The calculation was made for two Reynolds numbers and the results are shown as solid points in Fig. 5. The agreement between the measured and calculated values is very good. It was, however, found less satisfactory when the calculation was repeated for a triangular duct with 23-apex angle. The calculated friction factors were found to be only slightly higher than the values for the present duct, whereas the measured values reported in ref. [8] agreed well with the circular duct line in Fig. 5.

On the basis of this figure it can be assumed that turbulent friction factors for triangular ducts with small apex angle are smaller than the values calculated by the hydraulic diameter concept and can be calculated with better accuracy by the method of Deissler and Taylor. An experimental investigation of pressure drop in even more extreme cross sections is the subject of a current program in our laboratory.

Summarizing the pressure drop measurements, it may be said that the laminar flow pressure drop was found to be in good agreement with calculations and that the transition process was the same as previously observed. On the other hand, the turbulent pressure drop was approximately 20 per cent lower than predicted by Blasius' circular tube relation. Under these circumstances it would not be surprising if the fully developed turbulent heat transfer also deviated from the circular duct correlation. That this is the case, and that the deviation is many times greater, will be shown in the next section.

Results of Heat-Transfer Measurements

A series of runs was made, at a variety of duct Reynolds numbers, in which the wall-temperature distribution and the appropriate flow parameters were measured. In order to perform these measurements, the heating current was applied to the duct, the desired air flow was set, and the equipment was allowed to operate until a steady-state condition was reached. The existence of steady state was determined by the lack of change of the duct wall temperatures with time. Using the procedure given, a total of 15 runs was made. A summary of important measurements and operating parameters is given in Table 1. Reference to this table indicates that all measurements were taken in a Reynolds number range between 4300 and 24,000. It can be seen from Fig. 5, that the flow is already turbulent at the minimum Reynolds number. Therefore the data discussed in this section will be for turbulent conditions only.

It was originally intended to obtain data under conditions of laminar flow so that some comparisons could be made with the analytical solutions presented in ref. [9]. The experiments at low Reynolds numbers, however, indicated the existence of free convection flows which precluded such comparisons. These secondary flows were perceived indirectly by noting a difference between the temperature distribution on the top long side of the duct and on the bottom side. It was only when the flow became turbulent that these temperature differences disappeared and the temperature distribution along the two sides of the triangle became symmetrical. This experience indicates that caution should be exercised in applying laminar flow heat-transfer solutions for noncircular ducts to actual situations. The secondary currents engendered by the wall-temperature differences at a given cross section may produce free convection effects which are of the same order of magnitude as the forced convection heat transfer.

The measured wall temperature distributions for three Reynolds numbers are shown in Fig. 6(*a*, *b*, and *c*). In this figure, the difference between the local wall and the cross-section bulk temperature is plotted as a function of the dimensionless distance from the corner. The Reynolds numbers shown are the average between the values at duct inlet and exit. When the temperatures are plotted in such a way, the existence of a fully developed temperature field should be indicated by the coincidence of the temperature profiles for all sections in the developed region. In Fig. 6(*a*), it will be noted that the temperature distributions for Sections 7, 8, and 9 are nearly coincident. It

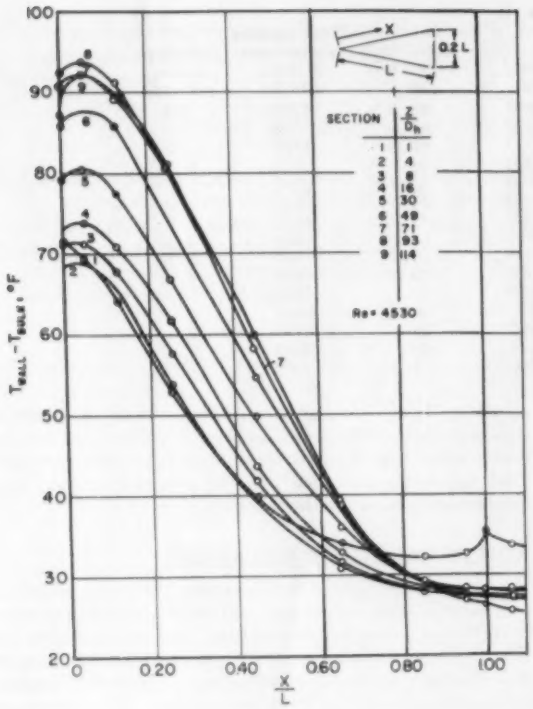

Fig. 6(a)

may therefore be inferred that the temperature field is fully established past the location of Section 7. Reference to the table in the figure indicates that a total of 71 hydraulic diameters were necessary in order to fully establish the turbulent temperature field. Fig. 6(*b* and *c*), however, shows that with increasing Reynolds number the temperature field does not become fully developed in the investigated duct length because a significant change in the temperature profiles persists in all sections to the end of the duct. The excessively long thermal starting lengths indicated by Fig. 6 are somewhat surprising, since measurements as well as calculations [11 and 12] predict that, for turbulent flow in a circular tube, the thermal entrance length is generally not in excess of 20 diameters.

The duct wall-temperature field was replotted in a manner shown in Fig. 7(*a*, *b*, and *c*). In this figure, the difference between the local wall and the fluid bulk temperature in the same cross section is plotted against the distance down the duct made dimensionless with the hydraulic diameter. The individual curves are for a constant wall location away from the duct corner. This figure again is plotted for three average Reynolds numbers and corroborates the information presented in Fig. 6. For the Reynolds number 4530, the temperature profiles, except in the immediate vicinity of the narrow corner, become horizontal indicating that the field is developed. At the higher Reynolds numbers, however, the profiles never attain a constant value, implying that the thermal field does not become established over the entire duct length of 116 diameters.

The region of a fully developed thermal field can also be defined as that region in which the heat-transfer coefficient is independent of axial location. This region can be determined from Fig. 8 in which the average Nusselt number, as defined by Equation (7), is plotted over the dimensionless distance z/D_h. Fig. 8 illustrates

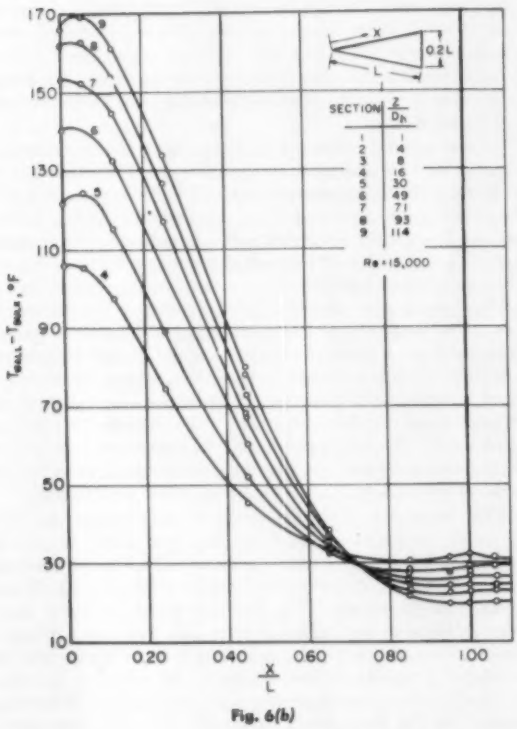

Fig. 6(b)

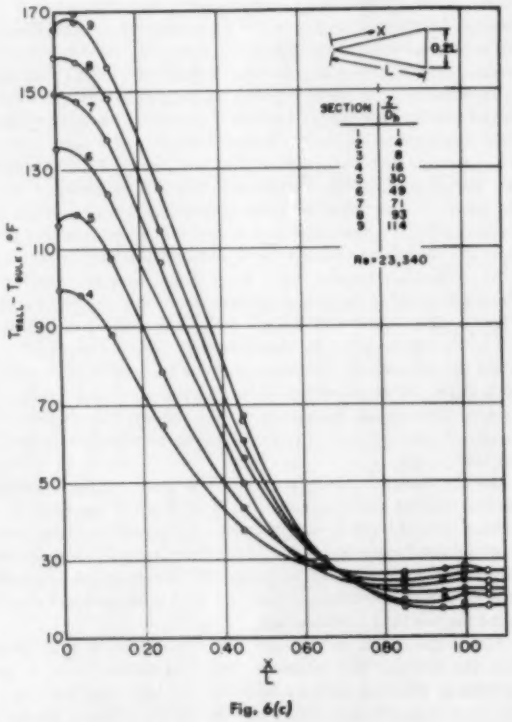

Fig. 6(c)

Fig. 6 Transverse wall-temperature distributions along heat-transfer duct

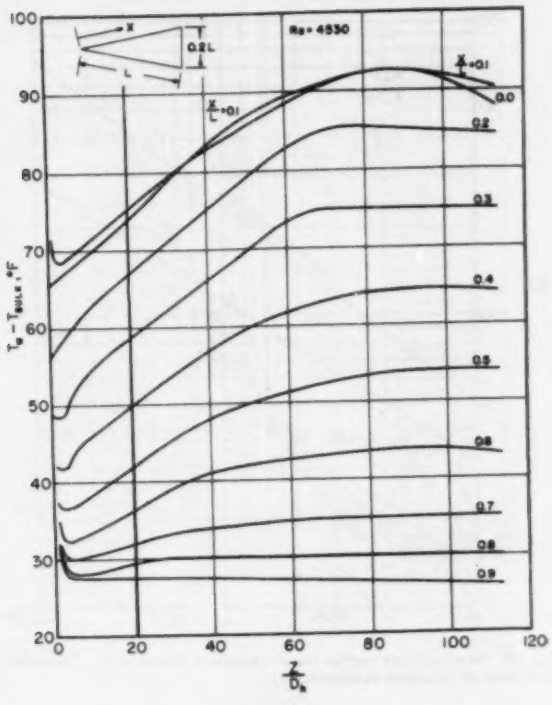

Fig. 7(a)

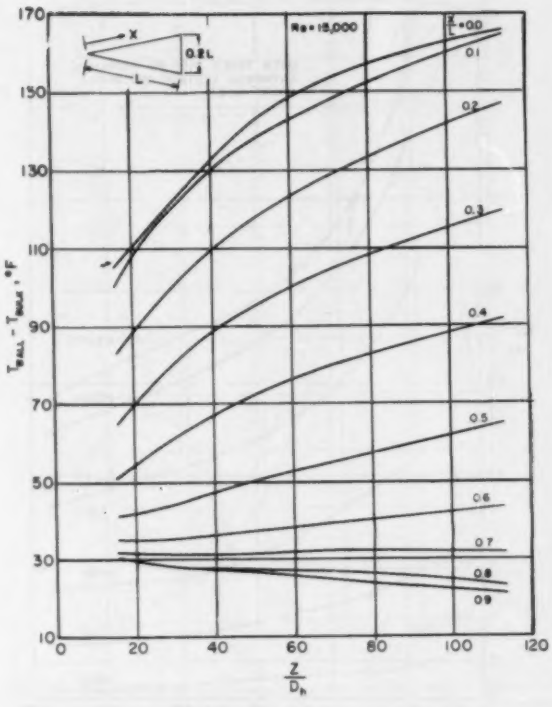

Fig. 7(b)

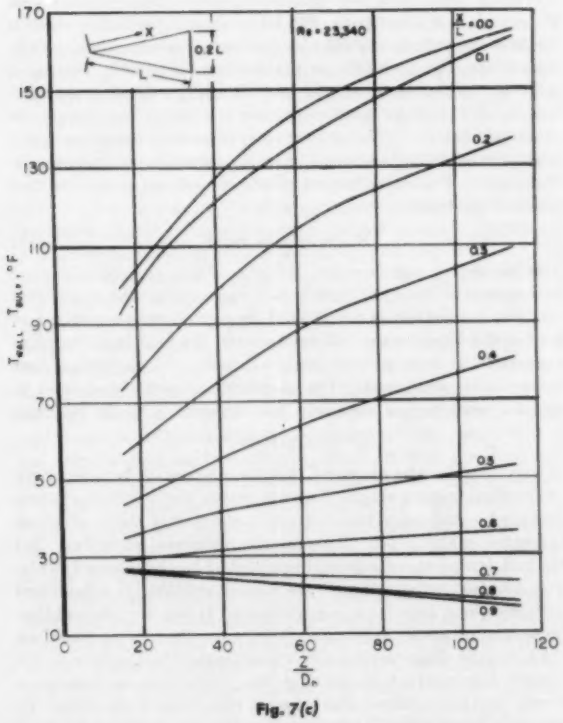

Fig. 7(c)

Fig. 7 Longitudinal wall-temperature distributions in heat-transfer duct

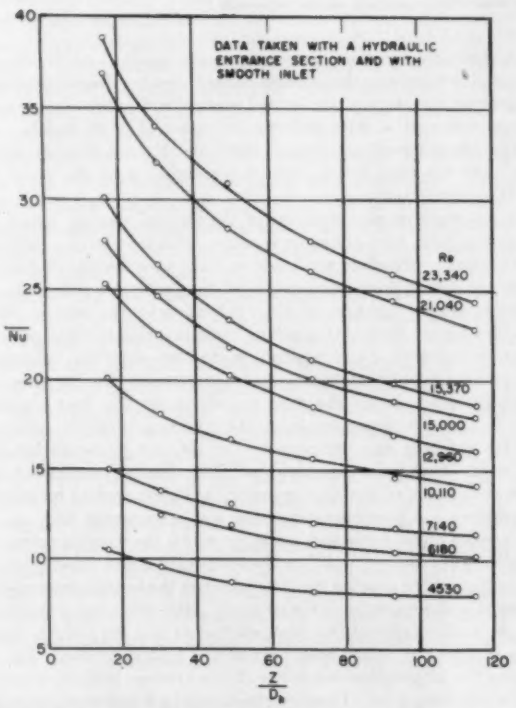

Fig. 8 Average cross section Nusselt numbers at various axial stations (hydrodynamic starting section in place)

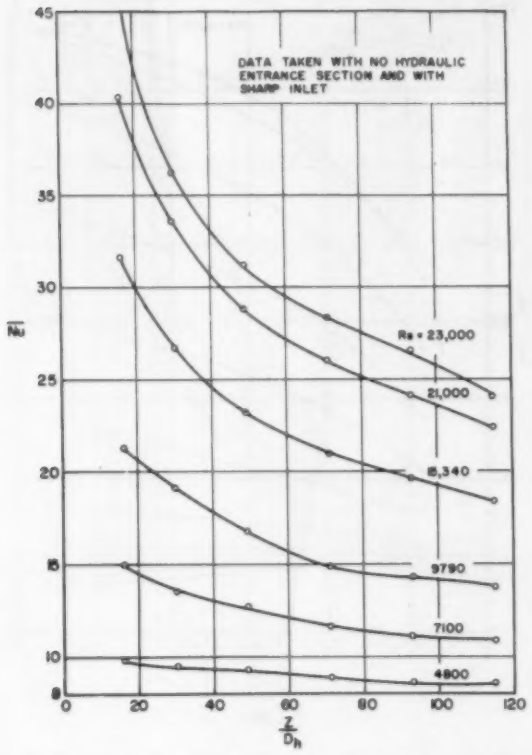

Fig. 9 Average cross section Nusselt numbers at various axial stations (hydrodynamic starting section removed)

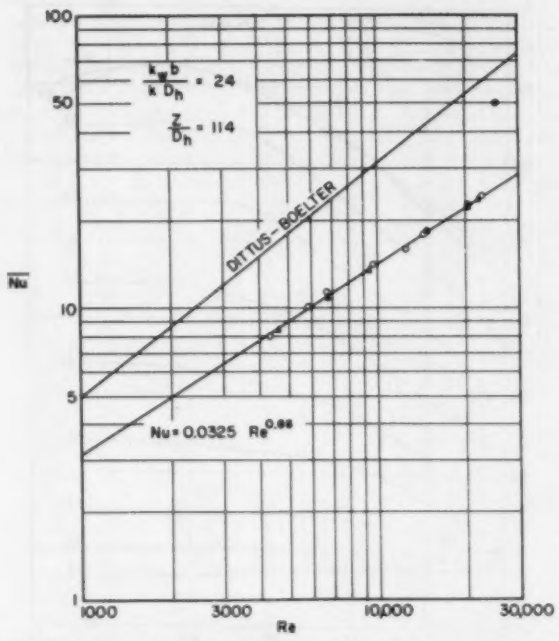

Fig. 10 Average cross section Nusselt numbers at Section 9. Properties evaluated at local bulk temperature.

the same phenomenon as discussed previously. At the lower Reynolds numbers, the average Nusselt number drops from large values at the start of the heated section and approaches a constant value at a duct location in excess of 70 diameters. At Reynolds numbers in excess of 6000, the Nusselt number never becomes constant but is always decreasing over the range of z/D_h investigated.

Since these measured values of the thermal starting length in the triangular duct are so at variance with the circular duct information, every effort was made to make sure that this behavior was not due to some peculiarities of the particular setup. Such factors as duct leakage and duct distortion by the interior pressure at higher Reynolds numbers were investigated but no fact was found that could contribute to the observed behavior. Physical property changes which accompany the increase in temperature level as the fluid travels down the duct are too small to cause departure from the constant property analysis which predicts an asymptotic value of the heat-transfer coefficient. It therefore appears that the extended starting length is a peculiarity of this duct geometry with the applied boundary conditions. A possible explanation will be presented later on.

A series of runs was also made for which the wooden entrance section was removed and thus the temperature and velocity fields were required to develop simultaneously in the heated test section. Except in the region near the entrance, little difference was noted in the performance of the duct whether or not the velocity field was established at the beginning of the heated section. Fig. 9 shows the longitudinal variation of the average Nusselt number with this sharp inlet. Cross reference to Fig. 8 will show that the performance is essentially the same.

The fact that the temperature field was not established within the duct length which was used for the experiments causes some difficulties. It means that strictly the Nusselt number obtained in the present tests should not be compared with information for thermally established flow in a round tube. Nevertheless, such a comparison is presented in Fig. 10 for the cross section 9 which is farthest away from the start of the heated section. Values obtained with the hydraulic entrance section and with a rounded inlet are indicated by circles and values for simultaneous hydraulic and thermal development by the triangles. It may be observed that the difference between both flow situations has a negligible effect on heat transfer at the distance of 114 hydraulic diameters. The experimental points lie well on a straight line which is represented by the equation

$$\overline{Nu} = 0.0325\ Re^{0.8} \tag{12}$$

The physical properties were introduced into the dimensionless parameters at the local fluid bulk temperature. An evaluation was also carried out in which fluid properties were evaluated at a reference temperature halfway between the fluid bulk temperature and the average wall temperature at the particular duct cross section were used. The experimental points evaluated in this way arranged on a straight line represented by the equation

$$\overline{Nu}^* = 0.0318\ Re^{0.8} \tag{13}$$

It may therefore be observed that the difference between both evaluations is quite small. For this reason the bulk temperature was used as reference temperature in the rest of the evaluations presented in this paper. This has the additional advantage that the bulk temperature is directly established by the measurements. Fig. 10 also contains the Dittus-Boelter relation for established turbulent heat transfer in a round pipe. It can be observed that Nusselt numbers obtained in the triangular duct, when based on the hydraulic diameter, are only approximately half as large as the Nusselt numbers for turbulent pipe flow. They also increase more slowly with Reynolds number than the pipe Nusselt numbers. In this connection it should be remembered that the temperature field in cross section 9 is further away from established state the larger

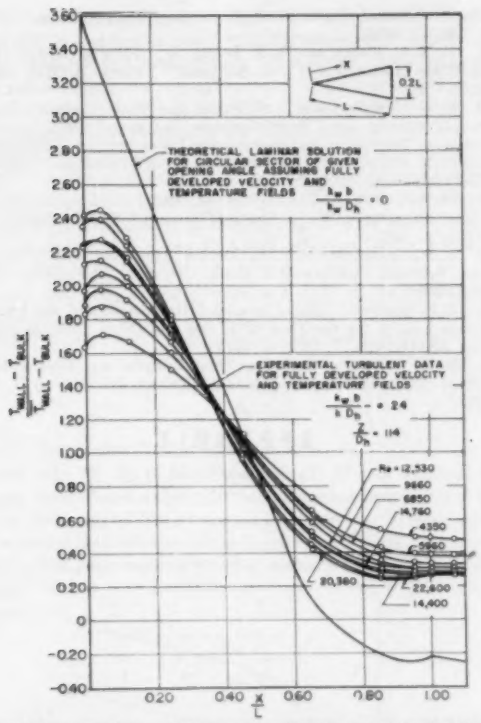

Fig. 11 Dimensionless wall-temperature distribution at Section 9 compared with laminar solution from reference [9]

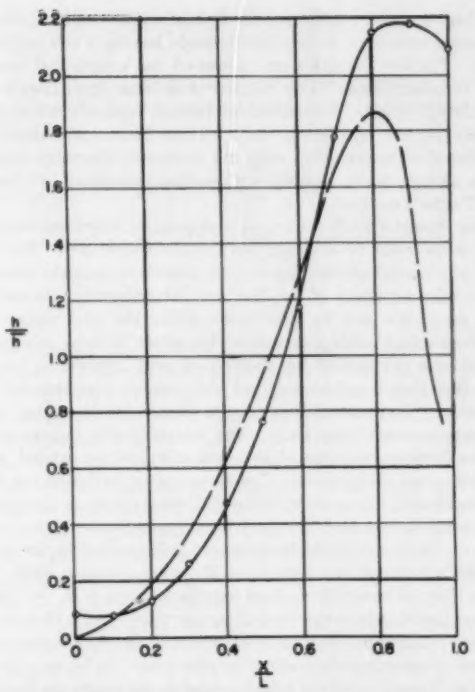

Fig. 12 Distribution of dimensionless local heat-transfer coefficient at Section 9 compared with isothermal calculation (dashed line) by method of reference [5], Re = 14,300

the Reynolds number. Therefore it is to be expected that, for completely established thermal situation, the increase of Nusselt number with Reynolds number will be even smaller.

Fig. 10 also contains a solid point which has been calculated by a method which is essentially a modification of Deissler and Taylor's procedure [5] and which is described in more detail in the Appendix. This point was determined for the condition that the heat flux to the fluid is constant around the duct periphery. The present experiments have a peripheral boundary condition for the temperature field of the fluid which lies between a constant heat flux and a constant wall temperature. For this situation one has to expect a Nusselt number larger than the value shown in Fig. 10 because of the influence of wall conduction. The measured Nusselt numbers are, however, very much lower than this calculated value. An explanation for this fact is suggested by an inspection of Fig. 11 in which the difference between the local wall temperature and the fluid bulk temperature is plotted over the distance from the duct corner. The figure indicates that the temperature variation around the duct wall is up to two and one half times as large as the difference between the average wall temperature and the bulk temperature. This means that in the corner region the heat entering the fluid from the duct wall has to flow in a direction toward the base of the triangle before it is picked up and carried away by convection in the bulk of the fluid. It may well be that the turbulent diffusivity describing the turbulent heat exchange in this direction is smaller than the turbulent diffusivity in a direction normal to the duct walls. This directional characteristic of the turbulent diffusivity may be connected with the fact that the velocity gradient in the direction from the sharp corner toward the base is much smaller than the velocity gradient normal to the duct walls [7]. It is also suggested by Prandtl's mixing length theory, according to which the turbulent diffusivity ϵ_m is $\epsilon_m = l^2 \left|\frac{dw}{dy}\right|$ with l indicating the mixing length. The diffusivity depends, according to this equation, on the velocity gradient. The assumption of a small turbulent diffusivity also explains the fact, discussed before, that an unusual duct length is required to establish the temperature field. One might attempt to account for the starting length by referring to the height of the duct rather than to the hydraulic diameter. The corresponding ratio is 5.43, and on this basis the length of our duct is 21.5 triangle heights.

The measured temperature variations around the periphery of the duct wall are compared in Fig. 11 with a calculated temperature variation for laminar flow. The calculation, however, is made for a peripherally constant heat flux q_w into the fluid which is produced in a duct with uniform heat generation when the parameter $(k_w b)/(kD_h)$ is equal to zero. Since the corresponding parameter for the experiments has the finite value 24, a direct comparison is impossible. In a qualitative way, however, the two curves have a similar shape. The drop of the measured wall temperatures near the sharp corner is probably due to increased heat losses on the outer surface of the duct in this region.

Fig. 12 presents the local heat-transfer coefficients for the same duct cross section as obtained by evaluation of the measurements. Theory indicates that the local heat-transfer coefficient should drop to the value zero in the duct corners. The fact that finite values have been obtained from the measurements is partially explained by the finite differences used in Equation (11), partially by the larger external heat losses from the corners, partially by radiative heat exchange from the corners toward the cooler parts of the duct wall. For comparison purposes, turbulent local heat-transfer coefficients are plotted as a dashed line as they have been calculated by the method of ref. [5] with the boundary condition that the duct wall temperature is peripherally constant.

Conclusions and Recommendations

Experiments have been performed to establish friction factors

and heat-transfer coefficients for flow of air through a duct with the cross section of an isosceles triangle having a side ratio of 5 to 1. Friction factors were measured for established laminar and turbulent flow. The laminar flow data agreed well with calculated values. The turbulent friction factors were approximately 20 per cent lower than friction factors obtained from circular duct information with the hydraulic diameter concept. They agreed, however, well with values calculated by Deissler and Taylor's method.

Heat-transfer coefficients and temperature distributions in the duct walls could be obtained for turbulent flow only. The duct wall was heated electrically and the distribution of the heat flux around the periphery of the duct was determined by the uniform heat generation and by conduction within the duct walls. The parameter $(k_w b)/(kD_h)$ describes this effect of heat conduction and it was established by analysis of heat transfer in laminar duct flow that it influences local and average heat transfer considerably. The present experiments were made for a fixed value of this parameter equal to 24. The measurements indicated that a considerable variation of the wall temperature existed in all cross sections of the duct. This temperature variation was from two to three times as large as the difference between the average wall temperature and the fluid bulk temperature at any cross section. An established temperature field existed in the downstream portion of the duct at a Reynolds number 4530. For larger Reynolds numbers, duct lengths beyond $z/D_h = 114$ are required to obtain an established temperature field. The average Nusselt number for the end cross section of the duct which comes closest to an established situation was found to be only half as large as Nusselt numbers calculated with the hydraulic diameter concept from circular duct relations. It also increases at a slower rate with Reynolds number than the heat transfer in circular ducts. It is suspected that the turbulent diffusivity on which the heat transport primarily depends is considerably smaller in the present duct than in a round pipe.

The results mentioned indicate that the maximum wall temperatures of similar duct geometries will be in any engineering application considerably larger than the values obtained from circular duct information with the hydraulic diameter concept. Additional research is therefore obviously required to clarify the energy transport mechanism and to obtain information from which wall temperature variations and maximum temperatures in heat exchangers can be predicted.

Acknowledgments

The authors wish to acknowledge the assistance of L. Carlson and R. Schmidt in the experimental program, and R. Sampson and E. Halasz in the calculations outlined in the Appendix. The research was sponsored by the Aeronautical Research Laboratory, Wright Air Development Center.

References

1 J. G Knudsen and D. L. Katz, "Fluid Dynamics and Heat Transfer," McGraw-Hill Book Company, Inc., New York, N. Y., 1958.

2 E. R. G. Eckert and G. M. Low, "Temperature Distribution in Internally Heated Walls of Heat Exchangers Composed of Non-Circular Flow Passages," NACA TN 2401, 1951.

3 E. R. G. Eckert, "Temperature Distribution in the Walls of Heat Exchangers With Noncircular Flow Passages," Proceedings of the Third Midwestern Conference on Fluid Mechanics, University of Minnesota, Minneapolis, Minn., 1951.

4 R. G. Deissler and M. F. Taylor, "Analysis of Axial Turbulent Flow and Heat Transfer Through Banks of Rods or Tubes," Reactor Heat Transfer Conference, New York, N. Y., November, 1956.

5 R. G. Deissler and M. F. Taylor, "Analysis of Turbulent Flow and Heat Transfer in Noncircular Passages," NACA TN 4384, 1958.

6 W. H. Lowdermilk, W. F. Weiland, and J. N. B. Livingood, "Measurement of Heat Transfer and Friction Coefficients for Flow of Air in Noncircular Ducts at High Surface Temperatures," NACA RM E53J07, 1954.

7 E. R. G. Eckert and T. F. Irvine, Jr., "Flow in Corners of Passages With Noncircular Cross Sections," TRANS. ASME, vol. 78, 1956, p. 709.

8 E. R. G. Eckert and T. F. Irvine, Jr., "Incompressible Friction Factor, Transition, and Hydrodynamic Entrance-Length Studies of Ducts With Triangular and Rectangular Cross Sections," Proceedings of the Fifth Midwestern Conference on Fluid Mechanics, University of Michigan Press, April, 1957.

9 E. R. G. Eckert, T. F. Irvine, Jr., and J. T. Yen, "Local Laminar Heat Transfer in Wedge-Shaped Passages," TRANS. ASME, vol. 80, 1958, p. 1433.

10 E. R. G. Eckert and R. M. Drake, "Heat and Mass Transfer," second Edition, McGraw-Hill Book Company, Inc., New York, N. Y., 1959.

11 J. P. Hartnett, "Experimental Determination of the Thermal Entrance Length for the Flow of Water and Oil in Circular Pipes," TRANS. ASME, vol. 77, 1955, p. 1211.

12 R. G. Deissler, "Turbulent Heat Transfer and Friction in the Entrance Regions of Smooth Passages," TRANS. ASME, vol. 77, 1955, p. 1221.

APPENDIX

R. Deissler and M. Taylor calculated in ref. [5] the velocity field in developed turbulent flow through a noncircular passage on the basis of two assumptions which will be discussed in connection with Fig. 13. Assume that the velocity field is known and described by lines of constant velocity as illustrated in Fig. 13(*b*).

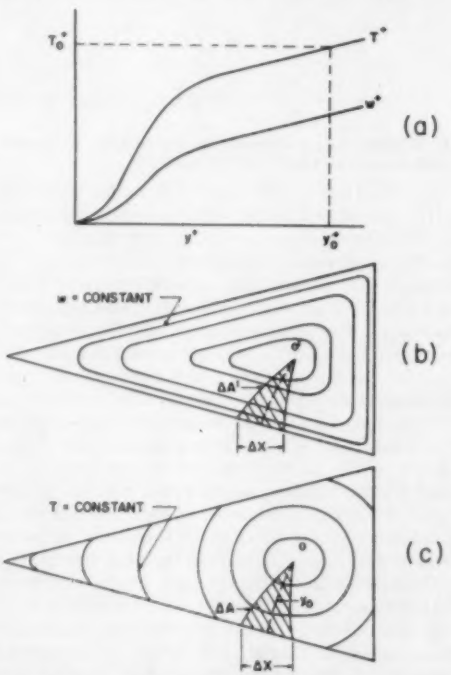

Fig. 13 Sketch of universal velocity and temperature profiles (a), velocity field (b), and constant peripheral heat rate temperature field (c)

Then attention is concentrated on the hatched small area $\Delta A'$, with the base Δx at the duct wall and bounded by two lines which are at any point normal to the lines of constant velocity. It is then assumed that no net flux of momentum occurs into the fluid moving in axial direction within the space appearing as area $\Delta A'$ in the plane of the drawing from the rest of the fluid. With this assumption, the following force balance exists

$$\tau_w \Delta x = \frac{dp}{dz} \Delta A' \qquad (14)$$

It is also assumed that the velocity profile along the dashed center line of $\Delta A'$ is identical in shape with the universal profile describing the velocities in a circular duct. In addition, it has, of course, to be required that proceeding from any location at the wall along a line normal to the curves of constant velocity one ends up with the same maximum velocity at the center point O'. The relation between the turbulent wall shear and the universal velocity profile in a circular duct gives thus a second possibility to calculate the wall shear stress in the noncircular duct at the location Δx. Lines of constant velocity in the duct have to be established by trial and error in such a way that both relations for the wall shear are simultaneously fulfilled.

To actually carry out this analysis, a diagram for the universal velocity profile in a circular tube is needed. Such a diagram is indicated in Fig. 13(a). It is presented as a dimensionless velocity

$$w^+ = \frac{w}{\sqrt{\tau_w/\rho}} \tag{15}$$

plotted over a dimensionless wall distance

$$y^+ = \frac{y}{\nu}\sqrt{\tau_w/\rho} \tag{16}$$

For our later calculations, a universal temperature profile will be needed which is also indicated in Fig. 13(a) as a dimensionless temperature

$$T^+ = \frac{\rho c_p (T_w - T)}{q_w\sqrt{\tau_w/\rho}} \tag{17}$$

plotted over the dimensionless wall distance. Such a curve exists for each Prandtl number provided the properties of the fluid can be assumed constant. Deissler and Taylor introduce, in addition, the following dimensionless parameters

$$w^{++} = \frac{w}{\sqrt{\frac{D_h}{\rho}\frac{dp}{dz}}} \tag{18}$$

$$D_h{}^{++} = \frac{D_h}{\nu}\sqrt{\frac{D_h}{\rho}\frac{dp}{dz}} \tag{19}$$

They extended their method to a calculation of the temperature field and heat transfer in a noncircular duct for established turbulent flow under the condition that the temperature gradient in the fluid in axial (z) direction is constant and that the wall temperature is constant around the periphery or varies by an amount which is small compared to the difference between wall temperature and bulk temperature. An inspection of Fig. 11 will show that this condition does not apply to our duct geometry.

For this reason we extended the method for the condition that the heat flux from the wall into the fluid is constant around the periphery and that the wall temperature differences around the periphery are large. The procedure is again based on the assumption that no energy transport occurs in directions which lie on the surfaces of constant temperature and that the temperature varies along lines which are everywhere normal to the surfaces of constant temperature in the way described by the universal temperature profile for a duct with circular cross section. Fig. 13(c) indicates, within the triangular duct cross section, lines of constant temperature. An area element ΔA may be bounded by the length Δx along the duct wall and by the two curved lines which are everywhere normal to the isotherms. This area element, hatched in Fig. 13(c), has the dashed center line. The following energy balance holds for a cylindrical control volume with the bases ΔA and with height dz:

$$\Delta x q_w = \rho c_p \frac{dT}{dz} w_m \Delta A \tag{20}$$

The term w_m in this equation denotes the average velocity through the area element ΔA. A similar relation holds for the whole duct cross section A

$$q_w C = \rho c_p \frac{dT}{dz} \bar{w} A \tag{21}$$

From both relations (20) and (21) one obtains

$$w_m{}^{++} = \frac{D_h}{4}\frac{\Delta x}{\Delta A} \bar{w}^{++} \tag{22}$$

In this equation the velocities w have been additionally replaced by the dimensionless parameters defined in Equation (18). Equation (22) gives a relationship by which an original assumption of the temperature field can be improved in an iteration process.

The procedure which we used is as follows: One assumes the location of point O within the cross section at which the temperature has a maximum or minimum. Then a number of isotherms are drawn as a first estimate and lines are inserted which start at the origin O and are everywhere normal to these isotherms. In this way the area elements ΔA are established. For any of these area elements, for instance, for the one hatched in Fig. 13(c), the length y_0 can be measured. With this value and with Equation (16), the parameter $y_0{}^+$ is calculated and the temperature parameter $T_0{}^+$ is read from the universal temperature profile in Fig. 13(a). The following parameter is used to describe the temperature field

$$\theta^{++} = \frac{(T - T_0)\rho c_p \sqrt{\frac{D_h}{\rho}\frac{dp}{dz}}}{q_w} \tag{23}$$

It is connected with the parameter T^+ by the equation

$$\theta^{++} = \frac{T_0{}^+ - T^+}{\sqrt{\frac{\Delta A}{\Delta x\, D_h}}} \tag{24}$$

This equation permits the calculation of the parameter $\theta_0{}^{++}$ when the term T^+ is made equal to 0. In order to establish a new, improved isothermal curve, a value θ^{++} is arbitrarily assumed. The corresponding temperature parameter T^+ is calculated from Equation (24), the corresponding value y^+ is read off Fig. 13(a), and the distance y is calculated from Equation (16). It is assumed in this connection that the velocity profile and the local wall shear stress τ_w have already been established by a previous calculation. A point of the isothermal curve is in this way obtained by plotting the length y along the dashed line in Fig. 13(c). A repetition of this procedure in other area elements ΔA results in other points of the same isotherm so that this isotherm can now be inserted in Fig. 13(c). Other isotherms are calculated in the same way and can be considered as a second approximation to the true temperature field. By a repetition of the procedure this temperature field can be approximated to any degree provided the procedure converges.

The dimensionless Nusselt number can now be obtained from the equation

$$\mathrm{Nu} = \frac{\mathrm{Pr}\, D_h{}^{++}}{\theta_0{}^{++} - \theta_B{}^{++}} \tag{25}$$

which is easily derived from Equations (9), (19), (23), and from the definition of a Nusselt number. The value $\theta_B{}^{++}$ is the di-

mensionless parameter describing the fluid bulk temperature and can be obtained from the velocity field and temperature field resulting from the calculation just described. An equation corresponding to Equation (25) describes the Nusselt number $\overline{Nu}$ when the parameter $\overline{\theta_0}^{++}$ describing the average wall temperature replaces the parameter $\theta_0{}^{++}$.

The actual calculation following this procedure turns out to be quite tedious because the location O as well as the shape of the isotherms has to be varied in the course of the iteration procedure. We were therefore satisfied to replace the curved boundaries of ΔA by straight lines. A variation of O along the duct center line leads to a position for which Equation (22) was fulfilled around the duct periphery within ±20 per cent. A study of the convergence obtained to that point indicated that the result is not accurate enough for a description of the local Nusselt numbers, but that it should approximate, on the other hand, the average Nusselt number fairly well. The value of the Nusselt number obtained in this way is inserted as a full point in Fig. 10.

DISCUSSION

L. C. Hoagland[3]

The authors should be commended for an excellent piece of experimental work and a very significant contribution to the rather sparse literature on the subject of heat transfer in noncircular ducts. Research on heat transfer to fluids in noncircular ducts is fraught with many difficulties not encountered in work with circular ducts. Perhaps the most significant difficulty is the sensitivity of the average heat-transfer coefficient or Nusselt number to changes in the thermal boundary condition applied around the duct periphery.

As stated by the authors, previous analytical work has shown that "the Nusselt number averaged over the periphery may differ by an order of magnitude depending on whether a constant (uniform) wall temperature or a constant (uniform) heat flux from the duct wall into the fluid is prescribed peripherally." These two extremes, of course, represent the limits of actual boundary conditions that may be achieved in practice. It appears that the authors have obtained experimental results for a boundary condition approaching the uniform peripheral heat-flux case. (It would be interesting to know how the heat flux into the fluid varied peripherally in these tests.)

Previous analytical work reported in the literature has indicated that for extremely noncircular shapes such as the 5 to 1 triangle, the average Nusselt numbers for uniform peripheral heat flux are considerably lower than those for uniform peripheral wall temperature. Therefore it is not too surprising that the average Nusselt numbers reported in Fig. 10 are considerably lower than one would predict from the Dittus-Boelter equation. It is hoped that the authors will continue their program to investigate other values of the parameter $k_p b/kD_h$ and, in particular, the uniform peripheral wall-temperature case to determine whether the Nusselt number for this case approaches the Dittus-Boelter correlation. This, of course, is easier said than done.

The experiments reported here indicated that very long duct lengths (measured in terms of number of hydraulic diameters) are required to develop the temperature profile along the axis of symmetry (across the long duct dimension). The author has recently been doing some work at M.I.T. on the thermal entrance region for laminar slug flow in rectangular ducts. Although it is impossible to make a direct comparison between laminar slug flow and turbulent flow, some of the results obtained to date may help to explain this seemingly strange discovery. Two thermal boundary conditions have been investigated, namely, (*a*) uniform heat flux to the fluid both peripherally and axially, and (*b*) uniform duct wall temperature both peripherally and axially. Fig. 14 shows for a 4:1 aspect ratio duct typical temperature distributions along the long and short axes of symmetry at various positions from the duct entrance [measured by the conventional Graetz number $Gz = Re \cdot Pr/(L/D_h)$]. These curves indicate that the temperature profiles along the long and short axes become fully developed at widely different values of the Graetz number (based on the conventional hydraulic diameter) or, in other words, at considerably different distances from the entrance to the heating section. This effect appears about the same qualitatively for both boundary conditions.

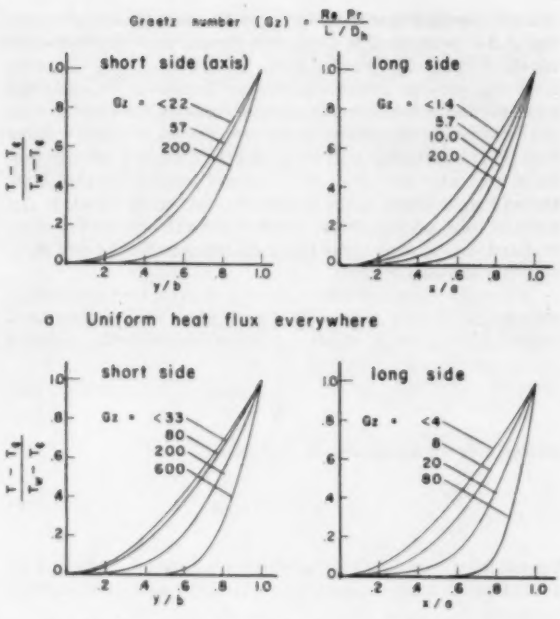

Fig. 14 Laminar slug flow in 4 to 1 rectangular duct—development of temperature profiles across long and short axes

Of special interest is the manner in which the Graetz number required to develop the temperature distribution across the long and short axes varies with the duct aspect ratio. Fig. 15 shows this relationship using the criterion that the temperature parameter (see Fig. 14) must everywhere be within 5 per cent of its value when fully developed. The Graetz number required for developing the short side profile increases by a factor of 3 as the aspect ratio goes from one to ten whereas the Graetz number required to develop the long side profile simultaneously "decreases" by a factor of 30. Note that a lower Graetz number means a larger L/D_h for fixed values of Re and Pr. For comparison, the Graetz number required to develop the temperature profile in a circular duct is about 15 or 20.

At this point it is interesting to philosophize a bit. Should the thermal entrance length for noncircular ducts be comparable to that for circular ducts? Should the hydraulic diameter be a meaningful parameter determining the thermal entrance length for noncircular ducts? Physically, in order to obtain a fully developed temperature profile (say, across the long axis of symmetry), the effect of the sudden change in the thermal boundary condition at the entrance of the heating section must propagate across the long axis from the wall to the center, a distance a. The propagation phenomenon is accomplished physically by heat conduction and is inhibited by convection and thermal storage

[3] Principal Engineer, Microtech Research Company, Cambridge, Mass. Assoc. Mem. ASME.

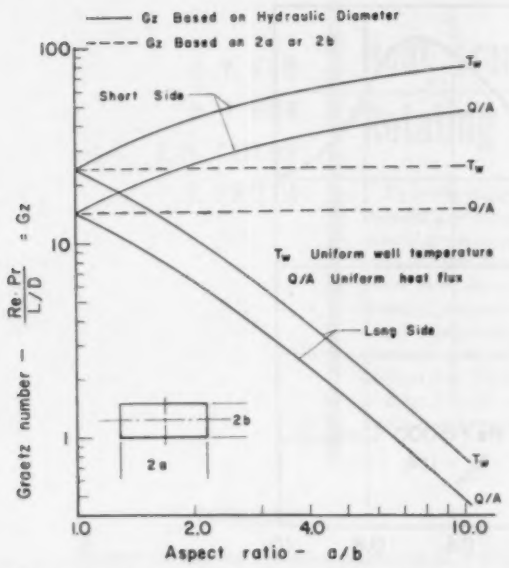

Fig. 15 Laminar slug flow in rectangular ducts—thermal entrance length required to develop temperature profiles across long and short axes of symmetry (within 5 per cent)

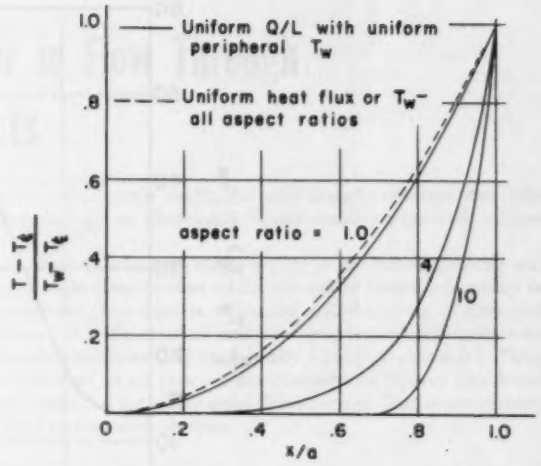

Fig. 16 Laminar slug flow in rectangular ducts—fully developed temperature profiles across long axis of symmetry

processes. Hence the thermal entrance length L required for the boundary effect to propagate across the distance a should be directly proportional to the fluid velocity u and the thermal capacity of the fluid through which the effect must propagate ($\rho c_p A_n \cdot a$) and inversely proportional to the thermal conductance of the fluid (kA_n/a) where A_n is the area normal to long axis or a. Thus

$$L \propto \frac{u\rho A_n \cdot ac_p}{kA_n/a} = \frac{u\rho a}{\mu} \cdot \frac{c_p \mu}{k} \cdot a$$

This physical notion suggests that a Graetz number built with the duct dimension representative of the temperature profile in question should provide a better thermal entrance length parameter than the Graetz number built with the hydraulic diameter. When the results shown in Fig. 15 are converted to Graetz numbers based on the width ($2a$) and height ($2b$) of the duct, respectively, the Graetz number required to obtain fully developed temperature profiles is indeed a constant (for a given boundary condition) and is the same for both long and short sides and independent of aspect ratio.

Although the solutions illustrated in Figs. 14 and 15 indicate large entrance lengths required to develop temperature profiles across the long duct dimension, another boundary condition of practical importance should be expected to have a much smaller thermal entrance length. Consider the boundary condition of uniform heat input per unit duct length with uniform peripheral wall temperature. For this case the fully developed temperature distribution across the long side is completely different in character from the "parabolic type" temperature profiles obtained with uniform wall temperature and uniform heat flux everywhere. Fig. 16 shows *fully developed* temperature profiles across the long axis of rectangular ducts with uniform heat input per unit length (uniform peripheral wall temperature). The temperature distribution is nearly parabolic for a square duct, but is markedly flattened in the center for the larger aspect ratios.[4] Because here the ultimate effect of the boundary condition is localized, the thermal entrance length required to develop the long side temperature profile is probably considerably smaller for this boundary condition than for those mentioned previously. As yet, no analytical solution is available for the thermal entrance length under the influence of this boundary condition. It will be interesting to see if this notion can be verified by a solution. If so, it appears that a knowledge of the wall conductivity parameter ($k_w b/kD_h$) is essential for determining the thermal entrance length when a uniform heat flux is generated in the duct wall.

Finally, it is interesting to compare the duct length required to develop temperature profiles along the long and short sides based on the results shown in Fig. 15. Consider a rectangular duct with an aspect ratio of 5:1, a Reynolds number of 1000, and a Prandtl number of 1.0. For the short side, a Graetz number of 40 is required. The corresponding length to hydraulic diameter ratio is 25. For the long side, the required Graetz number is 1.5 and the necessary length-diameter ratio becomes 667. The writer plans to finish this work soon and submit a paper with a complete description to the ASME.

[4] This fact can also be visualized physically by noting that the membrane or soap film analogy (generally used for torsion of noncircular bars) is applicable to this problem.

Authors' Closure

The preceding discussion of our paper by L. C. Hoagland focuses attention on the question: Which length should be used as basis for a dimensionless parameter characterizing the duct length required for the development of the temperature field? Mr. Hoagland was successful in finding such a parameter for laminar bulk flow through a rectangular duct the value of which is independent of the side ratio of the duct cross section. In a similar attempt, it was investigated in our paper whether the ratio of duct length L necessary for development of the temperature field to duct height would have a value which agrees better with the ratio of L to diameter D for a circular tube than the ratio L/D_h. The experiments showed, however, that the temperature field in turbulent flow through a triangular duct was not developed for a ratio of duct length to duct height equal 21.5, whereas it has been found to be developed for a ratio L/D from 10 to 15 in a circular pipe. This led us to the conclusion that the turbulent flow process itself must be different in the triangular duct and in the circular tube.

In answer to a suggestion by Mr. Hoagland, we are presenting in Fig. 17 a parameter which is proportional to the local heat flux q_w plotted over the distance x from the sharp corner of the

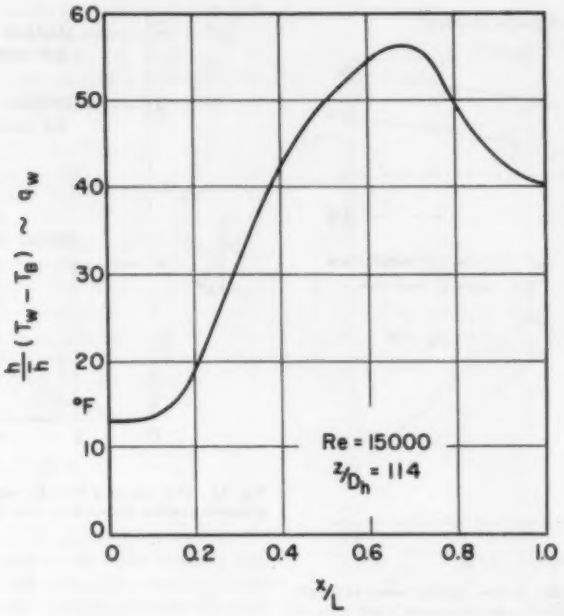

Fig. 17

duct for a specific Reynolds number. It may be observed that the heat flux varies considerably over the duct periphery indicating that the specific conditions applied in our experiments led to a situation approximately halfway between a constant heat flux and a constant wall temperature boundary condition.

Friction and heat transfer in turbulent flow through a rectangular duct are presently studied in our Heat Transfer Laboratory. A report on the friction characteristics is presently being prepared.

C. Y. KUO[1]
H. T. IIDA[2]
J. H. TAYLOR[3]
F. KREITH[4]

Heat Transfer in Flow Through Rotating Ducts

Experimentally measured heat-transfer coefficients and visually observed flow phenomena for water flowing through an electrically heated rotating pipe with various inserts are reported.

Convection heat transfer in flow through a rotating pipe or a rotating annulus was found to be an exceedingly complex mechanism which can not be treated adequately in terms of conventional parameters, but requires a detailed understanding of wave and vortex phenomena which were visually observed and photographed. Heat-transfer coefficients were measured in completely as well as partially filled flow channels. Three distinct flow regimes were observed in all cases; transition between regimes was found to depend on the rotational speed, but not on the axial flow velocity. Stationary vortexes and a counterrotational fluid motion were observed.

Introduction

ALTHOUGH CONVECTIVE HEAT TRANSFER in rotating systems is of importance in the thermal design of many types of industrial equipment, relatively little information on heat transfer in such systems is available in the literature, especially with fluids other than air.

This study was originally undertaken under the sponsorship of the National Printing Ink Research Institute in order to obtain information on the factors which control the cooling of printing ink roll mills in which an excessive temperature rise in the products is undesirable. The results of the initial phases of the research program raised, however, more questions than they answered. The scope of the study was therefore extended under a grant from the National Science Foundation to include a basic investigation of convection heat transfer to, and flow phenomena in, water flowing through a heated rotating pipe and annulus. Unfortunately, even the extended scope of the research program leaves many questions still unanswered and also raises new ones. It does, however, give an insight into some of the complexities of the transfer mechanism and can therefore serve as the basis for further study.

Heat transfer and flow phenomena in systems in which the fluid motion is influenced by body forces and Coriolis forces have until recently been investigated only by meteorologists and astrophysicists. In recent years, however, practical problems in aeronautics, atomic power, gas turbine cooling, printing and paper roll design, and chemical engineering have drawn the attention of engineers to problems associated with convection in fluids subject to various force fields.

This paper presents experimental results on heat transfer and flow phenomena in a fluid flowing through a horizontal, electrically heated pipe and annulus which are rotating and by virtue of their rotation cause the fluid to rotate. The rotation vector in this system is horizontal, and the temperature gradient is radially orientated. Table 1 summarizes the information available in the literature on some other rotating diabatic systems of interest. Papers dealing with heat transfer from bodies rotating in an infinite environment, such as cylinders and disks, are not included

[1] Research Assistant and Graduate Student, Lehigh University, Bethlehem, Pa.
[2] Convair Astronautics Corporation, San Diego, Calif.; formerly, Research Assistant and Graduate Student, Lehigh University. Assoc. Mem. ASME.
[3] Supervisor of Dispersion Research, N.P.I.R.I., Lehigh University.
[4] Professor of Aeronautical Engineering, University of Colorado, Boulder, Colo.; formerly, Associate Professor of Mechanical Engineering, Lehigh University. Assoc. Mem. ASME.

Contributed by the Heat Transfer Division of THE AMERICAN SOCIETY OF MECHANICAL ENGINEERS and presented at the ASME-AIChE Heat Transfer Conference, Storrs, Conn., August 9–12, 1959.
NOTE: Statements and opinions advanced in papers are to be understood as individual expressions of their authors and not those of the Society. Manuscript received at ASME Headquarters, May 15, 1959. Paper No. 59—HT-12.

Nomenclature

c_p = heat capacity, Btu/lb deg F
D = ID of test section, ft
D_e = equivalent diameter, ID of outer tube minus OD of inner tube, ft
= separation distance between surfaces rotating in opposite directions; $D_e/48$, in.
e = internal energy of water layer, Btu
g = gravitational constant, ft/hr^2
h = convective heat-transfer coefficient, Btu/hr ft^2 deg F
k = thermal conductivity, Btu/hr ft^2 deg F/ft
l = depth of fluid in free convection studies, ft
n = rotational speed, rev/sec
q = rate of heat transfer, Btu/hr
R_0 = radius of inner tube, in.
t_1 = inlet water temperature, deg F
t_2 = outlet water temperature, deg F
t_s = average wall surface temperature, deg F
t_f = average bulk water temperature, deg F
V = average water velocity, ft/sec
w = mass flow rate of water, lb/hr
y = radial distance from inner surface of outer tube, ft
N_{Pr} = Prandtl number, $c_p\mu/k$
N_{Re_f} = flow-rate Reynolds number, DV/ν
N_{Re_r} = rotational Reynolds number, $D^2\omega/\nu$
N_{Re_e} = flow-rate Reynolds number based on equivalent diameter, D_eV/ν
N_{Nu} = Nusselt number, hD/k
N_{Ta} = Taylor number, $\sqrt{\frac{d}{R_0}}\, d2\pi R_0 n/\nu$
β = coefficient of volumetric expansion, deg F^{-1}
δ = thickness of water film on upper inside surface of outer tube when tube is partly full, ft
μ = viscosity, lb/ft hr
ν = kinematic viscosity, ft^2/sec
ω = angular velocity, sec^{-1}
ρ = density of water, lb/ft^3

Table 1 Summary of types of flow investigated in rotating diabatic systems

Reference no.	1	2	3	4	5	6	7	8	9	This paper
Temperature gradient	R	V	V	V	R	R	R	R	R	R
Rotation vector	V	V	V	V	V	V	H	H	H	H
Geometry	A	HL	HL	HL	A	A	A	A	A	P, A
Type	E, T	T	T	T	T	E	E	E, S	T	E

Legend:

H—horizontal	P—pipe
V—vertical	HL—horizontal layer
R—radial	E—experimental
A—annulus	T—theoretical
	S—summary

in Table 1 because in these systems no phenomena directly pertinent to this study have been reported. Summaries of the information available on heat transfer from bodies rotating in an infinite environment are presented in Refs. [8 and 12],[1] and on the mechanics of the flow in rotating systems without heat transfer in Refs. [7, 8, and 11].

Equipment and Procedure

Heat Transfer. A schematic flow diagram of the equipment is shown in Fig. 1. Water was supplied to the constant head tank through valve A. The water flow rate was regulated by valve E and measured by a rotameter, R, before entering the test section.

Two piping arrangements were available at the test section outlet. In the first arrangement, shown in Fig. 1(*a*), the outlet duct was horizontal. With this arrangement, corresponding to that employed in many ink and paint dispersion mills, the test section was only half filled with water, and the space above the water was filled with air. With the alternate arrangement shown in Fig. 1(*b*), the test section was completely filled with water. The air was first removed through a hole in the top of the pipe, and the hole was then plugged. A standpipe with a vent at the outlet insured full flowing conditions in the test section during the test runs.

The heat-transfer test section is shown in detail in Fig. 2. It consisted of a horizontal, 3-in-ID steel tube, 25¼ in. long with ¼-in. thick walls. When assembled, the internal length was 24 in. Heat was supplied to the section by radiation and convection

[1] Numbers in brackets designate References at end of paper.

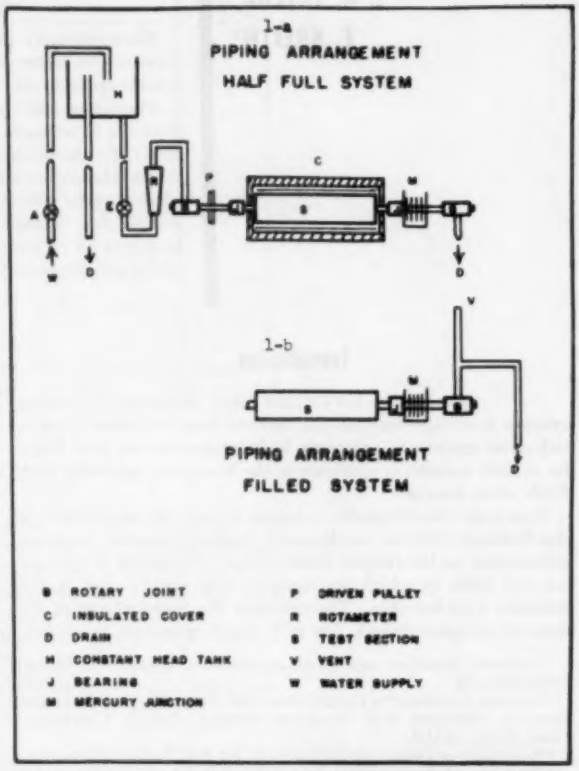

Fig. 1 Schematic sketch and flow diagram of experimental equipment (*a*, arrangement for partially filled ducts; *b*, arrangement for full flowing duct)

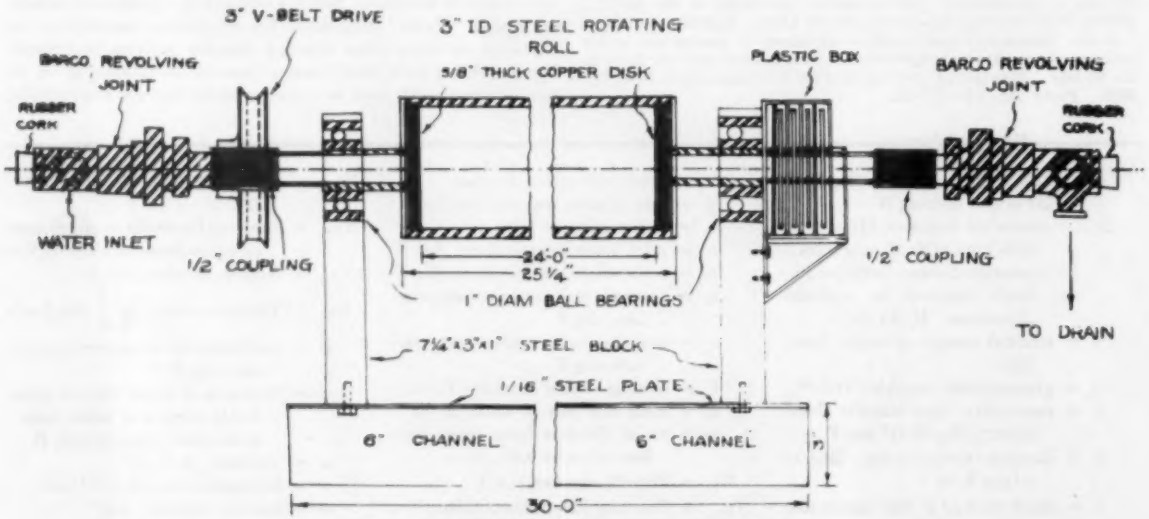

Fig. 2 Heat-transfer test section—construction details

from 32 stationary, electrically heated, No. 15 Nichrome, resistance wires, running parallel with the axis, near the outside surface of the tube. The test section was placed in an insulated cabinet to which the heating wires were attached. Electrical power input was regulated by a rheostat and measured with a wattmeter for establishment of operating conditions.

Inside surface temperatures of the tube were measured by three thermocouples embedded in the wall in accordance with the Patton-Feagan method [20]. These thermocouples were connected to a potentiometer through mercury pool junctions as shown in Fig. 4. Inlet and outlet water temperatures were measured with thermocouples immersed in the water stream. The wall and water thermocouple locations are shown in Fig. 3. Readings from thermocouples 1, 2, 3, 6, and 9 were used in the heat-transfer calculations.

Tests were conducted with two types of inserts in addition to the plain tube studies. These inserts are shown in Fig. 5. The first type, the paddles-insert, consisted of four baffles made of

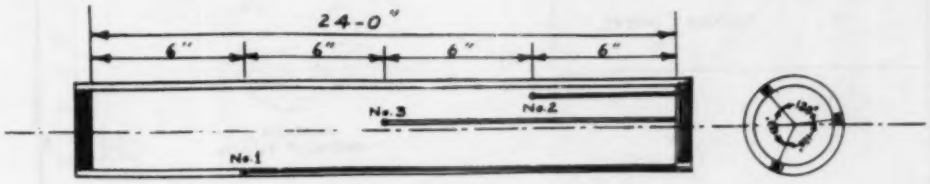

Wall Thermocouples

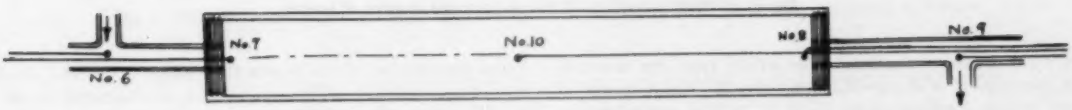

Water Thermocouples

Fig. 3 Location of thermocouples

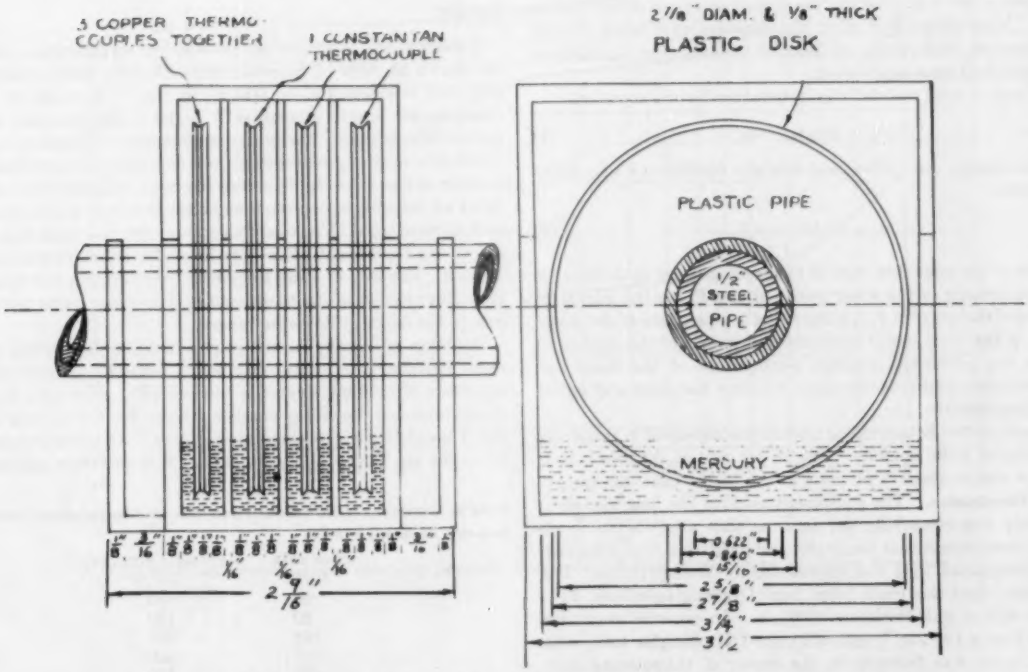

Fig. 4 Construction of mercury junction for connecting rotating thermocouple leads to potentiometer

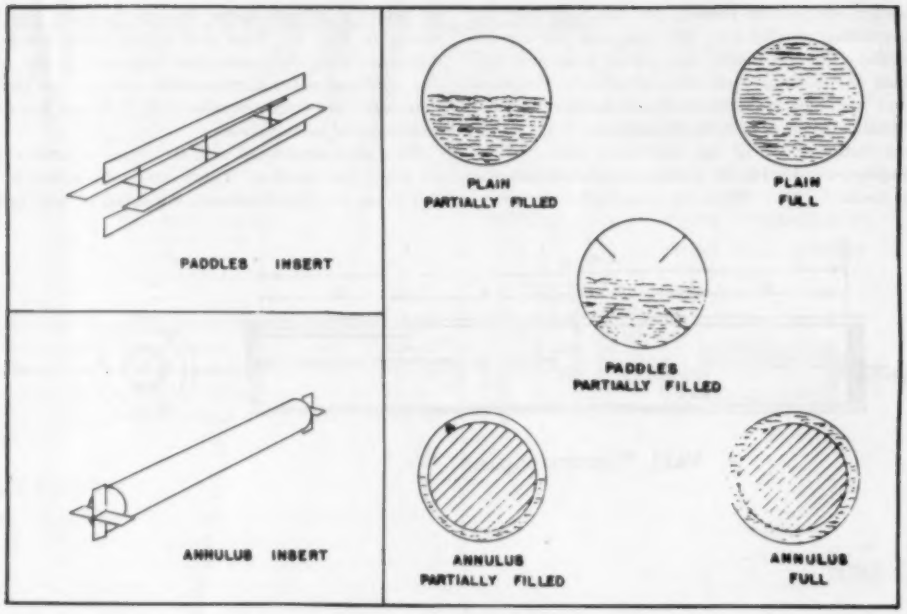

Fig. 5 Flow cross sections of test sections and sketches of inserts

$^1/_8 \times {}^3/_4 \times 24$-in. steel strips. The second type, the annulus-insert, consisted of a $2^3/_8$-in-OD steel tube, $22^1/_2$ in. long, sealed at both ends and supported by $^1/_8 \times {}^3/_4 \times 3$-in. crosspieces as shown in Fig. 5. Both types of inserts rotated along with the main tube.

Independent variables were the water flow rate, rotational speed, and power input. Dependent variables were the temperatures of the duct wall and the temperature rise of the cooling water. Measurements of all of the variables were taken at each experimental condition for at least 15 minutes after equilibrium conditions had been established.

The rate of heat transfer was determined by the equation

$$q = wc_p(t_2 - t_1), \tag{1}$$

and the average convective heat-transfer coefficient h was calculated from

$$h = q/A(t_s - t_f); \tag{2}$$

where w is the mass flow rate of the cooling water in lb/hr, c_p is the heat capacity of the water in Btu/lb deg F, t_1 is the inlet temperature of the water in F, t_2 is the outlet temperature of the water in F, A is the total inside heat-transfer surface of the duct in sq ft, t_s is the arithmetic average temperature of the three wall thermocouples, and t_f is the mean between the inlet and outlet water temperatures.

The convective heat-transfer coefficients measured in this study are estimated to be reliable within 28 per cent at the lowest heat flux, but within about 5 per cent in the higher heat flux range.

Flow Visualization. The equipment used for the flow visualization study was essentially the same as that used for the heat-transfer tests except that the heater and insulation were removed, and a transparent tube was substituted for the steel tube. The transparent duct was made from 3-in-ID plexiglas tubing, $22^1/_4$ in. long with a wall thickness of $^3/_{16}$ in. In order to study the annulus flow, a $19^1/_4$-in. length of $2^1/_2$-in-OD plexiglas tube, with plugged ends, was fastened in the center of the rotating duct. Crushed wheat particles were added to the system in order to aid visual observation of the water flow patterns. Visual studies were made with and without axial flow, at rotational speeds in the range from 10 to 500 rpm using water at an average temperature of 68 F. The movements of the wheat particles were observed both visually and with photographs taken with a 35-mm camera, tri-X film, f-11 lens opening, and $^1/_{30}$-sec exposure.

Results

Experimental results for the geometrical configurations studies are shown in plots of Nusselt number, hD/k, versus rotational Reynolds number ($\mathrm{Re}_r = D^2\omega/\nu$), in Figs. 6 through 10. The characteristic length dimension D is the inside diameter of the test section, 0.25 ft. The parameter employed in presenting different flow-rate curves in each of these figures is the water flow rate in lb/hr rather than the flow-rate Reynolds number, because the latter varied with temperature while the flow rate was constant in each series of tests. The relationship between flow rates and averages of the experimental flow-rate Reynolds numbers is shown in Table 2. The lack of strict proportionality between flow rate and Reynolds number is due to differences in average water temperature in the different flow-rate ranges.

The data of Fig. 6, for the partly full, simple rotating tube, yield straight lines when plotted as Nusselt number versus logarithm of the flow Reynolds number ($\mathrm{Re}_f = DV/\nu$), at constant rotational Reynolds number. Lines for the various rotational speeds have a common intercept at a Reynolds number of 24 on the log Reynolds number axis. It is therefore possible to

Table 2 Correspondence between flow rate and experimental average flow-rate Reynolds number

Flow rate, lb/hr	Reynolds number, DV/ν
29	60
60	120
168	300
317	550
465	800
530	950

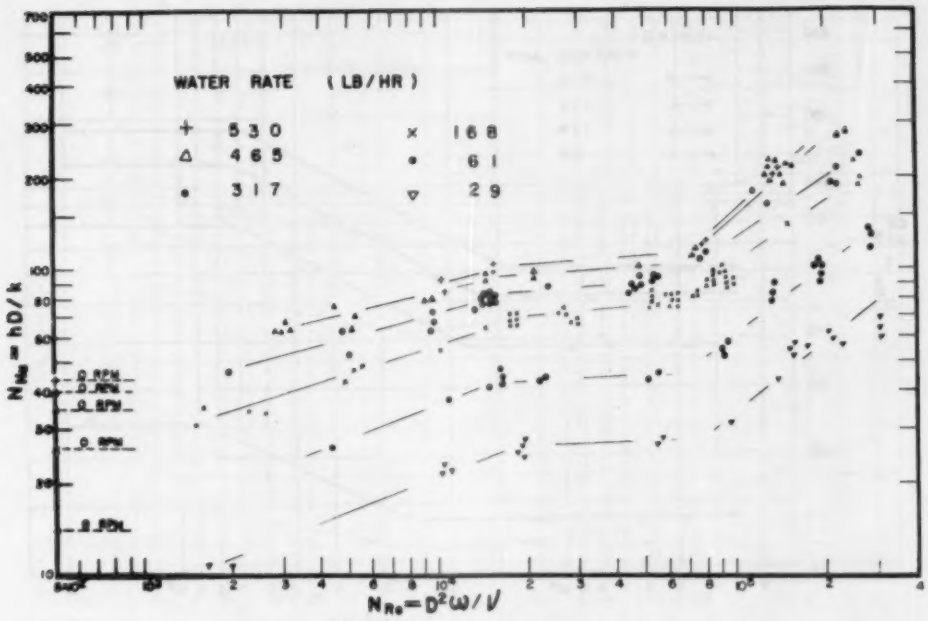

Fig. 6 Nusselt number versus rotational Reynolds number for partially filled plain tube at various flow rates

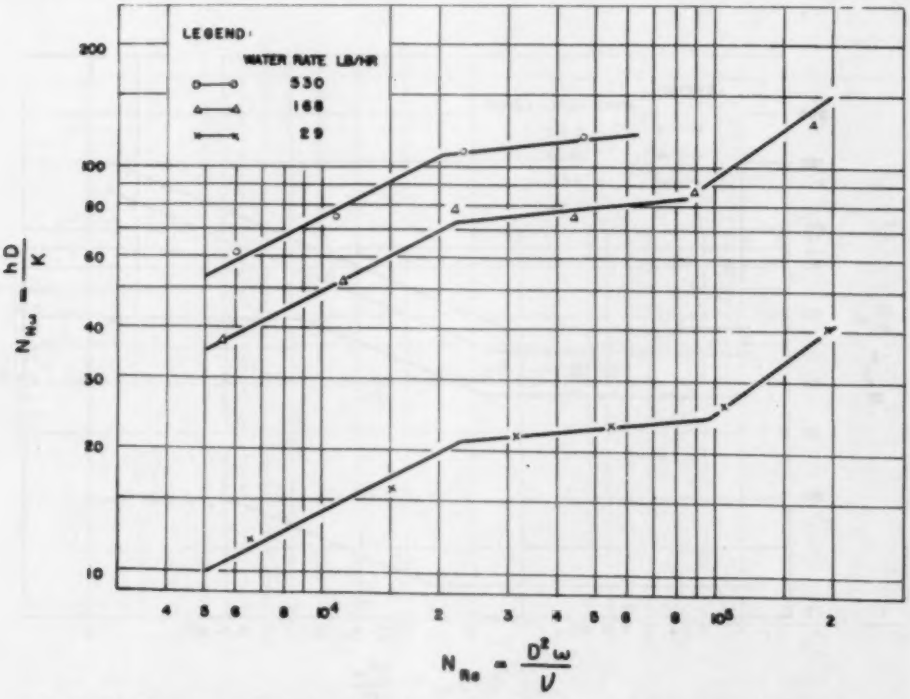

Fig. 7 Nusselt number versus rotational Reynolds number for full flowing plain tube at various flow rates

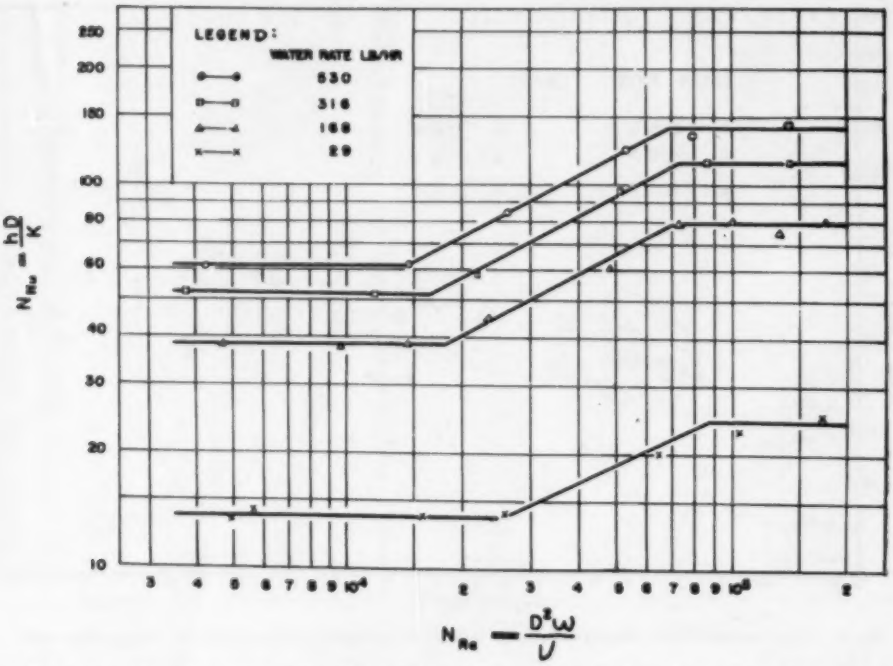

Fig. 8 Nusselt number versus rotational Reynolds number for partially filled annulus at various flow rates

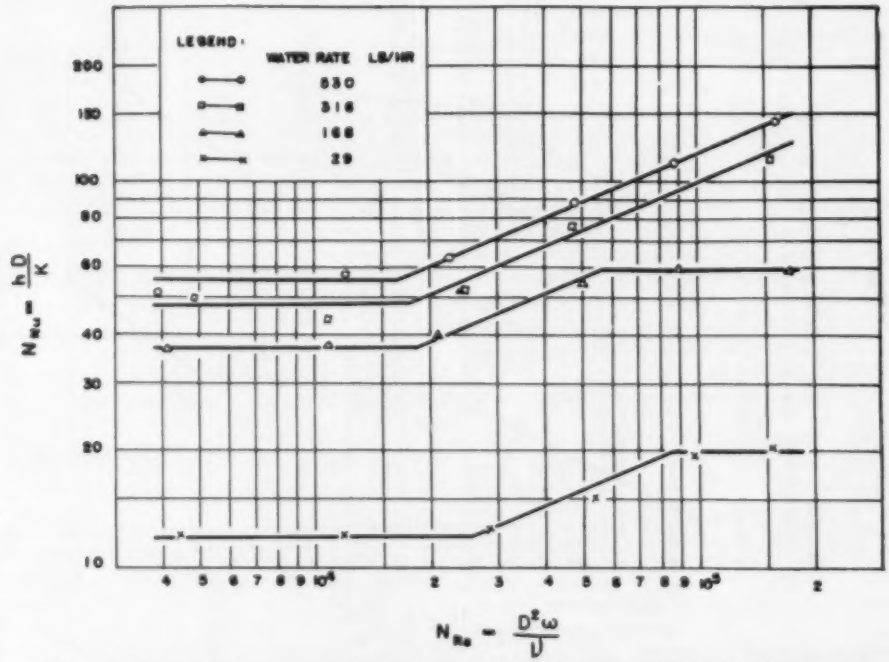

Fig. 9 Nusselt number versus rotational Reynolds number for full flowing annulus at various flow rates

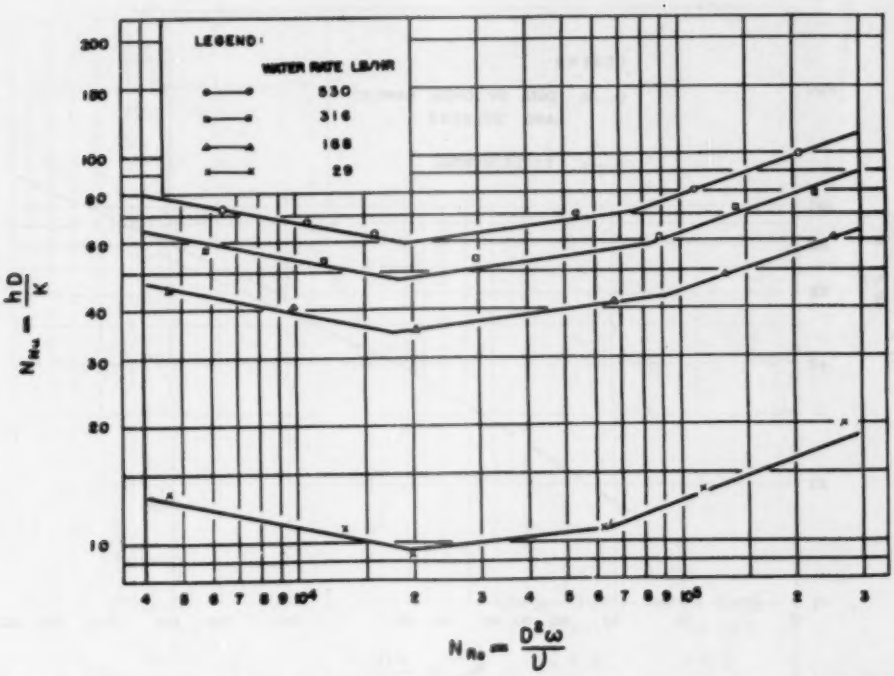

Fig. 10 Nusselt number versus rotational Reynolds number for partially filled pipe with paddle insert at various flow rates

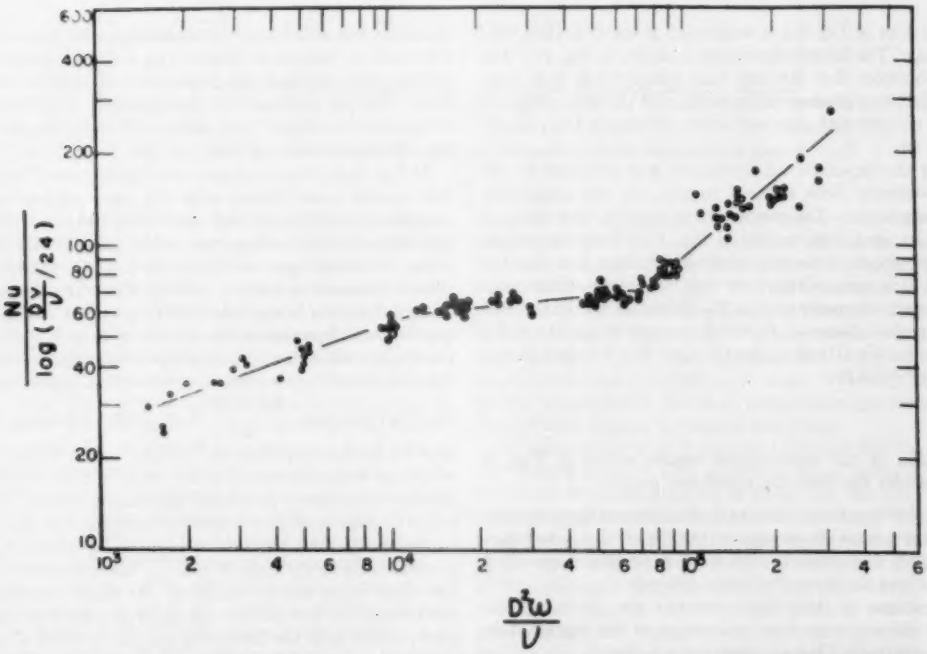

Fig. 11 Correlation of Nusselt number with flow rate and rotational Reynolds numbers for partially filled plain tube

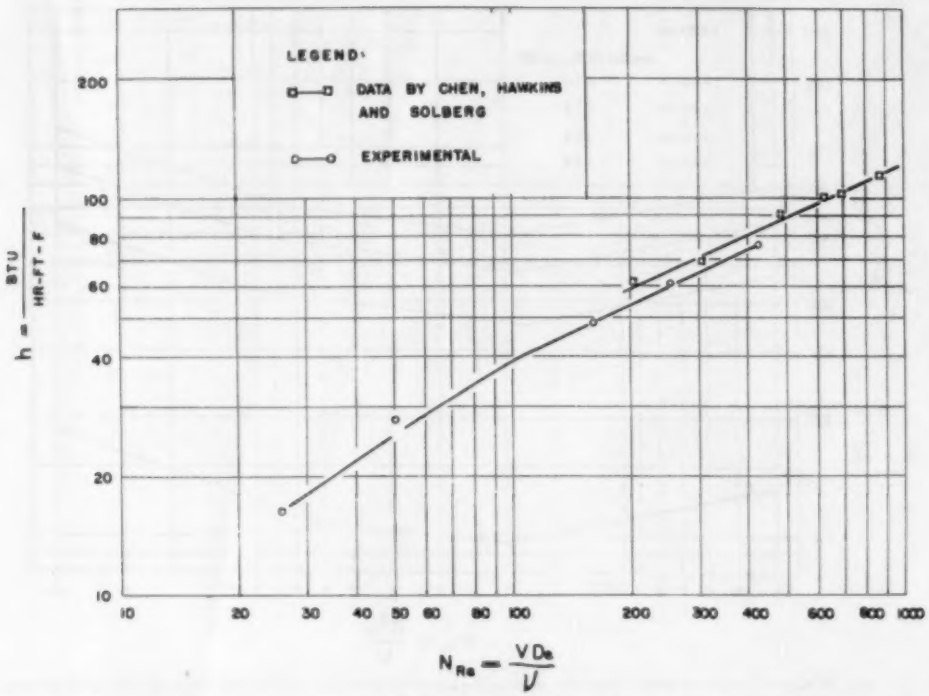

Fig. 12 Calibration of experiment—comparison of heat-transfer coefficient for flow through the annulus without rotation with data of Ref. [16]

correlate the data of Fig. 6 in a single plot of log [Nu/(Re$_f$/24)] versus log Re$_f$. The latter relationship is shown in Fig. 11. The relationship between flow rate and heat transfer was more complicated in the other geometrical systems, and the data presently available do not warrant more extensive correlation than shown in Figs. 7 to 10.

A check of the experimental equipment was provided by obtaining heat-transfer data without rotation in the completely filled annulus system. The results are compared with those of Chen, Hawkins, and Solberg [16] in Fig. 12. This comparison shows that the slopes of the two curves are similar, and that the experimental data agree within 8 per cent with those of Ref. [16]. The characteristic diameter used in the Reynolds number of Fig. 12 is the equivalent diameter D_e which is equal to the ID of the outer tube minus the OD of the inner tube. For the data of this paper, D was 0.0313 ft.

Discussion

An inspection of the experimental results shown in Figs. 6 through 11 reveals the following significant points:

1 There exist two discontinuities in the slopes of the curves of Nusselt number versus Reynolds number for all of the test sections. The first discontinuity occurs at a rotational speed of about 30 rpm, and the second at about 150 rpm.

2 The locations of these discontinuities are essentially independent of the net mass flow rate except at the highest flow rates in the completely filled annulus shown in Fig. 9.

3 At any given rotational speed and net flow rate the Nusselt number for a partially filled duct is equal to, and in some cases even slightly larger than, the Nusselt number for the same duct completely filled with water.

In the following discussion, an attempt is made to present plausible, but still tentative, explanations for these observations. The authors wish to emphasize the tentative nature of this discussion, but feel that its presentation is justified by its agreement with the experimental observations. Additional tests will be required to validate these arguments under conditions different from those investigated here.

At first sight, the conditions in a rotating annulus with fluid in the annular space heated from the outer surface resemble the conditions prevailing in free convection between two horizontal flat surfaces with heating from below [13]. In the rotating annulus the centrifugal body force is directed perpendicular and toward the heating surface, while in the free convection system the gravitational body force acts in a similar manner. For the gravitational free convection system it is well known that motion begins when the vertical temperature gradient becomes sufficiently large, a condition corresponding approximately to a Rayleigh number, $\frac{\beta g l^3 \rho^2 \Delta T c_p}{\mu k}$ of 1700. Chandra [17] showed that the motion can either be "cellular" or "columnar," the form of motion being dependent on the depth of fluid. When a steady flow is superimposed parallel to the heating surface, the fluid was found to align itself into a series of vortexes with axes transverse to the steady flow direction as soon as the steady flow velocity becomes sufficiently large to destroy the columnar flow pattern. For even larger steady velocities (the exact transition value is not known) the flow pattern changes into a series of vortexes with axes parallel with the flow direction, i.e., a series of longitudinal rolls.

The situation in the rotating annulus or pipe is, however, considerably more complicated, because within the range of rotational speeds investigated the gravitational force g is of the same order of magnitude as the centrifugal force. For example, at a rotational speed of about 150 rpm, the centrifugal force is just equal

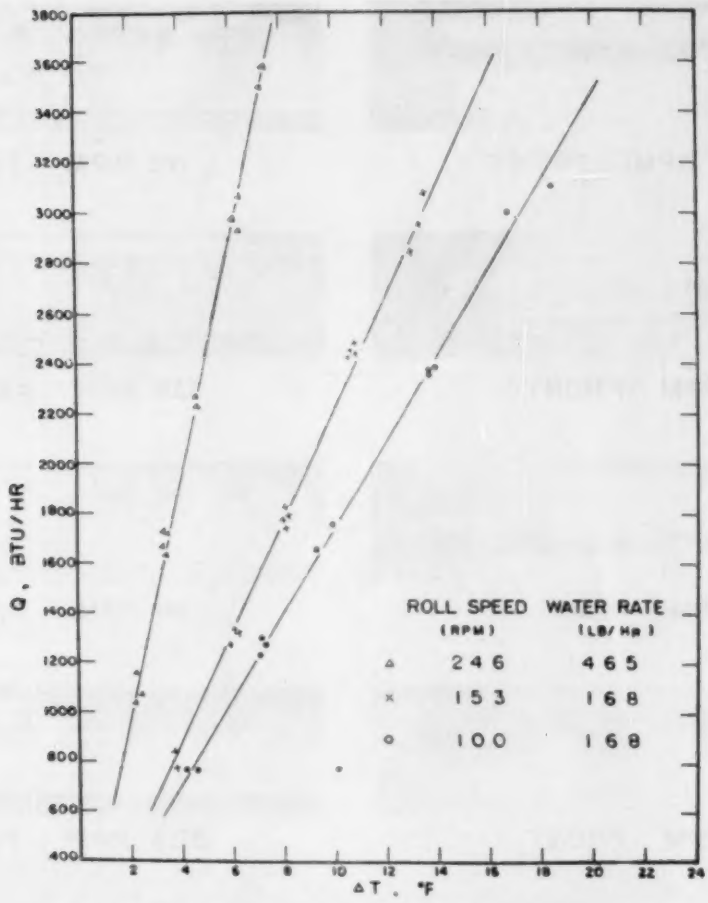

Fig. 13 Heat flux versus temperature potential for partially filled rotating plain tube

to one g. Since the component of the gravitational force perpendicular to the heating surface varies with angular position, the analogy between the rotating system and horizontal free convection is only approached at high rotational speeds when the gravitational force becomes negligible compared with the centrifugal force. It will be shown in the following discussion that in the lower range of rotational speeds investigated here, the flow conditions appear to be somewhat analogous to those found by G. I. Taylor [18] and others in an annular space between rotating co-axial cylinders. H. Jeffreys [10], who investigated mathematically the stability of a layer of incompressible fluid with a decreasing temperature in the vertically upward direction with a steady crossflow superimposed parallel to the surface, found that the instability in this system is analogous to that observed by G. I. Taylor [18] for flow without heat transfer between rotating co-axial cylinders. It is therefore reasonable to expect that a transition from conditions where the gravitational force is significant to the conditions under which centrifugal effects predominate would be subject to similar flow regimes and stability phenomena as have been found in each system separately. In order to determine experimentally whether or not pure free convection phenomena analogous to those between two horizontal surfaces are of importance for the rotating duct within the range of rotational speeds and temperature gradients investigated, the heat-transfer coefficient in the partially filled plain pipe was measured at various wall-to-fluid temperature differences while holding all other variables constant. As can be seen from Fig. 13, the heat-transfer coefficient is essentially independent of the temperature difference, since the rate of heat flow is directly proportional to the mean temperature difference. From these tests it was concluded that those flow phenomena which depend on the rotational speed and the mass flow rate predominate over those induced by pure free convection. This may, however, not be true at rotational speeds or temperature gradients considerably different from those used in this study.

An inspection of Figs. 6 through 10 reveals that the variation of the Nusselt number with rotational speed changes abruptly at rotational Reynolds numbers of about 2×10^4 and 7×10^4, corresponding to rotational speeds of about 30 and 150 rpm, respectively. In order to shed some light on the reason for the change in the functional dependence of N_{Nu} on N_{Re_r}, a transparent test section having a geometrical configuration similar to that of the section used for the heat-transfer study was built of plexiglas, and the flow was observed visually. It was observed that the general features of the flow pattern did not vary qualitatively with flow rate, but depended primarily on the rotational speed. Since it was considerably easier to photograph the flow pattern without any net through flow, the pictures shown here were taken without net flow through the system.

The series of photographs in Fig. 14 show the flow pattern in

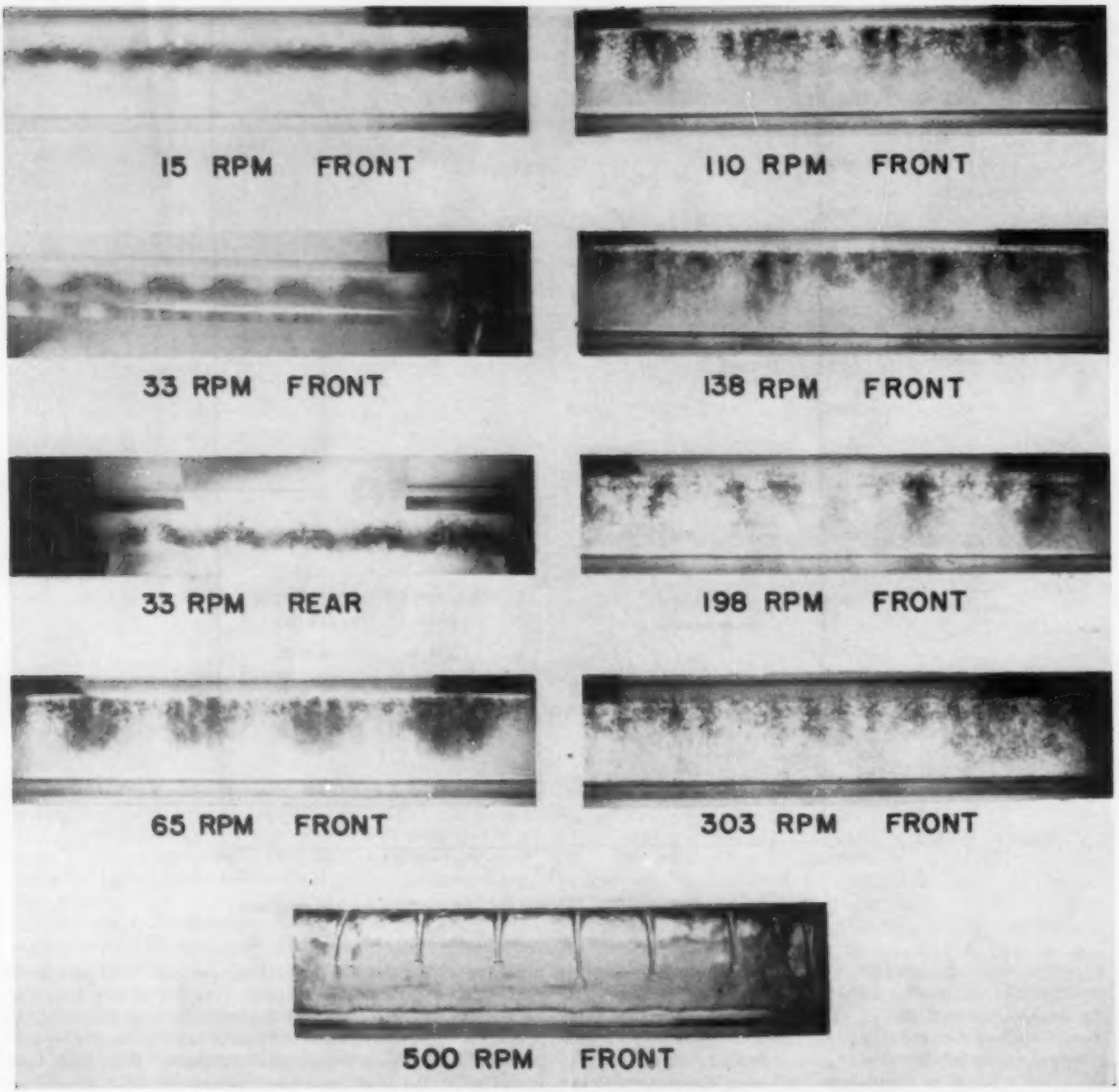

Fig. 14 Photographs of flow in partially filled plain pipe without net through flow

the plain pipe, half filled with water, at various rotational speeds. The dark areas in the photographs are the crushed wheat particles mentioned previously.

At 15 rpm the particles are almost uniformly distributed along the tube. At 33 rpm the particle motion indicates the existence of ring-shaped vortexes spaced regularly along the pipe. Two pictures are shown for this speed. One, identified as "Rear," was taken from 15 degrees below the horizontal, looking along the direction of rotation at the cylinder top. The picture marked "Front" was taken at an angle of 45 degrees from the horizontal, looking down in the direction opposite to that of rotation. The wave length of these vortexes, i.e., the spacing between their axes, is about one half the pipe diameter. At 65 rpm the wave length has increased to about one pipe diameter, but the main vortex is beginning to break up into smaller disturbances. This break up continues at 110 and 138 rpm, and at about 160 rpm a sheet of water of substantial thickness is carried along by the tube wall. It should be noted that at 150 rpm the centrifugal force just balances the gravitational force. At 200 rpm the flow pattern is irregular, but at 300 rpm a more regular vortex motion becomes apparent again. The wave length is now only about one fifth of the tube diameter. At 360 rpm a new flow pattern appeared. At this speed there were 6 distinct bands of entrapped air observed along the inner circumference of the tube. At 450 rpm the number of bands increased to 9; while at 500 rpm, the last picture shown, 11 bands were counted. Seven of these bands can be seen in the portion of roll photographed.

At speeds below 150 rpm the flow pattern in the bulk of the fluid, as seen from an end view, i.e., in a cross section perpendicular to the axis of rotation, is sketched in Fig. 15. The fluid in the central portion of the pipe rotates in a direction opposite to the pipe. This somewhat unexpected flow pattern may be neces-

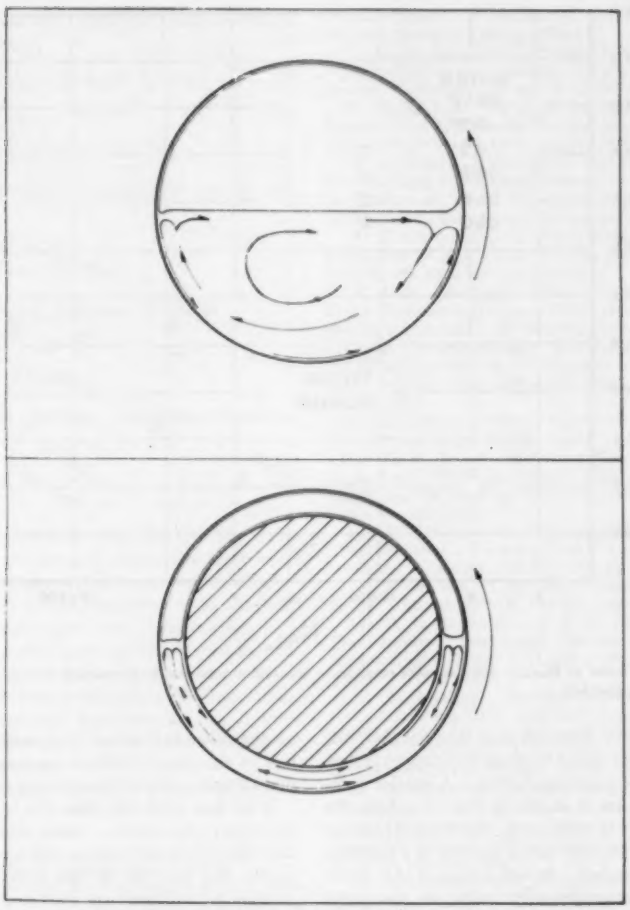

Fig. 15 Sketches of flow pattern in partially filled pipe and annulus in a cross section perpendicular to the axis of rotation

sary to conserve the moment of momentum of the air and water in the test section. A similar reversal in the flow was also observed in the water in the rotating annulus [see Fig. 15(*b*)]; it may serve to explain the discontinuity at 30 rpm.

In 1923, G. I. Taylor [18] investigated the stability of an incompressible viscous fluid contained in a narrow annulus between rotating concentric cylinders of infinite length for the case of zero axial flow. In 1937, S. Goldstein [19] extended the analysis to the case of a viscous flow through an annulus formed between a rotating inner cylinder and a stationary outer cylinder. These papers, as well as additional mathematical treatments and experimental investigations are summarized in Refs. [7 and 8]. Although Taylor's analysis leads to the conclusion that no instabilities should occur when the inner and outer cylinder rotate at the same speed, and Goldstein's analysis is inconclusive on that point, one can expect instabilities to arise in the partially filled annulus and pipe as shown by the following considerations. According to the observed cross-sectional flow pattern, the water in the center of the annulus rotates in the direction opposite to that of the walls at low speeds. The flow system, therefore, roughly resembles two concentric annuli in which the inner and outer surfaces rotate in opposite directions. Meskyn's analysis [15] predicts for this case a critical Taylor number of about 85 without net flow. For the idealized system above, the critical Taylor number at 30 rpm, the speed at which the first discontinuity in the slope of the curve of N_{Nu} versus N_{Re} occurs, is,

$$N_{Ta} = \sqrt{d/R_0}\, d2\pi R_0 n/\nu \tag{3}$$

$$= \sqrt{\frac{0.094}{1.5}}\ 0.094 \times 6.28 \times 1.5 \times 0.5/(144 \times 1 \times 10^{-5}) = 82$$

The agreement may be fortuitous, but the same approach has been used successfully by Brewster and Nissan [14] on a similar problem with satisfactory results.

A similar argument can be used to explain the origin of the vortex pattern in the partially filled pipe where the flow in the outer annulus resembles the flow between rotating co-axial cylinders.

The preceding arguments admittedly do not apply to the full-flowing pipe and annulus. In these two cases it was very difficult to observe the flow with the available equipment, and although vortexes were observed and the curves of N_{Nu} versus N_{Re}, show similar discontinuities in slope, neither a reliable description of the flow nor a satisfactory explanation of the cause of the instabilities can be given at this time.

Having shown that the discontinuities in slope of the curves of N_{Nu} versus N_{Re}, coincide, at least in the partially filled systems, with changes in the flow pattern, we now turn our attention to a comparison of the Nusselt number with rotation to the Nusselt number without rotation. For an annulus filled with air, Bjork-

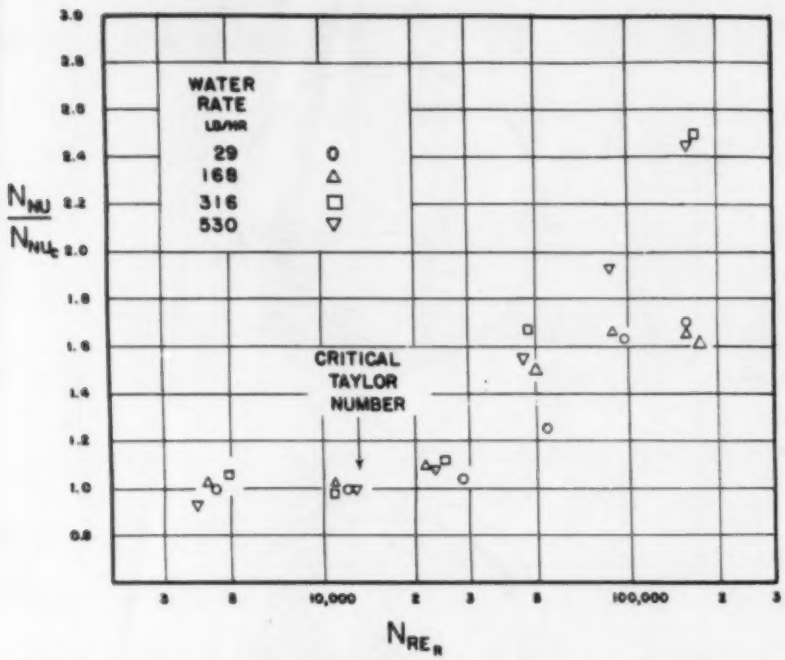

Fig. 16 Ratio of Nusselt number with rotation to Nusselt number without rotation versus rotational Reynolds number

lund [8] found that, at Taylor numbers less than critical, the Nusselt number in the annular space between rotating cylinders equals the Nusselt number for pure conduction. A similar comparison for the rotating annulus is shown in Fig. 16, where the ratio of the Nusselt number with rotation to the Nusselt number without rotation at the same net flow rate is plotted as a function of the rotational Reynolds number. An inspection of this curve reveals that this ratio is approximately unity at rotational Reynolds numbers below those corresponding to the critical value of Taylor numbers for the idealized system. In other words, rotation does not increase the Nusselt number until vortexes begin to appear.

The situation is qualitatively similar for the plain pipe, but in this system the Nusselt number was found to increase continuously with rotational speed, even at low rotational speeds.

The tests with the paddles insert were conducted chiefly to determine whether or not this type of insert would improve the heat transfer at a given flow rate. Contrary to expectations the paddles did not improve the heat transfer, but actually reduced the Nusselt number at rotational speeds above 30 rpm. A reasonable explanation for this observation is that the motion induced by the vortexes is more effective in transferring heat by convection than the motion induced by the paddles which undoubtedly interfered with the formation of the ring-shaped vortex patterns.

The third significant observation was that the heat-transfer coefficients for a partially filled duct at a given rotational speed and water mass flow rate is essentially equal to that for a completely filled duct at the same speed and flow rate. At first sight this seems unreasonable because in a partially filled duct only one half of the inside area is in contact with the main body of water, and consequently the convection heat-transfer surface area is much smaller. However, it was observed that under all conditions a film of water, approximately 0.025 in. thick, adhered to that portion of the inner pipe surface which was above the water level in partially filled flow. This thin layer of water will be heated by conduction from the pipe, but is effectively insulated on the other side which is in contact with the air in the upper half of the pipe. Little or no mass transfer is expected to take place because the air is saturated in the steady state.

If we now postulate that this layer of water which adheres to the upper pipe surface mixes effectively with the main stream after the rotational motion submerges it again in the bulk of the water, one can ask if this periodic heat flow mechanism can possibly be as effective as the transfer mechanism in a completely filled duct.

Assume for the sake of this argument that the convection heat-transfer coefficients over that portion of the duct surface which is in contact with the main stream are equal for partially filled and full flowing conditions. Then the rate of heat transfer through the lower half of the pipe surface per unit length is

$$q = h(\pi D/2)(t_s - t_f) \tag{4}$$

in a half full duct. In the upper half of the duct the internal energy of a water layer of thickness δ increases during one revolution by the amount

$$\Delta e = \rho c_p \left[\int_0^\delta t_2(y)dy - \int_0^\delta t_1(y)dy \right] (\pi D) \tag{5}$$

where y is the radial distance from the surface

$t_1(y)$ is the temperature profile of the film as it emerges from the main body of water

$t_2(y)$ is the temperature distribution of the film as it submerges again

Assuming that the temperature profile of the emerging film is linear and that the entire layer is heated up to t_s by conduction, the internal energy change per revolution becomes

$$\Delta e = \rho c \left\{ (t_s)\delta - \int_0^\delta [t_s - (t_s - t_3)(y/\delta)]dy \right\} (\pi D)$$
$$= \pi D \delta \rho c_p (t_s - t_3)/2 \tag{6}$$

where t_3 is the water temperature at the air interface.

If the water film mixes with the bulk upon being re-immersed, a heat balance per unit time yields

$$q = 900\omega\delta\rho c_p D(t_s - t_3) + h(\pi D/2)(t_s - t_f) \quad (7)$$

for the partially filled duct, while

$$q = h\pi D(t_s - t_f) \quad (8)$$

for the full flowing case. Combining Equations (7) and (8) and solving for δ yields

$$\delta = \frac{\pi h(t_s - t_f)}{1800\omega\rho c_p(t_s - t_3)} \quad (9)$$

Assuming $(t_s - t_f) = 2(t_s - t_3)$, Equation (9) yields

$$\delta = \frac{\pi h}{900\omega\rho c_p} \quad (10)$$

Equation (10) can be recast into the more convenient dimensionless form,

$$\left(\frac{\delta}{D}\right) = 4\pi \frac{N_{Nu}}{N_{Pr}N_{Re_r}} \quad (11)$$

Substituting the experimental data from Figs. 6 and 9 into Equation (11) shows that the film thickness δ required to have equal rates of heat transfer in a partially and a completely filled duct is about 0.08 in. at N_{Re_r} of 4×10^3 and decreases to about 0.008 in. at N_{Re_r} of 2×10^4. Although experimental observations indicate that the actual film thickness slightly increases with increasing speed, the preceding analysis is still valid because with increasing speed less time per revolution is available for heating the film. The change in internal energy, however, can still be more than sufficient to offset the reduction in surface area available for convection. This mechanism may have numerous practical applications in the thermal design of milling and calendering rolls.

References

1 G. I. Taylor, "Distribution of Temperature Between Concentric Rotating Cylinders," *Proceedings, Royal Society*, vol. 151, series A, 1935, p. 494.

2 S. Chandrasekhar, "The Instability of a Layer of Fluid Heated Below and Subject to Coriolis Forces," *Proceedings, Royal Society*, vol. 217, series A, 1953, pp. 306–327.

3 T. V. Davies, "The Forced Flow of a Rotating Viscous Liquid Which Is Heated From Below," *Philosophical Trans. Royal Society*, vol. 246, series A, 1954, pp. 81–112.

4 H. L. Kuo, "Symmetrical Disturbances in a Thin Layer of Fluid Subject to a Horizontal Temperature Gradient and Rotation," *Journal of Meteorology*, vol. 11, 1956, pp. 399–411.

5 H. L. Kuo, "Forced and Free Axially Symmetric Convection Produced by Differential Heating in a Rotating Fluid," *Journal of Meteorology*, vol. 13, 1956, pp. 521–527.

6 D. Fultz, "A Survey of Certain Thermally and Mechanically Driven Fluid Systems of Meteorological Interest," presented at a Symposium on Model Experiments, Johns Hopkins University, September, 1953, and cited in Reference [5].

7 J. Kaye and E. C. Elgar, "Modes of Adiabatic and Diabatic Fluid Flow in an Annulus With an Inner Rotating Cylinder," TRANS. ASME, vol. 80, 1958, pp. 753–765.

8 I. S. Bjorklund, "Heat Transfer From Rotating Bodies—Single Cylinder and Concentric Cylinders," Technical Report No. 34, Stanford University, December, 1957.

9 S. Chandrasekhar, "The Stability of Viscous Flow Between Rotating Cylinders in the Presence of a Radial Temperature Gradient," *Journal of Rotational Mechanics and Analysis*, vol. 3, 1954, pp. 181–207.

10 H. Jeffreys, "Some Cases of Instability in Fluid Motion," *Proceedings, Royal Society*, vol. 118, series A, 1928, pp. 195–208.

11 H. B. Squire, "Rotating Fluids: Survey in Mechanics," The G. I. Taylor 70th Anniversary Volume, edited by G. K. Batchelor and R. M. Davies, Cambridge University Press, Cambridge, England, 1956, pp. 139–161.

12 F. Kreith, J. H. Taylor, and J. P. Chong, "Heat and Mass Transfer From a Rotating Disk," TRANS. ASME, series C, JOURNAL OF HEAT TRANSFER, vol. 81, 1959, pp. 95–105.

13 S. Ostrach, "Convection Phenomena in Fluids Heated From Below," TRANS. ASME, vol. 79, 1957, pp. 299–305.

14 D. B. Brewster and A. H. Nissan, "The Hydrodynamics of Flow Between Horizontal Concentric Cylinders—I, Flow Due to Rotation of Cylinder," *Chemical Engineering Science*, vol. 7, no. 4, 1958.

15 D. Meskyn, "Stability of Viscous Flow Between Rotating Cylinders, Parts I, II, and III," *Proceedings, Royal Society*, vol. 187, series A, 1946, pp. 115, 480, and 492.

16 C. Y. Chen, G. A. Hawkins, and H. L. Solberg, "Heat Transfer in Annuli," TRANS. ASME, vol. 68, 1946, pp. 99–106.

17 K. Chandra, "Instability of Fluids Heated From Below," *Proceedings, Royal Society*, vol. 164, series A, 1938, pp. 231–242.

18 G. I. Taylor, "Stability of a Viscous Fluid Between Two Rotating Cylinders," *Philosophical Trans. Royal Society*, vol. 223, series A, 1923, pp. 284–243.

19 S. Goldstein, "The Stability of Viscous Fluid Flow Between Rotating, Cylinders," *Proceedings, Cambridge Philosophical Society*, vol. 33, 1937, pp. 41–48.

20 E. L. Patton and R. A. Feagan, "A Method of Installing Tube Wall Thermocouples," *Industrial and Engineering Chemistry*, Analytical Edition, vol. 13, 1941, pp. 823–824.

Journal of HEAT TRANSFER — Technical Briefs

This section consists of contributions of 750 words or less (about 2½ double-spaced typewritten pages, including figures). Technical Briefs will be reviewed and approved by the specific division's reviewing committee prior to publication. After approval such contributions will be published as soon as possible, normally in the next issue of the Journal.

Comparison of Turbulent Heat-Transfer Results for Uniform Wall Heat Flux and Uniform Wall Temperature

R. SIEGEL[1] and E. M. SPARROW[1]

Introduction

THE PURPOSE of this note is to examine in a more precise way how the Nusselt numbers for turbulent heat transfer in both the fully developed and thermal entrance regions of a circular tube are affected by two different wall boundary conditions. The comparisons are made for: (*a*) Uniform wall temperature (UWT); and (*b*) uniform wall heat flux (UHF). Several papers which have been concerned with the turbulent thermal entrance region problem are given in references [1 to 4].[2] Although these analyses have all utilized an eigenvalue formulation for the thermal entrance region (in contrast to reference [6] which used a boundary layer approach), there were differences in the choices of eddy diffusivity expressions, velocity distributions, and methods for carrying out the numerical solutions. These differences were also found in the fully developed analyses. Hence when making a comparison of the analytical results for uniform wall temperature and uniform wall heat flux, it was not known if differences in the Nusselt numbers could be wholly attributed to the difference in wall boundary conditions, since all the analytical results were not obtained in a consistent way. To have results which could be directly compared, computations were carried out for the uniform wall temperature case, reference [4*c*], using the same eddy diffusivity, velocity distribution, and digital computer program employed for uniform wall heat flux in references [4*a* and *b*]. In addition, the previous work was extended to a lower Reynolds number range so that comparisons could be made over a wide range of both Reynolds and Prandtl numbers.

The analysis of heat transfer in the turbulent thermal entrance and fully developed regions has already been thoroughly treated in references [4] and hence need not be presented here in detail. The calculations were carried out under the assumption of equal eddy diffusivities for heat and momentum. For the region near the tube wall, the diffusivity was evaluated from Deissler's formula [5], while for the region away from the wall, the diffusivity was found by differentiating the logarithmic velocity expression and using a linear variation of shear stress. For convenience, the Appendix gives a few of the final analytical expressions, and Table 2 provides numerical data for the cases which have not been previously tabulated in references [4].

In the next section, we then proceed directly to an examination of the Nusselt number results.

Nusselt Number Comparisons

Pr = 0.7. The results for Pr = 0.7 and four different Reynolds numbers are given in Table 1(*a*) as a function of the length-diameter ratio (x/D) from the tube entrance. The per cent difference is defined as $(Nu_{UHF} - Nu_{UWT})/Nu_{UWT}$. The largest differences are found in the low Reynolds number range, and for each case the differences become smaller at larger distances from the tube entrance. For the ranges of variables considered, the effect of the two different wall boundary conditions is never larger than 10 per cent.

Pr = 10 and Pr = 100. Results for the higher Prandtl numbers are given in Tables 1(*b*) and (*c*). For this range there is essentially no influence of the two different boundary conditions. Since the per cent difference does not become significant even for small x/D, the details in the thermal entrance region are only given as an example for one Reynolds number. Some of the Nusselt number results for uniform wall temperature are very slightly in excess of those for uniform wall heat flux. This is a somewhat surprising finding, and it may be inferred that the differences of a few tenths of a per cent are probably due to accuracy limitations of the calculations.

Conclusions. From these tabulations we may then conclude that for turbulent flow the heat-transfer mechanism in the thermal entrance and fully developed regions is quite insensitive to the two wall boundary conditions which were examined, at least for the range $Pr \geq 0.7$. This conclusion is in qualitative agreement with the findings of reference [6] for Pr = 0.73 (thermal entrance region calculations using a boundary layer model) and of reference [7] for Pr = 1.0 (fully developed region). The effect of other wall boundary conditions can be examined by the superposition techniques described in references [2 and 4*b*].

References

1 H. Latzko, "Heat Transfer in a Turbulent Liquid or Gas Stream," NACA TM 1068, 1944.

2 C. A. Sleicher, Jr., and M. Tribus, "Heat Transfer in a Pipe With Turbulent Flow and Arbitrary Wall-Temperature Distribution," TRANS. ASME, vol. 79, 1957, pp. 789–797.

3 H. L. Beckers, "Heat Transfer in Turbulent Tube Flow," *Applied Scientific Research*, vol. 6, sec. A, 1956, pp. 147–190.

4*a* E. M. Sparrow, T. M. Hallman, and R. Siegel, "Turbulent Heat Transfer in the Thermal Entrance Region of a Pipe With Uniform Heat Flux," *Applied Scientific Research*, vol. 7, sec. A, 1957, pp. 37–52.

4*b* R. Siegel and E. M. Sparrow, "Turbulent Flow in a Circular Tube With Arbitrary Internal Heat Sources and Wall Heat Transfer," JOURNAL OF HEAT TRANSFER, TRANS. ASME, series C, vol. 81, 1959, pp. 280–290.

4*c* E. M. Sparrow and R. Siegel, "Unsteady Turbulent Heat Transfer in Tubes," ASME Paper No. 59—HT-16.

5 R. G. Deissler, "Analysis of Turbulent Heat Transfer, Mass Transfer, and Friction in Smooth Tubes at High Prandtl and Schmidt Numbers," NACA Rept. 1210, 1955. (Supersedes NACA TN 3145.)

6 R. G. Deissler, "Turbulent Heat Transfer and Friction in the Entrance Regions of Smooth Passages," TRANS. ASME, vol. 77, 1955, pp. 1221–1233.

7 R. A. Seban and T. T. Shimazaki, "Heat Transfer to a Fluid Flowing Turbulently in a Smooth Pipe With Walls at Constant Temperature," TRANS. ASME, vol. 73, 1951, pp. 803–809.

APPENDIX

Summary of Analytical Results

Uniform Wall Temperature. The temperature distribution within the fluid is given by

$$\frac{T - T_w}{T_0 - T_w} = \sum_{n=1}^{\infty} C_n \Phi_n(r) e^{-4\beta_n^2 x/DRe}$$

[1] NASA, Lewis Research Center, Cleveland, Ohio. Assoc. Mem. ASME. E. M. Sparrow is now Professor of Mechanical Engineering, University of Minnesota, Minneapolis, Minn.

[2] Numbers in brackets designate References at end of paper.

Contributed by the Heat Transfer Division of THE AMERICAN SOCIETY OF MECHANICAL ENGINEERS.

Manuscript received at ASME Headquarters, January 28, 1960.

Table 1(a); Pr 0.7

x/D	Re = 10,000			Re = 50,000		
	Nu_{UHF}	Nu_{UWT}	% diff.	Nu_{UHF}	Nu_{UWT}	% diff.
2	42.83	39.28	9.0	131.6	125.3	5.1
5	36.90	34.68	6.4	116.7	111.9	4.2
10	34.15	32.44	5.3	108.7	104.8	3.7
20	32.72	31.32	4.5	103.8	100.5	3.3
30	32.42	31.11	4.2	102.4	99.40	3.0
∞	32.32	31.06	4.1	101.8	98.95	2.8
x/D	Re = 100,000			Re = 500,000		
	Nu_{UHF}	Nu_{UWT}	% diff.	Nu_{UHF}	Nu_{UWT}	% diff.
2	220.2	211.6	4.1	757.5	740.2	2.3
5	196.4	190.2	3.3	686.7	672.7	2.1
10	183.6	178.4	2.9	644.9	633.6	1.8
20	175.2	170.8	2.5	616.3	607.1	1.5
30	172.8	168.8	2.3	606.5	598.4	1.4
∞	171.4	167.7	2.2	599.7	592.9	1.1

Table 1(b); Pr 10

x/D	Re = 100,000		
	Nu_{UHF}	Nu_{UWT}	% diff.
2	733.6	732.0	0.2
5	711.3	710.4	.1
10	697.7	697.2	.07
20	688.5	688.3	.03
30	685.5	685.4	.01
∞	683.9	683.9	0

Fully developed Nusselt numbers

Re	Nu_{UHF}	Nu_{UWT}	% diff.
50,000	381.0	379.7	0.3
500,000	2722	2730	-.3

Table 1(c); Pr 100

x/D	Re = 100,000		
	Nu_{UHF}	Nu_{UWT}	% diff.
2	1554	1556	-0.2
5	1543	1545	-.2
10	1536	1539	-.2
20	1531	1534	-.2
30	1530	1532	-.2
∞	1529	1532	-.2

Fully developed Nusselt numbers

Re	Nu_{UHF}	Nu_{UWT}	% diff.
50,000	836.6	834.9	0.2
500,000	6352	6386	-.5

Table 2(a) Uniform wall temperature

(1) Re = 10,000; Pr = 0.7

n	β_n^2	$(d\Phi_n/dr^+)_{r_o^+}$	C_n
1	44.371	-0.036269	1.2664
2	454.26	.022654	-.49152
3	1137.4	-.018059	.43507
4	2106.2	.016892	-.41660
5	3346.0	-.016687	.41254
6	4864.0	.017637	-.41692
7	6617.8	-.018532	.41912

(2) Re = 50,000; Pr = 0.7

n	β_n^2	$(d\Phi_n/dr^+)_{r_o^+}$	C_n
1	141.36	-0.030622	1.2267
2	1676.2	.017838	-.42513
3	4184.6	-.013381	.39001
4	7679.4	.011209	-.37987
5	12167.0	-.0098511	.37320
6	17667.0	.0090539	-.36768
7	24167.0	-.0085049	.36286

Table 2(b) Uniform wall heat flux

Re = 10,000; Pr = 0.7

n	β_n^2	A_n
1	361.38	-0.21646
2	984.83	-.11776
3	1863.8	-.090430
4	2990.7	-.073326
5	4364.4	-.059857
6	6004.1	-.044084
7	7946.8	-.032717

For Re = 10,000; $r_o^+ = 324$

where T_w is the wall temperature, T_0 the entering fluid temperature, C_n are constants, β_n and Φ_n the eigenvalues and eigenfunctions, x the distance from the tube entrance, and r the radial coordinate. The Reynolds number is defined by $\bar{u}D/\nu$, where $\bar{u}$ is the mean fluid velocity.

The Nusselt number is given by

$$Nu_{UWT} = Pr \frac{\sum_{n=1}^{\infty} C_n \left(\frac{d\Phi_n}{dr}\right)_{r_0} e^{-4\beta_n^2 x/DRe}}{\sum_{n=1}^{\infty} \frac{C_n}{\beta_n^2} \left(\frac{d\Phi}{dr}\right)_{r_0} e^{-4\beta_n^2 x/DRe}}$$

Uniform wall heat flux. The fluid temperature distribution is given by

$$\frac{T - T_0}{q\frac{r_0}{k}} = \frac{2}{RePr}\frac{x}{D} + G(r) + \sum_{n=1}^{\infty} C_n \Phi_n(r) e^{-4\beta_n^2 x/DRe}$$

where q is the wall heat flux per unit area, r_0 the tube radius, and $G(r)$ is the fully developed temperature distribution. The Nusselt number is given by

$$Nu_{UHF} = \frac{2}{G(r_0)} \frac{1}{1 + \sum_{n=1}^{\infty} A_n e^{-4\beta_n^2 x/DRe}}$$

where $A_n = C_n\Phi_n(r_0)/G(r_0)$. The Φ_n, C_n, and β_n for uniform heat flux are different from those for uniform wall temperature.

For a detailed description of the analytical method, the reader is referred to references [4].

Journal of HEAT TRANSFER

Information for Authors

• Manuscripts should be submitted in final form to the Editor. Each manuscript must be accompanied by a statement that it has not been published elsewhere nor has it been submitted for publication elsewhere. A paper which would occupy more than 8 pages of the Journal may be returned to the author for abridgment.

• The author should state his business connection, the title of his position, and his mailing address. A short abstract (50 to 100 words) should be included on the first page immediately preceding the introductory paragraph of the paper.

Three copies of the manuscript are required. One of these must be a carefully prepared printer's copy, typed in double spacing, on one side of the page only, with wide margins, on $8\frac{1}{2}$ by 11-in. opaque white paper. Mimeographed manuscripts, if prepared with exceptional care, can be accepted provided they are completely edited.

• As far as possible, all mathematical expressions should be typewritten. Greek letters and other symbols not available on the typewriter should be carefully inserted in ink. Care should be taken to distinguish between capital and lowercase letter, between zero (0) and the letter (*O*), between the numeral (1) and the letter (*l*), etc. A letter representing a vector cannot be printed with an arrow above or below it. The letter should be underscored with a single wavy line, wherever it appears in the text, to designate boldface type.

• A list of symbols carefully marked for the use of the editor (thus: κ, Greek l.c. kappa), if it has not been included in the body of the paper, should accompany the manuscript on a separate page.

• Before preparing a manuscript the author should study printed articles in the Journal, with special attention to the form and style of mathematical expressions, tables, footnotes, references, and abstract. Numbers that identify mathematical expressions should be enclosed in parentheses. Numbers that identify references at the end of the paper should be enclosed in brackets. Care should be taken to arrange all tables and mathematical expressions in such a way that they will fit into a single column when set in type. Equations that might extend beyond the width of one column (fractions that should not be broken or long expressions enclosed in parentheses) should be rephrased to go on two or more lines within column width. Fractional powers are preferred to root signs and should always be used in more elaborate formulas. The solidus should be used instead of the horizontal line for fractions wherever possible.

• A normal paper should not exceed 8 pages in the Journal. It is about 8000 words or 20 double-spaced typewritten pages exclusive of drawings. A Technical Brief should not exceed 750 words or about one page in the Journal inclusive of drawings.

• Originals and two copies of figures must accompany the manuscript. Line drawings should not be larger than $8\frac{1}{2} \times 11$ in. and should be planned for reduction to column width. Lettering should be large enough to be clearly legible when the illustration is reduced. The originals of line drawings must be in India ink on white or pale blue tracing paper or tracing cloth. Photographs of equipment or test specimens must be glossy prints and should be used sparingly. Captions for figures should be typed double-spaced and included as the last page of the manuscript. The figure number and author's name should be written in the margin or on the back of each illustration.

• Titles of papers should be brief.

• Authors can obtain copies of the ASME Manual MS-4, "An ASME Paper," from the Editor and are urged to do so before drafting their papers in final form.

• Papers published in Journals of the Transactions of the ASME must be presented at a Meeting, either in person or by title.

• An author is entitled to 25 preprints free of charge (in the case of two authors, 15 each; three or more authors, 10 each). Larger quantities of preprints or reprints can be ordered from Editorial Department, The American Society of Mechanical Engineers, 29 West 39th Street, New York 18, N. Y. Quotations will be sent on request.

Please address all communications to:

Editor, ASME,

29 West 39th Street,

New York 18, N. Y.

ASME Publications Committee